SATELLITE-DERIVED MONITORING OF ASBESTOS MINE REHABILITATION IN THE POST MINING ENVIRONMENTS OF MAFEFE AND MATHABATHA. LIMPOPO PROVINCE, SOUTH AFRICA

by

Brilliant Mareme Petja

RESEARCH THESIS
Submitted in fulfilment of the requirements for the degree of

Doctor of Philosophy

in

Geography (GIS and Remote Sensing)

in the

FACULTY OF SCIENCE AND AGRICULTURE
(School of Agricultural & Environmental Sciences)

at the

UNIVERSITY OF LIMPOPO

SUPERVISOR: Dr. G.T. Tengbeh
CO-SUPERVISOR: Dr. Y.A. Twumasi

2009

DECLARATION

I declare that the thesis hereby submitted to the University of Limpopo for the degree of Doctor of Philosophy in Geography (GIS and Remote Sensing) has not been previously submitted by me for a degree at this or any other university; that it is my work in design and execution, and that all material contained herein has been duly acknowledged.

_____ _____

B.M. Petja (Mr) **Date**

[redacted]

ABSTRACT

Mining of the environment leaves scars of environmental damage and associated health consequences resulting from exploration, extraction and processing of minerals. These impacts tend to get worse during the post closure period on the abandoned derelict mines. The South African government is conducting environmental remediation on the mines which were abandoned by colonial mining companies. In this situation, monitoring and evaluation of such projects becomes a necessity to ensure sustainability of the mine rehabilitation process. However, the government did not have any plan and/or capacity to monitor the rehabilitation process. This study therefore utilizes remote sensing techniques to monitor the asbestos mine rehabilitation process at Mafefe and Mathabatha and to assess its effectiveness as short and long term strategies of environmental management.

This research used Landsat Thematic Mapper (TM) images (1989 - 2004) to assess and monitor mine degradation and rehabilitation efforts in the study area. Two scenes were acquired for each year, representing both low peak and high peak growing periods. An image differencing method (NDVI) was used to assess the condition of vegetation in the study area. Results showed both positive and negative trends in vegetation growth. In order to understand the dynamics depicted from satellite images in the post mining phase, a field campaign was conducted to understand the reflective properties of the variables (vegetation species) used for mine rehabilitation. Results using leaf area index (LAI) and fraction of photosynthetically active radiation (*f*PAR) provides a proper reasoning for the type of positive environmental change reflected from satellite images. This therefore makes remote sensing an important tool for the limited field monitoring capacity for observing the dynamics of mining environments in the post closure phase. The image differencing method also helped in identifying areas that needs further rehabilitation.

Despite the rehabilitation efforts, field evidence shows that traces of different asbestos minerals appear scattered even after the rehabilitation process has been conducted. This has not been properly reported since there was no effectively coordinated monitoring procedure in place to assess the progress of mine rehabilitation in mitigating asbestos pollution. This study therefore used *in situ* remote sensing techniques to spectrally differentiate various types of asbestos minerals with the aim of determining its potential in assessing asbestos pollution. Data generated from an X-Ray Diffraction and Scanning Electron Microscopy were also utilized for the identification and characterization of asbestos minerals in soil and water of the rehabilitated environments which were also examined using *in situ* remote sensing. An Analytical Spectral Devices (ASD) Field Spectrometer was used to collect spectra of asbestos minerals and that of soil and water samples for comparative analysis with laboratory results. Results showed that *in situ* remote sensing can play a significant role in monitoring the distribution of the asbestos minerals over rehabilitated surface areas. However, the spectral characteristics of asbestos minerals in the water bodies were not conclusive enough when compared to laboratory methods.

Within the context of South Africa as a developing country, remote sensing is recommended as an important tool for periodic assessment and monitoring of mine rehabilitation. This will fill the gap created from the limited capacity within the government for monitoring and evaluation of asbestos mine rehabilitation. It is also the most cost effective method of conducting natural resource monitoring.

DEDICATION

This work is dedicated to my late grandparents,

Rakgolo Amos Makafele Mabatamela and Koko Ramadimetja Mmapula Mabatamela.

TABLE OF CONTENTS

Declaration…..i
Abstract…..ii
Dedication…….iv
Table of contents……v
Lists of Figures and Tables…….viii
Abbreviations and Acronyms……xv
Acknowledgements……xvii
Citation……xix

Chapter 1: Introduction 1
1.1 Background……1
1.2 Asbestos Mining in South Africa……1
1.3 Statement of the Problem……6
1.4 Purpose and Objectives……7
1.5 Research Hypotheses……8
1.6 Summary……8

Chapter 2: The Environment of the Study Area..... 9
2.1 Introduction……9
2.2 Ecological Setting……9
2.2.1 Location..... 9
2.2.2 Physiography..... 10
2.2.3 Geology and Pedology..... 11
2.2.4 Climate……13
2.2.5 Hydrology 14
2.2.6 Biodiversity..... 15
2.2.7. Land use 17
2.2.8. Population and Settlement..... 18
2.3 Socio-economic drivers of environmental change in the asbestos setting. ……19
2.4 The state's involvement on the asbestos problem. ……21
2.5Environmental law perspectives in the asbestos situation..... 23
2.5.1 International environmental law…… 23
2.5.2 The South African legal perspective..... 25
2.5.3 Recommendations..... 31
2.6 Summary..... 33

Chapter 3: Literature Review 34
3.1 Introduction 34
3.2 Land Degradation: An Overview 34
3.3 Review of Mining Degradation and Rehabilitation using Remote Sensing 38
3.4 Review of Asbestos Dump Rehabilitation in Other Countries 57
3.5 Literature Survey of Imaging Spectroscopy and Field spectrometry applications, together with Laboratory Techniques 61
3.6 Summary 83

Chapter 4: Methodology 84
4.1 Introduction 84
4.2 Research design, data requirements and sampling procedure 84
4.3 Field data collection 86
4.4 Satellite imagery acquisition 87
4.5 Image processing (Landsat TM) 87
4.6 Reflectance Spectra Processing 92
4.7 Collection and processing of LAI/ fPAR data 93
4.8 Laboratory Methods 95
4.9 Summary 99

Chapter 5: Results and Discussion 101
5.1 Introduction 101
5.2 Satellite Derived Monitoring of the of Mine Rehabilitation on Vegetation Growth and Ecosystem recovery 101
5.2.1 Introduction 101
5.2.2 Background to the Control Site (Potlake Nature Reserve) 102
5.2.3 Results and Discussion (Experimental Sites) 105
5.2.4 Post-Rehabilitation Change Detection 111
5.2.5 Overview of the Findings 115
5.2.6 Summary 116
5.3. Fraction of Photosynthetically Active Radiation (fPAR) and Leaf Area Index (LAI) 118
5.3.1 Introduction 118
5.3.2 Results and Discussion 118
5.3.3 Summary 121
5.4. Spectral Separability of Euphorbia terucalli from other Natural Vegetation 122
5.4.1 Introduction 122
5.4.2 Results and Discussion 122
5.4.3 Summary 127

5.5. Analysis of Reflectance Spectroscopy of Asbestos Minerals..... ……128
5.5.1 Introduction ..... ……128
5.5.2 Results and Discussion..... ……..... 128
5.5.3 Overview of Findings..... ……..... 135
5.5.4 Summary ..... ……..... 135
5.6. Spectral Analysis of Soil and Water Samples..... ……..137
5.6.1 Introduction ..... ……..... 137
5.6.2 Results and Discussion..... ……..... 137
5.6.3 Summary ..... ……..... 146
5.7. Laboratory based identification and characterization of asbestos minerals in soil and water samples from Mafefe and Mathabatha, Limpopo Province..... ……..... 147
5.7.1 Introduction ..... ……..... 147
5.7.2 Results and Discussion..... ……..... 148
5.7.3 Summary ..... ……..... 184
5.8. Synthesis of the Study and Overview of the Findings..... ……..... 187
5.8.1 The use of remote sensing to Monitor Environmental Change associated with mining..... 187
5.8.2 Spectral Separability of Vegetation using field spectrometry... 189
5.8.3 Comparison of Reflectance Spectroscopy and Laboratory techniques in Monitoring Asbestos Pollution ..... ……..... 190
5.9 Overall Summary..... ……..... 194

Chapter 6: Conclusions and Recommendations 195
6.1 Conclusions..... ……..... 195
6.2 Recommendations..... ……..... 198

References..... 201
APPENDIX I: Minimum and Maximum Temperatures of the Study Area..... 213
APPENDIX II: Population……..... 214
APPENDIX III: Acquired Landsat TM images and Field Survey Sites……..... 216
APPENDIX IV: XRF AND ICP-MS Analyses……..... 218
APPENDIX V: PAR/LAI Values and Parameters……..... 224

Lists of Figures and Tables

Figures

Figure 2.1. Locality map of the study area showing the sample sites 10

Figure 2.2. Landsat TM bands 542 showing rugged topography overlaid with Bewaarkloof sample sites. 11

Figure 2.3. Simplified Geology of the study area overlaid with sample sites 12

Figure 2.4. Broad Soil pattern of the study area 13

Figure 2.5. Annual long term rainfall average 14

Figure 2.6. Hydrological pattern of the Mafefe and Mathabatha areas 15

Figure 2.7. Vegetation growth pattern in Mafefe 16

Figure 2.8. Landsat ETM derived land cover map 18

Figure 3.1. Typical spectral reflectance profile of vegetation 67

Figure 3.2. Spectra of vegetation at different phenological stages 68

Figure 3.3. High spectral resolution reflectance spectra of the first overtone of OH in talc, tremolite, actinolite, crysotile, lizardite, and antigorite 73

Figure 4.1. Landsat TM image showing locality of the control and experimental sites in the study area 87

Figure 4.2. An ERDAS GCP Tool showing GCPs of a second georectification process of an image subset 91

Figure 5.1. Landsat TM NDVI showing control and experimental sites 102

Figure 5.2. Landsat TM NDVI values of the early growing season showing vegetation condition of Potlake Nature Reserve 104

Figure 5.3. Landsat TM NDVI values of the end of growing season showing vegetation condition of Potlake Nature Reserve 105

Figure 5.4. Landsat TM NDVI values of the early growing season showing vegetation condition of Mafefe sites 106

Figure 5.5. Photo of site W58 in Cork, Mafefe 107

Figure 5.6. Landsat TM NDVI values of the end of growing season showing vegetation condition of Mafefe sites 107
Figure 5.7. A photo of site W69 in Mashilwane 108
Figure 5.8. Landsat TM NDVI values of the early growing season showing vegetation condition of Mathabatha sites 109
Figure 5.9. Landsat TM NDVI values of the end of growing season showing vegetation condition of Mathabatha sites 109
Figure 5.10. A photo of site W72 in Bewaarkloof 110
Figure 5.11. Landsat TM derived NDVI for 1989 (above) and 2000 (below) for the study area 112
Figure 5.12. Landsat TM NDVI derived analysis of post rehabilitation vegetation change for Mafefe sites (early part of the growing season) 113
Figure 5.13. Landsat TM NDVI derived analysis of post rehabilitation vegetation change for Mafefe sites (end of the growing season) 113
Figure 5.14. Landsat TM NDVI derived analysis of post rehabilitation vegetation change for Mathabatha sites (early part of the growing season) 114
Figure 5.15. Landsat TM NDVI derived analysis of post rehabilitation vegetation change for Mathabatha sites (end of the growing season) 115
Figure 5.16. *f*PAR/LAI values measured on 09 June 2006 at Mashilwane 119
Figure 5.17. *f*PAR/LAI values measured on 08 June 2006 at Bewaarkloof 120
Figure 5.18. *f*PAR/LAI values measured on 07 June 2006 at Cork (W58) 120
Figure 5.19. Spectral profile of *Euphorbica terucalli* canopy recorded at site W59 123
Figure 5.20. Spectral profile of *Euphorbica terucalli* canopy recorded at site W69 123
Figure 5.21. Spectral profile of Acacia canopy recorded at site W59 124
Figure 5.22. Spectral profile of Acacia canopy recorded at site W69 124
Figure 5.23. Spectral profile of *Ziziphus mucronata* canopy recorded at site W58 125
Figure 5.24. Spectral profile of grass cover recorded at site W58 125
Figure 5.25. Spectral profile of grass cover recorded at site W71 126
Figure 5.26. Spectral profile of mixed vegetation cover recorded at site W69 126

Figure 5.27. Spectral profile of Crocidolite (QJE314) obtained from Cubbic, Kuruman, North West Province 129

Figure 5.28. Spectral profile of Crocidolite (QJE317) obtained from Pietersburg Asbestos Company, Limpopo Province 130

Figure 5.29. Spectral profile of Crocidolite (QJE248) obtained from Kliprivier, Postmasburg, Northern Cape 130

Figure 5.30. Spectral profile of Amosite (QJE300) obtained from Penge, Limpopo Province 131

Figure 5.31. Spectral profile of Anthophylite (QJF007) obtained from the Soutpansberg, Limpopo Province 131

Figure 5.32. Spectral profile of Chrysotile (QNK176) obtained from Barberton, Mpumalanga 132

Figure 5.33. Spectral profile of Tremolite (QJE139) obtained from Prieska, Northern Cape 132

Figure 5.34. Spectral profile of Tremolite (QJE306) obtained from Kaapmniden, Mpumalanga 133

Figure 5.35. Spectral separability of crocidolite, amosite and chrysotile 134

Figure 5.36. Spectral differencing of amosite from crocidolite. 134

Figure 5.37. Spectral profile of cleaner drinking water 138

Figure 5.38. Spectral profile of sample 1 collected from flowing water at Cork River ... 139

Figure 5.39. Spectral profile of sample 2 collected from flowing water at Cork River ... 139

Figure 5.40. Spectral profile of sample 3 collected from dirty water at Cork River 140

Figure 5.41. Spectral profile of sample 4 collected from dirty water at Cork River 140

Figure 5.42. Spectral profile of sample 7 collected from dirty water at Mohlapitse (Mashilwane) River 141

Figure 5.43. Spectral profile of sample 8 collected from dirty water at Mohlapitse (Mashilwane) River 141

Figure 5.44. Spectral profile of sample 9 collected from flowing water at Mohlapitse (Mashilwane) River 142

Figure 5.45. Spectral profile of sample 10 collected from flowing water at Mohlapitse (Mashilwane) River 142
Figure 5.46. Spectral profile of sample 11 collected from river bed at Mohlapitse (Mashilwane) River 143
Figure 5.47. Spectral profile of sample 12 collected from river bed at Mohlapitse (Mashilwane) River 144
Figure 5.48. Spectral profile of sample 13 collected from river bed at Mohlapitse (Mashilwane) River 144
Figure 5.49. Spectral profile of sample 14 collected from river bed at Cork River 145
Figure 5.50. Spectral profile of sample 15 collected from river bed at Cork River 145
Figure 5.51. Spectral profile of sample 5 collected from river bed at Cork River 146
Figure 5.52. BSE images of asbestos minerals identified in sample BW2 152
Figure 5.53. BSE images of asbestos minerals identified in sample BW2 154
Figure 5.54. BSE images of asbestos minerals identified in sample CS1 155
Figure 5.55. BSE images of asbestos minerals identified in sample CS2 157
Figure 5.56. BSE images of representative specimens of asbestos minerals from sample MS1 158
Figure 5.57. BSE images of representative specimens of asbestos minerals from sample MS2 159
Figure5.58. BSE images of representative specimens of asbestos minerals from sample MS3 161
Figure 5.59. BSE images of representative specimens of asbestos minerals from sample Mt1 162
Figure 5.60. BSE images of representative specimens of asbestos minerals from sample Mt2 164
Figure 5.61. BSE images of representative asbestos minerals from sample SS cork 165
Figure 5.62. BSE images of representative asbestos minerals from sample WP58 cork1 166
Figure 5.63. BSE images of representative asbestos minerals from sample WP58 cork2 168

Figure 5.64. BSE images of representative asbestos minerals from sample WP66 169
Figure 5.65. BSE images of representative asbestos minerals from sample WP71 171
Figure 5.66. BSE images of representative asbestos minerals from sample WP72 172
Figure 5.67. BSE images of representative asbestos minerals from sample WP74 174
Figure 5.68. BSE images of representative asbestos minerals from water residue W1 ... 175
Figure 5.69. BSE images of representative asbestos minerals from water residue W2 ... 177
Figure 5.70. BSE images of representative asbestos minerals from water residue W3 ... 178
Figure 5.71. BSE images of representative asbestos minerals from water residue W4 ... 179
Figure 5.72. BSE images of representative asbestos minerals from water residue W7 ... 180
Figure 5.73. BSE images of representative asbestos minerals from water residue W8 ... 181
Figure 5.74. BSE images of representative asbestos minerals from water residue W9 ... 183
Figure 5.75. BSE images of representative asbestos minerals from water residue W10 183
Figure 5.76. Site rehabilitated using gravel and soil with loose asbestos fibres on a steep mountain slope (Site W58) 189
Figure 5.77. BSE image of sample W58 showing a fragment of stubby riebeckite with incipient fractionation along cleavage planes and massive grunerite (Riebeckite fragment size: 21.18 x 15.32 μm) 191
Figure 5.78. Spectral profiles of soil collected at Cork (W58) compared to the one of crocidolite 192
Figure 5.79. Spectral profiles of wet riverbed soil (CWS) and flowing water (CFL) collected at Cork (W58) compared to the one of crocidolite 193

Tables

Table 2.1. Current employment rate in Mafefe and Mathabatha 21

Table 3.1. Different types of field spectrometers 65

Table 4.1. Solid residue recovery and analytical test for the water sample 97

Table 5.1. Common asbestos minerals 148

Table 5.2. Bulk mineral compositions as determined by X-Ray Diffraction, expressed as semi quantitative estimates (wt%) 150

Table 5.3. EDS analyses of selected asbestos minerals from sample BW1 153

Table 5.4. EDS analyses of selected asbestos minerals from sample BW2 153

Table 5.5. EDS analyses of selected asbestos minerals from sample CS1 156

Table 5.6. EDS analyses of selected asbestos minerals from sample CS2 156

Table 5.7. EDS analyses of selected asbestos minerals from sample MS1 160

Table 5.8. EDS analyses of selected asbestos minerals from sample MS2 160

Table 5.9. EDS analyses of selected asbestos minerals from sample MS3 160

Table 5.10. EDS analyses of selected asbestos minerals from sample Mt1 163

Table 5.11. EDS analyses of selected asbestos minerals from sample Mt2 163

Table 5.12. EDS analyses of selected asbestos minerals from sample SS cork 167

Table 5.13. EDS analyses of selected asbestos minerals from sample WP58 cork1 167

Table 5.14. EDS analyses of selected asbestos minerals from sampleWP58 cork2 167

Table 5.15. EDS analyses of selected asbestos minerals from sample WP66 170

Table 5.16. EDS analyses of selected asbestos minerals from sample WP71 170

Table 5.17. EDS analyses of selected asbestos minerals from sample WP72 173

Table 5.18. EDS analyses of selected asbestos minerals from sample WP74 173

Table 5.19. EDS analyses of selected asbestos minerals from water residue sample W1 176

Table 5.20. EDS analyses of selected asbestos minerals from water residue sample W2 176

Table 5.21. EDS analyses of selected asbestos minerals from water residue sample W3 176
Table 5.22. EDS analyses of selected asbestos minerals from water residue sample W4 176
Table 5.23. EDS analyses of selected asbestos minerals from water residue sample W7 182
Table 5.24. EDS analyses of selected asbestos minerals from water residue sample W8 182
Table 5.25. EDS analyses of selected asbestos minerals from water residue sample W9 182
Table 5.26. EDS analyses of selected asbestos minerals from water residue sample W10 182
Table 5.27. Summary of results 186

Abbreviations and Acronyms

AMPLATS	Anglo American Platinum mine
ASD	Analytical Spectral Devices
Å	angstrom
BV	Brightness Values
BSE	Backscattered Electron Images
DSB	Dispute Settlement Body
DN	Digital Numbers
CSIR SAC	Council for Scientific and Industrial Research Satellite Applications Centre
EDS	Energy Dispersive Microanalysis System
ENVI	Environment for Visualizing Images
EPA	Environmental Protection Agency
EROS A 1	Earth Resources Observation System A 1
ERTS	Earth Resources Technology Satellite
ESU	Elementary Sampling Unit
ETM	Enhanced Thematic Mapper
*f*PAR	Fraction of Photosynthetically Active Radiation
FWHM	Full Width Half Maximum
GCP	Ground Control Point
GER	Geophysical and Environmental Research Corporation
GIS	Geographic Information System
GPS	Global Positioning System
IC	Ion Chromtography
ICP-MS	Inductively Coupled Plasma-Mass Spectrometry
IUCN	International Union for Conservation of Nature and Natural Resources
KeV	Kilo Electron Volts
LAI	Leaf Area Index
MANOVA	Multivariate Analysis of Variance
MDHS	Methods for the Determination of Hazardous Substances
MIR	Mid Infrared
MNF	Minimum Noise Fraction
MSAVI	Modified Soil Adjusted Vegetation Index
MSS	Multispectral Scanner
NDVI	Normalized Difference Vegetation Index
NEMA	National Environmental Management Act
NIOSH	National Institute for Occputional Safety and Health (USA)
NIR	Near Infrared
NIR/R	Near Infrared divided by Red
NPP	Net Primary Productivity
OH	Hydroxyl
OM	Organic Matter
PCA	Principal Component Analysis
PPI	Pixel Purity Index
PLM	Polarized Light Microscopy
PAR	Photosynthetically Active Radiation
REIP	Red Edge Inflection Point

RMS	Root Mean Square
RS	Reflectance Spectroscopy
RTM	Radiative Transfer Model
SAVI	Soil Adjusted Vegetation Index
SEM	Scanning Electron Microscopy
SMA	Spectral Mixture Analysis
SOC	Soil Organic Content
SNR	Signal to Noise Ratio
SPOT	*Systeme Probatoire poul d' Observatoire d' Terre*
SR	Simple Ratio
SVF	Single Variable File
SWIR	Shortwave Infrared
s	section
TEM	Transmission Electron Microscopy
TM	Thematic Mapper
TIR	Thermal Infrared
TRAC	Tracing Radiation and Architecture of Canopies
UDHR	Universal Declaration of Human Rights
USA	United States of America
USEPA	United States Environmental Protection Agency
USGS	United States Geological Survey
USSR	Union of the Soviet Socialist Republic
UTM	Universal Traverse Mercator
VI	Vegetation Indices
VNIR	Very Near Infrared
v	versus
WCMC	World Conservation Monitoring Centre
WGS	World Geodetic System
WTO	World Trade Organization
wt%	weighted percentage
XRD	X-Ray Diffraction
XRF	X-Ray Fluorescence spectrometry

Acknowledgements

I thank my supervisors Drs George T. Tengbeh and Yaw A. Twumasi for having guided and supported me in this research. Thanks also to the following: Klaas Nkoana for assistance during the initial field visit, Phila Sibandze and Shadrack Molokoane (Mathabatha Health and Asbestos Association) for assistance during the major field campaign and Dr Tengbeh for guidance during the fieldwork; Dr. Greg Swayze (USGS) for technical advice; Zacharia Thobejane and Mafefe Tribal Authority for supporting the project together with Phogole Thobejane for moral support. My sincere gratitude is also extended to, Maria Atanasova and Hilde Maritz, for their valued assistance in laboratory analysis and Leon Croukamp for funding the analysis both belonging to Council for Geosciences. I thank also my parents, David and Helen Petja for their continued support. I thank also the Council for Scientific and Industrial Research – Satellite Applications Centre (Elsa de Beer and Helmut Newman) for supplying me with Landsat satellite imagery. The Department of Science and Technology is gratefully acknowledged for funding, especially Pontsho Maruping (General Manager: Space Science and Technology). I also thank G. Mothibi Ramusi, former head of CSIR SAC for facilitating access to funding and Mzukisi Mazula, SumbadilaSat Project Manager, based at University of Stellenbosch for allocating the necessary funds. I express my sincere gratitude to Prof Tim Simalenga, Head of the Agricultural Research Council – Institute for Soil, Climate and Water, for funding in part this project and giving me enough time to study

despite my work responsibilities. I also thank Dr. T. Saidi for encouraging me to continue with asbestos research. Finally, I thank the St Engenas Zion Christian Church for the motivation and support given to me throughout my studies. Thanks for making education the top most priority in the church, your support has been incomparable.

Citation

Brilliant Mareme Petja was born on the 4th of October 1977 at Ga Mothiba a Ngwanamago in the Limpopo Province of South Africa. He attended his primary education at Ngwanamago Primary School (1983-89). He further obtained his secondary at Mphachue Secondary School (1990-94) at Mogodi ga Mphahlele.

He received a Bachelor of Environmental Sciences in Ecology and Resource Management, and Geography (1999), Bachelor of Environmental Sciences Honours in Ecology and Resource Management (2001), both from the University of Venda, South Africa. He also obtained a Master of Science in Geosciences (with specialization in Remote Sensing) from University of the Witwatersrand (2004). He received certificates in remote sensing and environmental science from various institutions. These include:

(i) SADC Hyperteach Training in Imaging Spectroscopy Certificate, The Flemish Institute of Technology at University of Stellenbosch (2007),

(ii) Certificate in Fundamentals of Erdas Imagine II/Advanced Remote Sensing from Geographic Information Management Systems PTY LTD (2007),

(iii) Certificate in Processing of Radar Data, International Society for Photogrammetry and Remote Sensing at Costa Rica (2007),

(iv) Certificate of participation in MODIS/AIRS Remote Sensing Workshop, Universities of Johannesburg and Winsconsin-Madison (2006),

(v) Certificate in Fundamentals of Erdas Imagine I, Geographic Information Management Systems PTY LTD (2006),

(vi) Certificate in Usage and Interpretation of Meteosat Second Generation Satellites, EUMETSAT (2005),

(vii) Certificate in Advanced Remote Sensing for Quantitative Analysis from

Agricultural Research Council – Institute for Soil, Climate and Water (2005),

(viii) Certificate in Air Quality Management and Pollution Control from University of the Witwatersrand (2001).

He also participated at SAFARI 2000 Remote Sensing Data Workshops at Zambia and University of Virginia in 2001 and 2002, respectively. He attended a Scientific Writing Workshop at Wits Rural Facility in 2002.

He has worked as a Remote Sensing Researcher at Agricultural Research Council – Institute for Soil, Climate and Water, Pretoria since April 2001 where he is currently a Project Manager and Remote Sensing Research Scientist.

He served the World Meteorological Organization (WMO) in 2006 as a WMO Regional Expert on Management of Natural and Environmental Resources for Sustainable Agricultural Development (Africa Region) to which he was also a member of the WMO Commission for Agricultural Meteorology. He also serves as an Expert Advisor for agricultural risk and disaster management to the National Agrometeorological Committee (Department of Agriculture, South Africa). He is an Expert Advisor in satellite derived monitoring of land degradation to the South African focal point of the United Nations Convention for Combating Desertification. He is a participant of the United Nations Office for Outer Space Affairs Expert Team focusing on applying space technology for disaster management and sustainable development. He is a professional member of the Institute for Electronics and Electrical Engineers (USA) and a Manuscript Reviewer for International Journal of Environmental Research and Public Health and Sensors Journal (Both published in Switzerland). He has addressed the International Geoscience and Remote Sensing Symposium (IGARSS) as an Invited Speaker in Alaska (2004) and Barcelona (2007). He currently serves the Technical

Program Committee for IGARSS 2008 to be held in Boston and the Organizing Committee of IGARSS 2009 to be held in Cape Town.

Among his achievements, he received the 1999 Mail and Guardian/ World Wide Fund for Nature Green Trust Award (Community Projects) for the research he conducted on the impacts of asbestos on rural communities. He has also received the Vice Chancellor's Merit Award in 1999 at University of Venda. He is also the recipient of the 2006 IEEE Travel Award for Academic visit to USA. He is the grantee of The International Society for Photogrammetry and Remote Sensing (ISPRS) Honor Roll of 2007, for which he was given the travel award to San Jose, Costa Rica. His biography has been published in Who's Who in Science and Engineering 2006/2007, Who's Who in Science and Engineering 2008/2009, Who's Who in the World 2008 published by Marquis in USA. He is a part-time academic at University of Limpopo focusing on Environmental Management and Impact Analysis.

Author's Bibliography

Petja, B.M., Tengbeh, G.T. and Twumasi, Y.A. (2008) Using Remote Sensing and Geographic Information System (GIS) to Monitor Environmental Change in the Post Asbestos Mining Environment, South Africa, *World Resources Review*, (Submitted 12 June 2007, Under Peer Review).

Petja, B.M., Twumasi, Y.A. and Tengbeh, G.T. (2008) Assessment of Asbestos Pollution using *in situ* remote sensing together with X-Ray Diffraction and Scanning Electron Microscopy. *Sensors Journal* (Submitted 31 August 2007, Under Peer Review).

Petja, B.M., Tengbeh, G.T. and Twumasi, Y.A. (2008) Using Earth Observation for Challenges Facing Monitoring Environmental Remediation of Derelict Mines in South Africa. *African Skies / Cieux Africains*, Volume 12, pp 71-76.

Petja, B.M. (2008) Review of Case Studies of Successful Measures to Protect Land, Manage Land Use and Mitigate Land Degradation. In Stefanski, R. and P. Pasteris (Eds) (2008) *Management of Natural and Environmental Resources for Sustainable Agriculture. Proceedings of the USDA/WMO Workshop on Management of Natural and Environmental Resources for Sustainable Agricultural Development*, 13-16 February 2006, Portland, Oregon, USA. Washington, D.C., USA: United States Department of Agriculture; Geneva,

Switzerland: World Meteorological Organization; Technical Bulletin WAOB-2008, NRCS-2008, and AGM-10, WMO/TD No.1428. pp147-157.

Dissertations/ Academic Research Reports

Petja, B.M. (2004) *Remote Sensing Approach for Sustainable Natural Resource Management in Umkhanyakude Development Node.* M Sc Dissertation, University of the Witwatersrand, Johannesburg.

Petja, B.M. (2001) *An Evaluation of the Rehabilitation Process in the Post Asbestos Mining Environment of Mafefe and Mathabatha, Northern Province.* Honours Dissertation, University of Venda, Thohoyandou.

Petja, B.M. (1998) *The Effects of Asbestos Mining in Rural Communities: A case of Mafefe and Mathabatha, Northern Province.* Department of Ecology and Resource Management, University of Venda, Thohoyandou.

Conference Papers/ Proceedings

Petja, B.M., Tengbeh, G.T. and Twumasi, Y.A. (2007) Using Earth Observation for Challenges Facing Monitoring Environmental Remediation of Derelict Mines in South Africa. Paper Presented at the Second African Leadership Conference on Space Science and Technology for Sustainable Development, 02-05 October 2007, Pretoria, South Africa.

Petja, B.M., Twumasi, Y.A. and Tengbeh, G.T. (2007) Comparative Analysis of Reflectance Spectroscopy and Laboratory Based Assessment of Asbestos Pollution in the Rehabilitated Mining Environment, South Africa. Proceedings of the 27th International Geoscience and Remote Sensing Symposium (Invited Paper), 23-27 July 2007, Barcelona, Spain.

Petja, B.M., Twumasi, Y.A., Tengbeh, G.T. and Croukamp, L. (2007) Reflectance Spectroscopy and Laboratory Based Analysis of Different Asbestos Minerals in South Africa for Potential Use in Pollution Monitoring. *Proceedings of the 32nd International Symposium for Remote Sensing of Environment*, 25-29 June 2007, San Jose, Costa Rica.

Petja, B.M., Tengbeh, G.T. and Twumasi, Y.A. (2006) Satellite Derived Monitoring of Derelict Asbestos Mine Rehabilitation in Mafefe and Mathabatha, Limpopo Province. *Proceedings of Limpopo Environmental Research Conference*, 28-30 November 2006, Polokoane, South Africa (In Press).

Petja, B.M., Twumasi, Y.A.,Tengbeh, G.T., Sibandze, P.C. and Croukamp, L. (2006) Spectral Differentiation of Asbestos Minerals in South Africa for Potential Use in Pollution Monitoring. *Proceedings of the First Annual International Conference and Exhibition on Geospatial Information Science, Technology and Applications*. 20 – 22 November 2006, Sandton Convention Centre, Johannesburg, South Africa.

Petja, B.M., Twumasi, Y.A. and Tengbeh, G.T.(2006) The use of Remote Sensing to Detect Asbestos Mining Degradation in Mafefe and Mathabatha, South Africa. *Proceedings of International Geoscience and Remote Sensing Symposium,* 31 July-04 August 2006, Denver, Colorado (USA).

Petja, B.M. (1999) An Evaluation of the Asbestos Rehabilitation Programme in the Post Mining Environment of Mafefe and Mathabatha, Northern Province. Annual National Students Geographical Conference, Fort Hare University, Alice.

CHAPTER ONE

INTRODUCTION

1.1 Background

This chapter provides an introduction and background of this research project. It starts by providing an introductory historical background to asbestos mining in South Africa. This is then followed by an overview of the problem of traditional field based monitoring versus the use of satellite remote sensing techniques in natural resource monitoring, with reference to the monitoring of the asbestos mine rehabilitation in the Mafefe and Mathabatha areas. Thereafter, the research problem statement is presented followed by the aim and objectives of the study.

1.2 Asbestos Mining in South Africa

The first recorded large-scale asbestos mining in South Africa started in the 1890s in the Prieska area of the Northern Cape. The mines were owned and operated by a British company by the name of the Cape Asbestos Company (now Cape plc.). By the 1920s the company extended its operations into the Northern Province at Penge, and later into the Mafefe and Mathabatha areas. As early as 1930, the dangers posed by asbestos emerged, and in 1931 the first restrictions regarding the use of asbestos were introduced in Britain. Although the dangers of asbestos became well documented in the 1950s, environmental legislation remained extremely lax and the Cape Plc. continued to mine in the Prieska, Penge and Mafefe and Mathabatha areas until the company withdrew its investments from South Africa in 1979 (Turkington, 2000).

The major environmental health problems associated with asbestos mining and processing are diseases caused by exposure to fine asbestos fibres. The diseases can also be contracted as a result of coming into contact with asbestos mine tailing dams during and even after the closure of the mines. A survey of asbestos-related diseases in the Northern Cape showed that more than half of the former mine workers suffers from lung diseases caused by asbestos, with about one individual out of twelve affected in the general population in the Prieska area (SAEP, 2000). In recognition of the extent of the problem, the South African Parliamentary Committee on Environmental Affairs and Tourism convened a National Asbestos Summit in 1998, with a view to seeking compensation for the cost of the long term health care for asbestos victims. The asbestos victims have since filed a lawsuit in the United Kingdom seeking for compensation for asbestos-related diseases (SAEP, 2000).

Although asbestos mines have been decommissioned, people who continue to live in the post-mining environments that have been either partially or not rehabilitated, or that have un-rehabilitated asbestos waste dumps, continue to contract asbestos-related diseases. This is because the exposed deadly fibres continue to be spread in the environment by wind and overland flow. The mining and processing of asbestos in the Mafefe and Mathabatha areas has been undertaken since the early 1920s. These activities necessarily lead to the release into the atmosphere of fine particles of asbestos that could then be inhaled not only by the mine workers but also by all those living in the mining vicinity. As asbestos has chronic effects on human beings, its effects took about 20 to 30 years to start being noticed. Over this time, the level of fine asbestos fibres released in the atmosphere increased to critical levels. Apart from the impact of the fine asbestos fibres

on the social health, the mining also had an increasingly negative impact on the environment. In addition to mined-out scars, asbestos wastes were dumped within the workers settlements of Mafefe and Mathabatha. These dumps have subsequently been eroded by wind and overland flows, with the eroded materials polluting the surrounding terrain and Mohlapitse river that flowed through these settlements. As a result of these consequences, the mines were decommissioned in 1979.

After the decommissioning of the mines, a strategy of managing the degraded mined environment was desired by the South African government. This led to the Department of Minerals and Energy contracting the Research Institute for Reclamation Ecology of the then University of Potchefstroom (now University of North West) to rehabilitate the asbestos mines and dumps. The government invested over fifty million Rands in this programme (British Asbestos Newsletter, 1999).

After the capital and technical infrastructure has been put in place, a problem of environmental concern arose. The government did not have any plan and capacity to monitor the rehabilitation process. This is despite the severity and the seriousness of the asbestos problem. To date there has not been any efficient monitoring procedure in place. This therefore prompted the current study. Other problems include physical limitations and access to the rehabilitation areas. Asbestos mining in this area was undertaken in a mountainous environment - a very difficult terrain with very steep and rugged topography, and also now home to wild life that could be a danger to humans. Accessibility is therefore a very serious problem that would make it very difficult, if not

impossible, to efficiently undertake and sustain traditional field-based monitoring methods. Also, these field methods are labour intensive, time consuming, and can be dangerous to life and very costly. For instance, personal experience has shown that an average four-wheeled drive fieldwork vehicle could access only very few of the rehabilitated sites in the study areas and even these, only with great difficulty. Access to most of the sites require climbing very steep and rugged terrain, and walking with much difficulty, even with appropriate clothing, through thick and very thorny acacia vegetation.

Because of the above practical problems, in this study, a satellite-derived monitoring approach is being attempted with the hope that it provides an efficient, continuous or repeatable and long term approach for the monitoring of the rehabilitated asbestos mine sites in the study environment.

According to Håme et al. (1998), monitoring of natural resources involves both short term and long term monitoring. He further indicates that in the short term monitoring, changes can deviate from the normal vegetative succession and seasonal variation, which are of particular interest. This may include man made disturbances and damage. In the long term monitoring, trend detection and forecasting are of special interest (Håme *et al*., 1998). Apan (1997) indicates that one of the causes of rehabilitation failures are poor spatial planning and lack of monitoring of projects, due to weaknesses in land resource surveys and evaluation systems. Satellite-derived land cover information is important for spatial analysis of the rehabilitation. He experimented with it for forest rehabilitation planning, where the basic information required was the knowledge of the boundary

between vegetated and non vegetated areas, which is important for identifying potential rehabilitation areas (Apan, 1997).

Satellite remote sensing can therefore be a useful tool for the environmental monitoring of the reclamation and rehabilitation of open cast mining areas. Mining areas are characterized by a high temporal and spatial dynamics in their environment. Satellite images offer a repeat coverage of the environment which makes their use useful in relatively accurately observing changes over time and space. Mining companies have previously carried out analyses of environmental change caused by mining based on analogue and digital interpretation of multitemporal aerial photographs. However, the main technique used has been analogue interpretation of aerial photographs in order to distinguish open mining areas from the already reclaimed areas. Intensive monitoring of disturbed lands is necessary for the effective management and control of surface mine recovery. This can be properly accomplished by regular (annual) monitoring using remote sensing systems (Schmidt and Glaesser, 1998).

This research therefore adopts the use remote sensing techniques to monitor the process of asbestos rehabilitation in the Mafefe and Mathabatha areas. Laboratory techniques and field instrumentation are also used to validate satellite data, to ensure that future reliance on satellite data is sustainable. Remote sensing is provided as an alternative and cost effective approach for long term monitoring of mine rehabilitation as opposed to traditional field based approaches, which can only be complementary.

1.3 Statement of the problem

Mine rehabilitation has been undertaken in Mafefe and Mathabatha as a way of trying to repair the damage caused by asbestos mining to the environment. The environmental problems that resulted from asbestos mining are now being alleviated through mine rehabilitation. The rehabilitation of asbestos mines is intended to serve as a long-term strategy for mitigating the negative health effects. It involves covering the open cast asbestos mines and dumps that served as a source of asbestos dust. The main problem is that there has not been a reliable and sustainable procedure in place to monitor the process of asbestos mine rehabilitation. This is because it is not practical and sustainable to reliably and regularly (annually) use the traditional field-based survey methods to monitor the rehabilitation process in the study area. Rehabilitation as a strategy of environmental management needs to be properly planned and executed to prevent it from creating more environmental problems. There has been lack of good monitoring procedure for asbestos rehabilitation. An internal assessment provided by the company conducting the rehabilitation process is not good enough to monitor the process and it is only done during the implementation as a report. This research therefore aims at evaluating the progress and monitoring the effectiveness of asbestos rehabilitation in the post mining environment of Mafefe and Mathabatha using Landsat 5 Thematic Mapper (TM) satellite imagery, combined with ground truthing and laboratory analysis.

1.4 Purpose and Objectives

1.4.1 Purpose

The purpose of this study is to use remote sensing techniques to monitor the asbestos mine rehabilitation process at Mafefe and Mathabatha and to examine its effectiveness as short and long-term strategies of environmental management.

1.4.2 Objectives

The objectives of the study are:

i) To use satellite imagery to:

a) Monitor the progress of asbestos mine rehabilitation.

b) Detect vegetation change as a result of the rehabilitation process.

c) Assess the effectiveness of using revegetation or gravelling as a rehabilitation procedure.

d) Assess the effectiveness of vegetation establishment on rehabilitated asbestos mines in combating erosion.

ii) To undertake field surveys to verify and validate satellite observations.

iii) To investigate the spectral separability of vegetation used for rehabilitation from natural vegetation.

iv) To provide a replicable remote sensing technique for use in the continuous monitoring of asbestos mine rehabilitation.

v) To assess the level of different asbestos fibres in the soil and water bodies within the rehabilitated areas.

1.5 Research Hypotheses

i) Satellite imagery can provide a cost effective method of monitoring open cast mining and dump rehabilitation.

ii) Satellite images can be used to provide a quantifiable timeous monitoring of vegetation establishment on the rehabilitated asbestos mining sites.

iii) Modeling of medium spatial resolution imagery can assist in maximizing the use of such images in monitoring progress of rehabilitation on rehabilitated sites.

iv) Satellite derived assessment of asbestos rehabilitation can be more cost effective compared to intensive field-based surveys.

1.6 Summary

In this chapter, the background of this research project has been presented. It focused on how the asbestos mining processes in South Africa degraded the mined out lands, including the atmosphere, and also caused and continue to cause health problems to the mine workers and to all those who lived and continue to live in the mining environments. It then points out how these problems needed addressing through the rehabilitation of the mined-out areas. Since rehabilitation of such areas need efficient and reliable long term monitoring, and because of the very practical difficulties associated with the use of the conventional field monitoring methods in such a trying environment, a case is made for an attempt to use remote sensing in this study as an alternative environmental monitoring approach. The chapter ends with the aims and objectives of the study, followed by the hypotheses that will be tested.

CHAPTER TWO

THE ENVIRONMENT OF THE STUDY AREA

2.1 Introduction

The nature of the environment has a bearing on the influence of land use on environmental deterioration. The landscape of Mafefe and Mathabatha has those features which makes it prone to degradation when subjected to improperly planned land uses. The chapter describes the physical and the social environment of the study area. It further highlights the social and the biophysical factors that drove the process of environmental change. The role of environmental legislation in guiding land use and protecting the environment is also reviewed.

2.2 Ecological Setting

2.2.1 Location

Mafefe and Mathabatha areas are located in the Republic of South Africa at Lepelle – Nkumpi Municipality of the Limpopo Province. The area is situated at approximately 70km South-east of Polokoane, 36km east of Lebowakgomo and about 50km west of Burgersfort. Mafefe and Mathabatha areas are situated 35km west of Penge which was the main branch for asbestos mines in the Limpopo Province. They are located approximately 20km north of the Anglo American Platinum mine (AMPLATS) in Atok which was formerly known as the Lebowa Platinum Mine. Mathabatha is located 5km

north of the main road R37 which is the main way from Polokoane to Burgersfort. Mafefe lies about 15km north east of Mathabatha.

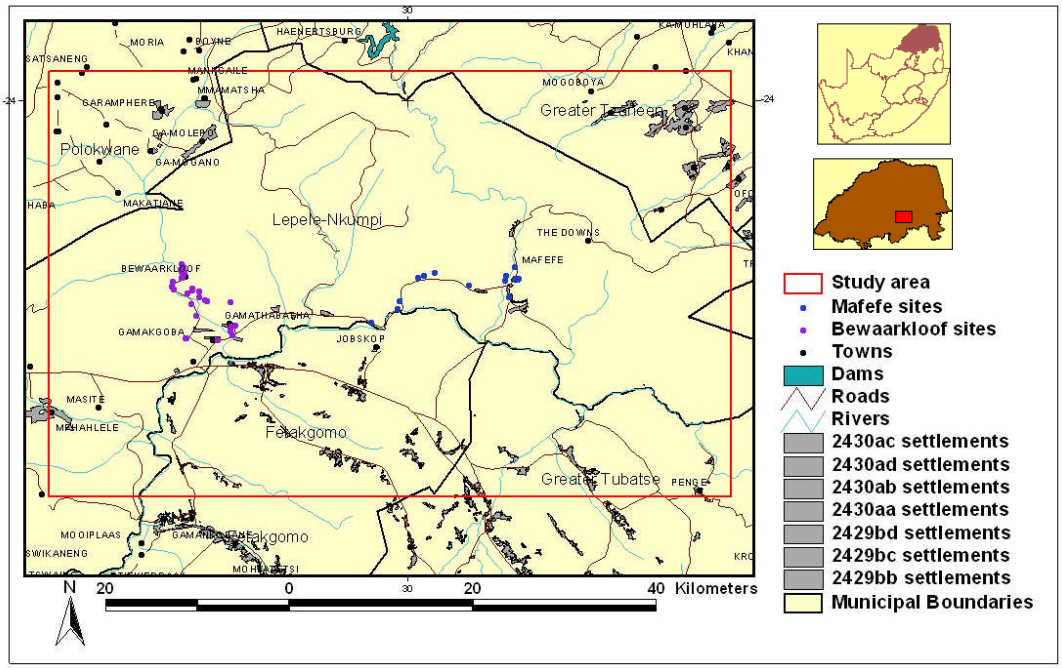

Figure 2.1. Locality map of the study area showing the sample sites.

2.2.2 Physiography

Asbestos mining in Limpopo Province was undertaken on mountainous environment, with a steep to relatively flat slope (Fig. 2.2). Both Mafefe and Mathabatha areas are situated between Wolkberg and Steelpoort Mountains which form part of Drakensberg Mountains. The landscape has been ravaged by folding, weathering and erosion. The area is situated a few kilometres away from the escarpment and it is also characterized by hilly topography. A majority of the slopes are north facing with the ups dominant. The steepy nature of the slope influences the rate of run off and erosion. This particularly makes rehabilitated areas more prone to forces of erosion.

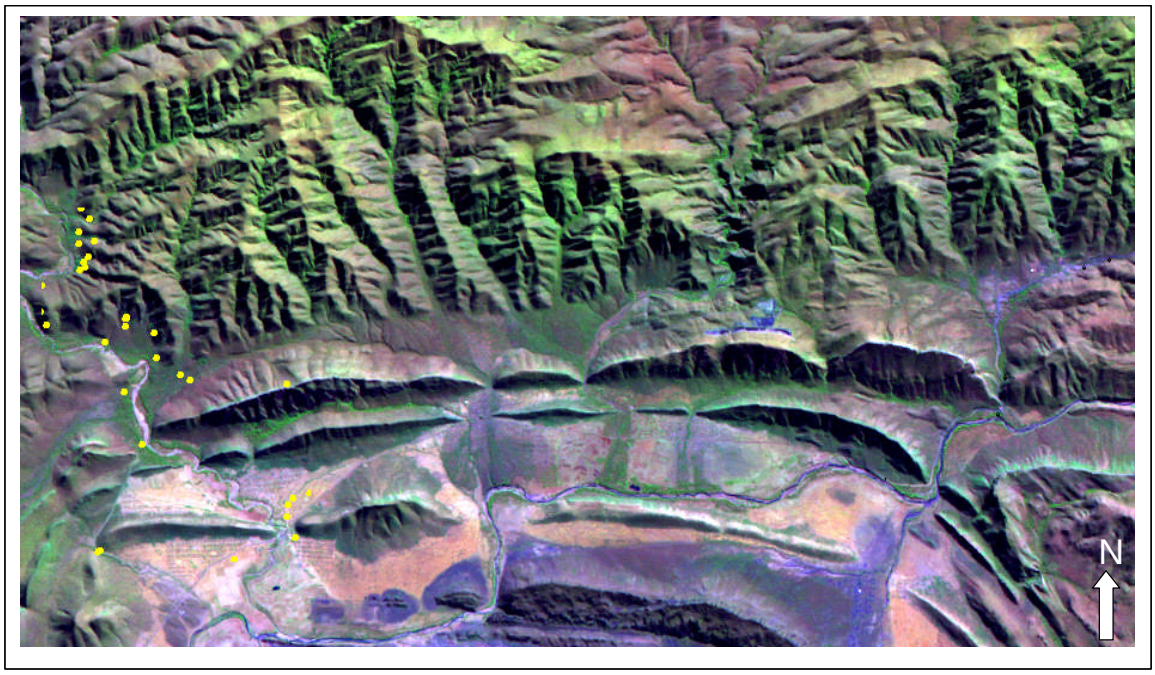

Figure 2.2. Landsat TM bands 542 showing rugged topography overlaid with Bewaarkloof sample sites.

2.2.3 Geology and Pedology

The crocidolite and amosite asbestos in Mafefe and Mathabatha constitute the Transvaal Crocidolite-Amosite field which occupies portions of Polokoane and Letaba districts and it stretches from Chueniespoort in the west to Steelpoort river in the east. The asbestos occurs in the Banded Ironstage of the Dolomite series. The ironstone is underlain by a great thickness of dolomite of the main dolomite stage and overlain by dolomite and shale of the upper dolomite stage (Figure 2.3).

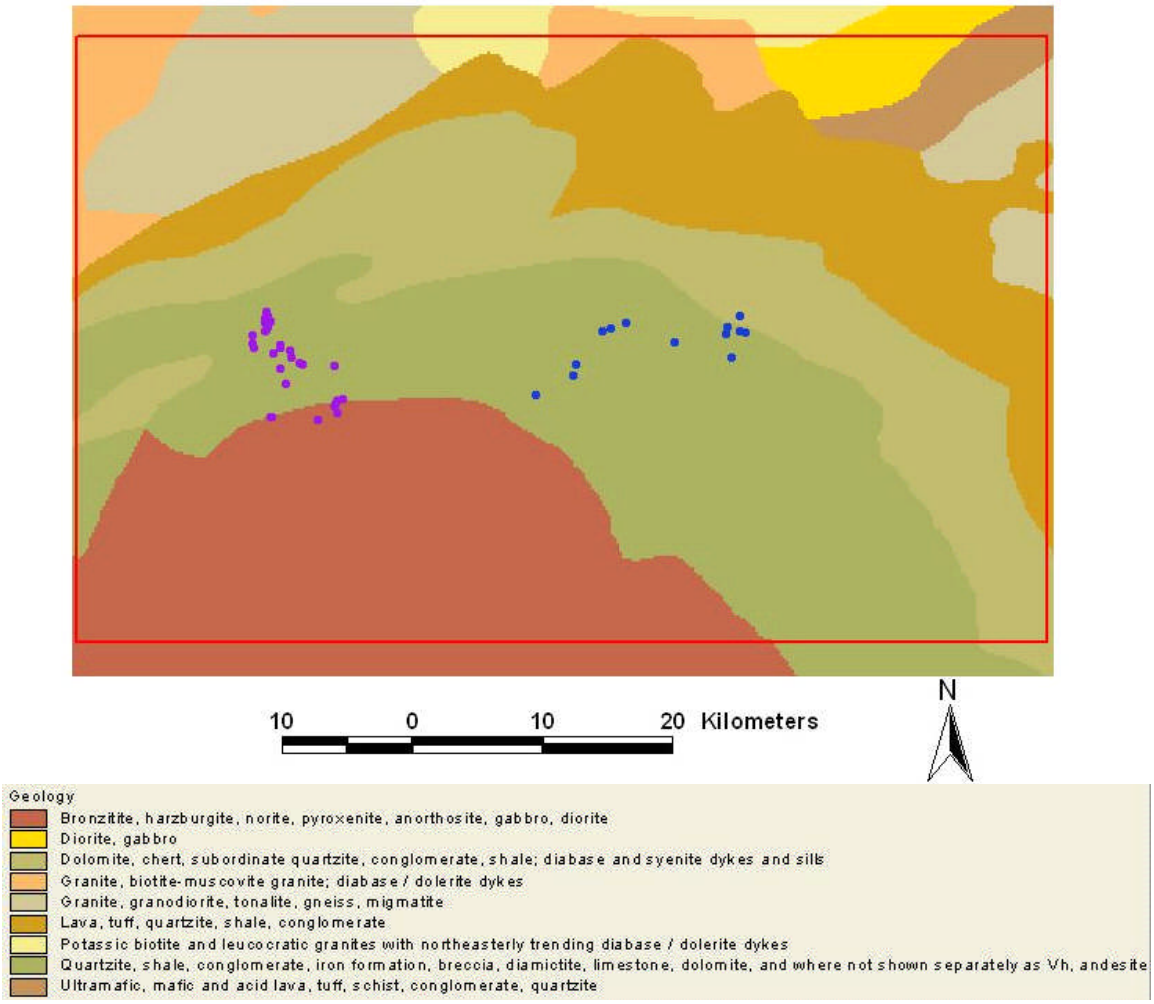

Figure 2.3. Simplified Geology of the study area overlaid with sample sites.

The banded ironstone reaches a maximum thickness of over 800m in the centre of the field around Mohlapitse River. The thickness decreases westwards rapidly due to postdepositional erosion so that the thickness at Penge is 160m and 30m at Kromelboog. The diabase sills of up to 70m thick have been intruded into the succession. The banded ironstone succession has been subjected to folding into numerous synclines and anticlines with a general east west strike. The asbestos occupies definite stratigraphic horizons in succession which are generally known as the lower zone, the main zone, the short fibre zone and upper zone. Each zone consists of a large number of individual asbestos fibre

seams or groups of fibre seams which comprise the main asbestos zone in the Malips river area (Coetzee et al., 1992).

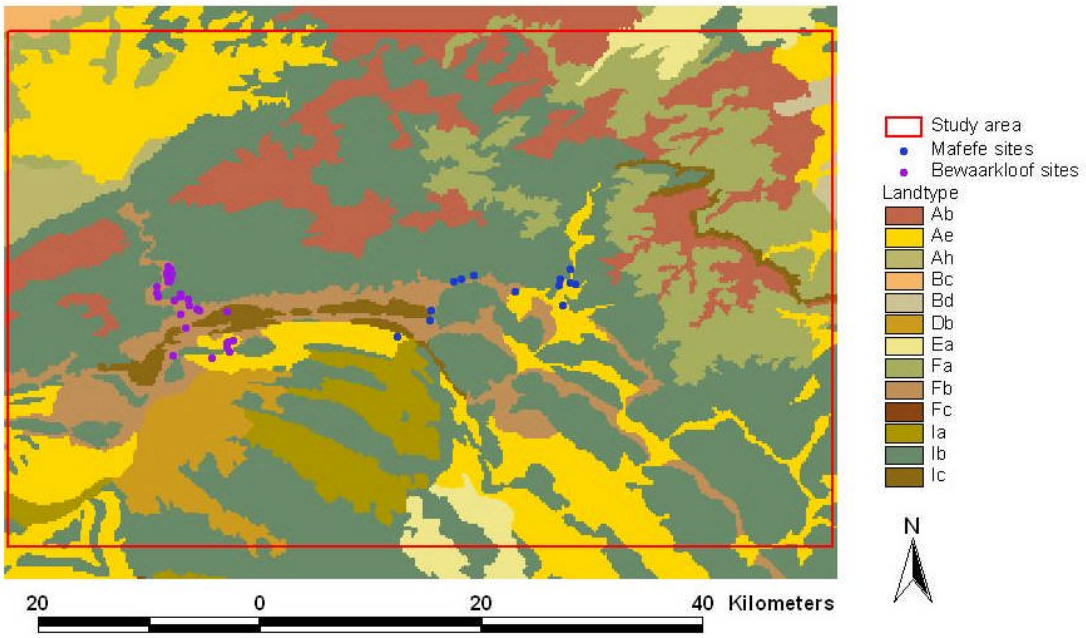

Figure 2.4. Broad Soil pattern of the study area.

The soil types that are dominant are loamy, clayey loam and sandy. The loamy soil favours the growth of *Ficus thonningii*. The broad soil patterns of Mafefe and Mathabatha as shown in Fig 2.4 are characterized by Ae (Freely drained Red yellow apedal: Red high base status of > 300mm deep), Fb (Glenrosa and/or Mispah forms with lime rare or absent in the upland soil but generally present in low lying soils), Ib (Rock areas with miscellaneous soils) and Ic (Rock with little or no soil).

2.2.4 Climate

The climate of the study area is categorised as temporal experiencing changes in seasons and associated with a wide range of temperature. The area is semi-arid with an annual

rainfall between 463 mm to 970 mm (Figure 2.5). A larger amount of rainfall is experienced in summer season extending from October to January. There is normally no rainfall in winter. The minimum temperature ranges from 8°C to 19°C particularly in winter, whereas the average maximum temperatures range from 20°C to 30°C (Appendix I).

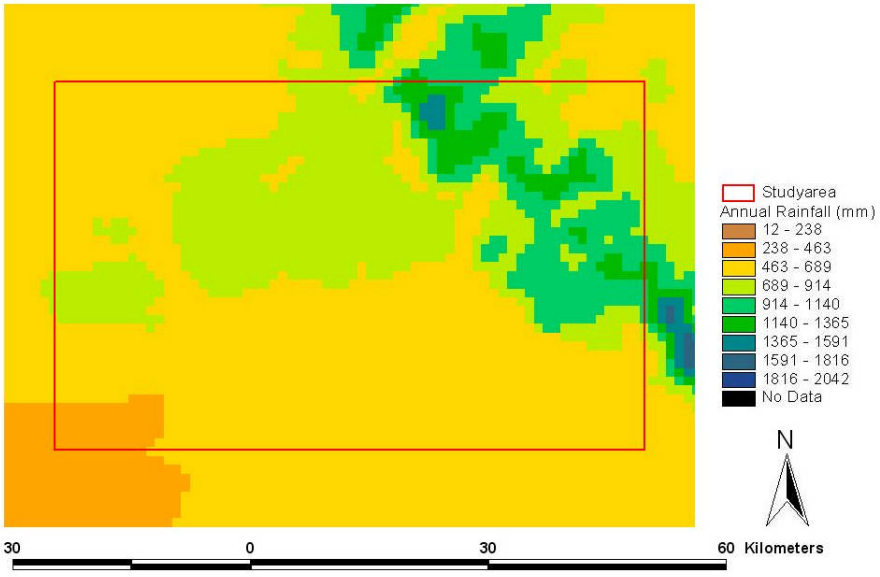

Figure 2.5. Mean annual rainfall.

2.2.5 Hydrology

Both Mafefe and Mathabatha have several streams which are perennial and non-perennial. The non-perennial streams include Tongwane River in Mathabatha and Dipintshane and "Cork " Rivers in Mafefe. Mohlapitse is a perennial river which drains into Lepelle (Olifants) river system. It is the main river passing through Lepelle–Nkumpi municipality to the Kruger National Park. The rivers are the main driving forces behind the agriculture, local brickworks and small scale building industries in the community.

Most of the rivers follow a trellis flow pattern. The diverse vegetation in most parts of the study area indicates a well drained pattern.

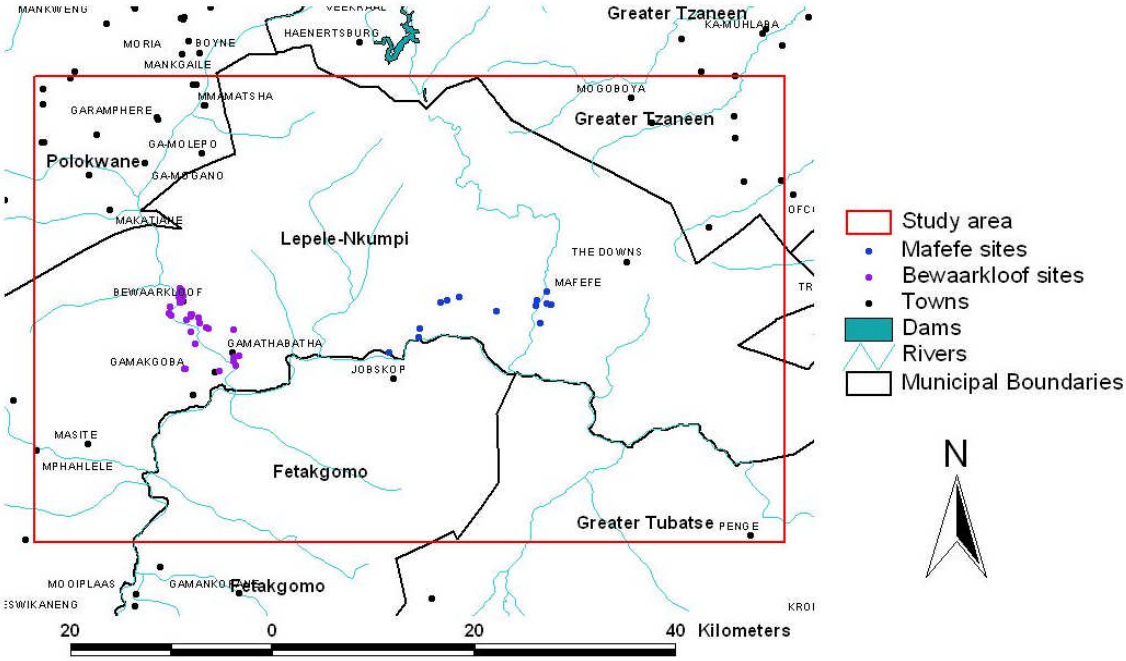

Figure 2.6. Hydrological pattern of the Mafefe and Mathabatha areas.

2.2.6 Biodiversity

The area falls under savanna biome with the vegetation type of a mixed bushveld. The dominant vegetation lifeform in the area include trees, shrubs and grasses (Figures 2.7 and 2.8). The dominant tree species belong to the Fabaceae, Rhamnaceae, Moraceae, Anacardiaceae and Combretaceae families. These species include *Peltophorum africanum, Acacia burkei, Acacia caffra, Rhus lancea, Ziziphus mucronata, Ficus thonningii, Combretum imberbe* and *Sclerocarrya birrea. subsp.caffra*.

Figure 2.7. Vegetation growth pattern in Mafefe.

Most *Acacia* trees are deciduous with rounded, flattened or open crown, dominant on both river valleys and mountain slopes. The *Peltophorum* species are semi-deciduous with a dense rounded to spreading crown. Other tree species are mostly semi deciduous to deciduous with a roundish crown. The dominant shrub species belongs to the families of Euphorbiaceae and Tiliaceae. These species include *Euphobia terucalli*, *Ricinus communis*, *Grewia flava* and *Cassine aethopica*.

Most shrubs are evergreen and deciduous with a rounded and open crown growing up to 4 metres tall. *Ricinus communis* is a characteristic of the disturbed areas. Both the trees and shrubs are utilised by cattle, baboons, vervet monkeys, squirrels, rodents and

pigeons. The dominant grass species belong to the Poaceae family which include mostly *Melinis repens*, *Cyanodon dactylon*, *Dactyloctenium aegyptium*, *Panicum maximum*, *Cenchrus ciliaris*, *Eragrostris guliflovia* and *Echinochloa colona*.

The animal species present in the area include the baboons, vervet monkeys, domestic cattle and bird species such as pigeons.

2.2.7 Land use

The area was previously used for asbestos mining. The broad land use and landcover derived from Landsat Enhanced Thematic Mapper (ETM) is shown in Figure 2.7. The dominant land use in Mafefe and Mathabatha are subsistence agriculture and livestock. The crops cultivated include maize, sugar cane, groundnuts and water melon. The crops are cultivated for both local consumption and selling. Most cultivated plots are situated near the river banks. The driving force behind this riparian cultivation is the need for water from the rivers which is used for irrigation. The area is also used for small scale brick manufacturing industries which are dependent on water and sand from the rivers.

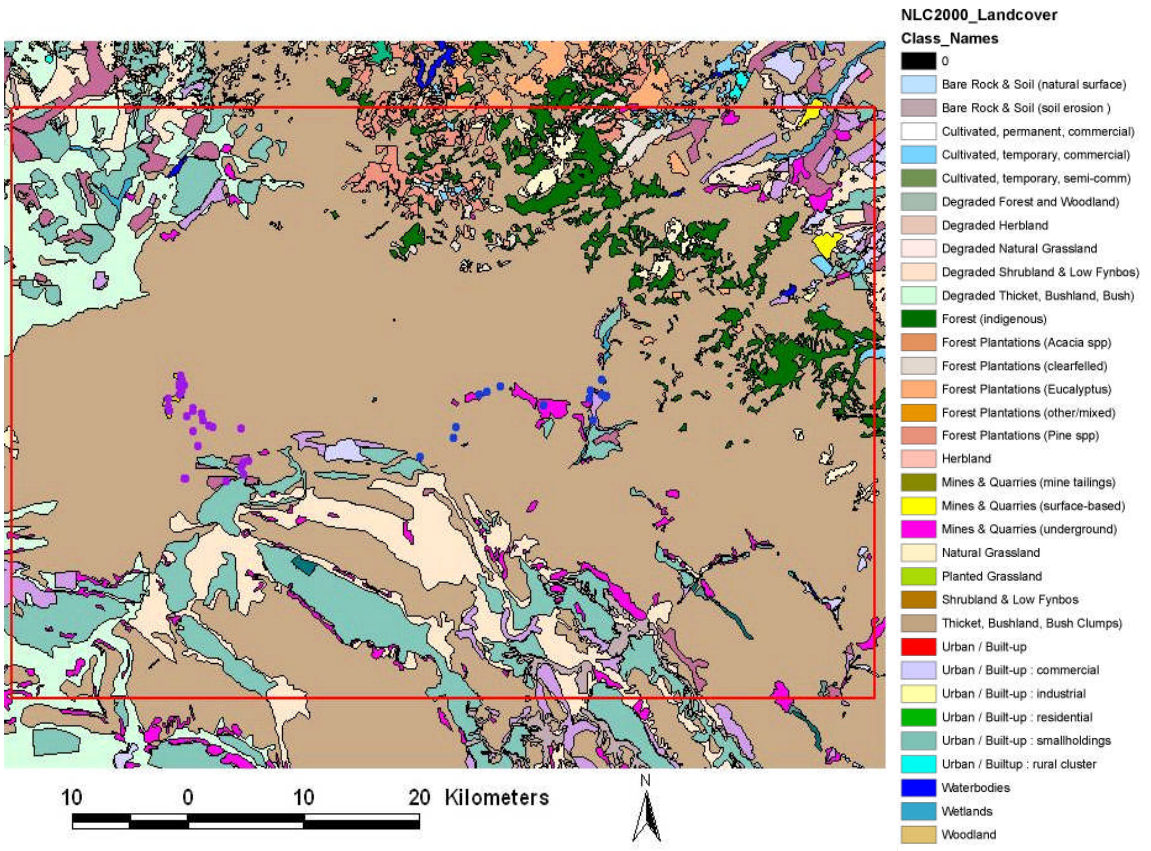

Figure 2.8. Landsat ETM derived land cover map.

2.2.8 Population and settlement

The major people residing at Mafefe and Mathabatha are Bapedi tribe falling under the tribal authority Chiefs: Thobejane in Mafefe and Mathabatha in Mathabatha area. Because of the employment which was offered by the asbestos mines, Mafefe and Mathabatha used to accommodate a variety of ethnic groups from within and outside South Africa. These included the Xhosa, Zulu, Tsonga, Venda people and also people from Zimbabwe, Lesotho and other countries in Southern Africa. The current population in Mafefe and Mathabatha is estimated at 15000 (Appendix II). For the past 16 years there has been a continuous decline in

the number of adult population (retired) as a result of fatal diseases caused by asbestos exposure. The majority of settlements in Mafefe and Mathabatha follows a linear pattern which is influenced to a greater extent by the topography. The settlements are used as residential areas which consists of schools, clinics, tribal offices and local business, and also shops and brick manufacturing yards.

2.3 Socio-economic drivers of environmental change in the asbestos setting

2.3.1 World markets

The asbestos production had significant contribution to the economy of South Africa. South Africa's total production of all asbestos fibre types from 1941 to 1978 was 6555896 tonnes made up of 33.65 % amosite, 41.99% crocidolite, 22.30% chrysotile and 2.06% anthophyllite. The asbestos production had a significant contribution to the economy of South Africa. Vermaak (1979) indicates that from the period 1958 to 1978 South Africa exported 4.89% of asbestos to USA and the production of asbestos in South Africa was ranked third after Canada and USSR. In 1977 South Africa produced 4.99% of the world's asbestos and was ranked among the chief producers (Vermaak, 1979).

Vermaak (1979), shows that South Africa increased the pricing of amosite and crocidolite asbestos. The reason is that demand continued to exceed supply in those industries during the early periods of recession which was the bright aspect of asbestos marketing and thus justified for more production. The slackening of demand started during the middle of 1977 and accelerated towards the end of that year with deepening recession in the building industry. South African sales trends followed the worldwide pattern of recession especially in the building industries. Modernisation in the pressure packing, pressballing

and pallets improved the packaging and transport facilities of asbestos industry in South Africa over the latter years. An adverse factor in the asbestos industry became the highly emotional campaign on a worldwide basis against the negative health impact of asbestos. The supply of chrysotile asbestos was hampered by the strike at Thetford mines in Canada which lasted from March to October 1975. This made the world's asbestos supply to exceed demand and thus stimulated the exploration and expansion of asbestos mining in Russia, Greece and Brazil. This caused a geometric increase in the demand of asbestos from South Africa.

2.3.2 Employment

Asbestos mining became a major source of employment for the people living in villages surrounding the mines. The local people were also selling the local products including fruits and vegetables in villages surrounding the mines. Because of the employment which was offered by the asbestos mines, Mafefe and Mathabatha used to accommodate a variety of ethnic groups from within and outside South Africa. These included the Xhosa, Zulu, Tsonga, Venda people and also people from Zimbabwe, Lesotho and other countries in Southern Africa. Table 2.1 shows the current employment rate in the post mining situation.

Table 2.1: Current employment rate in Mafefe and Mathabatha (Source: Stats SA, 2006).

	Employed	Unemployed	Not economically active
Mafefe	283	1264	4134
Mafefe SP	5	55	112
Dublin	15	-	70
Fertilis	24	6	769
Ga Mafefe	140	502	1313
Ga-Mokgotho	10	89	147
Gemini	13	169	327
Geneva	5	63	81
Mahlatjane	45	158	544
Masusele	3	7	76
Mataung	16	71	273
Mobosobohlogo	-	72	98
Osterd	3	67	77
Setaseng	3	6	247
Mathabatha	16	-	223
Madikeleng Kuduskop	16	-	223

2.4 The state's involvement on the asbestos problem

The National Parliamentary Portfolio Committee on Environmental Affairs and Tourism arranged a meeting attended by 250 experts including scientists, doctors, government officials, trade union representatives, asbestos industry representatives, and the local communities. The meeting was held for three days to address the urgent health and welfare problems relating to asbestos induced diseases in South Africa. This was also attended by Ministers from South Africa and Zimbabwe, experts from USA and Australia and observers from the regional workshops. Calls to ban chysotile asbestos and implement polluter pay principle were reported in the submissions from the Northern Province. Environmental consultants from USA supported proposals for banning chrysotile asbestos pointing out that in three years time the country's remaining asbestos mine at Msauli will be exhausted.

South Africa is currently facing an epidemic of asbestos diseases but still not only the past practices are the problem. This is because about 2000 tonnes of Chrysotile asbestos is still used annually wherein seven companies employ three thousand workers to manufacture asbestos-containing building materials and pipes. Levels of environmental pollution are colossal. Huge asbestos dumps including 82 in the Northern Cape alone are scattered throughout the countryside. The government has already spent R44 million (US$7.5 million) on rehabilitation of derelict and ownerless mines. It has been estimated that R52 million more will be needed to complete the task.

For Mafefe and Mathabatha areas, the total budget utilized for the financial year 1999/2000 was R10.725.336.97 which constituted 36.41% of the overall budget of R3.905.035.63. For Masupalonie the total budget constituted 15.00% which was R2.316.096.96. Completion of Baboons mine costed R232.569.45 which constituted 211.40% of the completed budget. For finalizing Baboon mine the total budget was R3.265.051.64 which constituted 92.07% of the completed budget. An amount of R60.000.00 was used for the tender procedure. The total budget for phase 1 of Voorspoed mine complex was R3.227.570.17 whereas for phase 2 it was R1.560.470.95. The total budget for establishment of the Voorspoed mine complex was R63.577.80. The budget for completing Masupalonie (retaining walls) for the financial year 2000/2001 was R257.086.11. For completing the remainder in both Masupalonie and Baboons the budget was R561.966.83. The budget for new exposed asbestos in the riverbed at Masupalonie was R94.978.34. For risk assessment the original budget for the medical practitioner was R162.400.00 and R245.486.40 for occupational hygienist. The balance of budget for 2000/2001 was

R142.501.00 for medical practitioner and R199.021.01 for occupational hygienist. The total budgeted for occupational hygiene consultants was R67.128.68 and R7.560.00 for Tembo Civil Engineering Contractor (Institute for Ecological Rehabilitation, 1999, 2000).

2.5 Environmental law perspectives in the asbestos situation

2.5.1 International environmental law

The World Trade Organisation (WTO)'s legal role on the asbestos situation

The World Trade Organisation's Dispute Settlement Body (DSB), the source of its strong arm tactics, operates anonymously in secret and behind closed doors. The WTO first came to prominence for its regrettable judgement against the European Union for refusing to import hormone treated meat from the United States to France. The ruling provoked a chain reaction starting with initiatives by the Roquefort cheese producers of Aveyron in France. Currently with no more publicity, the DSB is preparing to rule on Canadian complain challenging the French decision to ban asbestos, in force since 1 January 1997. By so doing, it was acting in the name of freedom of international trade. On May 28 1998, Ottawa initiated dispute proceedings against France. That was when the battle of experts began. This was taking place far away from countless victims who have already experienced the effects of asbestos at first hand. On one hand, asbestos production is a strategic industry for Canada, Zimbabwe and Russia. France, backed by the European Union, adopted a directive banning of trade in and use of asbestos in July 1999. Although the ban will not become active until 2005 (at the latest), only three

member states of the European Union (Spain, Greece and Portugal) still have to implement it. Paris has the support of the US which considers all types of asbestos carcinogenic. What is at stake with the DSB's judgement has to be understood in the light of the war that has set the asbestos industry lobby against the deadly fibres millions of victims for the last hundred years. Between 1930 and 1960 manufacturers did all they could to prevent the link between asbestos and the respiratory diseases including cancer to become known, so that they can avoid prosecution. However, an American worker sued John Mansville Company as far back as 1932, but it was not until 1962 that the epidemiologists finally established beyond reasonable doubt what company bosses have known for a long time, that asbestos cause cancer. The asbestos victims' counterattack took place before the law. Legal proceedings uncovered the tragedies of victims and their families, the criminal practices of the employers, and the culpable failure to act. All this gave the scandal a real political dimension.

In the US, the 'trial of the century' with nearly 300 000 complaints filed, ended abruptly. John Mansville declared itself bankrupt in August 1982 and set up a compensation fund, followed by other manufacturers and their insurance companies. In France, the National Association for the Defence of Victims of Asbestos has brought more than 1000 civil and criminal actions from 1996(9). Both the system for preventing and compensating for occupational disease and the relevent institutions, industrial medicine, were on trial with them.

In Brazil the military dictatorship helped the asbestos operations (Eternit and Saint-Gobain) which therefore censored all information about occupational health and industrial hazards. At the investigation of the Brazilian Association of Workers Exposed

to Asbestos formed in 1997, hundreds of workers and families of the deceased went to court. Eternit and Brasility then offered their former employees an amicable agreement whereby workers would refrain from bringing proceedings in exchange for the lump sum compensation in the event of illness. In a study carried out for the Trade Union of Technical Bureau, Samien Zia-Zarifi and Mary Footer showed that, even if the DSB's decision does not call into question the French decision to ban asbestos, the very proceedings are bringing human health and workplace safety within the remit of the WTO, although they had hitherto been matters of national sovereignty.

2.5.2 The South African legal perspective

Environmental criminal law

The legislation which deals with environmental protection prohibits a range of behaviour, provides that contravention of any of the prohibitions is an offence and makes provisions for penalties for such contravention. Any contravention of the legislation is declared to be an offence, regardless of the seriousness of the offence or whether it causes harm or not, and often the legislation does not even distinguish between the seriousness of different offences by providing different penalties for different offences. For example, in the Atmospheric Pollution Prevention Act 45 of 1965, a number of different offences are created, ranging from carrying on a process which emits noxious or offensive gases without a prescribed registration certificate [section 9, (s 9)], to failure to stop a vehicle on a public road when requested to do so by an authorized person (s40(4). Alternative methods of control were rarely provided in the legislation. In addition to the usual penalty provisions, certain legislation makes provision for remedies over and above criminal

penalties, but these are always available only once the offender has been convicted of a criminal offence. Therefore, they are not alternatives to the criminal law but complimentary to it. However, there has been lack of regulatory controls for asbestos mining. The Atmospheric Pollution Act 45 of 1965 adopted a procedure for prevention and control of pollution which of 'the best practicable means'.

The Act makes provision for a chief control officer who grants a registration certificate authorising the continuation of the process if satisfied that the best practicable means against pollution has been adopted. Application of the 'best practicable means' involves a subjective evaluation on the part of the Chief Air Pollution Control Officer. However, most industries performed self regulation which resulted in lack of clear standards. The regulations may be made prescribing the steps to be taken to prevent the creation of a nuisance due to the dispersion of dust. This is done once the area has been declared as a dust control area. The Mining Rights Act 20 of 1967 provides for the establishment of mine dumps, comprising tailings, slimes, waste rock, sand or residues produced in the course of mining operations. However, the Act didn't look at the real health hazards by allowing the deposit of asbestos dumps.

Constitutional rights

In keeping with international human rights provisions regarding environmental rights, both the interim Constitution (Constitution of the Republic of South Africa Act 200 of 1993) and final Constitution (Constitution of the Republic of South Africa Act 108 of 1996), provide for environmental rights. While section 29 of the interim Constitution simply provided that, every person shall have the right to an environment which is not

detrimental to his or her health or well-being', the provisions of the final Constitution (1996) are more elaborate.

Section 24 of the Constitution provides that everyone has the right - to an environment that is not harmful to their health or well-being; and to have the environment protected, for the benefit of present and future generations, through reasonable legislative and other measures that - (i) prevent pollution and ecological degradation; (ii) promote conservation; and (iii) secure ecologically sustainable development and use of natural resources while promoting justifiable economic and social development

In terms of Section 7(2) of the Constitution, the State will be required to respect, promote and fulfill the rights provided for by the Constitution. In so doing, the state will have to enact legislative measures to give effect, inter alia, to the constitutional rights to an environment that is not harmful to the health and well-being of all persons in South Africa. The state also has international obligations to provide and maintain a clean and healthy environment because it signed the UDHR and the Covenant on Social, Economic and Cultural rights (1966), and it has ratified The Convention on the Rights of the Child (1995) and the Convention on the Elimination of All Forms of Discrimination against Women (1995), which have provisions related to environmental issues. In view of the direct horizontal application of the Bill of Rights, natural and juristic persons are now also obliged to respect the environmental rights of others (section 8 (2)).

Liability

The law of delict and nuisance are relevent to the imposition of liability for the harm to the environment. The utility of delict with regard to environmental damage is limited by

the difficulty that litigants encounter in proving fault and causation. Another limiting factor is the restrictive approach taken by the South African courts to extend delictual liability to novel situations, a category into which many environmental liability cases fall. The provisions related to environmental liability in NEMA (Act 107 of 1998) are stipulated in sections 28 and 30. With these provisions as the polluter pay principle is manifested in sections 28 and 30. Section 28 establishes a general duty of care and imposes liability for clean up costs on a range of persons. Section 30 makes certain persons liable for the consequences of emergency incidents of serious nature.

S (28)1 provides that every person who causes, has caused or may cause significant pollution or degradation of the environment must the reasonable measures to prevent such pollution or degradation from occurring, continuing or recurring, or in so far as such harm to the environment is authorised by law or cannot reasonably be avoided or stopped, to minimize and rectify such pollution or degradation of the environment.

This phrase is significant because it generalises and applies to every person. Subsection 2 says this includes owner of land, premises, person in control of land, premises, or person who has the right to use land/premises (may include the contractor or subcontractor). It is retrospective as applies to pollution/degradation in present and past. Appears to impose strict liability- does not have to prove the person acted negligently/intentionally. S(28)3 measures to be taken are in broad terms. Expropriation in terms of (ito) s (28)6, if for a person to carry out rehabilitation or other remedial work on land of another. Minister can expropriate the land and recover the costs from a person to carry out measures.

The Cape plc did not have a mandate to rehabilitate when the asbestos mines were decommissioned. This was because before 1991 there was not legislation enforcing miners to rehabilitate after closure of the mines. The provisions for rehabilitation were put in place when the Minerals Act 50 of 1991 was enacted. South African tax payers' money will have to be used for environmental rehabilitation of the asbestos mines abandoned by the Cape plc. Upon settling out the compensation for the asbestos victims, it based on the condition that the South African government must waive any claims against the Cape plc for environmental rehabilitation. The Cape plc wanted an assurance from the government that it will forego any claims for the rehabilitation of the polluted land. The Chief State legal advisor indicated that an earlier settlement condition suggested by the British Mining Company was that the South African government introduces legislation barring any locals from suing the Cape plc again. This was rejected because it could have been inter alia unconstitutional. By that the Northern Province and Northern Cape governments agreed to waive environmental rehabilitation claims and awaiting the final approval from the Cabinet. However, this directly meant that the government would be responsible for the environmental rehabilitation worth of millions. On the other hand the British government's Department of International has indicated a willingness to get involved in the rehabilitation of the Cape plc's mine dumps.

In Lubbe and others v Cape plc in England, the plaintiffs who were South African citizens resident in South Africa claimed damages for personal injury, and in some case death against the defendant. The plaintiffs alleged that, in respect of periods before 1979, the defendant, while knowing of the injurious effects of exposure to asbestos, had failed as the parent company, to take appropriate steps to ensure the adoption of proper working

practices and safety precautions throughout its subsidiary companies or those living in the area of their operations. The company was liable to the costs and damage incurred and insisted that the application be heard in South Africa which will in anyway be a disadvantage to the plaintiffs because they would not get legal aid. The judge granted the stay, concluding that South Africa was the national forum and that justice would not require him to order otherwise. The plaintiffs appealed and throughout the process, 9 other applications were submitted with similar claims. However after a long process, the decision of the Court of Appeal was reversed and therefore considering the public interest and public policy which did not relate to the private interests of any parties.

Locus standi (Legal standing)

The current state of locus standi is being advanced to a reasonable level. The NEMA grants legal standing to persons acting as members of or in the interest of a group or class of persons and persons acting in the public interest, with respect to the infringements of environmental rights.

In terms of S(32)1 –any person /group can seek relief for breach of provisions of NEMA (including principles) or any other statute concerned with protection of the environment and use of natural resources including *inter alia* own interest/ in interest or on behalf of group, in public interest, or even in interest of protecting the environment.

In terms of S(23)2 –the court of law may decide not to award costs against person if lose, of the opinion that person acted reasonably out of concern for the public interest or in interest of protecting the environment and had made due efforts to use other means reasonably for obtaining the relief.

If succeeded ito S(23)3 –in addition to granting relief sought, the court may award costs to attorney/advocate who gave applicant free legal advice/represented them on an appropriate scale and may also order that pay applicants reasonable costs for their investigation and preparation of the proceeding.

2.5.3 Recommendations

The state's responsibility

The state has a duty to protect the welfare and health of its legal subjects and to protect the environment and the people living in it from the detrimental effects of environmental degradation. The right to the healthy environment that is not harmful to the well being is imposed in the constitution. As the Constitution is the supreme law of the country, it proclaims the state' duty to respect, protect, promote and fulfill the rights in the Bill of Rights (Act 108 of 1996) and this includes s24. The state's obligation to protect its citizens is moreover a well known constitutional principle in South African law as well as in other legal systems and in international law. However, in respect of the asbestos issue, the South African state previously have failed both the environment and its citizens, leaving them inadequately protected against the effects of environmental degradation. The failure has been illustrated by lack of control of unsafe asbestos mining.

The responsibility of mining companies

Mining companies in South Africa have reaped profits of asbestos mining but never had to pay the real costs of cleaning up the dumps, medical expenses and loss of income. Pollution control in South Africa is mainly addressed through legislation and so is the

liability for personal injury due to asbestos related diseases. The Compensation for Occupational Injuries and Diseases Act 130 of 1993 provides for compensation for workers who have contracted asbestos related diseases. However most of the people who were ill were not covered by the act since it came into effect in 1993. Section 9(1) also creates a duty of care towards non employees and people who suffered damage may bring a claim against an employer in addition to the common law claim.

Provisions for rehabilitation

Section 38 of the Minerals Act of 1991 (Act no 50 of 1991) in the South African Mining legislation, stipulates that the rehabilitation of the surface of the land concerned in any prospecting or mining shall be carried out by the holder of the prospecting permit or mining authorization in accordance with the environmental management programme approved in terms of section 39 (Environmental management programme). This provision gives the miner a full responsibility for the rehabilitation of any mine after the operations has ceased. It is further required that the miner in question prove to the state that he has or will have funds to undertake the rehabilitation.

Current asbestos regulations

The Minister of Labour has under section 43 of the Occupational Health and Safety Act (Act 85 of 1993), after consultation with the Advisory Council for Occupational Health and Safety, made the regulations in the schedule hereto referred to as asbestos regulation. The asbestos regulations are provided for matters relating to asbestos which include among others exposure to asbestos, air monitoring, medical surveillance, asbestos related products and control measures. The regulations prohibit the use and operation of any

asbestos or asbestos related material which result in the release of asbestos dust. However, given the extent and severity of the asbestos problem, and looking at the current costs of asbestos rehabilitation, the penalties provided in the regulations are not enough and have been overlooked. Regulation 23 of the asbestos regulations provides that any person who contravenes or fails to comply with any provisions of the regulations stipulated, shall be guilty of an offence and liable on conviction to a fine not exceeding 81000 or imprisonment for a period not exceeding 12 months and, in the case of continuous offence, to an additional fine of 8200 for each day on which the offence continues: provided that the period of such additional imprisonment shall in no case exceed 90 days. The fine however doesn't bring into account the damage that will result thereof and thus have an extra allowance continuous pollution for a specified period with a fine of 8200 per day.

2.6 Summary

This chapter has reviewed the environmental characteristics of the study area. It described different parameters that characterize the environment of Mafefe and Mathabatha. It also reviewed the drivers of environmental change, particularly focusing on the socio-economic and the biophysical aspects. The chapter ends by reviewing the legal aspects revolving around management and utilization of asbestos environments.

CHAPTER THREE

LITERATURE REVIEW

3.1 Introduction

The focus of geography of environment is directed primarily towards space in time. Time is considered as one of the subsystems of geographical landscapes. A temporal parameter is important in the interpretation of satellite imagery. Remote sensing devices which operate on a regular basis can be used to detect dynamic trends and direction of growth. Once changes are recorded, locational factors responsible for change may be identified (Simonett, 1976). This chapter reviews the historical trends in using satellite imagery to monitor mine rehabilitation, applicable methodologies, relevant applications and the current trends in the research of such nature. This part however begins by reviewing the global issue of degradation focusing on the drivers of degradation and emergence of degradation in Africa.

3.2 Land Degradation: An Overview

When land become degraded, its productivity declines and it becomes no longer useful unless steps are taken to restore its productivity (Blaikie et al., 1987a; MacDonald et al., 1993). The social significance of degradation has far reaching implications in economic, social and environmental terms. Central to the issue of land degradation is the land manager, who often responds to changes in their social, political, and economic circumstances. This may include among others access to common resources, market or social demands and state responsibilities. Human induced degradation occurs when the land is poorly managed. Some degradation occurs when the land that should never have been interfered with is brought into use. An increase in

cash incomes from those areas of mining which can yield a temporary increase in rural incomes over several generations, but can lead to degradation through lack of attention to management of land and hence to subsequent income reduction (Blaikie et al., 1987a).

3.2.1 The role of Colonial Development on Degradation in Africa

The impact of colonialism on indigenous land users was extraordinarily diverse across space and time (Blaikie et al., 1987b; MacDonald et al., 1993). In Africa, this happened most heavily in the southern part of the continent and also in East and North Africa. In Algeria, 20 000 Europeans occupied about 2.5 million hectares (ha) of the best land while about 630 000 Algerians were left with 5 million ha of land. In Zimbabwe the sixth of the entire country (6 million ha) was taken by Europeans after 1890. In South Africa successive Europeans relocated and marginalized the rural African population into areas proportioned according to the legislation between 1877 and 1913, with the resettlement further expanding in 1936. The remaining land for the masses of African population was about 12% of the total area. Even Swaziland which retained its political identity had only 37% of the land remaining for the indigenous population. Blaikie et al., (1987b) notes that the massive disruptions of society brought under colonialism in Africa bear a major share of the deteriorated quality of land. African systems of land use had their own protective devices against erosion. When native reserves were first created in southern Africa, the aim was to produce a labour shortage for European farmers. However, the restriction of Africans to inadequate land and the enforcement of taxation made temporary labour migration to the mines and cities a necessary strategy for survival. Colonial attitudes toward land degradation problems have varied considerably through time. There was not much concern before 1900. Erosion was recognized as a settler (colonialists) problem but from 1920 until 1940 the focus was shifted to soil conservation.

3.2.2 General Approaches to Degradation

Biot et al., (1995) identified three approaches of land degradation which have been examined in developing countries. The first one was categorized as the classic approach which assumes that the extent of and solutions to the problems of land degradation are well known to the people but the problem is to implement them. The classic approach is constituted by four major components which include; identification of an environmental problem with an environmental solution; mismanagement of the environment by the users; overpopulation and subsistence fundamentalism. The concept of marginalization was applied to understand the way in which the expanding population on a restricted resource base might have been forced to degrade its environment. Growing inequality and socioeconomic differentiation within peasant communities, and their relationship with traders and state agencies has contributed to degradation of environment (Biot et al., 1995; Blaikie et al., 1987b). The classic approach also assumes that the nature and the extent of degradation are imperfectly understood, that local people often reject conservation technologies for a good reason and adopts their own individual and collective technologies that have resulted in sustainable livelihood practices. This often resulted from the top – down systems of administration. The other approach referred to as the populist approach evolved as a result of the critiques to the classic during the late 1970s. Biot et al. (1995) emphasizes that the populist approach was people centred with elements of a bottom - up system thus reflecting the need to redistribute land and political changes to empower people. The Neo-liberal approach was also established which brings to attention that suitable technology exists to understand the present structure of incentives that prevents land users from adopting them and to design incentives that will induce adoption. This approach also focuses on the understanding of the significance of population growth in exacerbating pressure on natural resources and the

relationship between land degradation and poverty.

3.2.3 The Nature and Characteristics of Mines that make them prone to degradation

Sengupta (1993) emphasized unique characteristics that make mines prone to degradation of the environment when compared to other resources. Mines have unique characteristics that make them prone to degradation of the environment. Mineral deposits have fixed locations and as such are not subject to rational selection or advanced planning. Due to physical conditions associated with their location, there is no choice about the characteristics of their ecological setting, biological and chemical characteristics, mineral composition, or grade of the ore in question. All of these factors influence the design, layout, and size of the operation, as well as the basic environmental problems and the potential longer range of regional impacts. The nature of the ecological setting also determines other land uses or activities that may be affected by mining. Mines have a finite life span. Because of the nonrenewable nature of mineral deposits, mining becomes a temporary land use. However, ore reserves in some situations are so abundant that mining activities appear to be permanent fixtures in the life of the region inhabitants. Mines are usually located in a setting of relatively unspoiled nature. In many instances, the original mine is the reason for existence of a town. Other means of economic support are then generated. Another important aspect of mine development is time lag. After initial discovery and evaluation of a potential mine, years of development and construction pass before a mine begins production. Time have an important effect on the ultimate impact of mining operations on the environment. Unforeseen chemical and physical changes to the environment can emerge at any stage of the life of the mine, or even long after closure, despite precautions.

3.3 Review of Mining Degradation and Rehabilitation using Remote Sensing

3.3.1 Ecological Research Needs from Remote Sensing

Modern ecological research places emphasis on the variability in structure and function at all spatial and temporal scales. However, changes in function may or may not manifest in measurable structural changes across scales of interest. Knowledge of this scaling issues has largely fueled the interest of both top – down and bottom – up approaches to studying ecological processes. Ecological research efforts tend to focus at specific spatial scales ranging from individual plants, plant populations, and multi - species communities to whole ecosystems, biomes and the globe. For most part, ecological studies at ecosystem to global scales have benefited from remote sensing research. The remote sensing needs of the ecological communities are diverse and are dependent upon the spatial and temporal scales of individual applications. The land reflectance anisotropy fundamentally represents an independent and potentially important source of information for increasing the accuracy of vegetation parameter estimates at all scales (Asner et al., 1998).

Landsat TM data provide a means by which vegetation biophysical conditions can be mapped and monitored over larger geographic regions. Studies using satellite multi-temporal data to map and monitor forest succession have generally used one of the two possible approaches in most cases. This included spatially based studies which examine changes in spectral response across a successional gradient and using a single date of imagery. The second is a temporally based approach which examines changes in spectral response for specific sites over time, using multiple dates of imagery (Jakubaskas, 1996).

3.3.2 Monitoring Environmental Impacts of Mining using Satellite Imagery

Legg (1990) recommended Landsat TM and SPOT data as effective remote sensing in monitoring surface mining activities in a rapid and cost-effective way.

Rathore and Wright (1993) emphasize the importance of periodic mapping and monitoring of the areal extent and location of land degradation associated with mining, for use in formulating strategies for land reclamation once mining has ceased.

Chase and Pettyjohn (1973) were among the earliest to report the utility of Earth Resources Technology (ERTS) 1 – MSS data in mapping land disruption due to strip mining in east central Ohio. They reported that it was feasible to use ERTS 1 data without the need for maps or aerial photos to identify open cast mines. However, it was not easy to identify reclamation work done near the site as it was barely detectable using ERTS 1 imagery. Most activities however, focused on monitoring of strip mining activities rather than the reclamation process (Wier et al., 1973; Alexander et al., 1973; Anderson and Shubert, 1976; Anderson et al., 1977). Most studies found that Landsat MSS data was not suitable to monitoring and study aspects related to surface mining (Anutha and Bahethi, 1982; Peplies et al., 1982).

Irons and Kenhard (1986) investigated the suitability of Landsat TM data for surface mine monitoring. They found that the contributions of individual TM characteristics to utility depend considerably on the scene. Legg (1986) used a combination of multidate TM and MSS imagery to monitor open cast mining and reclamation activity of Butterwell open cast coal mine and Druridge Bay area of the United Kingdom. He concluded that the extent of open cast mine workings could be monitored using satellite imagery where TM's higher spatial resolution was

much better for the purpose. Almeida – Fihlo and Shimabukuro (2002) used Landsat TM to map and monitor the evolution of degraded areas caused by independent miners in search for gold and diamond. A similar study was reported by Petja et al., (2003) who investigated the degradation caused by open cast diamond mining using EROS A 1 imagery.

3.3.3 Mine Revegetation and Reclamation Monitoring

Abandoned mines are characterized by environments unsuitable for plant growth. Successful monitoring and reclamation programmes rely heavily on periodic monitoring of planted areas such that plant growth and vigour can be regularly estimated and corrective action undertaken if required (Rathore and Wright, 1993). Mrczynski and Westmiller (1982) have used colour aerial infrared photography for evaluating reclaimed and non reclaimed land in south-western Indiana. Legg (1986) undertook vegetation vigour studies on the reclaimed lands using band ratioing for monitoring.

3.3.4 Satellite derived methodologies for monitoring mine rehabilitation and vegetation change

3.3.4.1 Common Methods for Change Detection

Spectral information is the most commonly used measurement variable for detecting change. Algorithm based approaches most likely focus on the use of spectral data and spectral variability. The commonly used techniques are image differencing, image ratioing and Principal Component Analysis (PCA). Post-classification comparison of multiple thematic cover classification has the advantage of creating a complete descriptive matrix. Change vector analyses provide a high level of information regarding the magnitude and the nature of surface change, and have been widely

used to monitor vegetation conditions. Other methods include analysis of trends in various vegetation indices and other spectrally based band ratios and indices. Object-based classification offer an improvement that goes beyond spectral information alone. Object based classification segment imagery into discrete image objects (contiguous groups of pixels with similar properties). Spectral information is not only one component on which segmentation is based. Characteristics such as shape, texture and neighborhood relationships are incorporated into the segmentation algorithm (Sohl et al., 2004).

Fung and Siu (2000) applied image differencing (NDVI) and PCA using SPOT HRV images to conduct change detection. NDVI image differencing was used as a first step of investigation. The resulting images reflect the increase or decrease in vegetation cover. The effects of land reclamation were depicted on NDVI difference images.

Fung and Siu (2000) found in their results that PCA 1 explained most of the variance and provided a picture of the average pattern of the data. The highest NDVI values were woodlands as compared to built up areas with low values. Subsequent components reflected land cover changes in different time periods. They further found that PCA 2 had the highest loading in 1997, representing change since 1987. Major reclamation sites after 1987 were all clearly shown. However, PCA 3 and 4 had the highest loadings in 1991 and 1993, respectively. These loadings highlighted land cover changes that took place after 1991 and between 1993 and 1995.

Prakesh and Gupta (1998) found that change detection using satellite data allow for timely and consistent estimates of change in land use trends over large areas, and has an additional advantage of the ease of data capture into GIS. They used remote sensing because of its advantage in providing multispectral and multitemporal synoptic coverages for any area of

interest. The satellite data provides a permanent and authentic record of land use patterns of a particular area at any given time which can be re-used for verification and reassessment. On the other hand, GIS provides the facility to integrate multidisciplinary data for dedicated interpretation in an easy and logical way.

3.3.4.2 Change detection using Thermal Infrared bands (TIR)

Mikkola (1996) used thermal radiation information for tentative mapping of severe vegetation degradation and erosion. He found that damaged areas can be detected more precisely using either TM or MSS ratios, however, by utilizing thermal image information, severely damaged areas could be quite easily and simply employed. The spectral variation between images from different acquisitions is due to a number of factors. The state of the atmosphere is never stable, and the azimuth varies throughout the day and summer. Soil and vegetation moisture contents also differ markedly between different days, and thus generate periodic changes in spectral radiation.

3.3.4.3 Associated drawbacks in change detection methodologies and recommended strategies

Munyati (2000) studied errors that could be encountered during image processing and analysis when using satellite imagery for change detection. He found that change detection errors arising from seasonal differences (vegetation phenology cycles) were therefore, minimized by the near anniversary September images. Change detection errors arising from sensor differences were partly minimized by using sensor calibration parameters, although other imaging systems like SPOT would have provided additional images.

In solving such errors Luque (2000) recommends radiometric normalization of multidate images to be an important step in the monitoring studies. Image normalization reduces pixel brightness value (BV) caused by non surface factors so that variations in pixel BVs between dates can be related to actual changes in surface conditions. Normalization enables the usage of image analysis logic for a base year scene to be applied to other scenes. Normalization targets are assumed to be constant reflectors, therefore any changes in their brightness values are attributed to detector calibration, astronomic, atmospheric and phase angle differences. Once these variables are removed, changes in BV may be related to changes in surfaces conditions.

Luque (2000) used about 30 training sites in each data set, which constituted among others, quarry areas, reservoirs, clear water bodies, airports and military sites. The mean BVs of the base image targets (Date *j*) were regressed against the mean BVs of Date *i* +1 targets for the bands in the red and the NIR of the data. This regression model produced an NDVI image of Date *i* +1 into Date *i* (converted NDVI). Then Image Algebraic Change Detection was performed according to the following expression.

D*ijk* = Converted NDVI/Date *i* NDVI Equation 1

where NDVI = NIR-R/NIR+R and D*ijk* = change pixel value.

Karnielli et al. (2002) acknowledges that there are still several difficulties in detecting and monitoring vegetation using multispectral imagery from airborne and space-borne sensors. These are due to temporal change in the vegetation state, temporal change in soil/rock signature and difficulty in discriminating vegetation from soil or rock background. The growth stage of plant communities may result from a combination of changes in plant leaf structure, pigments, and/ or

canopy area throughout the growing season. Consequently, phenology has some influence on seasonal reflectance dynamics. Different spectral vegetation indices have been proposed during the last three decades of monitoring the physiological and spatial distribution of vegetation from remote sensing data.

3.3.5 Basic image processing and analysis procedures for change detection and monitoring

3.3.5.1 Image processing of multidate Landsat TM

Almeida – Fihlo and Shimabukuro (2002) identified the following factors which are related to sensor systems and natural conditions as important variables to be considered as they may affect the results of the change detection studies. For their study area, they identified, factors related to the sensor system which include differences in satellite passes, differences in spatial resolution and variations in radiometric response. Natural conditions include atmospheric scattering and absorption, presence of clouds and cloud shadows, variation in solar irradiance and solar angles, seasonal variation in vegetation phenology and soil moisture.

However, they emphasized that the influence of the sensor factors is partially minimized by using multi-date images acquired by the same satellite in their area. To minimize variations in the spectral response of the ground targets, cloud free images should be used and images correspond to the dry season such that they are imaging vegetation cover under similar phenological conditions. The images should be acquired at higher solar elevation angles. This condition, combined with topography of the plateau, produce results without terrain shadowing effects. This is followed by radiometric normalization of images and geometric corrections. To

compensate for variations in sensor radiometric responses over time and for variations in natural conditions of solar irradiance and solar angles, digital numbers must be converted to reflectance values.

Almeida – Fihlo and Shimabukuro (2002) also used the PCA procedure. Landsat TM multispectral bands are generally highly correlated. To overcome the problem of dealing with highly correlated data and try to enhance information that is unique to each spectral band, PCA must be applied to each of the multi-date images. Results showed that the first three PCA images concentrated more than 98 % of the total variability of the data, for all the dates considered. Due to enhancement of the degraded areas relative to the surrounding savanna vegetated terrain, the third PCA image was chosen for segmentation and classification.

3.3.5.2 Image analysis

Analysis of optical satellite data from Landsat TM permits accurate estimation of deforestation areas and rates. Most studies reported accuracy levels of over 95 % (Sader et al., 1991; Steininger, 1996). Progress has also been made in the area of secondary forests with high resolution optical data. The estimation of regrowth biomass over large areas with satellite imagery, enable understanding about the ecological functioning of natural and human induced landscapes. The independent studies using TM observations have reported similar changes in canopy spectra with age over the first fifteen years of forest regrowth in the Brazilian Amazon. The visible (TM 3) reflectance is low for all ages of regrowth while NIR channel (TM 4) reflectance increase for four to eight years and then decreases for the following five to ten years of forest regeneration. Reflectances in both the MIR (TM 5, TM7) gradually decrease throughout the first 15 years of regrowth. The common trends in regrowth canopy reflectance with age have

been attributed to the changes in canopy leaf area and geometry as secondary vegetation regrow.

3.3.5.3 Integrating raster data with vector based GIS for land use change detection

Mattikalli (1995) provided the integration methodology required an interface to be developed between vector GIS and raster image processing system, since basic data structures of the two systems are different. The methodology involves a data conversion algorithm that can handle both raster and vector format types. The methodology makes use of some built in routines commonly available in most vector GIS. The data conversion algorithm involves the use of intermediate data formats (lattice, grid or single variable file (SVF)). The lattice formats interprets the raster data as a series of regularly spaced mashed points to represent pixel values, and it does not imply an area of constant value. In contrast, the interpretation of SVF format considers each cell a square area with a constant attributable value, and all locations within the cell are assumed to have the same value. Firstly, the raster image is transferred into a lattice data structure. Data in lattice format could easily be read and imported by most GISs at the time of the publication. The raster data is transformed into a polygon vector layer. In the resulting layer, polygons were built from groups of contiguous pixels having the same pixel value. Coordinates of the resulting vector layer were based on the minimum (x,y) coordinates of the input satellite image and the pixel dimension. This algorithm was employed to integrate three land use classifications derived from remotely-sensed images into a GIS interface.

3.3.5.4 Change vector analysis

Malila (1980) used the change vector analysis as an approach to detect and identify changes

automatically. This method uses spectral and spatial information to perform a spectral spatial clustering on a two temporal image data set in order to find homogeneous areas. The change vector is computed between the area spectral mean in the earlier and the latter images. The magnitude of vector gives the extent of change, while the angle gives the type of change.

The common method to observe change on the image as used by Sunar (1998), was a photographic comparison of a single band of data from the two dates. The image is prepared by making a photographic two colour composite showing the two dates in separate colour overlays. The colour in the resulting image indicates the changes in reflectance values between the two dates. Land use change over time in response to economic, social and environmental factors.

3.3.5.5 Using change curves for analysis of multi-date imagery

Lawrence and Ripple (1999) investigated the use of change curves in quantifying vegetation change. Change curves can be effective tools in characterizing vegetation change as mapped by digital imagery. Variability in change curves might be attributed to annual variability in soil moisture, uncorrected radiometric differences, annual climatic differences resulting in phenological variability, and differences each in length of the growing season prior to the growing season. Lawrence and Ripple (1999) demonstrated the importance of using computed curves for change analysis. The change curves reflected various parameters related to the trend in cover changes over time. This approach is useful where the interests are related to pixel level trends, as opposed to categorical changes. The study concluded that the change curve analysis will be important in the following applications:

1 Growth rates of forest stands, such as increases in biomass in managed forests,

2 Successional processes, such as changes from deciduous forests to mixed stands to conifers,

3 Seasonal changes associated with plant phenology,

4 And rate of urbanization.

Such changes at the pixel level in percent of land converted from agriculture to urban, but not categorical changes in pixels from agriculture to urban. This applies to sets of continuous data.

3.3.5.6 Spatial analysis of landscapes

Henebry (1993) used remote sensing for the spatial analysis of landscapes. He found it to be of a great challenge to monitor and measure landscape change in a manner that shed light on concominant ecological processes. Measurement of change relies on some quantification of observed patterns. Data that is spatially extensive, such as satellite imagery, can be understood in terms of interaction of spatial dependence and spatial heterogeneity, and a time series. Anisotropic influences such as topography and precipitation, can generate spatial heterogeneity across a range of scales. To monitor regional vegetation change effectively, levels of variability must be identified so that observed changes can be placed within a broader spatio-temporal context.

3.3.5.7 Analysis of canopy spectra

Steininger (2000) analyzed the canopy spectra on the surveyed stands which were identified in the georeferenced imagery. Means of corrected stand reflectance in each of the TM channels were calculated and plotted against above ground biomass and structural variables. Linear

regressions of each channel reflectance against biomass were performed using a general linear model. Stepwise regression was used to compare biomass estimation using single versus multiple band reflectances. Stand canopy reflectances were plotted against the other stand structural characteristics to assist interpretation of the biomass-canopy reflectance relationship.

3.3.5.8 Analysis of field data

Jakubaskas (1996) studied 69 sites which were classified into six successional stages/ cover types, based on specified ecological criteria. A multivariate analysis of variance (MANOVA) was used to test the significant differences among cover types. Since cover type groups were defined on the basis of biotic characteristics, statistical tests were applied solely to spectral differences of the six groups. Univariate two – tailed *t* – tests were then used to determine which TM bands were contributing to the significant multivariate pairwise differences. Discriminate analysis was used to examine the spectral separability of each cover type and determine the probability of a site belonging to one of the six cover types. Spectral reflectance as recorded by TM bands 1,2,3,5 and 7 decreases with increasing age and development of forest canopy. Middle infrared bands of the TM allow early successional stages to be differentiated from mature forest sites. Late successional cover types may be distinguished from each other based on TM 3 and 4 reflectance.

In a similar study, Foody et al. (1996) found a high degree of separability in the six age classes of regenerating tropical forest from an analysis performed using TM bands 3, 4, and 5. The highest accuracy observed was a weighted kappa coefficient of 0.8569.

Overlay operations within GIS were contingent upon the existence of a layer containing known old growth polygons and layers consisting of old growth polygons as identified by remote sensing techniques. Subscenes composed of the six forest stands in question were extracted so that the ability of remote sensing techniques to differentiate between old growth and younger stands could be evaluated. The NDVI and the Simple Vegetation Index (NIR/R) were successful in differentiating between old growth and the younger post fire stands (Nel et al., 1993).

3.3.6 Relevent applications from satellite derived analyses

3.3.6.1 Phenology based evaluation of vegetation change in assessing the progress of revegetation

Justice et al., (1985) found that the study of phytophenology provides an insight into the temporal organization, evolution and functioning of the ecosystem. Knowing phenology of plant communities is relevant to estimating biological productivity, biome dynamics and management of vegetation resources. Observed phenological changes are important in the identification of vegetation cover and communities with the aid of remote sensing techniques.

3.3.6.2 Monitoring of successional stage in assessing the state of rehabilitation

Remote sensing information can be used to investigate the consistency and steady improvement of the vegetation cover. Finding a natural equilibrium can keep erosion and sedimentation at reasonable levels where natural vegetation growth can be maintained. Geerken and Ilawi (2004) used Landsat TM scenes to identify the impacts of rehabilitation measures in the study of sedimentation. Results of their study showed that vegetation cover has significantly covered the

sand sheets in the plains of a rangeland environment.

Apan (1997) studied the rehabilitation of tropical forest ecosystems using remote sensing. He found that high crown class cover reflects the highest value in the NIR band and the lowest in the red and MIR bands. Low crown class cover has the highest reflectance in red and MIR bands with the lowest in the NIR band. Similar classes in successional stage reflect a similar pattern of reflectance. Different stages of vegetation growth may be spectrally separable. The low crown cover class in the initial successional stage has the highest red and MIR reflectance values, whereas having the lowest in the NIR band. On the other hand, the advanced successional stage class has the highest NIR reflectance but the lowest in red and MIR bands. This is because of the increased greenness in the growing vegetation. The spectral response of growing vegetation helps in monitoring ecological rehabilitation.

3.3.6.3 Using Middle Infrared (MIR) for terrestrial environmental studies

Boyd and Petitcolin (2004) experimented the applications of middle infrared bands for terrestrial environment. They adopted the use of MIR reflectance in their study, in order to improve the accuracy with which vegetation properties and their change can be mapped and monitored using optical remote sensing. They found that the use of MIR radiation will be helpful in areas where vegetation attains a large biomass and / or the atmosphere features large aerosol loadings. They found the following results for vegetation, soil, and rocks.

Green leaves display a uniformly low reflectance (< 10 %) in the MIR spectral region. Despite this low reflectance, vegetation type specific responses attributable to leaf water content, leaf structure and biochemical constituents has been observed. MIR radiation is reflected at the outer epidermal surface of the leaf with about one – fifth or less of the reflection arising from the epidermal palisade boundary. Since transmissivity in this region is negligible, the rest of the radiation not reflected enters the parenchyma layer to be absorbed by the photosynthetic pigments. The spectral reflectance of senescent vegetation contrasts widely from that of fresh leaves. Liquid water is a major component of fresh leaves comprising between 40 % and 90 % of the fresh weight.

Soils have a relatively high reflectivity in the MIR spectral region, reflecting up to one third of the incident radiation. Reflectance types vary between soil types and are a function, to a lesser extent of its organic matter. The presence of organic matter in soil has the effect of reducing soil reflectance.

Rocks are generally less reflective than soils. However, they exhibit more distinctive spectral signatures exclusive to each rock type. Rocks display a broad reflectance maximum towards the middle of the MIR region.

3.3.6.4 Spectral separability of canopy vegetation from understory growth

Ghitter et al. (1995) produced a conifer understory map and inputted it into a GIS, to provide the basis for image training and development of class signatures, and calculation of separability measures. The overstory map was derived from a reconnaissance map supplied by the timber/ forest company. The discrimination between light and heavy understory was based on a threshold of 60 % crown closure in the understory interpreted on 1: 20 000 colour infrared leaf of metric aerial photographs.

Haralick and Fu (1983) computed a B – distance as a measure of statistical separability between pairs of signatures that were previously generated from training areas of understory polygons. B – distance is a measure of the probability of correct classification that has been used as a measure of discrimination between a set of classes based on a set of spectral bands. A pixel sampling program was employed to arrange Landsat TM data for each of the 71 sites that were used to field check the aerial photo interpretation into an attribute table. Digital Landsat TM data was used to discriminate among several combinations of coniferous understory within the overstory stands that are pure or predominantly deciduous. Training areas of understory polygons imported from the GIS had shown on average poor overall separability because the understory is often unevenly distributed within overstory stands. Mapped polygons are often an average descriptor of a forest stand.

3.3.6.5 Linear spectral unmixing and spectral mixture analysis

Linear spectral unmixing modeling assumes that each pixel's value is a linear combination of reflectance from a limited set of constituent elements called endmembers. Coops et al. (2006) demonstrates that for a given wavelength channel (*i*), the constrained pixel reflectance (R*i*) of a given reflectance can be expressed using Equation 1 and the constrained be equation 2.

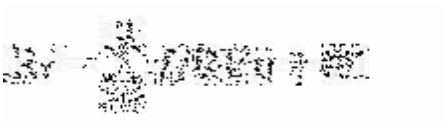

Equation 2

$$O \leq \sum_{J=1}^{n} fj \leq 1$$

Equation 3

Where f_j = the endmember image fraction, REij is the reflectance of image endmember j and band i, n is the number of endmembers, and $\in$ is the residual error of band i. If the number of wavelength channels is at least as large as the number of endmembers, then endmember spectral values observed in the field or using image interpretation, can be used to obtain estimates of the fraction of each pixel that is in the endmember. The method according to Coops et al. (2006) assumes that the reflectance from each pixel is a linear combination of each endmember and the fractional abundance are computed on a pixel by pixel basis. The assumption of linearity is arguably the most important problem with linear mixture modeling. Non linear mixture modeling can be expected in vegetation canopies as green vegetation transmission is high at certain wavelengths; however, in the shortwave infrared within coniferous forests, transmission is generally low making the assumption reasonable for most studies. Coops et al. (2006) used a minimum noise fraction (MNF) technique in ENVI to derive spectra of pure cover types by

transforming the spectral data into reduced number of channels containing independent information by reducing noise in the data. These new MNF transformed bands were then analyzed to find the most “spectrally pure” (extreme) pixels in the image using a Pixel Purity Index (PPI) classifier. Clusters of extreme pixels in the image were then displayed and through an iterative process which involves comparing spectra with ground - based collected reflectance spectra, examining spatial mapping of endmembers, and comparing it with local knowledge and field observations. A label was assigned to each “pure pixel” cover class (Coops et al., 2006).

Rashed et al. (2005) also investigated the spectral mixture analysis (SMA). According to their study, mixture models are based on the assumption that the landscape is formed from continuously varying proportions of idealized types of landcover referred to as endmembers. Endmembers are features recongnizable in the imagery as being abstractions of landcover materials with uniform properties. Through spectral mixture analysis, the areal fractions of the endmembers are quantified at the subpixel level, allowing the inference of morphological characteristics of the landscape in terms of the endmembers composition. Linear SMA is the process of solving for endmember fractions, assuming that spectrum measures for each pixel represents a linear combination of spectra endmember that corresponds to the physical mixture of some components on a surface weighted by surface abundance (Rashed et al., 2005).

3.3.6.6 Analysis of Leaf Area Index (LAI) and vegetation indices (VI)

Leaf area index (LAI) is a structural vegetation parameter of fundamental importance for quantitative analysis of many physical and biological processes related vegetation dynamics. LAI is defined as the half of the total all-sides green leaf area per unit ground surface area

(Xavier and Vettorazzi, 2004; Lu et al., 2005). Lu et al. (2005) used LAI 2000 (LI-Cor Inc, Lincoln, Nebraska) and TRAC (3rd Wave Engineering, Napean, Ontario) to measure LAI in an alpine meadow site. In each elementary sampling unit (ESU), they carried out nine LAI measurements evenly and densely within the 400 m^2 area. They also processed NDVI and Soil Adjusted Vegetation Index (SAVI) from Landsat ETM. They found LAI values to be mostly low (ranging from 0.2 to 1.2) within the base site. This attributed to the fact that alpine meadows have relatively fine leaved and short biome properties. However, some species found in the study site creep close to the ground and could have been difficult to measure by LAI 2000 and TRAC. The LAI measurements were overlaid with the vegetation indices maps derived from ETM using ENVI software. The pixel value of NDVI, Simple Ratio (SR) and Modified SAVI (MSAVI) in each ESU were then extracted. For the 31 retained elementary sampling units at the meadow base site elicits a positive correlation. The relationship between LAIs and VIs were non linear, but rather showed an exponential relationship. The standard deviations were high in the LAI/VI relationships, which might have originated from among others errors in the instrument operations, errors associated with cloudiness and wind conditions and errors due to time difference of phenological stages and the acquisition time of the ETM+ scenery. They concluded that the accuracy and consistency of in situ LAI measurements were strongly affected by weather conditions. They found useful relationships between ground LAIs and vegetation indices, and that the NDVI is the most promising estimator for the extraction of LAI in the Alpine meadows (Lu et al., 2005).

Xavier and Vettorazzi (2004) also examined the relationship between LAI (derived from ETM+ data) and LAI derived from field measurements together with those of vegetation indices. They used LAI 2000 to collect field LAI measurements. However, their measurements were

undertaken on cloudy days in order to avoid underestimations and always keeping the sensor in shadow. The measurements on sugarcane and corn were taken varying the sensor position between plant rows. Maximum and minimum LAI values were 4.48 and 0.47 for riparian forest and sugarcane, respectively. LAI values for the two plots of riparian forest were 3.21 and 4.48. LAI values for sugarcane ranged from 0.47 to 2.37. LAI estimates for corn were 1.49 and 2.11. The relationship between LAI and VIs (SR/NDVI and SAVI) was found to be similar. It was observed that NDVI and SAVI values increase faster for lower LAI values, tending towards stabilization for higher values. A better relationship was also observed for LAI/NDVI ($r^2 = 0.76$) compared to SAVI ($r^2 = 0.56$). They concluded that spectral vegetation indices derived from Landsat images can be successfully used in the estimation of LAI for different landcovers.

3.4 Review of Asbestos Dump Rehabilitation in other countries

3.4.1 Ontario, Canada

Ontario spent $27 million on a mine rehabilitation programme which focused on eliminating the risks to public safety. Workers in Ontario conducted a four year mine rehabilitation programme which was launched in September 1999 in the former North coldstream Mine near Thunderbay and at the former Hollinger mine in Timmins. At the North Coldstream mine site, buildings and mine structures were removed in Munch and Granding and it was indicated that the area would be revegetated in the summer 2000. There were also contracts to backfill physical hazards at the Kam Kotia mine. The sites for rehabilitation were to be assessed to ensure that rehabilitation dollars were spent more effectively by identifying locations where there were greater environmental risks (Ministry of Northern Development Mines, 2000).

3.4.2 New South Wales, Australia

The opencast asbestos mining was first introduced at Woodstreef in 1918 but ceased in 1923 as the production was not competitive with imported fibre. However large scale mining was carried out between 1970 and 1983 by the Chrysotile Corporation of Australia. The mine was closed due to financial difficulties despite the assistance from both state and federal governments. As a result very little rehabilitation has been undertaken. The company does no longer exist and the mine is categorised as derelict. In 1986, consultants prepared a government commissioned report which provided a range of options for site rehabilitation. The costs were estimated as high as $80.7 million (Mineral Resources New South Wales, 2000).

3.4.3 South Africa

South Africa is currently facing an epidemic of asbestos diseases but still not only the past practices are the problem. This is because about 2000 tonnes of Chrysotile asbestos is still used annually wherein seven companies employ three thousand workers to manufacture asbestos-containing building materials and pipes. Levels of environmental pollution are colossal, huge asbestos dumps including 82 in the Northern Cape alone are scattered throughout the countryside. The government has already spent R44 million (US$7.5 million) on rehabilitation of derelict and ownerless mines. It has been estimated that R52 million more will be needed to complete the task (British Asbestos Newsletter, 1999).

3.4.3.1 Asbestos Rehabilitation in the Northern Cape

According to Turkington (2000), only one out of 23 asbestos mines in the Northern Cape has been rehabilitated. This site is found at Koegas which is about 30 km from Prieska. It has been indicated that the rehabilitation process cost R7 million and was not properly done because the site is still covered with fibres. It is estimated that it will cost about R200 million to rehabilitate all the dumps in the Northern Cape which the Department of Minerals and Energy indicates that it will be unable to afford. Turkington (2000) further indicates that the department would spend R100 million over 15 years to rehabilitate the abandoned asbestos mines (Turkington, 2000).

3.4.4 Mitigation strategies

3.4.4.1 Mine rehabilitation in Zimbabwe

Asbestos mining activity in Zimbabwe has been undertaken since the early 1900's. There are many tailing dumps on the mining area. Gath mine alone spends Z$150000 a month on rehabilitation and another Z$250000 on reducing the dust pollution on a monthly basis. About 250000 square metres of Gath's dump area have been revegetated. Despite the rehabilitation process, Zimbabwe's chrysotile asbestos output was expected to increase in the year 2000 (Crankshaw, 1999).

3.4.4.2 Rehabilitation as part of mining process in Ontario, Canada

It is expected that every private company that begins either advanced exploration or mine production must provide a closure plan to rehabilitate the land to an acceptable state upon completion of exploration and mining activities. The rehabilitation procedure is that after various

stages of production, surface structures are removed, underground stability is assessed, tailing areas are assessed for both physical and chemical stability, and finally appropriate areas are revegetated to recover the land for other uses. There are a number of abandoned mines in Ontario which are more than a century old. Capping and backfilling of 31 sites across the province have already started. The Ontario government will spend Can $ 516,000 to work upon those sites. Capping involves the placement of an engineered concrete over the mine shaft (Ministry of Northern Development Mines, 2000).

3.4.4.3 The Dutch scenario for rehabilitation

Harms et al. (1993) developed the scenario ELK strategy which aims at developing wilderness and self sustaining complete ecosystems. The emphasis is on ecosystems with processes which are not managed by human beings. This strategy should secure ecological prerequisites over a long period of time. This strategy recommends that land uses that do not differ in the rate of change should be combined. These include nature conservation, recreation and forestry (Harms et al, 1993).

3.4.4.4 The situation of rehabilitation in South Africa

Section 38 of the Minerals Act of 1991 (Act no 50 of 1991) in the South African Mining legislation, stipulates that the rehabilitation of the surface of the land concerned in any prospecting or mining shall be carried out by the holder of the prospecting permit or mining authorization in accordance with the environmental management programme approved in terms of section 39 (Environmental management programme).

3.5 Imaging Spectroscopy and Field spectrometry applications and related Laboratory Techniques.

3.5.1 Background

Lucas et al. (2004) described extensively the subjects of imaging spectroscopy, field spectrometry and their relevant applications. This sections refers to their deliberations, focusing specifically on aspects relevant to this study and so to other studies elsewhere. According to Lucas et al. (2004), an improved technology based on spectroscopy was developed whereby the limited number of discrete spectral bands was enhanced by a series (nominally > 50 bands) of narrow (Full-Width-Half- Maximum (FWHM) of 2 – 20 nm) contiguous bands (Aspinall et al., 2002) over the VNIR and SWIR wavelength regions. Similar advances were also made in the thermal infrared (TIR) regions within the main aim of reducing the limitations posed by the multispectral systems. Matrices of spectral samples where then designed to be built up on a line by line basis to form a two dimensional image (*x*- and *y*-axes), with a third dimension (*z* axis) holding the spectral data for each sample (pixel). These new imaging spectrometers were subsequently able to retrieve near-laboratory quality reflectance spectra such that the data associated with each pixel approximated the true spectral signature of a target material, with sufficiently high signal-to-noise ratio (SNR) across the full contiguous wavelength range (nominally 400 – 250 nm) to ultimately form a *3*-dimensional datacube. Specific reflectance or absorption features could also be associated with different minerals or even biological and chemical processes, thereby providing an opportunity to better characterize surface environments and dynamics. With this advancement, the era of hyperspectral imaging was developed with airborne sensors deployed initially albeit largely for research purposes. Several spaceborne

hyperspectral sensors have also been deployed although, to date, the data have been used largely for technology demonstration and research.

Clark (1999) indicates that reflectance and emittance spectroscopy of natural surfaces are sensitive to specific chemical bonds in materials, whether solid, liquid or gas. He further emphasizes that spectroscopy has the advantage of being sensitive to both crystalline and amorphous materials, unlike some diagnostic methods, like X-ray diffraction. Spectroscopy's other main advantage is that it can be used up close (For example in the laboratory) to far away (For example to look down on the Earth, or up at other planets). Spectroscopy's historical disadvantage is that it is too sensitive to small changes in the chemistry and/or structure of a material. The variations in material composition often cause shifts in the position and shape of absorption bands in the spectrum. Thus, with the vast variety of chemistry typically encountered in the real world, spectral signatures can be quite complex and sometimes unintelligible. However, that is now changing with increased knowledge of the natural variation in spectral features and the causes of the shifts. As a result, the previous disadvantage is turning into a huge advantage, allowing us to probe ever more detail about the chemistry of our natural environment. Clark also attempted to define imaging spectroscopy. He recognizes that it has many names in the remote sensing community, including imaging spectrometry, hyperspectral, and ultraspectral imaging. Spectroscopy is the study of electromagnetic radiation. Spectrometry is derived from spectro-photometry, the measure of photons as a function of wavelength, a term used for years in astronomy. However, spectrometry is becoming a term used to indicate the measurement of non-light quantities, such as in mass spectrometry. Hyper means excessive, but no imaging spectrometer in use can hardly be considered hyper-spectral, after all, a couple of hundred

channels pales in comparison to a truly high resolution spectrometer with millions of channels. Ultraspectral is beyond hyperspectral, a lofty goal I do not believe we have reached. Terms like laboratory spectrometer, spectroscopist, reflectance spectroscopy, thermal emission spectroscopy, and others, are in common use. One rarely, if ever see the converse: spectrometrist, reflectance spectrometry, etc. So it seems prudent to keep the terminology consistent with "imaging spectroscopy."

3.5.2 Field Spectroscopy

Lucas et al. (2004) further emphasize on the use of field spectral measurements for the purpose of validating and calibrating data obtained using airborne and space borne sensors. They indicate that data acquired by airborne or spaceborne sensors cannot be considered in isolation since effective data interpretation requires a detailed understanding of the processes and interactions occurring at the Earth's surface. In this respect, a fundamental component of understanding hyperspectral sensors is the laboratory and field measurement of the spectral reflectance of different surfaces. A number of portable field and laboratory spectroradiometers have been developed for this purpose, ranging from the Milton spectroradiometer to the more advanced spectroradiometers that include the Analytical Spectral Devices (ASD) Fieldspec Pro FR and the IRIS spectroradiometer developed by GER (Table 2.1). Technological advances in a number of areas have led to improvements in the field of spectroscopy. Advances in spectroradiometer technology, specifically with respect to the electro-optical systems, have resulted in an increase in sensor sensitivity and a decrease in scan times, permitting greater data collection in a shorter period of time. This has enabled researchers to acquire high quality reflectance data rapidly, both in the field and under laboratory conditions. A second advancement has been the increase in the processing sophistication of computer technology and the reduction in the cost of data storage.

These technological improvements have also reduced the overall costs so that a greater number of users are able to acquire portable spectrometers, particularly for use in the field. Field spectroscopic studies are important in hyperspectral remote sensing for a number of reasons. The first is calibration of airborne and satellite-based image products. All remotely sensed datasets have been imaged through a variety of atmospheric conditions, which usually incorporate varying amounts of water vapour, CO_2, O_2, and particulate matter. In addition, imaging is carried out at various times of the year and, in some cases, during different times of the day and under sometimes highly variable atmospheric conditions. To account for this variability, image spectra can generally be compared to spectra that have not been affected by these conditions. One method is to capture spectra from a disparate range of pseudo-invariant targets (reference targets) at the time of remote sensing data acquisition. As these ground-based spectra are not collected through a large atmospheric path, they should be relatively free of the adverse "noise" influences that are common in spectra recorded by airborne and spaceborne sensors. By comparing spectra to those retrieved from the imaging spectrometers, these noise influences can be largely removed and the data can be converted from units of radiance to that of scale surface reflectance. The latter represents a simple standardization that allows comparison of spatially and/or temporally diverse data. The second reason is that field and laboratory spectra can be collated into spectral libraries which can be useful for a number of purposes. For example, field spectra of certain mineral assemblages can be used to train the classification of geologically diverse areas and have been used frequently to derive geological maps.

Table 3.1 Different types of field spectrometers (adapted from Lucas *et al*., 2004).

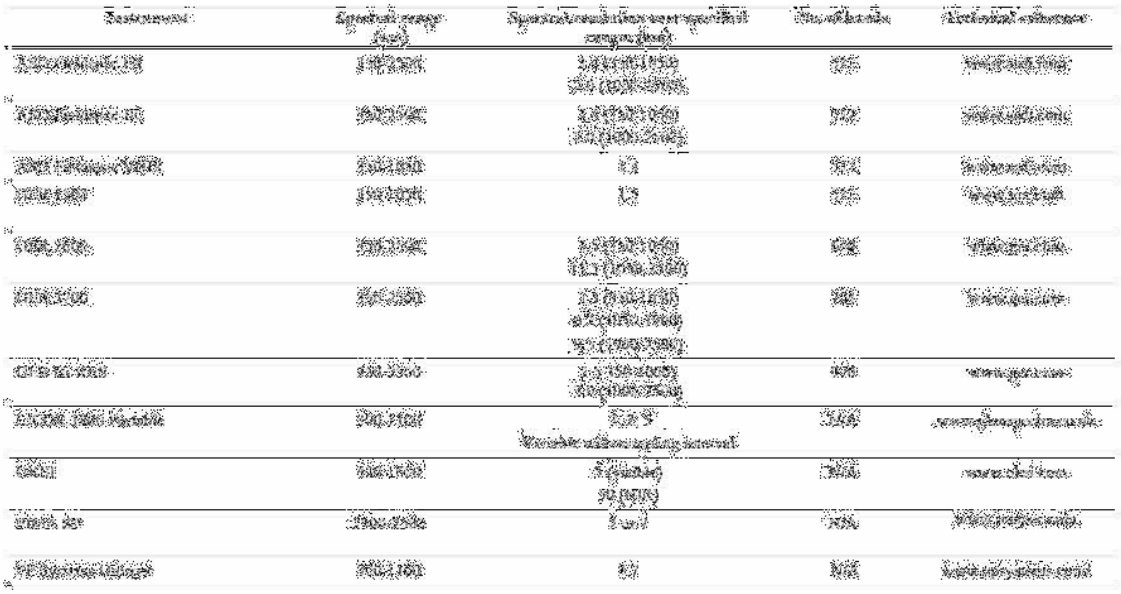

Lucas et al. (2004) elaborates that spectral libraries can also play a key role in selecting endmembers for subsequently spectral unmixing of hyperspectral data. This process decomposes individual pixels into their reflectance components based on a knowledge of and comparison with the spectral characteristics of known target materials. These known materials, also referred to as *endmembers*, are then used as references to decompose the pixels. Endmembers for spectral decomposition can be extracted by locating "pure" targets in the image through manual or automated techniques. Such an approach assumes that such pure targets exist in the image, which may be the case for very fine (< 1 – 2 m) spatial resolution images but becomes less likely as the spatial resolution coarsens (*esp*. mixed pixels). An alternative approach therefore is to use spectral libraries generated from field-based spectroscopy or even from the finer spatial resolution data themselves.

Much of the theory related to spectral endmembers has originated from minerals exploration applications with pure targets that do not vary greatly. However, it should be noted that the

spectral signatures of vegetation are dynamic in spectral-, spatial-, and temporal-space, and should cautiously be constructed into spectral libraries.

3.5.3 Vegetation applications

Hyperspectral sensors are well suited for vegetation studies as reflectance/absorption spectral signatures from individual species as well as more complex mixed-pixel community scale spectra can be utilised as a powerful diagnostic tool for vegetation sciences. The spectral geometry of vegetation signatures vary according to, for example, biochemical content and the physical structure of plant tissues, and is further influenced by phenologic factors and natural and anthropogenically induced factors creating a complex matrix of influencing variables. To "unscramble" the weighted influence of these variables upon the resultant vegetation spectral signature remains the perennial challenge to the monitoring of vegetation with hyperspectral systems. Lucas et al. (2004) showed that knowledge of the causes of variation in the spectral reflectance of vegetation (Fig. 3.1) has been fundamental to understanding the information content of spectra derived from ground-based or airborne/spaceborne spectrometers. In the visible (red, green, and blue) wavelength regions, plant reflectance is dictated by the amount and concentration of photosynthetic pigments, namely chlorophyll a, chlorophyll b, xanthophylls, anthocyanins and carotenoids. In the NIR wavelength region, the internal structure of leaves and, in particular, the size, shape and distribution of air spaces and also the abundance of air-water interfaces (and hence refractive index discontinuities) within the mesophyll layers exert the greatest influence on reflectance. Much of the radiation that is scattered within the leaf is reflected back through the leaf surface, with a proportion transmitted through the leaf. SWIR reflectance is determined largely by moisture content with water absorption features centred

primarily at 2660 nm and 2730 nm. SWIR reflectance is also influenced by leaf biochemicals such as lignin, cellulose, starch, proteins, and nitrogen but absorption is relatively weak and often masked by the more dominant water absorption features.

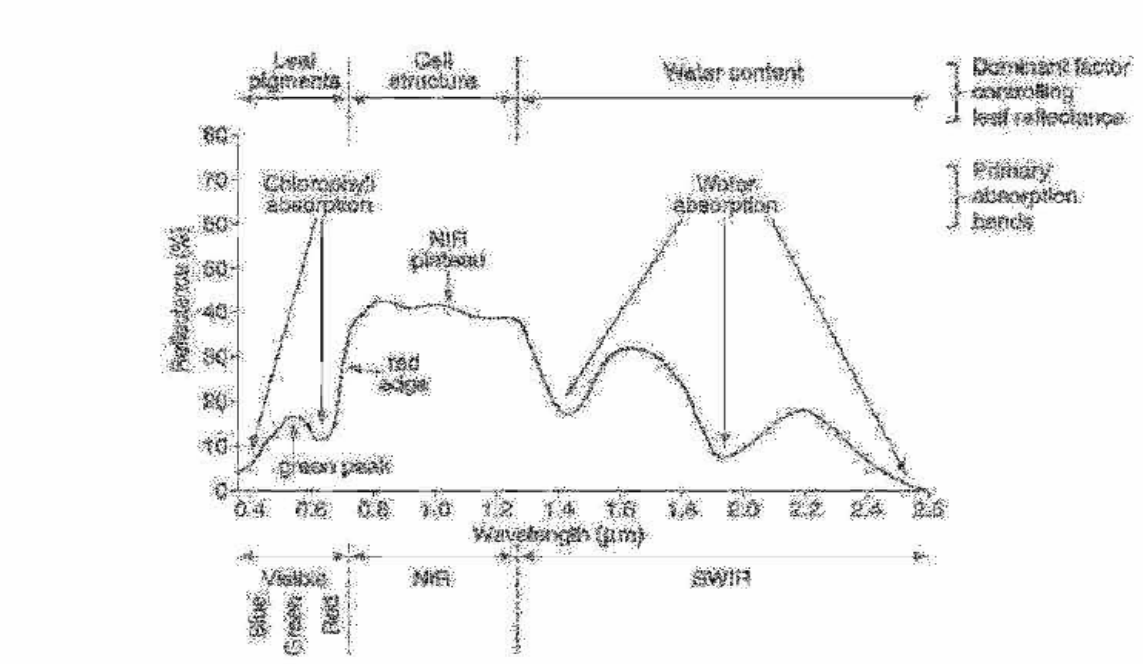

Figure 3.1 Typical spectral reflectance profile of vegetation.

Key descriptive elements of the vegetation spectral reflectance signatures include the green peak, the chlorophyll well, the red-edge, the NIR plateau, and the water absorption features. Of particular importance is the red-edge, which is defined as the rise of reflectance at the boundary between the chlorophyll absorption feature in red wavelengths and leaf scattering in NIR wavelengths. The red-edge, which displays the greatest change in reflectance per change in wavelength of any green leaf spectral feature in the VNIR regions, is identified typically using the red-edge inflection point (REIP) or point of maximum slope and is located between 680 and 750 nm regardless of species (Clark, 1999; Coops et al., 2006).

Clark (1999) divides spectra of vegetation in two general forms: green and wet (photosynthetic), and dry non-photosynthetic but there is a seemingly continuous range between these two end members. The spectra of these two forms are compared to a soil spectrum in Figure 3.2.

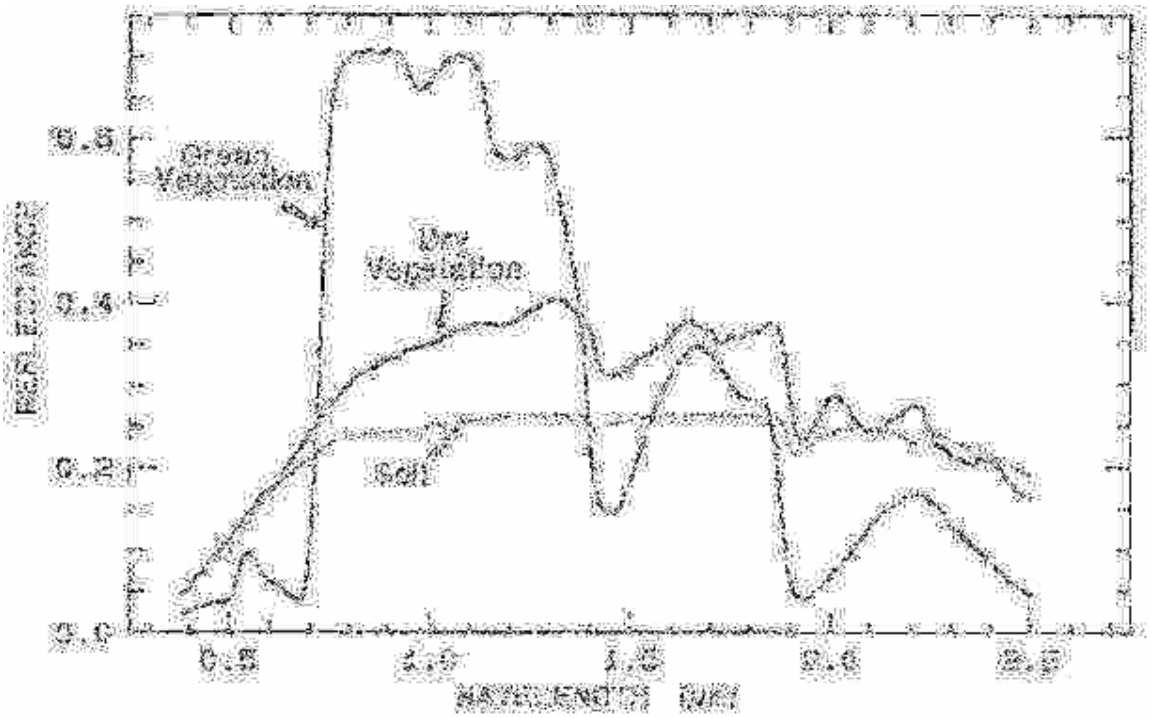

Figure 3.2 Spectra of vegetation at different phenological stages.

Because all plants are made of the same basic components, their spectra appear generally similar. The near-infrared spectra of green vegetation are dominated by liquid water vibrational absorptions. The water bands are shifted to slightly shorter wavelengths than in liquid water, due to hydrogen bonding. The absorption in the visible is due to chlorophyll. The dry non-photosynthetic vegetation spectrum shows absorptions due to cellulose, lignin, and nitrogen. Some of these absorptions can be confused with mineral absorptions, unless a careful spectral analysis is done.

Mutanga et al. (2004) investigated whether remote sensing can be used to detect the presence of certain minerals in plants of a rangeland environment. The main purpose was to discriminate different levels of sodium concentrations in grass. They used a Geophysical and Environmental Research Corporation (GER3700) spectrometer to measure the spectral reflectance of grass in the field. They also investigated the use of hyperspectral remote sensing techniques with narrow channels of less than 10 nm in estimating foliar sodium using the GER3700 spectrometer. The GER records measurements in the wavelength range of 350-2500 nm. It has a spectral sampling of 1.5 nm in the 350-1050 nm, 6.2 nm in the 1050-1900 nm range and 9.5 nm in the 1900-2500 nm range. The bandpass is 3 nm in 350-1050 nm, 11 nm in the 1050-1900 nm and 16 nm in the 1900-2500 nm range. From this study, they found a large range of foliar sodium concentration which resulted from sampling different species. Average amounts ranged from 0.02 percent in *Themeda triandra* to 0.2 percent in *S. ioclados*. They concluded that different species yielded different foliar concentrations of sodium. This was attributed to disparities among species in the uptake of sodium by the roots. They also classified the reflectance values according to three different levels of foliar sodium concentrations. They found the significant differences between low and medium classes for most wavelengths ranging from 560 nm to 730 nm. Significant differences between low and high sodium classes were found in the blue wavelength region (410-430 nm). Their study revealed that it is not only sodium concentration but also the mixture of species in different savanna environment affect spectral reflectance. The study provided important implications for using airborne and satellite remotely - sensed data to detect and map sodium concentration in grass (Mutanga et al., 2004).

3.5.4 Soils and Geological applications

Lucas et al. (2004) recognize that soils are complex and typically heterogeneous, so their properties therefore cannot be assessed easily and directly as a function of their composite spectral reflectance profiles, even under controlled laboratory conditions. The entire vertical soil profile cannot be imaged using multispectral or hyperspectral sensors and inferences have to be made about the soil based on the surface veneer. In most cases, vegetation (dry or green) obscures the soil surface either partly or completely. Using reference reflectance spectra from soil samples and established procedures, the relationships of soil organic carbon (SOC) to moisture, exchangeable calcium and magnesium cation exchange capacity and also soil colour were able to be quantified. Many of these variables actively influence the response across the reflectance region and, for this reason, only a small selection of spectral channels is required for their quantification. Colour is also a key attribute as it allows characterization, differentiation and ultimately classification of soil types. In general, colour is determined by the amount and state of iron and/or organic matter (OM) contained, with darker soils tending to be more indicative of higher OM contents, although manganese can also produce dark colouration. The colour of soils with low OM is often dominated by pigmenting agents such as secondary iron oxides. As many mineral components of rocks and soils have distinct spectral signatures, hyperspectral data have also played a key role in identifying and mapping expansive soils.

Geological applications have been the principal driving force behind much of the early development phases of imaging spectrometry. The development can be attributed partly to the recognition that a wide range of rock forming minerals, have distinct spectral signatures. Numerous publications have provided detailed laboratory spectra of rocks and minerals and their

mixtures as well as accurate analyses of absorption features, many of which have been obtained from laboratory measurements. These serve as spectral references obtained by ground radiometers or airborne/spaceborne sensors, with spectroscopic criteria applied to identify and map minerals and alteration zones.

Despite the availability of suitable reference sources, spectral references use in rock-type matching has been complicated by several interacting variables including original parent mineral associations, diagenesis, transformation/alteration through time and micro- to macro-scale morphology. A further limitation is that the dominant mineral components of a rock, which generally determine their petrographic classification, do not necessarily produce the most prominent spectral features. Even so, dominant spectral patterns produced by minor mineral components with strong absorption features can significantly assist to characterise rocks, at least within well constrained geological settings.

Clark (1999) has demonstrated the sensitivity of absorption bands to chrystal structure and chemistry. Spectroscopy is an excellent tool not only for detecting certain chemistries, but also at abundance levels unmatched by other tools. For example, each layer of a layered silicate absorbs radiation almost independently from its neighbors. The absorption of photons does not depend on the longer range crystallographic order as is required to give distinctive X-ray diffraction patterns. Thus, many processes, for example clay dehydroxylation, are detectable with spectroscopy before other methods. Spectroscopy is more sensitive to the presence of clays, iron oxides, iron hydroxides, quartz, and other minerals with strong absorption bands at levels significantly lower than other methods such as X-ray diffraction. In OH examples, the sharper

OH-related absorption bands allow smaller band shifts to be measured. These bands can be so sensitive that it is possible to distinguish between the isochemical end-members of the Mg-rich serpentine group, chrysotile, antigorite, and lizardite (Fig. 2.3). The Fe:Fe+Mg ratio can be estimated from reflectance spectra of minerals with brucite-like structure (Fig 3.3).

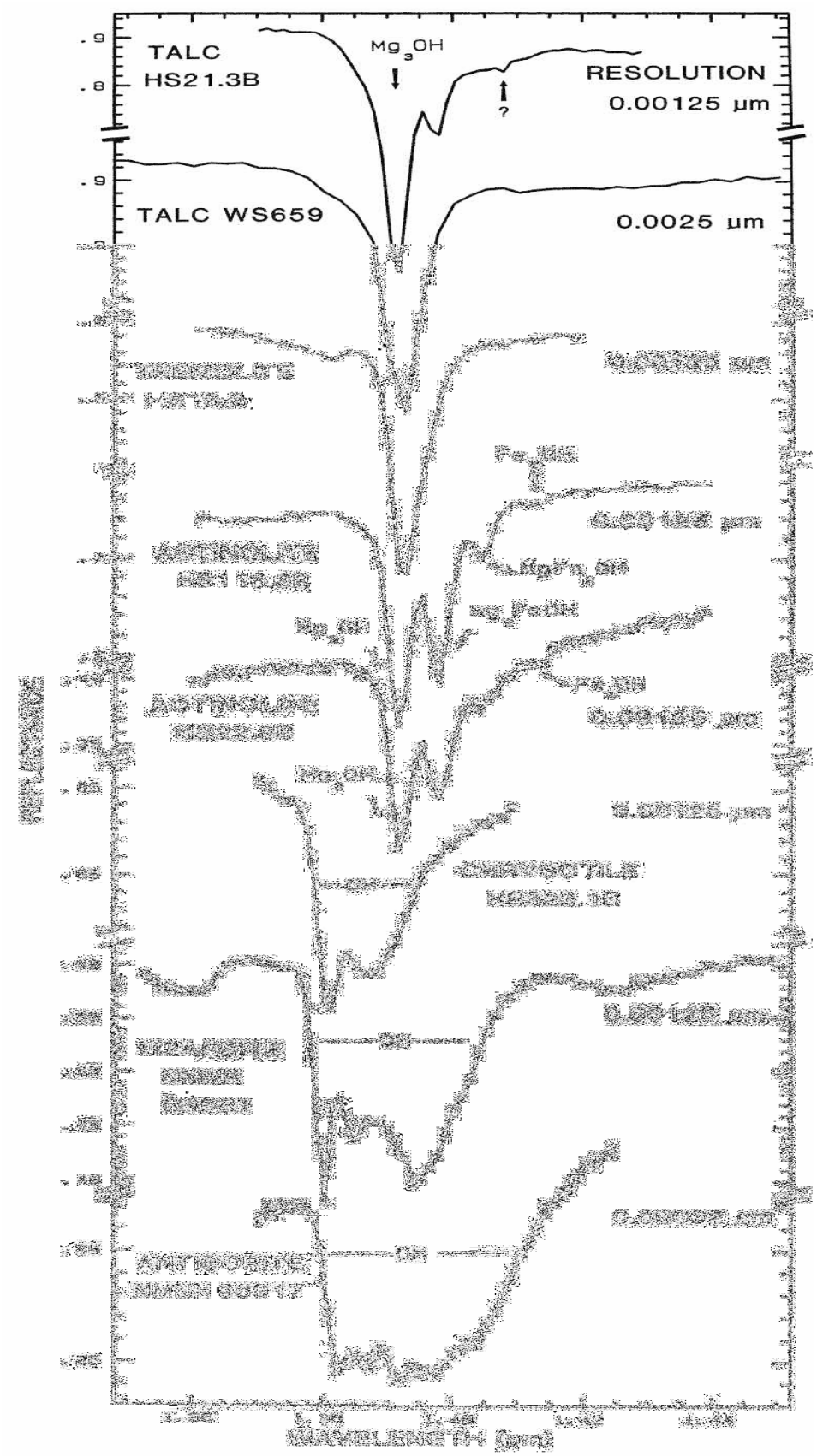

Figure 3.3. High spectral resolution reflectance spectra of the first overtone of OH in talc, tremolite, actinolite, crysotile, lizardite, and antigorite. The three sharp absorption bands in talc, tremolite and actinolite are caused by Mg and Fe ions associated with the hydroxyls, causing small band shifts. The Fe:Fe+Mg ratio can be estimated. In chrysotile, lizardite and antigorite, the absorptions change with small structural differences even though the composition is constant (from Clark *et al*., 1990a).

Saldanha et al., (2004) investigated the effectiveness of discriminant analysis techniques to discern different types of soils that originates from serpentinites, mylinitic schists rocks, to mafic volcanic rocks and the encasing rocks that are found in the Cero Mantiqueira region, in southern Brazil. They used a GER Mark V-IRIS Spectroradiometer in the laboratory environment to measure the spectral characteristics of soil, with the aim of correlating the spectral reflectance data with the mineralogical and chemical composition of soils. They also used the United States Geological Survey (USGS) Digital Spectral Library to interpret the resulting spectral curves. The first group was characterized by two strong absorption bands at 1400 nm and 1900 nm, and two weaker absorption bands at 2000 nm and 2500 nm, due to vibrational processes caused by the radial OH and the second group by a higher albedo. They found that the first component accounts for the total reflectance, or albedo, of the sample. The second component relate to the sample's curve of the spectral reflectance between the visible and the near infrared portions of the electromagnetic spectrum. The third component reflected the sample's iron bearing minerals and calcium/ magnesium bearing minerals. They concluded that the analysis may be helpful in understanding the soils chemical and mineral composition based on its spectral features.

Torres-Vera and Prol-Ledesma (2003) used Landsat TM to identify the presence of key minerals in mineral exploration. They identified the presence of oxides and hydroxyl-bearing minerals in the Guanajuato district in Mexico. They used different methods of spectral enhancement to determine hydrothermally altered areas. Hydrothermal alteration may be indicated by the presence of iron oxides and hydroxyl, they are frequently identified as surface manifestations of mineralized zones. These minerals have spectral features in the visible and infrared parts (0.4-1.1 μm) of the electromagnetic spectrum. The main problem in the identification is the

interference of vegetation that has a strong reflectance in the infrared. The abundance of iron oxides helps in the identification of altered rocks because their spectral characteristics affect TM bands in the part of the visible to the middle infrared part of the electromagnetic spectrum (0.4 to1.1 μm). The jarosite spectrum showed a well defined absorption features at 0.43 μm and 0.92 μm, haematite has a reflectance minimum at 0.85 μm and goethite at about 0.94 μm. Torres-Vera and Prol-Ledesma (2003) have observed that absorption anomalies at wavelength less than 0.9 μm is a good indication that haematite is the predominant mineral. The middle infrared region contains high reflectance anomalies for most hydroxyl-bearing minerals and, sulphates and carbonates at about 1.65 μm with high absorption at approximately at 2.2 μm. Vegetation absorption features from 0.45 μm to 0.68 μm related to water content, and high reflectance in the near infrared, between 1.6 μm to 2.2 μm due to chlorophyll content in leaves. These water absorption features are also observed in the spectra of minerals that contain water or OH^- in their chrystalline structure. Iron oxides and vegetation have similar reflectance in TM 1(0.45-0.69 μm) and TM 2(0.52-0.60 μm) and as such this makes it useful for these bands to separate both minerals. From the reflectance plots for minerals and vegetation, Torres-Vera and Prol-Ledesma (2003) observed that the spectrum region covered by TM 3(0.63-0.69 μm) shows a high reflectance from iron oxides and a strong absorption for vegetation. Band 4 which is typical used for identifying vegetation, also has an absorption feature for iron oxides at 0.9 μm, which can separate oxides from vegetation. TM bands 5 and 7 were found to be helpful in differentiating vegetation from hydroxyl and iron oxides because they have distinct reflectance curves. They obtained best results using TM5, TM4, TM1 combinations, where the high albedo of altered areas and the distinctive spectral features in the middle infrared allow delineation of few areas. They concluded that detailed processing of selected areas made it possible to decrease

the interference due to the response of other materials present in the Guanajuato image and a good identification of areas where altered rocks predominate in the rock outcrops.

3.5.5 Applications of Reflectance Spectroscopy to the detection of Asbestos Minerals

Clark et al. (2003) undertook a study utilizing reflectance spectroscopy to detect certain asbestos minerals. They tried to differentiate asbestiform amphiboles from the vermiculite in the Libby mineral deposit, Montana. Detection of asbestiform amphibole contamination proves to be difficult in certain situations. For example, in the case of Libby vermiculites, amphibole fibers can grow in between vermiculite layers. The index of refraction of vermiculite and the tremolite-richterite-winchite amphibole compositions found at Libby are nearly identical, thus normal optical microscopy methods will likely not be able to distinguish the presence of embedded amphiboles. Surface methods such as Transmission Electron Microscopy (TEM) and Scanning Electron Microscopy (SEM) do not probe into the vermiculite grains. In other cases, the fibers may be too small to easily detect with standard optical microscopy methods. Therefore Clark et al. (2003) used the reflectance spectral properties of geologic materials from the Libby region and showed how reflectance spectroscopy can be used as a rapid assessment tool.

3.5.6 Laboratory Techniques for Assessment of Asbestos

3.5.6.1 X-Ray Diffraction Method

X-ray diffraction is coherent elastic scattering of x-rays by atoms or ions in a crystal. Because the wavelength of photons with energy of order 10 KeV (kilo electron volts) is a little smaller than the spacing of atoms in solids, a crystal will act as a sort of diffraction grating for x-ray. As

a crystal is three dimensional, the diffraction conditions are more stringent than for a two-dimensional grating. For certain alignments of the crystal and detector relative to the x-ray beam, all atoms in the crystal scatter in phase. Characteristic x-rays can be generated by bombarding a metal target with electrons sufficiently energetic to knock a core electron out of a metal ion. A characteristic x-ray is emitted when an electron from a higher energy level makes a transition to fill the vacancy. The principal quantum number of the vacancy (n = 1, 2, 3,...) is designated by K, L, M, ... respectively. The principal quantum number of the upper level of the transition, relative to the vacancy, is indicated by a subscript α, β ,δ ,... Fine structure levels are indicated by a further numerical subscript. Thus $K_{\alpha 1}$ and $K_{\alpha 2}$ designate x-rays due to vacancies in the lowest core level (n=1) being filled by a transition from the next level (n=2), specifically from the $P_{3/2}$ and $P_{1/2}$ angular momentum states of n=2, respectively (University of Virgnia, 2006).

3.5.6.2 ICP-MS Analysis

Inductively Coupled Plasma-Mass Spectrometry (ICP-MS) is a technique for multi-element analysis. In a single scan in the semi-quantitative mode the analyst is able to acquire estimates on practically every element in the periodic table. In the quantitative mode accuracy and precision is comparable to existing techniques for every calibrated element. Samples for trace metals analysis are acid digested on a hot-plate to solubilize the elements of interest. The digested solutions are pumped into the plasma as a liquid stream at the rate of about 1 mL per minute with a peristaltic pump. At temperatures of 5000-8000°K in the argon plasma, all compounds in the sample stream are dissociated into their most basic components elemental ions. The success of ICP in producing the stream of ions for MS analysis relies on two features: attainment of a controlled environment of sufficiently high temperature for dissociation and ionization of

elements and rapid sample throughput. From the plasma, the ion stream enters a vacuum through a pinhole. The ions are focused by a series of voltage modulated lenses into the quadrupole mass analyzer which only allows ions of a single mass-to-charge ratio through at a time. Ions are directed into an electron multiplier to increase the signal and be detected. It typically scan the range from mass 2 to 300 atomic mass units. The ICP-MS is not capable of distinguishing between two sources of signal at a single mass. For example, 58Ni is the most abundant isotope for Ni and would therefore provide the greatest number of ions for low level measurement. However, 58Fe interferes. Other interferences are molecular ion combinations arising from the sample matrix (oxygen, nitrogen, carbon, chloride) and the plasma itself (argon). 80Se is the most abundant isotope for selenium, but there is interference from 40Ar40Ar+ at mass 80. 77Se is interfered with by 40Ar37Cl. The analyte masses used for quantitative measurements are carefully chosen to avoid problems with isotopic as well as molecular overlaps. Every instrument has its own set of limitations and the ICP-MS is no exception. However, the ICP-MS multi-element measurement capability coupled with high sensitivity offers a highly efficient approach to routine monitoring and research activities. High sample throughput and very low detection limit capability (lower than the graphite furnace) makes this instrument an important advantage for the analysis. The ability to perform qualitative analysis in a single scan for a quick survey is a unique and powerful feature. The ICP-MS has become one of our most important techniques for assessing environmental pollution (Alforque, 1996).

3.5.6.3 Laboratory Properties of Libby Vermiculite and Amphiboles

Clark et al. (2003) measured the reflectance spectra of thousands of Environmental Protection Agency (EPA) samples of rocks, soils, and other materials from the Libby, Montana region.

Several dozens of these samples have also been analyzed by X-Ray Diffraction (XRD), Scanning electron microscopy (SEM) with energy dispersive spectroscopy for elemental compositions, and Electron Microprobe for elemental compositions. From these analyses, they found that the "Vermiculite" ore contains at least 3 sheet-silicate phases: vermiculite, hydrobiotite (mixed layer vermiculite-biotite), and biotite. The above 3 minerals were then referred to as "vermiculite." Electron microprobe analyses of 30 samples shows the Libby amphiboles have a range of compositions spanning 6 different mineral names. While the spread of compositions cover 6 amphiboles, each individual sample from the 30 collection locations show smaller compositional range. The average of the 30 falls into the winchite category, but individual samples we used in testing straddle the richterite-winchite border. For simplicity, hereafter, the compositions used in testing are referred to as "richterite," or "Libby amphibole." The Libby minerals display different levels of electrostatic charge. Each vermiculite, hydrobiotite, or biotite flake has shown some electrostatic charge, some more than others. Biotite flakes show the least charge, vermiculite the most. Ultrasonically washed "vermiculite" flakes still show charge. Richterite grains show significant charge. Richterite has been observed to electrostatically cling to vermiculite flakes.

Richterite grains have been observed to electrostatically jump to and/or cling to rubber, glass, porcelain, aluminum, and Libby vermiculite ore. The closest analogy to the observed properties is "the richterite grains appear like iron filings with everything being a magnet." These extreme electrostatic properties imply unusual mixing properties which make standards difficult to prepare. Libby amphibole fibers sometimes grow between vermiculite layers. The index of refraction of vermiculite and the tremolite-richterite-winchite fiber compositions are nearly identical (vermiculite = 1.55-1.58, biotite = 1.61-1.70, tremolite = 1.61, Actinolite = 1.64:

Hurlbut and Klein, 1993). Thus, normal optical microscopy methods may have difficulty distinguishing the presence of the Libby amphiboles intergrown with vermiculite and perhaps biotite (biotites tend to be very dark at optical wavelengths, adding additional difficulty). Surface methods such as TEM and SEM do not probe inside the vermiculite grains. In other cases, the fibers may be too small to easily detect with standard optical microscopy methods like PLM.

3.5.6.4 Standards for Testing Spectroscopy Methodology

The USGS (Clark et al., 2003) has been funded by the EPA to develop a set of standards for testing methodologies to detect Libby amphiboles. Briefly, selected materials have been collected, ground and/or sieved to various grain sizes, appropriate fractions weighed, and physical mixtures created with soils and powdered minerals. Among the concerns in standards preparation is uniformity on some reasonable scale so that methods can obtain close to the same answer within some error limit if that method was valid. For example, if testing needs 1% accuracy, the standard should be uniform on the scale of the sample measurement to at least 1%. The electrostatic properties noted above poses challenges in preparation of uniform standards. As a result, we have constructed numerous test standards to find a good procedure that can be used on a large scale. We produced standards with small-scale heterogeneity as well as small-scale homogeneity. Thus, the standards provide a possible cross section of different mixtures and uniformity that might be encountered in natural samples from the Libby region.

Of the methods being tested in this program, including PLM, SEM, TEM, XRD, and Reflectance Spectroscopy (RS); RS can rapidly probe the largest physical sample volume. Near-infrared spectrometer can probe, for example, millimeters to many square meters in area. Photons

penetrates tens of microns to several millimeters into a sample, depending on wavelength. This means that milligrams to kilograms of sample may be probed with RS. Thus, while uniformity may be an issue with some methods and some scales, RS can be used to probe the largest volume of material in a single measurement thus providing, in theory, a more uniform answer independent of small scale heterogeneities in the sample. These standards, regardless of their uniformity, provide interesting tests of different matrices to which the amphibole is added and thus test a likely range of conditions that may be encountered in the real-world. They constructed mixtures using quartz, Libby soils, Denver Federal Center soils, and Libby vermiculite. Because Libby vermiculite may contain richterite fibers, we washed vermiculite flakes in an ultrasonic bath 19 times (14 times in water, 5 times in isopropyl alcohol). SEM images showed some flakes still contain richterite. Libby vermiculite includes some tremolite/winchite/richterite amphibole and the standards of vermiculite plus richterite therefore show more scatter in the lower concentrations. Amphibole used in the standards was obtained from fibrous amphibole veins at the Libby mine site. In general, standards were prepared for about 10% and less amphibole by weight. An exact listing of every standard will not be provided here as some standards are currently being used in blind tests at EPA and contractor laboratories. They concluded that reflectance spectroscopy can detect Libby amphiboles with detection limits near 0.5 wt % amphibole on unprepared samples. In some samples, those with a weakly absorbing matrix, detection limits are as low as 0.01 wt %, using currently available commercial portable field spectrometers. Increasing spectral resolution (using commercially available laboratory spectrometers) can improve detectability up to about 5 times (0.1 wt % on typical Libby samples and to about 0.002 wt % on weakly absorbing samples). Reflectance spectra measured on unprepared samples can achieve excellent signal-to-noise ratio in about 0.5 minutes. More than

60 samples can be measured per day by a 2-person team (5-minutes per sample), including necessary calibrations. With efficient sample handling, this number can be doubled. Analysis of Libby and World Trade Center samples to date show that reflectance spectroscopy can be an effective rapid screening tool. Reflectance spectra are a digital record of the sample. Thus in the future, better algorithms could be applied to the same data if lower detection limits become important. Analysis can be minimally biased by a human, and, depending on the algorithm, analysis can be automated. Reflectance spectroscopy can be deployed in a laboratory, in the field, and from aircraft. As a rapid screening tool, reflectance spectroscopy can reduce analysis loads on more expensive but detailed analyses using the "sieve" analysis methods.

A similar approach was used in South Africa by IOM Consulting (2003), but focused only on laboratory analysis. The aim was to collect representative samples from each grade of vermiculite, split them and analyse them for asbestiform mineral and crystalline silica to detect the presence of asbestos fibres. They carried out initial examination using stereo-binocular microscopy and polarised light. A portion of each sample was examined for the presence of fibrous asbestos minerals at X8 - X40 magnification, using stereo-binocular microscopy. Any fibres detected, were mounted in appropriate refractive liquid and identified at 125X magnification using Polarized Light Microscopy (PLM) and dispersion staining microscopy. Quantitative assessment of amphibole asbestos by electron microscopy and X-ray diffractometry was then carried out for samples in which asbestos fibres were detected. In this instance, this was not done as there were no fibres identified. For crystalline silica, a portion of each sample was ground up and analysed using X-ray diffraction techniques using modified versions of MDHS 51/2 and MDHS 76. Additional preparation of the Superfine PP&V sample was done to achieve a lower detection limit. In their findings, Polarised Light Microscopy examinations did not detect

any amphibole or chrysotile asbestos fibres present in any of the samples of vermiculite. As there were no amphibole or chrysotile asbestos fibres detected in any of the samples of vermiculite collected, quantitative analysis of the vermiculite materials was not undertaken. X-ray diffractometry did not detect any crystalline silica in any of the samples of vermiculite. They concluded there is no significant asbestos-related health hazard. The same applied to the chrytalline silica analysis.

3.6 Summary

Remote sensing technology plays a significant role in various sectors of development which are affected by degradation. It reduces costs and time that originally would have taken a longer form when conducting field surveys for environmental assessments. Calibrations of remotely - sensed data with laboratory analysis are making satellite data more reliable for decision making.

CHAPTER FOUR

METHODOLOGY

4.1 Introduction

This chapter describes the research methodology used in this study. This includes the research design, the methods of field data collection and the acquisition, processing analyses and interpretation of remote sensing satellite data. The results are presented as maps, images and statistics in a form of tabular and graphical representations.

4.2 Research design, data requirements and sampling procedure

The design is that of a post-test only control group (Saidi, 2000). This design involves the selection of samples where apriori observation is not required before the treatment of sample sites. This design was deemed necessary because the data was collected after the mining process has been decommissioned. It does not require much information about the environment before the mining activity started as it would usually be the case in other experimental designs. This research method used is a quasi-experimental design.

Experimental and control sites were selected. The control sites were selected from natural sites with minimal anthropogenic disturbance at Potlake Nature Reserve. The experimental sites were selected from former mining sites and asbestos dumps that have been either, rehabilitated, partially rehabilitated or not rehabilitated.

Information about the sites was acquired from multidate satellite imagery and current field observation data. The remotely sensed images obtained from previous years are used to assess pre-test conditions. Current images and images acquired after the mine rehabilitation process was completed were used to assess the post-test conditions to assess any significant changes in a mining environment over a specified time period.

Other data about the sites included both primary and secondary data. Primary data was collected by undertaking field surveys. This involved physically observing and characterizing sample sites with the purpose of obtaining ground truth data. These surveys were significant in validating data obtained from satellite imagery. A Global Positioning System (GPS), an Analytical Spectral Device (ASD) Field Spectroradiometer, an AccuPar PAR/ LAI Ceptometer, and a camera were used in field data collection. Soil and water samples were also collected for analysis in the laboratory. Details on primary data collections are explained in the following sections. Secondary data was mainly collected in the form of official statistics, documents, reports and maps obtained from government and research institutions. Data on various factors (including land use) affecting natural resources have been acquired.

The underlying purpose of this research was to use remote sensing and geographic information system (GIS) to monitor environmental conditions in the post mining situation. The monitoring aspect guided the sampling procedure in order to effect long term satellite derived observations. The original sampling method used in both Mafefe and Mathabatha for selection of sites was based on systematic stratified sampling as described in Petja (2001), which stratified the area according to systematic quadrats. This

stratified systematic sampling was informed by the fact the area is relatively homogeneous despite the disturbance by the mining activity (Petja, 2001). The purposive nature of the this study led to the selection of more sample sites through a systematic random sampling procedure. This was done in order to cover sites significant to the research as determined from the field surveys. The use of GPS helped in marking sites for permanent monitoring.

4.3 Field data collection

Field surveys were undertaken to characterize the vegetation cover of the sample sites, to conduct physical observation of degradation sites and to verify satellite data. The study location is shown in Fig 4.1 overlaid with sample sites. A total of thirty six survey points (Appendix III) were selected for the physical observation of rehabilitated, partially rehabilitated and un-rehabilitated sites classified as experimental and natural sites classified as control sites. Seventeen sites were identified in the undisturbed nature reserve adjacent to the study area as control sites, whereas experimental sites included eight sites in Mathabatha (Bewaarkloof) and eleven in Mafefe. The surveys determined vegetation establishment on rehabilitated sites and assessed the extent to which revegetation affects degradation.

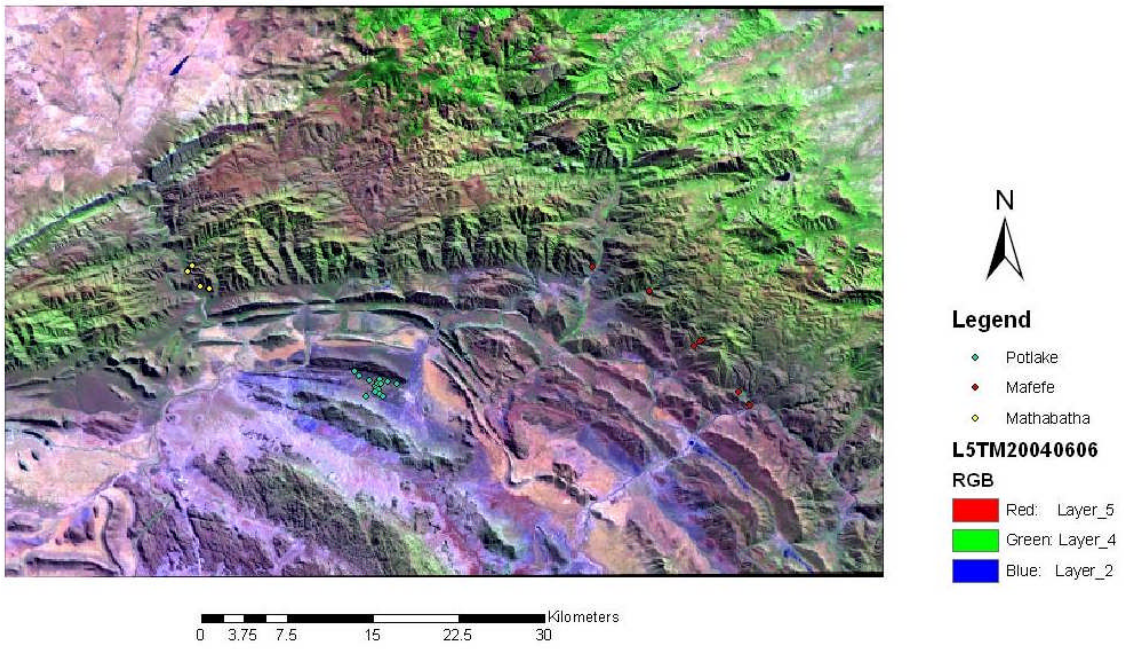

Figure 4.1 Landsat TM image showing locality of the control and experimental sites in the study area.

4.4 Satellite imagery acquisition

The Landsat Thematic Mapper (TM) images (1989-2004) were obtained at level 1 b format from the Council for Scientific and Industrial Research - Satellite Applications Centre (CSIR-SAC). Two scenes (169/077) per year were acquired for both dry and wet seasons (Appendix III).

4.5 Image processing (Landsat TM)

Several image processing techniques described below were applied to the acquired set of imagery. Normalized Difference Vegetation Index were processed and interpreted for change detection analysis.

4.5.1 Radiometric Normalization

Radiometric normalization was applied to a set of images using sensor calibration parameters in order to ensure consistence in multidate images for analysis. Almeida–Fihlo and Shimabukuro (2002) recommends that the influence of the sensor system factors affecting satellite images is partially minimized by using multidate images acquired by the same sensor. They further show that to minimize variations in the spectral response of the ground targets, cloud free images should be used and images should also correspond to the dry season such that they are imaging vegetation cover under similar phenological conditions. To compensate for variations in sensor radiometric responses over time and for variations in natural conditions of solar irradiance and solar angles, digital numbers (DN) were converted to reflectance values. During this process image pixels were converted to units of absolute radiance using 32 bit floating point calculations. Pixels values were then scaled to byte values prior to media output. The following equation was used to convert DN to radiance in a model run in ERDAS using calibration parameters obtained from the header files of raw images.

Radiance = gain*DN+offset Equation 4

which is also expressed as:

Radiance = ((LMAX-LMIN)/(QCALMAX-QCALMIN))*(QCAL-QCALMIN)+LMIN

where: QCALMIN = 1

QCALMAX = 255

QCAL = Digital Number

The LMINs and LMAXs are the spectral radiances for each band at digital numbers 1 and 255. For clear Landsat scenes a reduction in between scene variability is achieved through a normalization of solar irradiance by converting spectral irradiance to reflectance.

4.5.2 Atmospheric Correction

Electromagnetic energy passing through the atmosphere is often distorted depending on the wavelength. This normally takes a form of absorption, reflection, scattering and fluorescence. Scattering has the largest effect and is dependent on fluctuating gas concentrations. Different models are used for atmospheric correction. The model used in this case was the radiative transfer model (RTM). This model calculates the *effect* present aerosol concentrations have on electromagnetic radiation and corrects it on the image. The RTM models implemented in ERDAS are ATCOR 2 and 3. Once an Atmospheric Correction Configuration window is opened in ERDAS, an input image is selected for correction. The parameters are set to ATCOR3 under the elevation information subwindow and sensor type to Landsat TM with the pixel size of 30m and also putting the relevant date, together with the calibration file under sensor information. Atmospheric definition area is set to rural input with the condition and thermal atmospheric definition of the area. Correction parameters which include sun angles and a radiance to temperature conversion factor are also set. The correction is then run to derive outputs.

4.5.3 Geometric Correction

The images were obtained in a level 1 b format. Geometric corrections were undertaken using ERDAS Imagine version 8.7. The images were geometrically corrected using an orthorectified Landsat ETM (Enhanced Thematic Mapper) image of the same area acquired 22 August 2000. A spatial interpolation method was used to geometrically correct the images. This is a common way of creating a geometrically correct image of XY coordinates. The least square regression is applied to establish the relationship between two sets of variables. That basically means using ground control points (GCPs) and a computation of Root Mean Square (RMS). From the ERDAS Imagine an icon on Data Prep is clicked to display a data preparation window. Then an image geometric correction icon is clicked which provides an opportunity to select a geo correction input file (an image to be rectified). The geometric model was set to polynomial. The images were projected to a Universal Traverse Mercator (UTM) projection at a spheroid and datum name of World Geodetic System 1984 (WGS 84). The UTM zone was set at 35 south. A Geo - Correction Tool and a reference image was displayed with a GCP Tool window showing the X and Y coordinates of both the input (uncorrected) and reference image. A total of 25 control points were selected and referenced using the Geo Correction Tool for the whole 169/077 scene. The rectified image was subset into a new image covering four corners of the study area for further processing and analysis. Similar geometric correction steps where followed as described above to rerectify the subset image. However in this case only a total of 10 GCPs were used equally distributed over the image (Figure 4.2) as guided by the reduced size of the subset image. A total RMS error of 0.0003 was achieved for the final product.

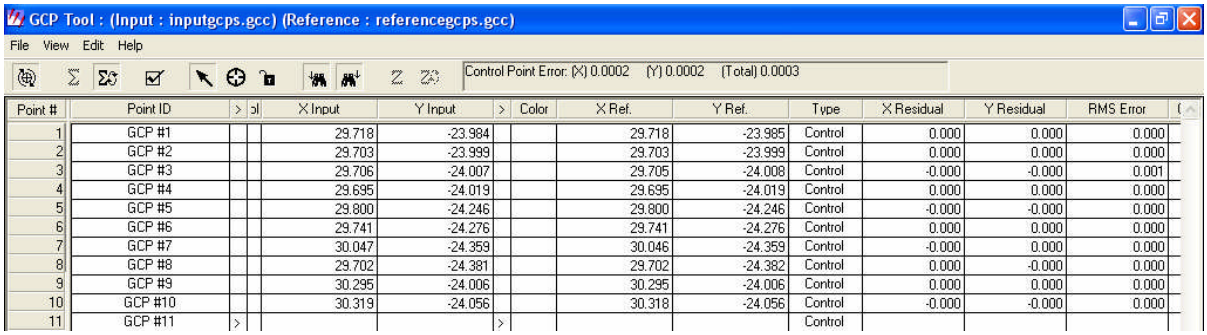

Point #	Point ID	X Input	Y Input	Color	X Ref.	Y Ref.	Type	X Residual	Y Residual	RMS Error
1	GCP #1	29.718	-23.984		29.718	-23.985	Control	0.000	0.000	0.000
2	GCP #2	29.703	-23.999		29.703	-23.999	Control	0.000	0.000	0.000
3	GCP #3	29.706	-24.007		29.705	-24.008	Control	-0.000	-0.000	0.001
4	GCP #4	29.695	-24.019		29.695	-24.019	Control	0.000	0.000	0.000
5	GCP #5	29.800	-24.246		29.800	-24.246	Control	-0.000	-0.000	0.000
6	GCP #6	29.741	-24.276		29.741	-24.276	Control	0.000	0.000	0.000
7	GCP #7	30.047	-24.359		30.046	-24.359	Control	-0.000	0.000	0.000
8	GCP #8	29.702	-24.381		29.702	-24.382	Control	0.000	-0.000	0.000
9	GCP #9	30.295	-24.006		30.295	-24.006	Control	0.000	0.000	0.000
10	GCP #10	30.319	-24.056		30.318	-24.056	Control	-0.000	-0.000	0.000
11	GCP #11						Control			

Figure 4.2. An ERDAS GCP Tool showing GCPs of a second georectification process of an image subset.

4.5.5 Product Generation and Value Adding

The Normalized Difference Vegetation Index (NDVI) was calculated for each image acquired. An image differencing (NDVI) technique was employed to assess the condition of the vegetation in the study area (Serra et al., 2003; Liu and Zhou, 2004, Twumasi, 2005). NDVI values were extracted for each experimental site to derive the analysis in order to observe trends and changes on the mining surface.

NDVI is the Normalized Difference Vegetation Index that has values varying between -1 and 1, where increasing positive values indicate increasing green vegetation and negative values indicate non vegetated surface features such as water, barren, ice, snow, or clouds. To scale the computed NDVI results to byte data range, the NDVI computed value, which ranges from -1 to 1, is scaled to the range of 0 to 255, where computed -1 equals 0, computed 0 equals 100, and computed 1 equals 255. As a result, NDVI values less than 100 represent clouds, snow, water and other non-vegetative surfaces and values equal to or greater than 100 represent vegetative surfaces. NDVI is calculated from the red and

near-infrared light reflected by vegetation. Healthy vegetation absorbs most of the visible light that hits it, and reflects a large portion of the near-infrared light. Unhealthy or sparse vegetation reflects more red light and less near-infrared light (Justice *et al*., 1985; Upper Midwest Aerospace Consortium, 2002).

4.6 Reflectance Spectra Processing

Collection of spectral reflectance of different asbestos minerals, plant canopies, soil and water samples were undertaken using the ASD (Analytical Spectral Devices Inc., 2002) FieldSpecFR spectroradiometer. This instrument records the reflectance within the range 350 nm to 2500 nm. The sampling interval for the FieldSpecFR is 1.4 nm for the region 350-1000 nm and 2 nm for the region 1000-2500 nm. The full-width-half-maximum (FWHM) spectral resolution of the FieldSpecFR spectroradiometer is 3 nm for the region 350-1000 nm and 10 nm for the region 1000-2500 nm. Spectral reflectance were recorded for each asbestos rock type collected from the rock library of the Council for Geoscience, canopies of plant species and the soil and water samples were collected from the study area. The spectral signatures of asbestos minerals were collected to determine the spectral separability of different types and also to determine if the collected asbestos spectral profiles can be used to detect the presence of asbestos in soil and water. Spectral signatures of selected vegetation species were collected to determine their spectral separability and distinction at different wavelengths.

On recording the spectral signatures, the ASD field spectroradiometer was first calibrated with a calibration panel before measurements were recorded. The procedure was repeated

continually every fifteen minutes after taking the readings. This procedure involves optimizing the instrument in order to adjust it to the sensitivity of various conditions of illumination. The instrument is then calibrated using a white reference. The spectral reflectance of the targets was then recorded.

The analysis of the spectral profiles was conducted using the ASD Viewspec pro software (Analytical Spectral Devices Inc., 2002) and the output in the form of spectral reflectance averages and graphs was exported in an ascii format for further analysis. The exported data was then imported to Microsoft Excel spreadsheet for detailed analysis and interpretation. These included converting the nanometers to micrometers, plotting the graphs and computing the difference spectra.

4.7 Collection and processing of LAI/ fPAR data

The AccuPAR model LP-80 instrument is menu-driven, battery-operated linear PAR Ceptometer. It is used to measure light interception in plant canopies, and to calculate Leaf Area Index (LAI). It consists of an integrated microprocessor-driven datalogger and probe. The probe contains 80 independent sensors, spaced 1cm apart. The photosensors measure PAR (Photosynthetically Active Radiation) in the 400-700 nm waveband. The AccuPAR displays PAR in units of micromols per meter squared per second ($\mu mol\ m^{-2}\ s^{-1}$). The instrument is capable of handheld or unattended measurement (Deacagon Devices Inc., 2004).

AccuPAR model LP-80 uses the following mathematics equation to calculate the leaf area index. The procedure is fully described in Deacagon Devices Inc. (2005).

$\tau = \exp(-KL)$ Equation 5

τ is the probability that a ray will penetrate the canopy, L is the leaf area index of the canopy, and K is the extinction coefficient of the canopy. When photosynthetically active radiation both above and below a canopy is measured on a bright sunny day, the ratio of the two (PAR below to PAR above) is approximately equal to τ. If K is known, then the leaf area index (L) can be found by inverting the equation:

$L = -1n\ \tau/K$ Equation 6

The LP80 basically solves this equation to find leaf area index. But there are a couple of complicating factors. In constructing the model, it was assumed that the leaves in our artificial canopy were horizontal and black, and that all radiation came directly from the sun. In reality, the angle of the sun changes over the course of the day, and real canopies have quite complex architecture. Also, some radiation is scattered both from leaves in the canopy and from the sky. A full model for finding the leaf area index from a measure of photosynthetically active radiation includes corrections for all of these factors.

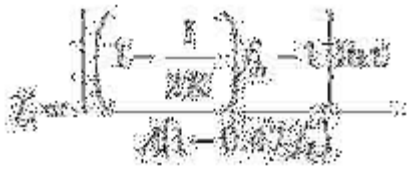

Equation 7

This equation is used by the LP80. It adjusts the amount of light absorbed (and not scattered) by the leaves in the term *A* and for the fraction light which enters the canopy as a beam (as opposed to diffuse light from the sky or clouds) in the term *fb*. *K*, the extinction coefficient of the canopy, includes variables for the zenith angle of the sun and for leaf distribution. The LP80 calculates the zenith angle of the sun at the time of each measurement. Leaf angle distribution is assumed to be spherical.

4.8 Laboratory Methods

4.8.1 Mineralogical Investigation

Mineralogical investigations were done using X-Ray Diffraction (XRD) and Scanning Electron Microscopy (SEM) with Energy Dispersive Microanalysis System (EDS). Major and trace element compositions of the soil samples were determined with the use of an X-Ray Fluorescence spectrometry (XRF) and the water analyses were done by means of ICP-MS and IC (Appendix IV).

In this study, the identification and characterization of asbestos minerals were done by a combination of structural, morphological and chemical information. The structural information was obtained as X-ray diffraction patterns and the identification of the main mineral groups, i.e. serpentine and amphibole. The morphological measurements which include grain size, shape and habit (e.g. fibrous nature and aspect ratio -L/D, given as

length/diameter measurement) were evaluated on a SEM. The chemical composition of individual asbestos particles was determined by EDS attached to the SEM.

Sample preparation was applied appropriate to the nature and state of the material and the various test assigned for analyses. Samples were submitted in the form of dry soil (10 samples), wet soil (6 samples) and eight water samples with visible solid residue. The wet soils (mud) were dried in an oven at 40ºC prior to processing. All soil samples were split; thereafter a representative portion of each sample was milled and homogenized to a fine powder at approximately 10-15 mm in size for XRD and XRF analyses. After the ICP-MS analyses of the water samples, the solid component of the water samples was settled by centrifuging and as quantities allowed used for XRD and SEM analyses (Table 4.1). For the SEM observations a polished section from the <75 μm fraction of all soil samples and water residues W3, W4, W7 and W8 was prepared. Due to insufficient quantities residues W1, W2, W9 and W10 were prepared as a non polished grain mount on a SEM stub with the aid of double sided adhesive tape. Prior to examination all preparations were coated with a carbon evaporator for conductivity.

XRD analysis of the mud, soil and water residue samples from Mafefe and Mathabatha was performed and the results are presented as semi-quantitative estimates of the phase abundances expressed in wt%. The analysis was conducted at the laboratories of South African Council for Geosicence. The study was aimed to establish if asbestiform varieties are present in the samples, based on their crystal morphology and elemental composition. Goethite/Hematite, Kaolinite/Chlorite and Kaolinite/Chlorite/Serpentine were quantified

and analyzed together and should be considered as either one or the other or a bit of both to be present in a sample. This is because of either closely spaced or overlapping XRD peaks and high background that make trace mineral identification and quantification difficult and thus they can not be reported separately. Samples were scanned from 2 to 65° 2θ $Cu_{K\alpha}$ radiation at a speed of 0.02° 2θ steps size/1 sec and generator settings of 40 kV and 35mA. Phase concentrations were determined as semi quantitative estimates, using relative peak heights/areas proportions as described in Brime (1985).

XRD was employed to determine the bulk mineral compositions for which a SIEMENS D500 diffractometer was used. The samples were run as a random powder preparation, in step scan mode from 2 to 65º 2θ CuK((λ=1.54060) radiation at a speed of 0.02º 2θ steps size/1 sec and generator settings of 35 kV and 25 mA. The JCDD (JCPDS) Inorganic/Organic Data base, PDF- 2 Data sets 1-50 was used for identification. Phase concentrations are determined as semiquantitive estimates, using reference intensity ratio and relative peak heights/areas proportions (Brime, 1985).

Table 4.1. Solid residue recovery and analytical test for the water sample

Water Sample	Water residue	Solid residue weight (g)	Analytical tests		
			XRD	SEM unpolished grain mount	Polished section
Sample 1	W1	< 0.23		x	
Sample 2	W 2	<0.23		x	
Sample 3	W 3	0.99	x		x
Sample 4	W 4	1.57	x		x
Sample 7	W 7	0.26	x		x
Sample 8	W 8	0.26	x		x
Sample 9	W 9	< 0.23		x	
Sample 10	W 10	<0.23		x	

Special Considerations: XRD cannot determine crystal morphology. Especially in asbestos, XRD does not differentiate between fibrous and nonfibrous polymorphs of the serpentine and amphibole minerals. Additional limitations may arise by the presence of other interfering minerals in the bulk sample the diffraction patterns of which may overlap thereby obscure. For naturally-occurring materials, those commonly associated with serpentine asbestos could be kaolinite, chlorite, vermiculite, sepiolite and gypsum in the regions between 7.1 ´ - 7.5 and 3.62 ´ - 3.67´ and with amphibole asbestos - talc and carbonates in the region 8.3 ´ - 8.5 ´ and 3.03 ´ - 3.14 ´. In addition mutual interference between various amphibole minerals at approximately 8.3 ´ and 3.1 ´ can also cause a problem when they occur in the presence of one another. However, these interferences can usually be anticipated and resolved by the use of special sample preparation such as extraction of clay fraction and various chemical and thermal treatments and/or instrument conditions modification. Furthermore, when used in conjunction with SEM or other optical methods, the XRD technique can provide a reliable analytical method for the identification and characterization of asbestiform minerals in soil samples.

Some basic mineralogical and structural terminology such as massive, cleavage and parting, used in the characterization of asbestos particles below will be briefly discussed because they affect the morphology of mineral fragments. Cleavage refers to breakage of a mineral along planes parallel to actual or possible crystal faces and is controlled by its crystal structure. Parting refers to a planar breakage along planes that are not cleavage planes and it is usually induced by planar defects, such as twin planes or exsolution

lamellae. Massive habit is usually applied to a particle with homogeneous structure and texture, i.e. no signs of cleavage or parting are observed.

SEM (Scanning Electron Microscopy) was used to determine the amphibole and serpentine polytypes and study their physical appearance. The study was also aimed to establish if asbestiform varieties of these minerals are present based on their crystal morphology and elemental composition. Detailed searches for fibrous mineral occurrences and their chemical characterization were performed on a Leica 440 Stereoscan SEM with INCA (OXFORD) Energy Dispersive System (EDS). The search was done at ~800-1000 times magnification and the brightness/contrast settings adjusted to emphasize the silicate minerals of interest. The results are presented in form of backscattered electron (BE) images for each sample. The BE image contrast is generated by the different average atomic mass of the phases, resulting in different backscatter intensities, e.g. the higher the average atomic mass the brighter the image of a phase. Mineral chemistry was determined by means of spot analyses with EDS. Counting time was set as 50 s; probe current at 2 nA and accelerating voltage of 20 kV was used.

4.9 Summary

This chapter discussed research methods that were followed in this study. It started by highlighting the research design and sampling procedure together with a focus on data required for this research. This was followed by the explanation of satellite image processing procedures and steps involved in collection of spectral reflectance data

together with other methods of field data collection. Laboratory techniques used were also explained. The output of this research methodology is presented Chapter Five.

CHAPTER FIVE

RESULTS AND DISCUSSION

5.1 Introduction

In this chapter the results are presented and discussed. The chapter starts by providing the results and discussion of satellite derived images for monitoring mine rehabilitation. It further focuses on the fraction of photosynthetically active radiation and leaf area index as derived from the field campaign. The chapter also covers extensively the use of field spectroscopy specifically focusing on vegetation and asbestos minerals together with soil and water samples. Laboratory results for determining asbestos pollution are presented, followed by an overview and summary of the chapter with some concluding remarks.

5.2 Satellite Derived Monitoring of the role of Mine Rehabilitation on Vegetation Growth and Ecosystem Recovery

5.2.1 Introduction

This section investigates the use of Landsat TM imagery to monitor mitigation of environmental degradation caused by asbestos mining, as well as to evaluate the progress of mine rehabilitation efforts. An image differencing method (NDVI) was used to assess the pre- and post-rehabilitation condition of vegetation in the study area. The purpose was to assess whether the rehabilitation efforts are making any significant change in transforming the degraded sites to habitable vegetation tracts that can restore ecosystem

life. The section starts by looking at the control sites (Potlake Nature Reserve) before presenting the assessment of investigated targets (experimental sites).

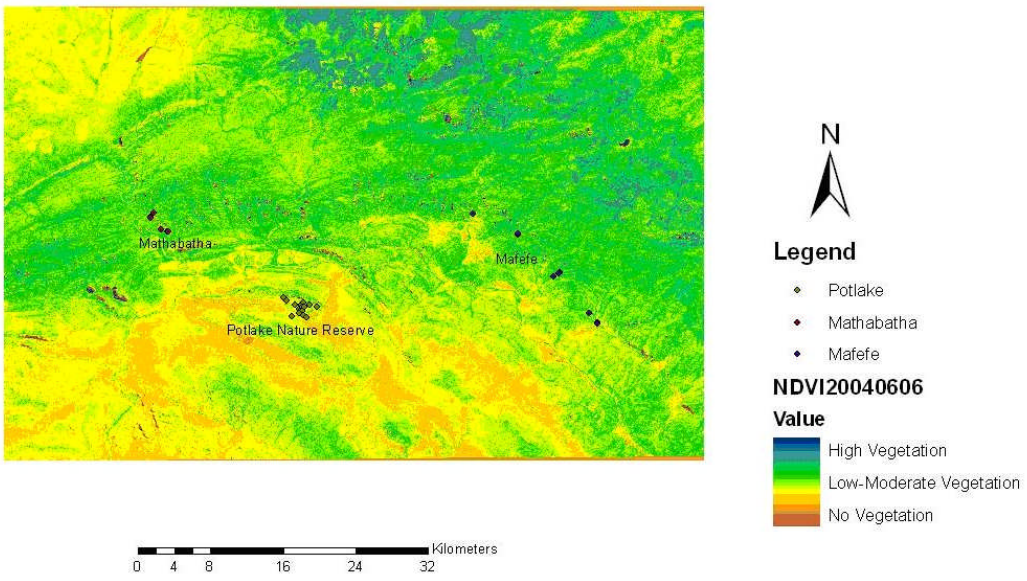

Figure 5.1 Landsat TM NDVI showing control and experimental sites.

5.2.2 Background to the Control Site (Potlake Nature Reserve)

Potlake Nature Reserve is located in Fetakgomo Municipality of Limpopo Province, South Africa at the following geographic coordinates 24°13'-24°16'S, 29°53'-29°58'E. It was established in August 1977 by the former Lebowa Government. Potlake is about 2928 ha in size and it is situated at approximately 20 km south of the experimental sites. It was categorized in the International Union for Conservation of Nature and Natural Resources (IUCN) Management Category IV (Managed Nature Reserve). It is classified by the UNEP WCMC as a South African Woodland/ Savanna. The physiography is more or less the same as those of experimental sites characterized by largely mountain and mountain slopes (about 50%), together with the flat land. The Olifants River touches the

western boundary. There are large areas of bare rock, and mixed sandy or clay loams. Annual average temperature range minimum: 18.4°C, maximum: 30°C. Annual rainfall is about 430 mm, falling mainly in summer (September-March).

Vegetation types consist of Arid Sweet Bushveld. Acacia woodland are the dominant species which include: *Acacia tortilis*, *A. grandicornuta*, *A. mellifera*, *Albizia adianthifolia*, *Ehretia rigida*, *Boscia foetida*, *Commiphora pyracanthoides*, *Boscia albitrunca*, *Capparis* spp., and *Maerua* spp.. Grasses include: *Themeda triandra*, *Cymbopogon plurinodis*, *Eragrostis* spp., *Aristida congesta*, and *Digitaria* spp. Except for a few impala and kudu, all large mammals were introduced: impala *Aepyceros melampus*, greater kudu *Tragelaphus strepsiceros* and lesser kudu *T. imberbis*, blue wildebeest *Connochaetes taurinus*, eland *Taurotragus oryx*, gemsbok *Oryx gazella*, waterbuck *Kobus ellipsiprymnus*, giraffe *Giraffa camelopardalis*, Burchell's zebra *Equus burchelli*, and red hartebeest *Alcelaphus buselaphus*. Ostrich *Struthio camelus* also occurs. Endangered species include sable *Hippotragus niger* (UNEP WCMC, 2007).

Landsat TM Derived Vegetation Analysis of Potlake Nature Reserve

Figures 5.2 and 5.3 show the vegetation condition of Potlake Nature Reserve as reflected from Landsat TM NDVI. A majority of sites experienced a healthy vegetation conditions from 1989 to 2002 as expected. Due to inter-seasonal variability, the highest vegetation conditions were reflected at the end of the growing season (Figure 5.3). This is the normal peak growth period at this region. Because of the fact that the area is undisturbed, a relatively higher vegetation condition is maintained throughout the growing season. A

major drought was experienced during 2000/2001 in Limpopo Province and as such most of the sites showed a low NDVI because of the dried leaves and decreased vigour.

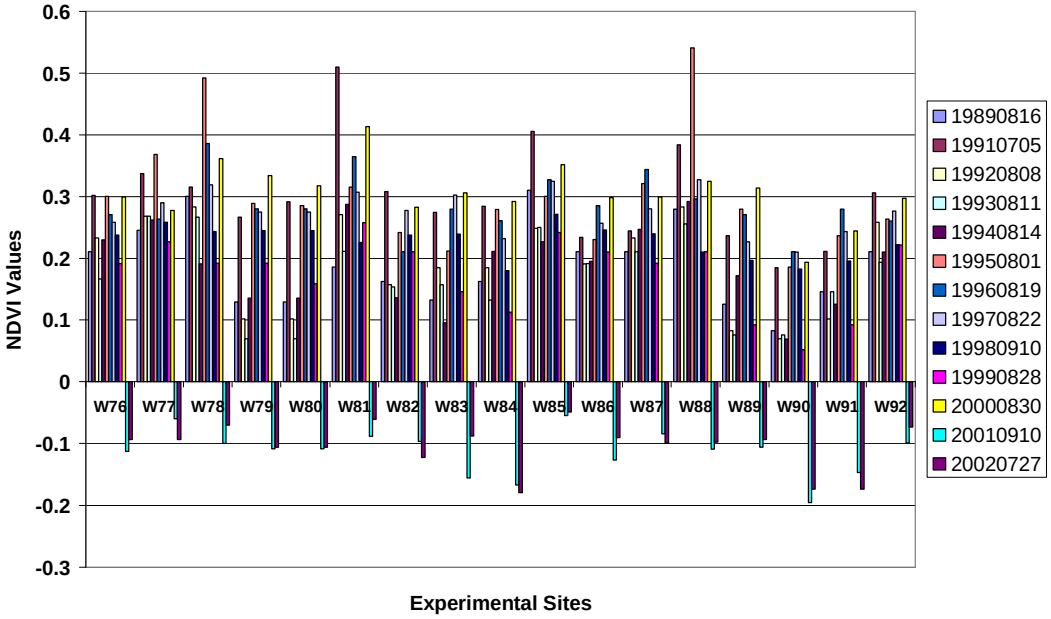

Figure 5.2. Landsat TM NDVI values of the early growing season showing vegetation condition of Potlake Nature Reserve.

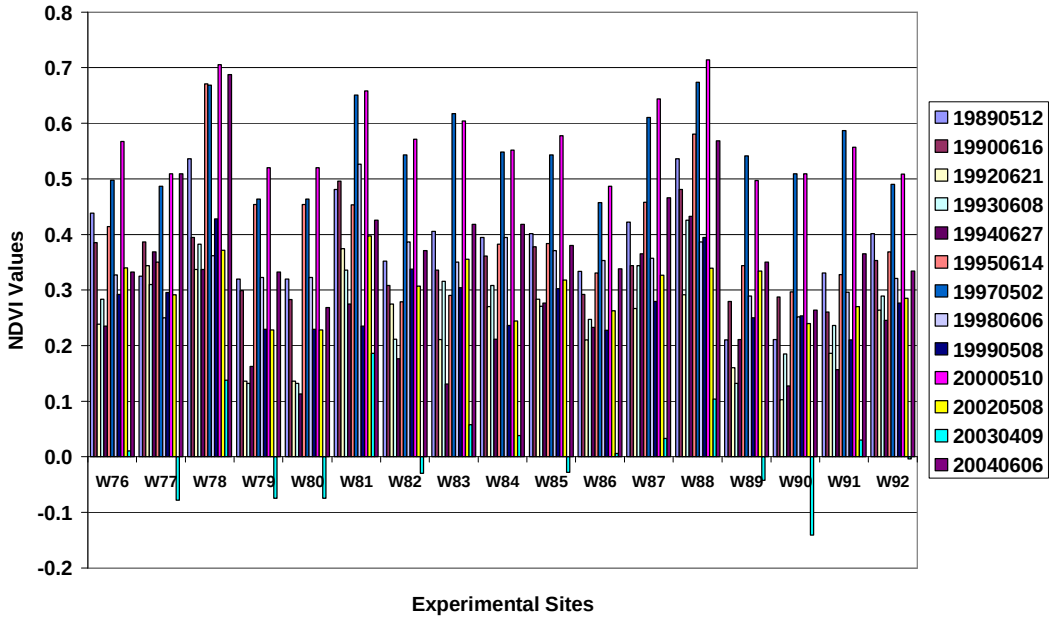

Figure 5.3. Landsat TM NDVI values of the end of growing season showing vegetation condition of Potlake Nature Reserve.

5.2.3 Results and Discussion (Experimental Sites)

Using Landsat 5 Thematic Mapper (TM) Vegetation Indices (VI) to investigate Ecosystem Recovery through Mine Rehabilitation

Mafefe Sites

The vegetation conditions of the experimental sites were assessed using remote sensing with reference to control sites. Figures 5.4 and 5.6 show the vegetation condition of Mafefe sites from 1989 to 2004. Mafefe is characterized by moist surfaces and wetlands thereby supporting a good vegetation growth. Site W58 is situated at Cork which was an open cast mine. Despite the fact that traces of asbestos are evident on the covered adit, the surrounding vegetation is good enough to reflect a high NDVI average because of its locality on the river bank. The lush green vegetation surrounding the covered adit (Figure

5.5) are a reason for a higher NDVI reflectance as Cork site is smaller than one Landsat pixel. On average the vegetation shows a positive increase. Site W59-62 is a rehabilitated Cork Asbestos Mill which is covered by fully grown *Euphorbia terucalli* with little understory cover (shrubs, grass and herbs growing below the tree canopy) on a relatively steep slope near the river.

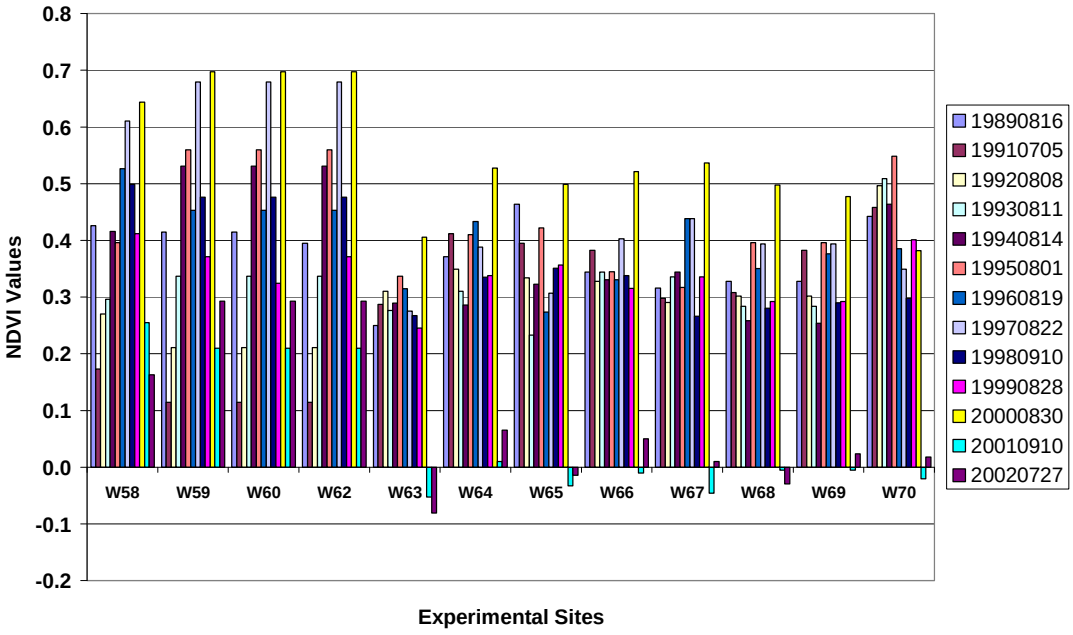

Figure 5.4. Landsat TM NDVI values of the early growing season showing vegetation condition of Mafefe sites.

Figure 5.5 Photo of site W58 in Cork, Mafefe.

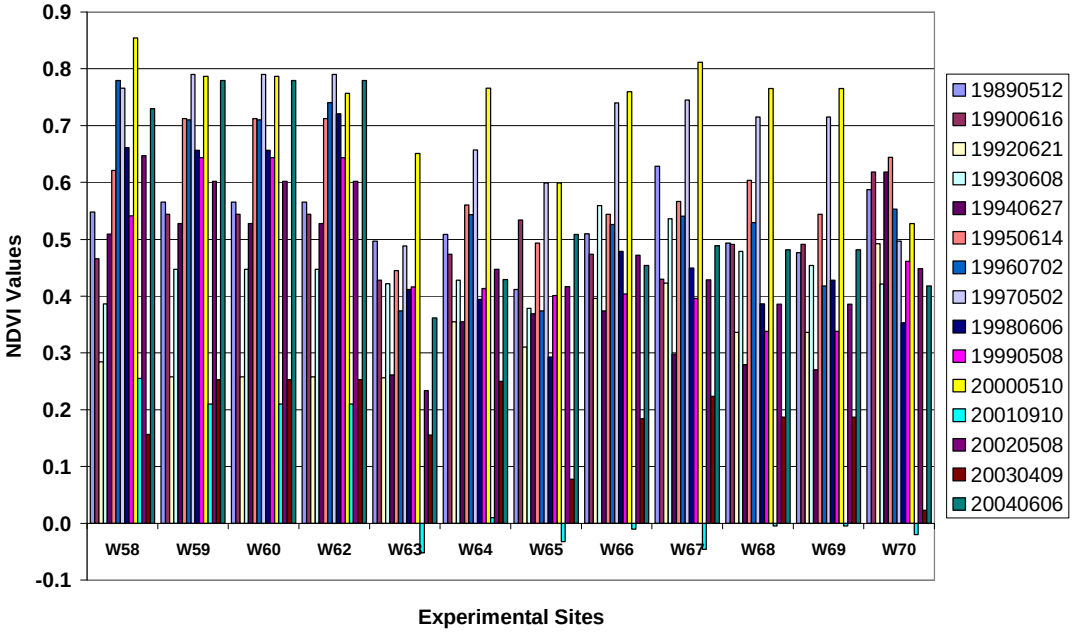

Figure 5.6. Landsat TM NDVI values of the end of growing season showing vegetation condition of Mafefe sites.

Sites W63 and W64 represents unrehabilitated mines in Mafefe (Motsane) which have developed natural vegetation through ecological succession. W66 and W67 represent rehabilitated mines at Dublin with a positive vegetation growth. Sites W69 and W70 represent rehabilitated sites in Mashilwane with a higher vegetation growth (Figure 5.7). In addition to the rehabilitation species, bush encroachment is enriching the species diversity at the sites in Mashilwane which may help in restoring ecosystem functions in the near future. Most of the former asbestos mines are situated near villages and the river. The vegetation growth generally shows an improvement. It is normal that the early part of the season shows relatively lower vegetation compared to the end of the growing season. This is attributed to inter-seasonal rainfall variability as observed also on the control sites.

Figure 5.7. A photo of site W69 in Mashilwane.

Mathabatha Sites (Bewaarkloof)

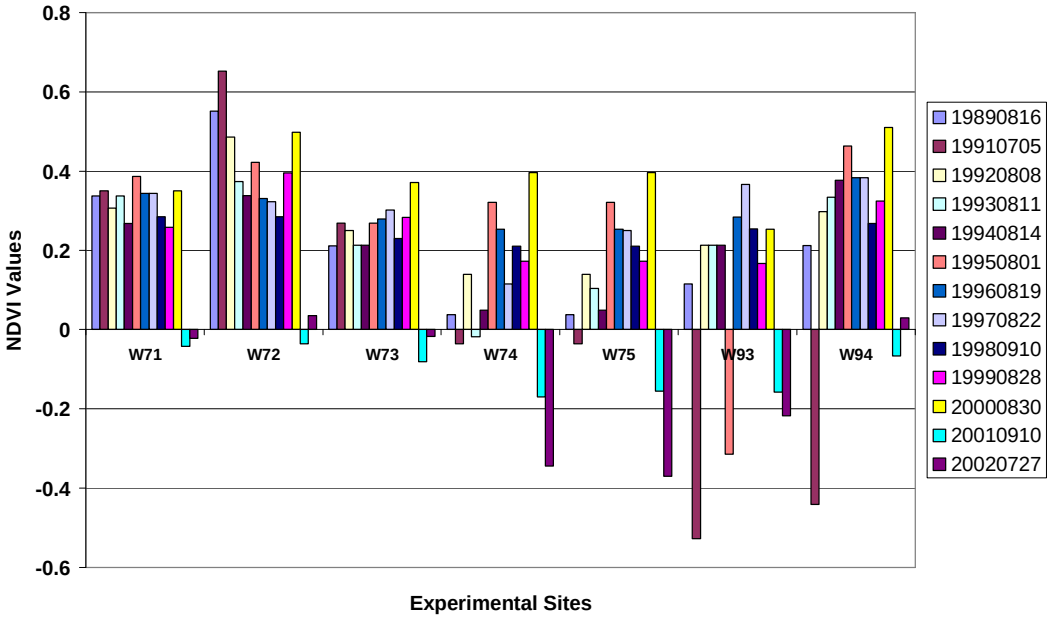

Figure 5.8. Landsat TM NDVI values of the early growing season showing vegetation condition of Mathabatha sites.

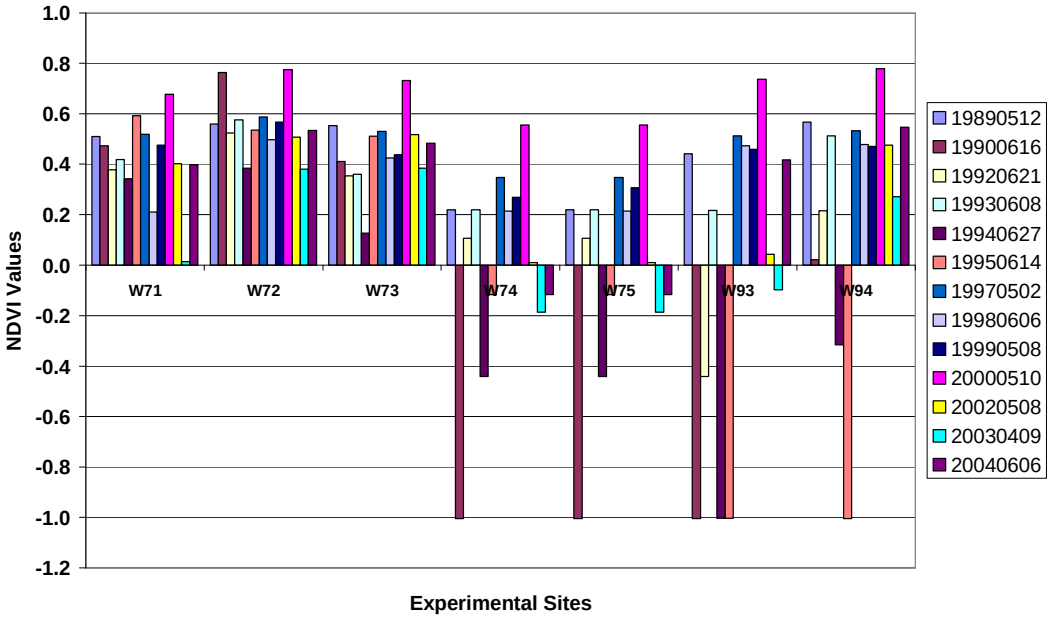

Figure 5.9. Landsat TM NDVI values of the end of growing season showing vegetation condition of Mathabatha sites.

Figures 5.8 and 5.9 show the vegetation condition in Mathabatha sites in the beginning and end of the growing season. Site W71 represents a former asbestos mine in Mathabatha (Bewaarkloof) which has been rehabilitated. Sites W72 (see Figure 5.10) and W73 are former asbestos mill in Bewaarkloof which has also been rehabilitated. Sites W74, W75, W93 and W94 represent former asbestos mines in Bewaarkloof located at the foot of the mountain (mostly in their early successional stages) which have been rehabilitated and/ or partially rehabilitated over the past six to ten years. Most rehabilitated sites experienced the lowest vegetation condition in 1994 because of the low rainfall. On average there has been a positive increase in vegetation growth on the rehabilitated sites of Mathabatha.

Figure 5.10. A photo of site W72 in Bewaarkloof.

5.2.4 Post-Rehabilitation Change Detection

Figure 5.11 shows the Landsat TM NDVIs for the study area for 1989 and 2000, respectively. A positive increase in vegetation is clearly reflected on the 2000 image when compared to the 1989 image. This positive change is also reflected at a site level in Figures 5.12 to 5.15.

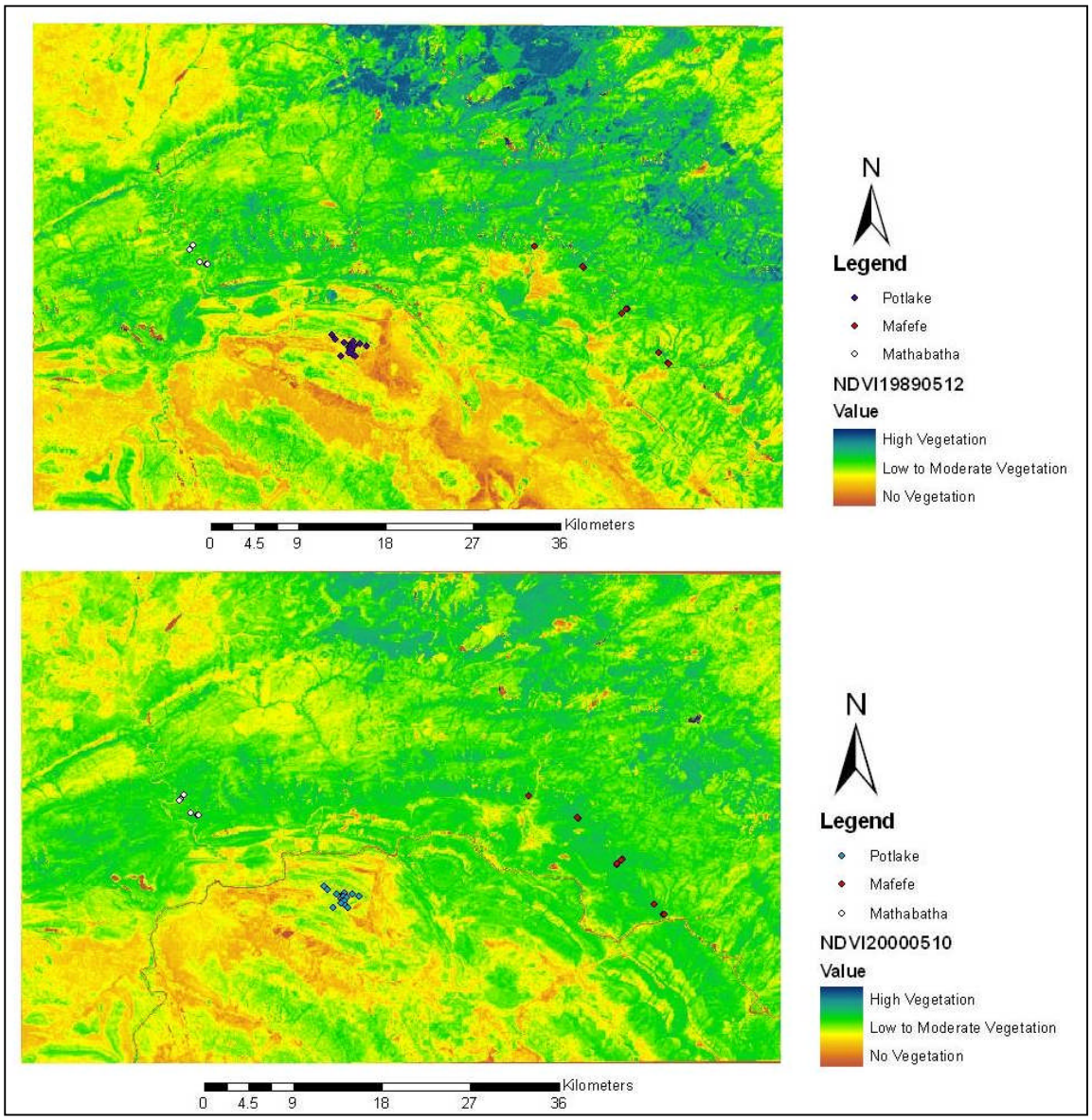

Figure 5.11. Landsat TM derived NDVI for 1989 (above) and 2000 (below) for the study area.

Mafefe

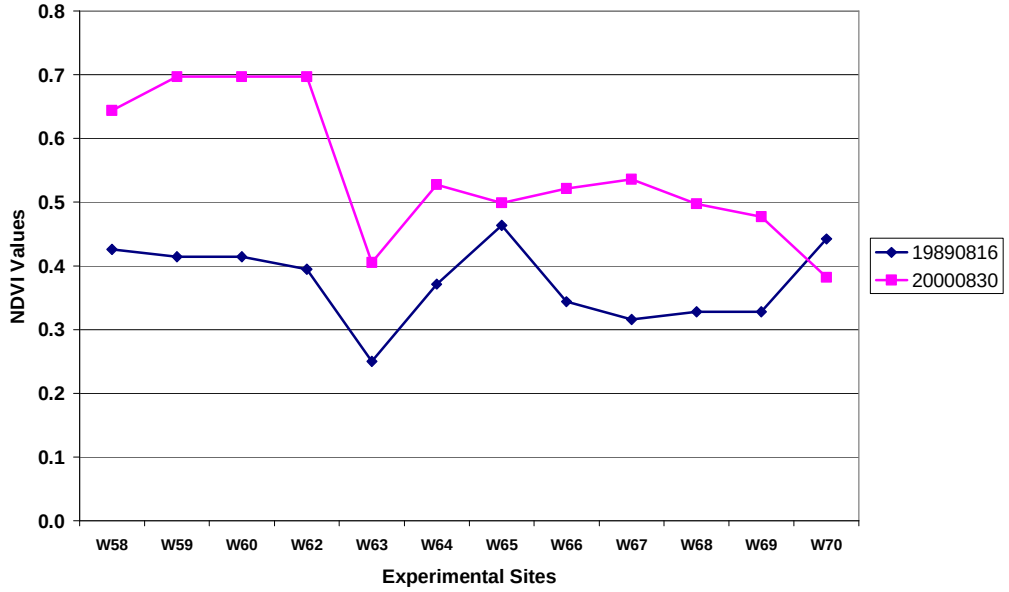

Figure 5.12 Landsat TM NDVI derived analysis of post rehabilitation vegetation change for Mafefe sites (early part of the growing season).

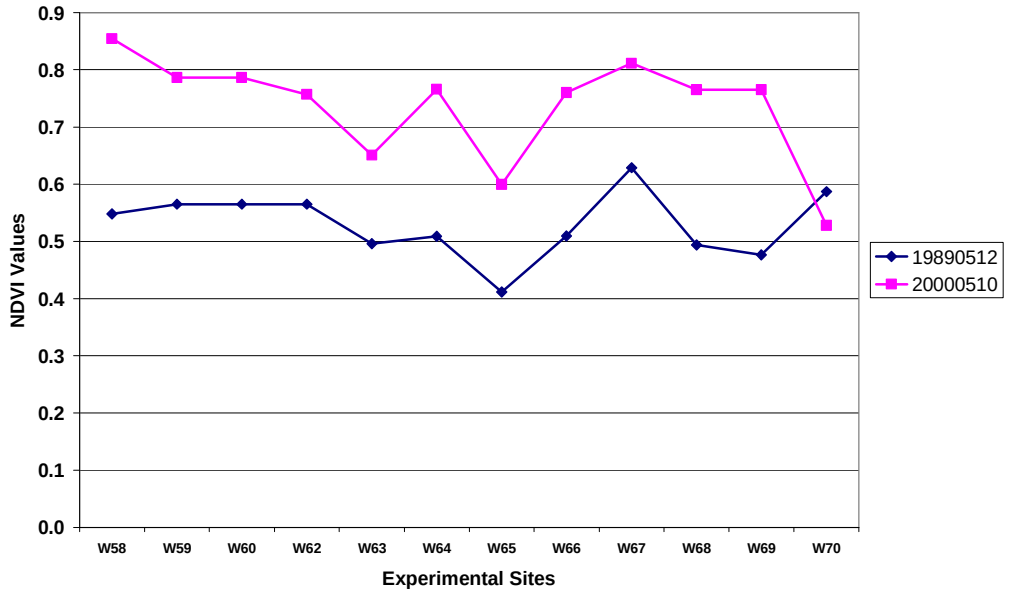

Figure 5.13 Landsat TM NDVI derived analysis of post rehabilitation vegetation change for Mafefe sites (end of the growing season).

Mathabatha (Bewaarkloof)

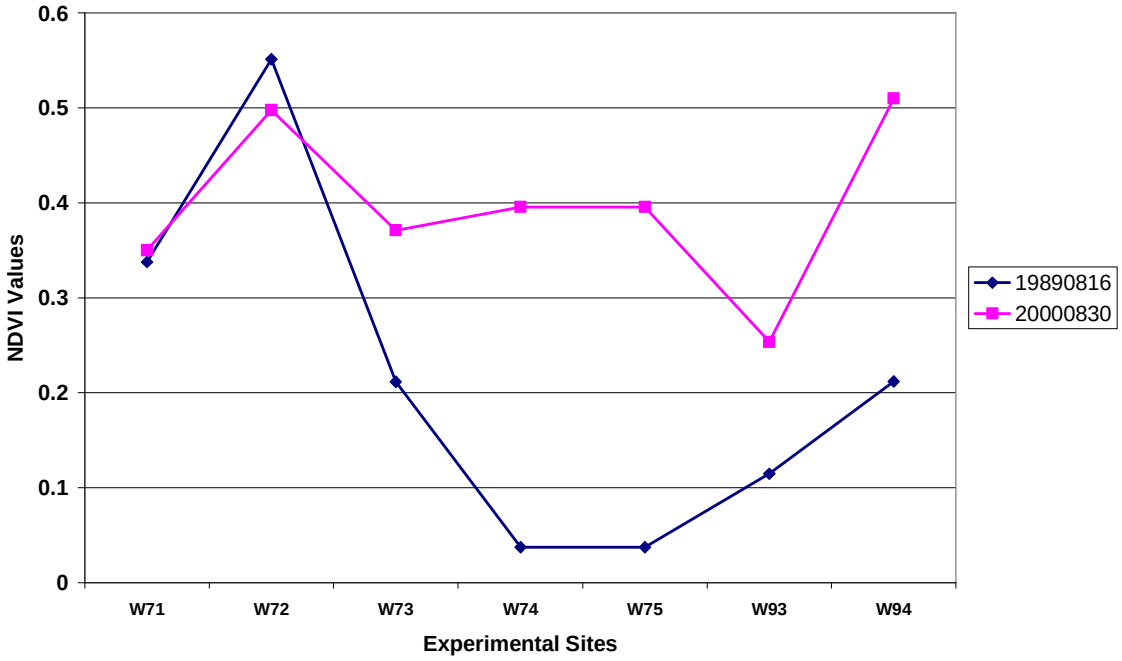

Figure 5.14 Landsat TM NDVI derived analysis of post rehabilitation vegetation change for Mathabatha sites (early part of the growing season).

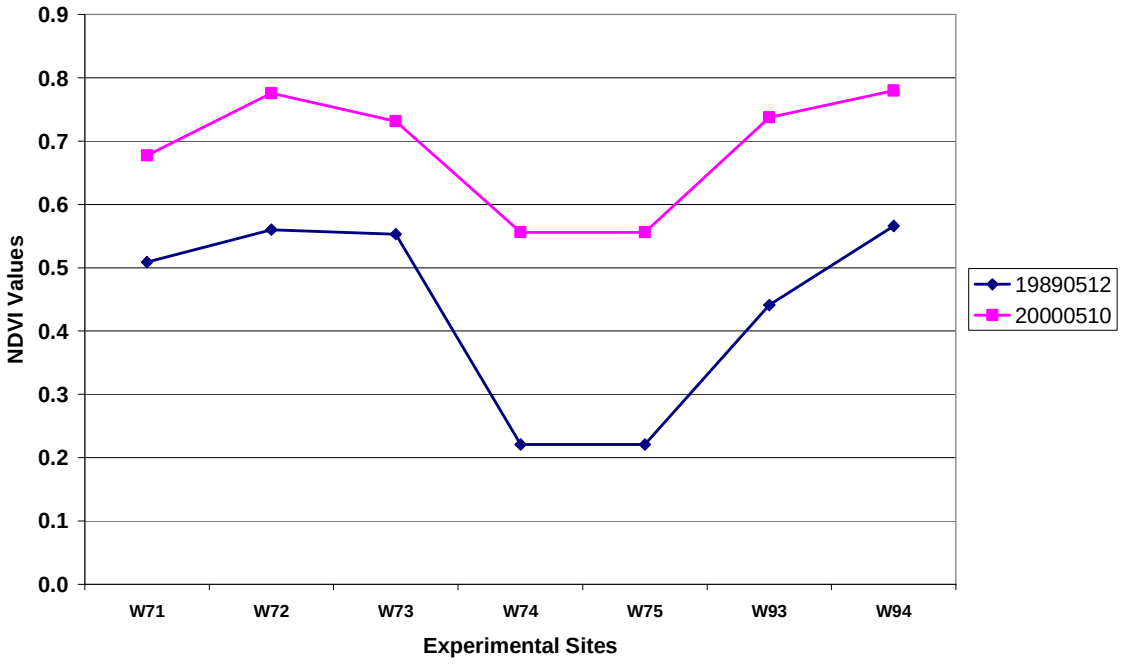

Figure 5.15 Landsat TM NDVI derived analysis of post rehabilitation vegetation change for Mathabatha sites (end of the growing season).

Figures 5.12 to 5.15 show a vegetation change situation between 1989 and 2000 for both Mafefe and Mathabatha as influenced by rehabilitation efforts. On average, there has been a positive increase in vegetation on rehabilitated sites for both Mafefe and Mathabatha, except for partially rehabilitated sites and sites covered only with soil. Site W70 in Mafefe did not record any change because it was rehabilitated using gravel and soil, and also delayed by a slow process of ecological succession.

5.2.5 Overview of the Findings

Most rehabilitated sites showed a positive increase in vegetation establishment. The use of NDVI for both low and high peak periods of the growing season enabled validation of vegetation conditions as a factor of seasonal variations. These confirm among others, findings by Lawrence and Ripple (1999) that variability in change curves might be

attributed to annual variability in climatic differences and phenological variability. The risk for resurfacing asbestos fibres is high on partially rehabilitated sites and sites rehabilitated using gravel and soil. This is exacerbated by exposure to forces of erosion on the steep slopes. The eroded materials are deposited into the streams. An analysis of medium term change detection shows a positive increase in vegetation. This positively implies that in most sites, vegetation establishment mitigates environmental degradation caused by asbestos mining. Field evidence shows that degradation will not be possible in densely vegetated rehabilitated areas. However, partially rehabilitated sites face the danger of erosion. Sites rehabilitated using only gravel and soil are less resistant to forces of degradation when compared to fully vegetated surfaces. Therefore, the revegetation method is a more effective and relatively proper way for mine rehabilitation.

5.2.6 Summary

This section demonstrated that satellite imagery is an important tool to monitor the extent to which mine rehabilitation mitigate environmental degradation. For the inaccessible areas of Mafefe and Mathabatha satellite images are the most cost effective monitoring tools compared to traditional field based methods. The NDVI showed the rate of vegetation growth /change in the study area and that the rehabilitation process in most sites is suppressing physical degradation. Rehabilitation using soil and gravel to cover open cast mines is less effective compared to the one using vegetation. Satellite-derived vegetation indices can be used as a technique to monitor environmental rehabilitation in the mining sector especially when using revegetation methods for rehabilitation. However, vegetation indices per se cannot determine if the rehabilitation has mitigated soil and water pollution but rather, that the increasing species diversity is suppressing

erosion of asbestos fibres to the streams in most sites except for the partially rehabilitated sites. Partially rehabilitated areas pose a danger of resurfacing asbestos due to soil erosion. A detailed soil and water pollution study follows in the next sections.

5.3. Fraction of Photosynthetically Active Radiation (*f*PAR) and Leaf Area Index (LAI)

5.3.1 Introduction

Leaf Area Index and Photosynthetically Active radiation are two parameters describing canopy structure and its energy absorption capacity. Both are used in evaluating the ecosystem Net Primary Production (NPP). Solar radiation scattered from a vegetation canopy and measured by satellite sensors results from interaction of photons traversing through the foliage medium, bounded at the bottom by a radiatively participating surface. This radiation regime is influenced by the architecture of individual plants and the entire canopy, optical properties of vegetation elements (leaves, stems) as well as soil and atmospheric conditions which determine the incident radiation field (Myneni *et al.*, 1999). Monteith (1973) assumed an exponential *f*PAR - LAI relationship for vegetation evenly distributed over a surface and linear for vegetation concentrated in clusters (Huemmrich and Goward, 1992). This section investigates the *f*PAR - LAI relationship using data collected from the field.

5.3.2 Results and Discussion

From the field measurements, the zenith angle in the study area range from 49 to 57 degrees. The estimated *f*PAR transmitted by the canopy recorded between 0.01 and 1.10 whereas the LAI values ranged between -0.05 and 2.14 (Figures 5.16 – 5.18, Appendix V). The beam fraction ranged between 0.68 and 0.9. LAI was calculated using equation 7 input with parameters computed in Appendix V.

Figures 5.16 – 5.18 demonstrates the relationship between LAI and *f*PAR. An inverse linear relationship is observed between LAI and *f*PAR (r^2=95% for Figure 5.16, 92% for Figure 5.17 and 94% for Figure 5.18). PAR measured by the AccuPar PAR/LAI ceptometer within the plant canopy is a combination of radiation transmitted through the canopy and radiation scattered by leaves within the canopy (Deacagon Devices Inc., 2004). When the value of PAR is low and the value of LAI is high, it implies that sufficient radiation has been absorbed for photosynthesis (Figures 5.16 – 5.18). The opposite occurs when PAR is high and the LAI is low it means that the canopy has not properly intercepted sufficient radiation. In this case, the higher LAI values are associated with *Euphorbia terucalli* and Acacia species, whereas the lower values were reflected from the grass canopy.

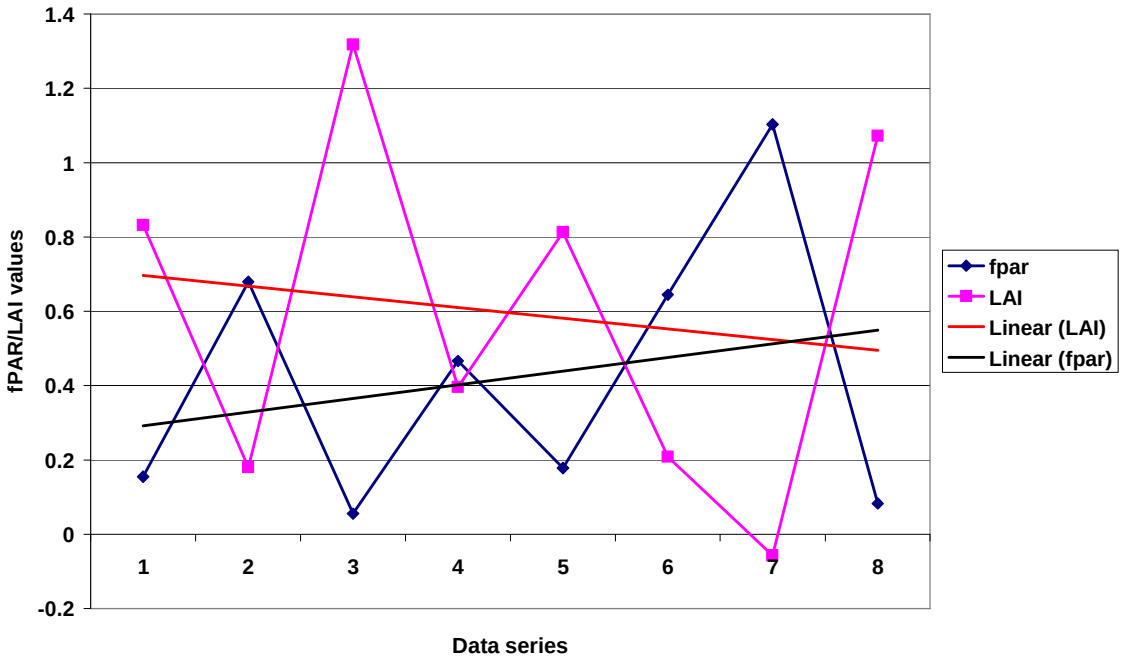

Figure 5.16. *f*PAR/LAI values measured on 09 June 2006 at Mashilwane.

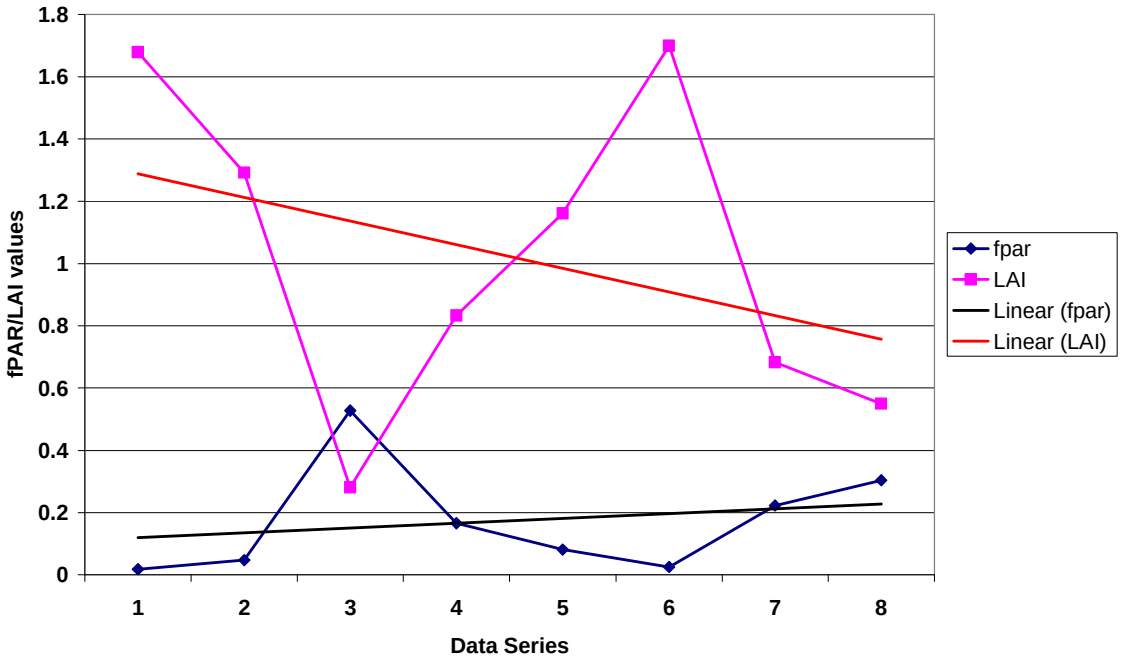

Figure 5.17. *f*PAR/LAI values measured on 08 June 2006 at Bewaarkloof.

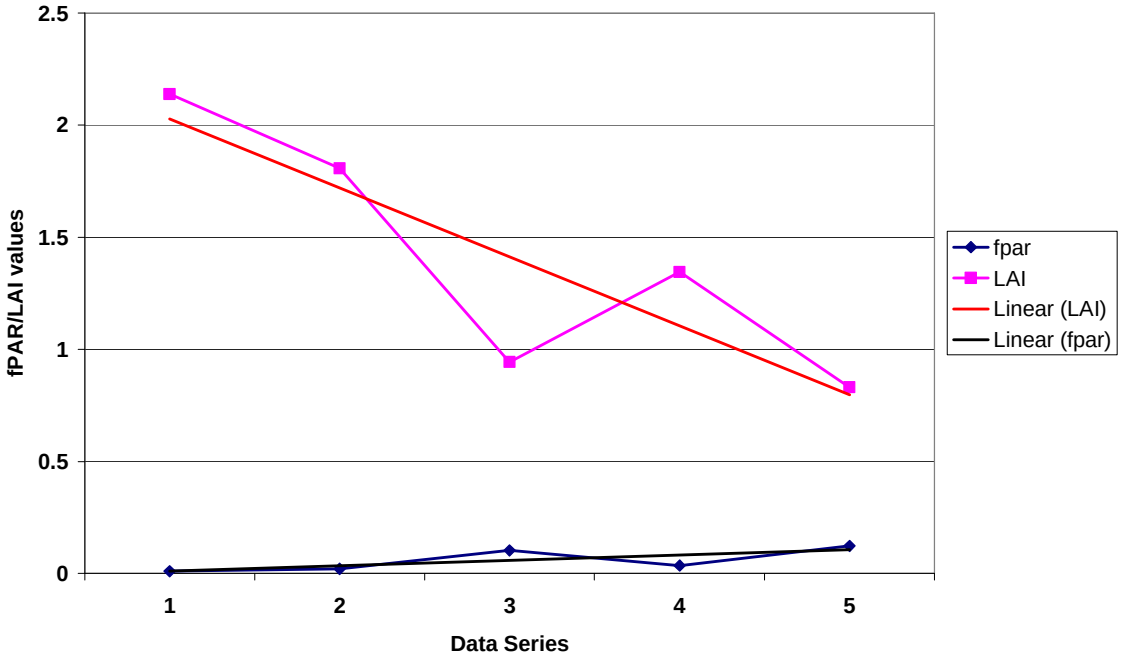

Figure 5.18. *f*PAR/LAI values measured on 07 June 2006 at Cork (W58).

5.3.3 Summary

An inverse relationship was observed for *f*PAR and LAI. Higher LAI values when compared to *f*PAR have positive implications of the photosynthetic activity. It means that much active radiation is being absorbed by plants for photosynthesis rather than reflected back into the atmosphere. The plant species used for rehabilitation showed higher LAI values. This explains to a greater extent the positive vegetation growth which has been shown from the satellite imagery (section 5.1). Their canopies capture enough radiation for the process of photosynthesis.

5.4. Spectral Separability of *Euphorbia terucalli* from other Natural Vegetation

5.4.1 Introduction

This section investigates the spectral separability of vegetation used for the rehabilitation process from natural vegetation. This essentially helps when interpreting the vegetation indices for change detection to avoid producing misleading results when determining the establishment of vegetation due to the rehabilitation process. Different plants are expected to have a broad reflectance pattern of a similar nature because of the presence of photosynthetic pigments. Despite the broad similarity, different plant species will exhibit different levels of reflectance because of type, physiology and vigour, among others. It was therefore important to investigate the separability of rehabilitation vegetation from natural vegetation.

5.4.2 Results and Discussion

Figures 5.19 to 5.26 shows the spectral reflectance profiles of different plant species recorded at the study sites. *Euphorbia terucalli* species recorded a reflectance of less than 50%. The rest of the vegetation recorded above 50% except for the *Ziziphus mucronata* which recorded below 30%. Acacia species reflected over 60% in the wavelength region 1.3-1.4μm. The grass cover, together with a mixed canopy, recorded a relatively higher reflectance. Both species are spectrally separable from each other. This implies that they can be distinctly analyzed when using satellite images of very high spectral resolution.

Euphorbia terucalli species have been used at most sites for mine rehabilitation. Others occur naturally within the area and grow gradually within rehabilitated sites through ecological succession.

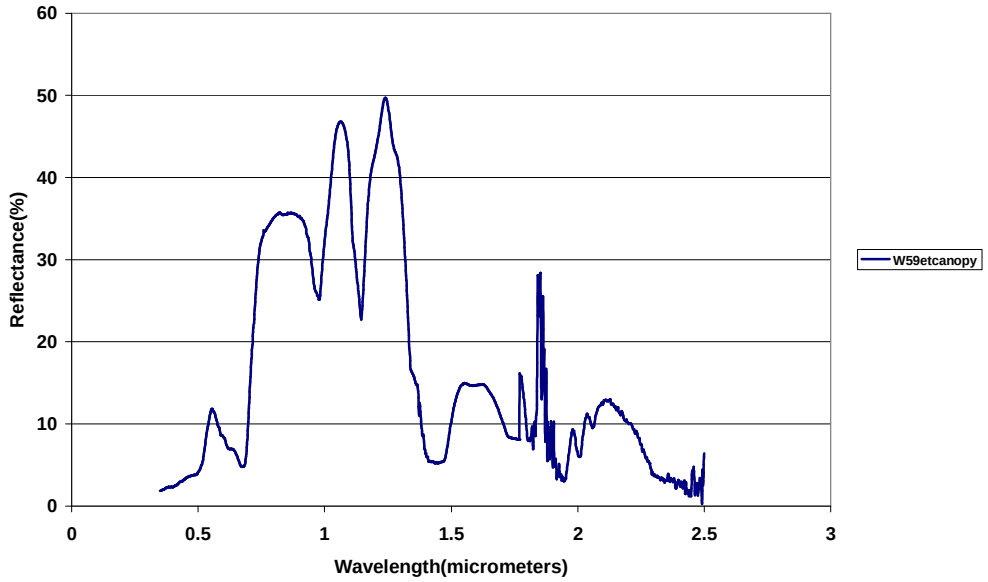

Figure 5.19. Spectral profile of *Euphorbia terucalli* canopy recorded at site W59.

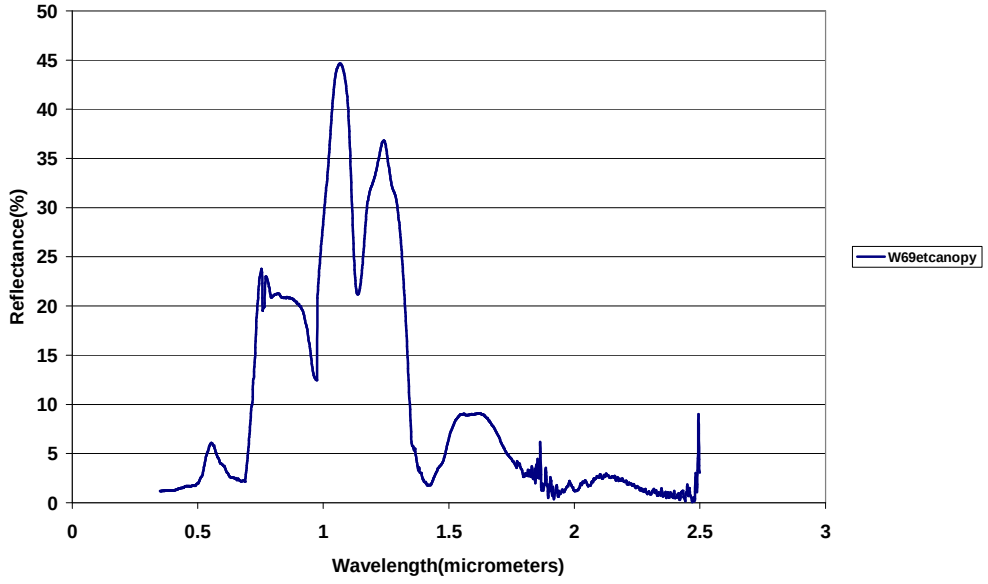

Figure 5.20. Spectral profile of *Euphorbia terucalli* canopy recorded at site W69.

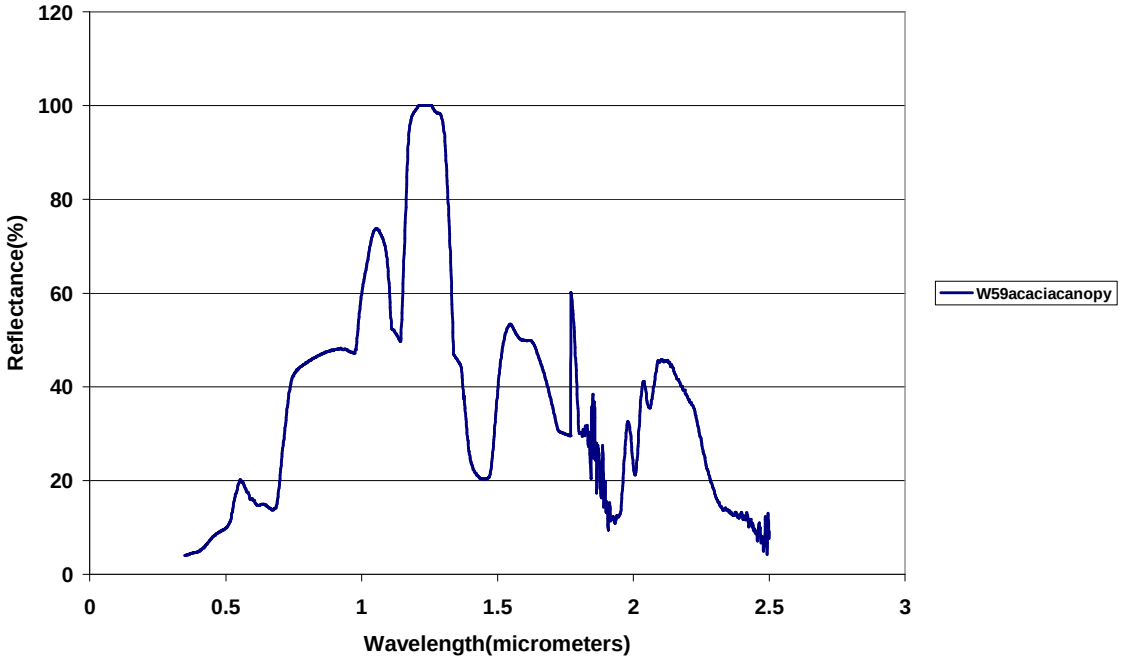

Figure 5.21. Spectral profile of Acacia canopy recorded at site W59.

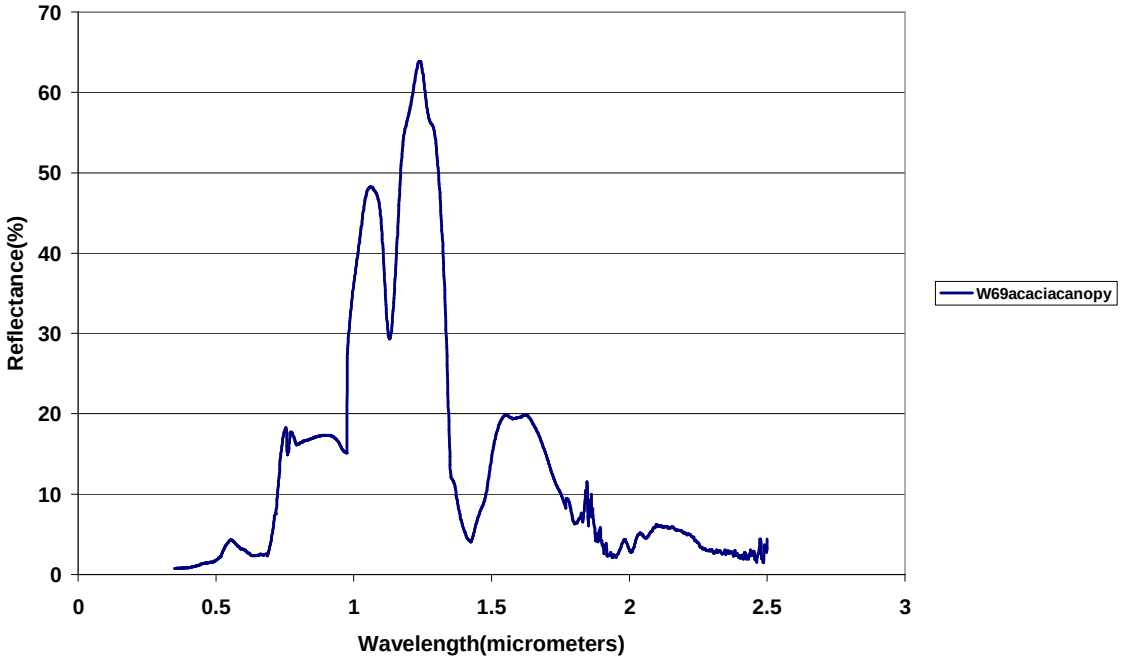

Figure 5.22. Spectral profile of Acacia canopy recorded at site W69.

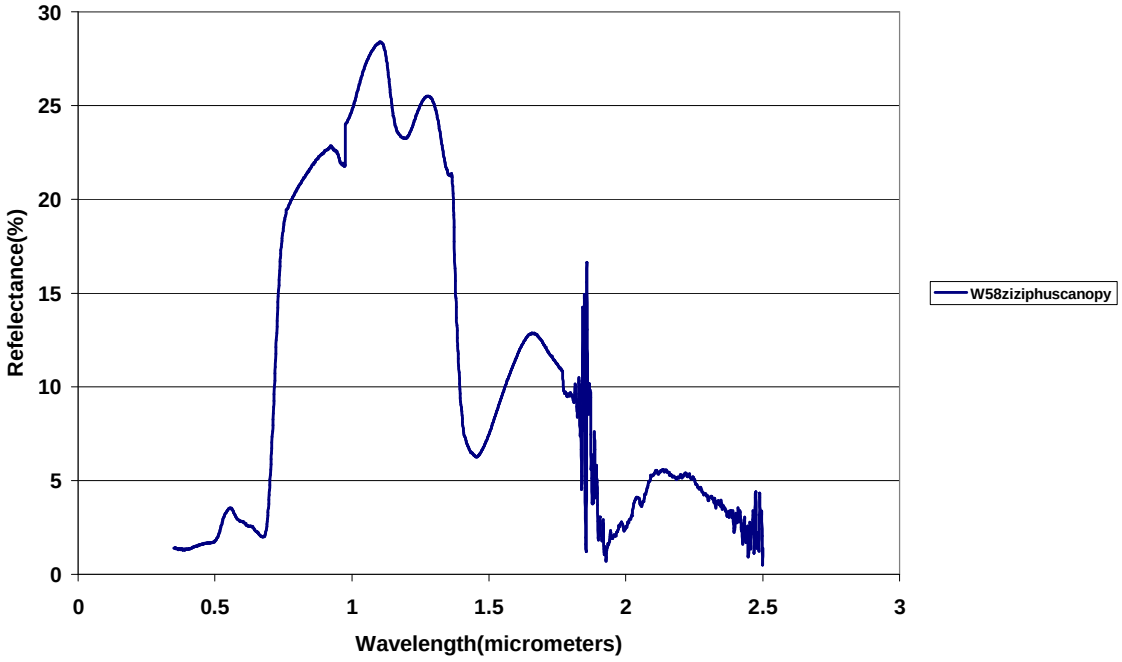

Figure 5.23. Spectral profile of *Ziziphus mucronata* canopy recorded at site W58.

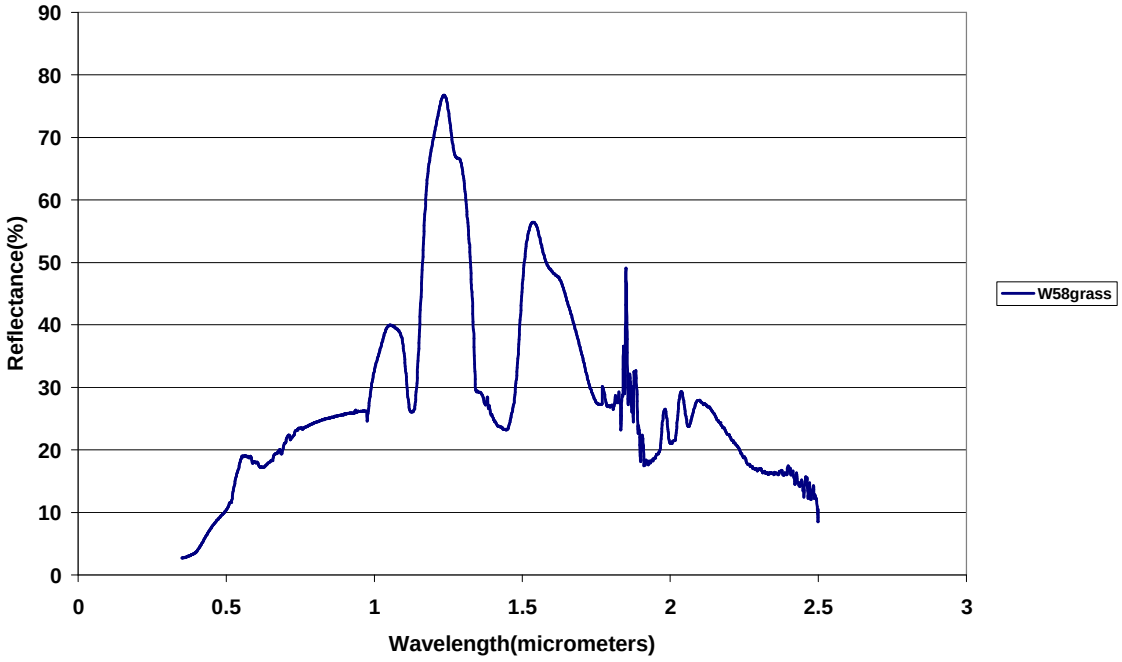

Figure 5.24. Spectral profile of grass cover recorded at site W58.

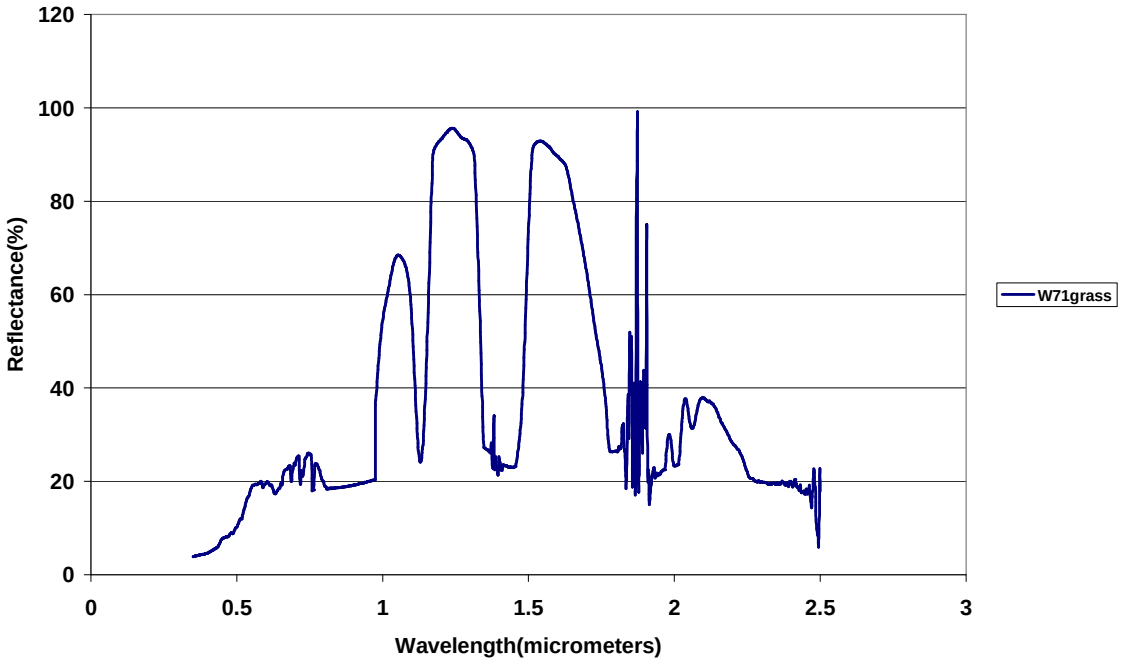

Figure 5.25. Spectral profile of grass cover recorded at site W71.

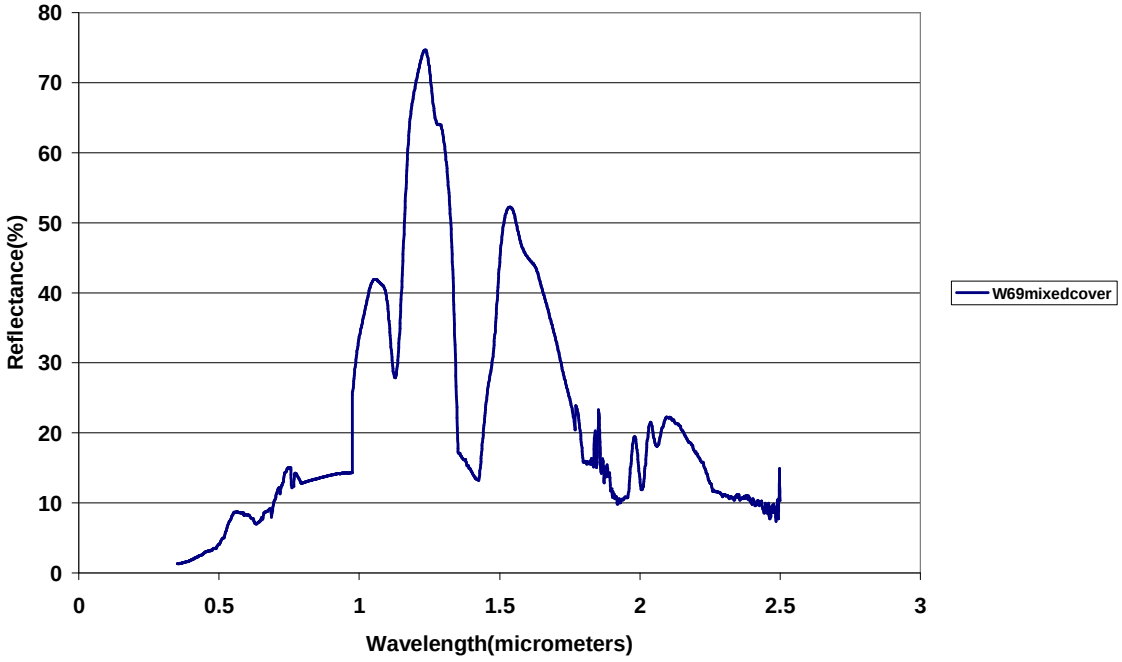

Figure 5.26. Spectral profile of mixed vegetation cover recorded at site W69.

5.4.3 Summary

It was found that the plant species used for mine rehabilitation reflects differently from natural vegetation. Therefore, they are regarded as being spectrally separable. Different species can therefore be classified and analyzed separately on images with high spectral resolution.

5.5. Analysis of Reflectance Spectroscopy of Asbestos Minerals

5.5.1 Introduction

This section investigates the feasibility of using remote sensing to differentiate different types of asbestos minerals by conducting spectroscopy analysis. It also investigates if traces of asbestos minerals can be detected using spectral signature analysis from collected soil and water samples on the rehabilitated environments. Separability of different types of asbestos will play a significant role in spectrally mapping methods to detect the spread of asbestos. The asbestos minerals studied here are Amosite, Crocidolite, Chrysotile, Anthophylite and Tremolite. The common asbestos minerals which are found in the study area are Amosite, Crocidolite and Chrysotile, respectively.

5.5.2 Results and Discussion

Spectral Reflectance of Asbestos Minerals

Figures 5.27 to 5.34 show the spectral reflectance profiles of asbestos minerals. Crocidolite, amosite, anthophylite and chrysotile depict a similar general pattern of reflectance which clearly shows that these minerals belong to the same group. A slightly different pattern is observed from tremolite. Figures 5.27 to 5.29 show the spectral reflectance of crocidolite minerals collected from different areas. Crocidolite collected from North West and Limpopo Provinces show a relatively similar percentage of reflectance. Crocidolite collected from the Northern Cape shows lower reflectance values

but with a similar reflectance pattern compared to the other two. This may be attributed to variations in the environmental setting. Figure 5.30 shows the spectral profile of amosite with Figures 5.31 and 5.32 showing those of anthophyllite and chrysotile, respectively. A similar pattern of reflectance is also observed, with variations in the level of reflectance at various wavelengths. Anthophylite and tremolite shows a similar reflectance and saturates at about 1.2 – 1.4 μm wavelengths. They can both be separated spectrally at about 1.5 – 1.6 μm because anthophyllite does not saturate at this region when compared to tremolite. The two minerals can be separated from each other by differencing the percentage spectral reflectance.

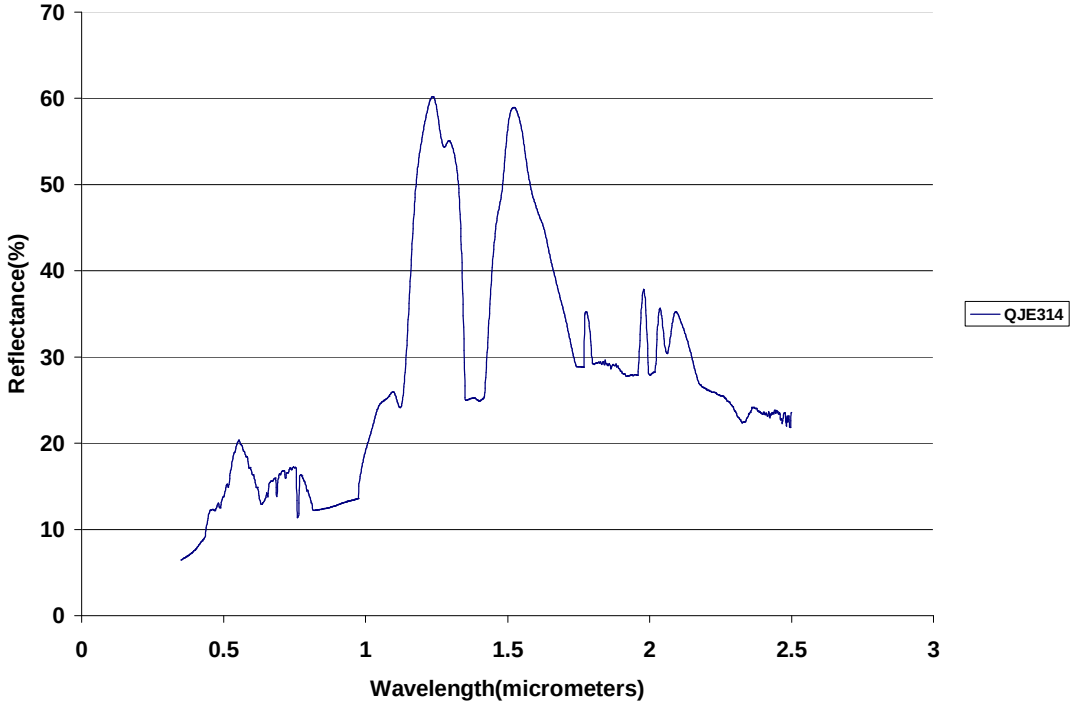

Figure 5.27. Spectral profile of Crocidolite (QJE314) obtained from Cubbic, Kuruman, North West Province.

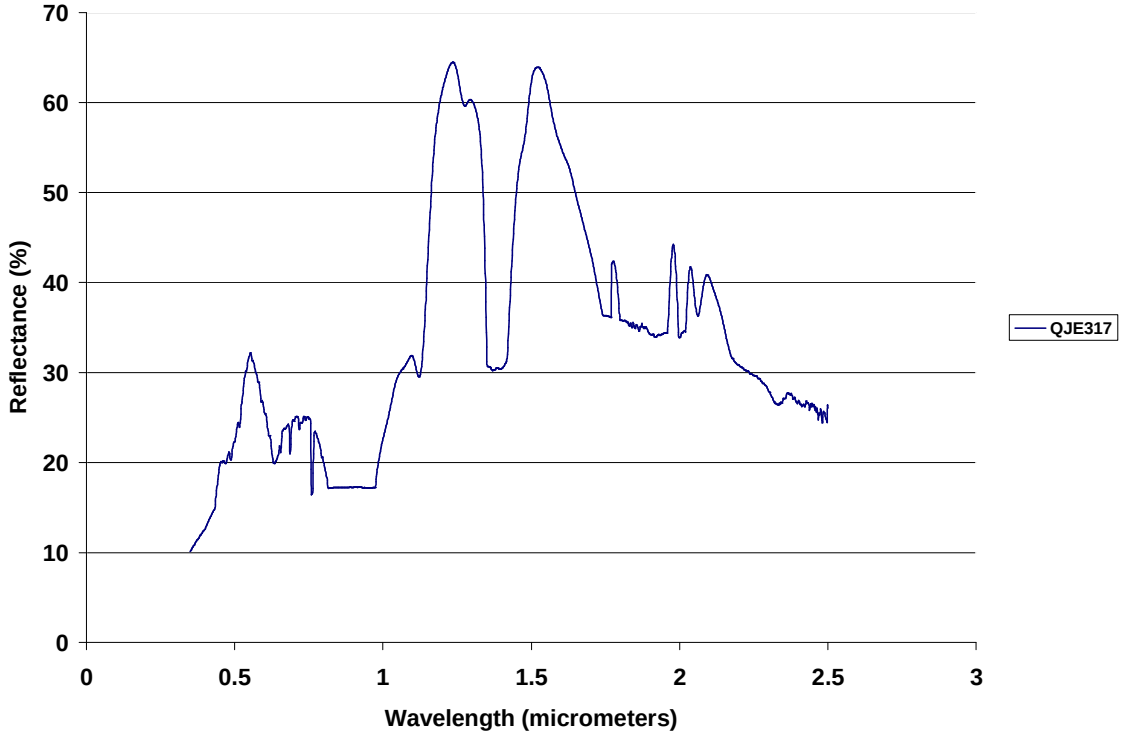

Figure 5.28. Spectral profile of Crocidolite (QJE317) obtained from Pietersburg Asbestos Company, Limpopo Province.

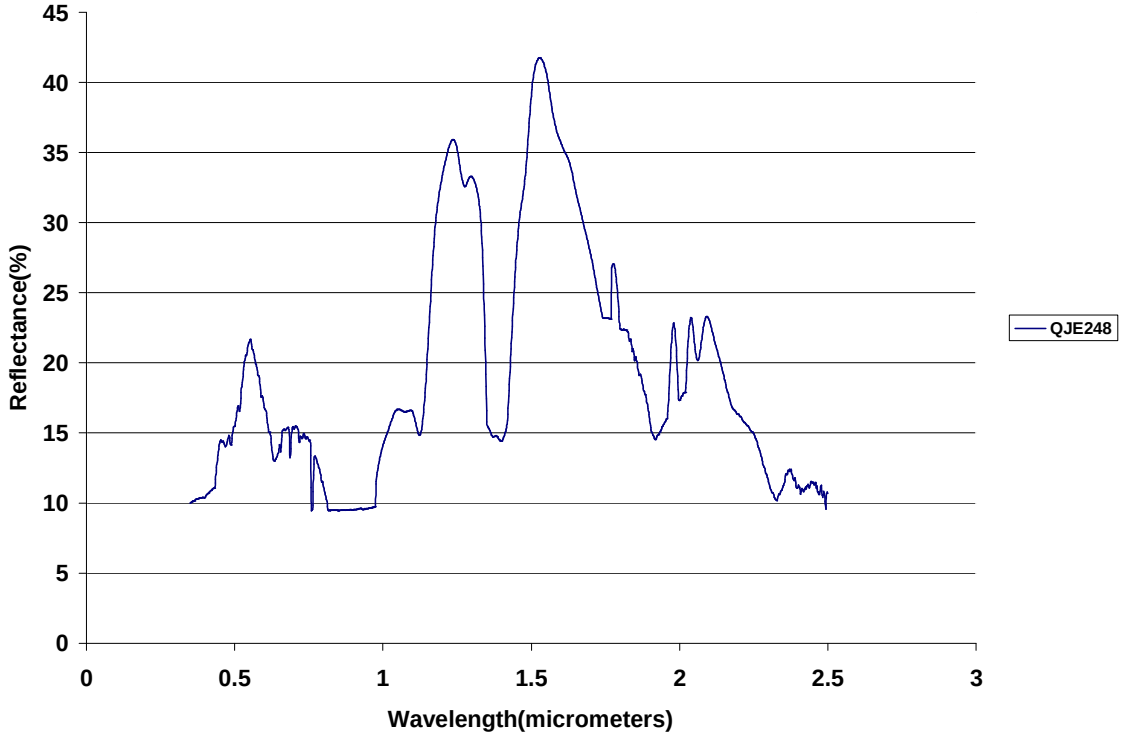

Figure 5.29. Spectral profile of Crocidolite (QJE248) obtained from Kliprivier, Postmasburg, Northern Cape.

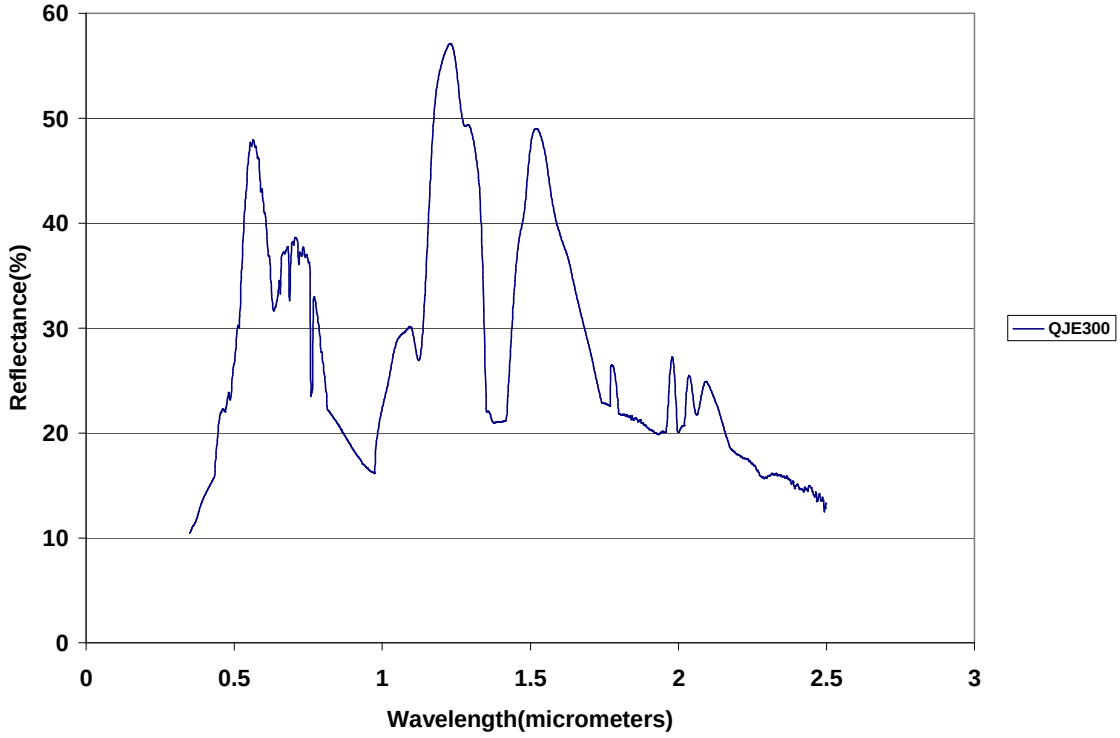

Figure 5.30. Spectral profile of Amosite (QJE300) obtained from Penge, Limpopo Province.

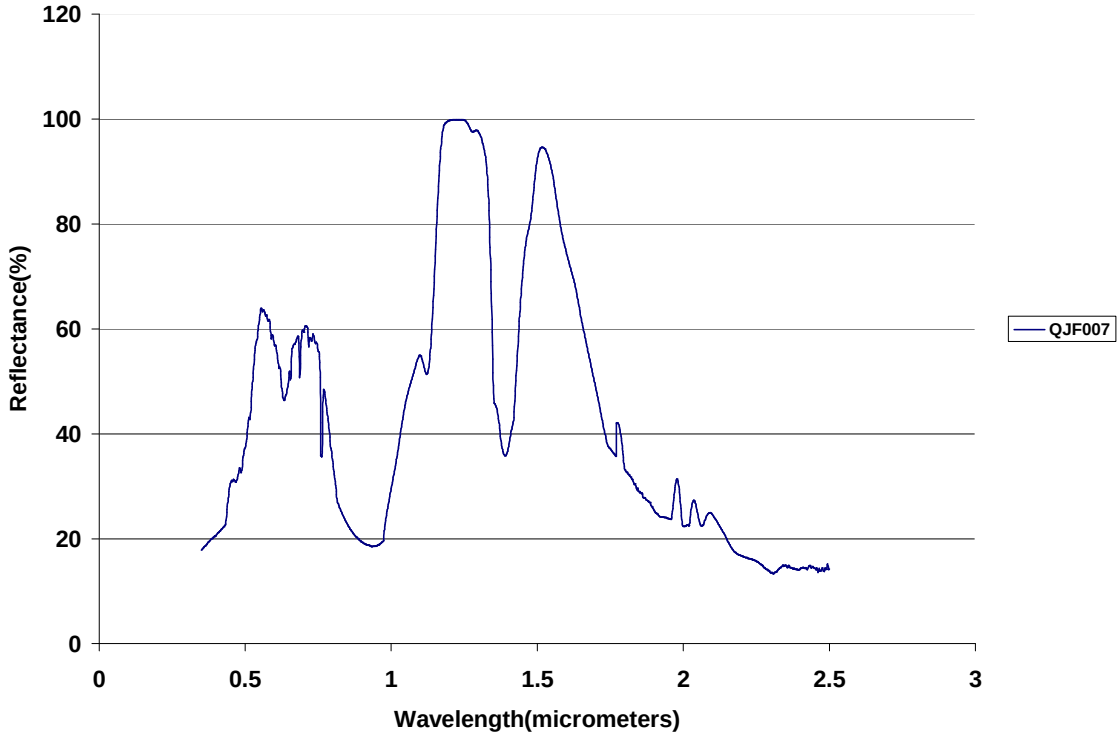

Figure 5.31. Spectral profile of Anthophylite (QJF007) obtained from the Soutpansberg, Limpopo Province.

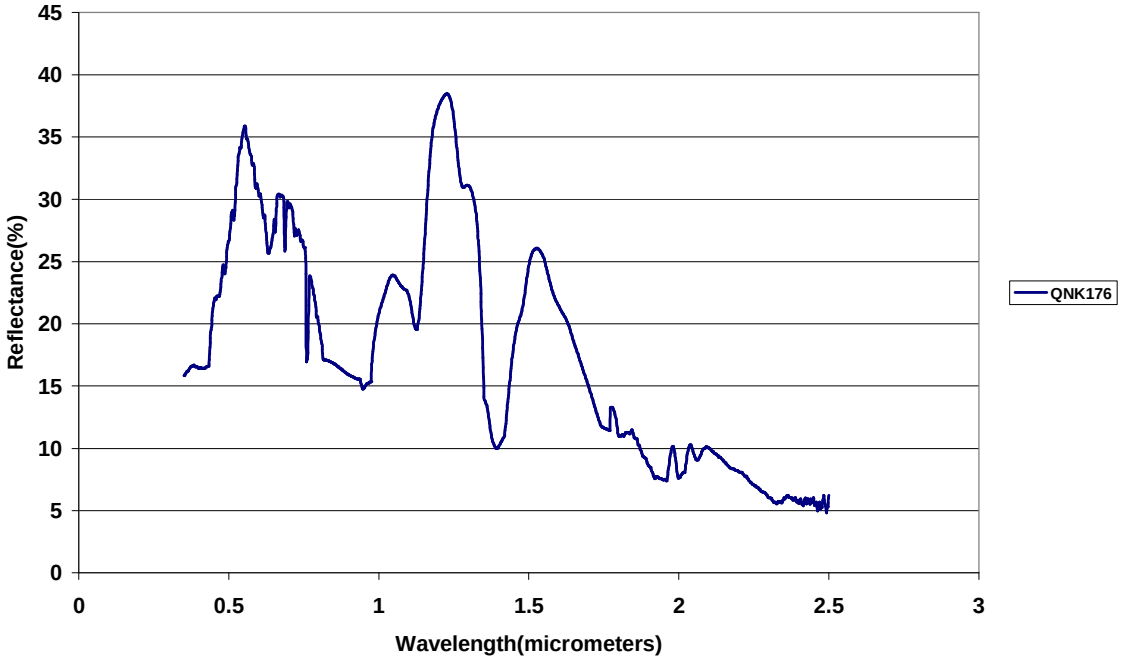

Figure 5.32. Spectral profile of Chrysotile (QNK176) obtained from Barberton, Mpumalanga.

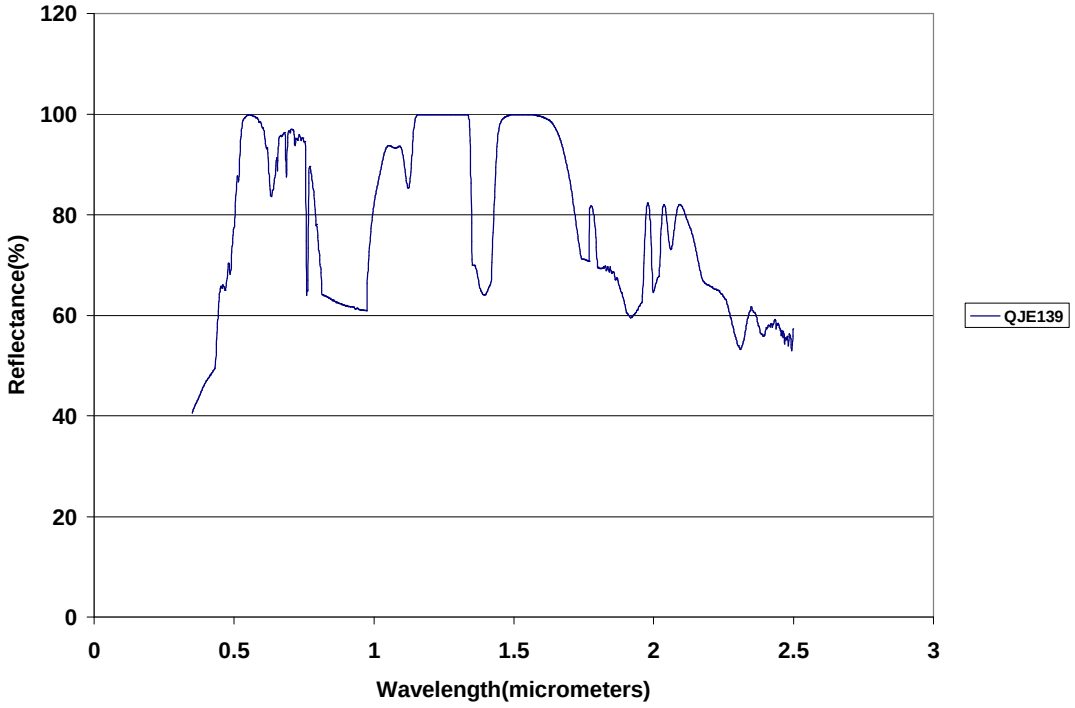

Figure 5.33. Spectral profile of Tremolite (QJE139) obtained from Prieska, Northern Cape.

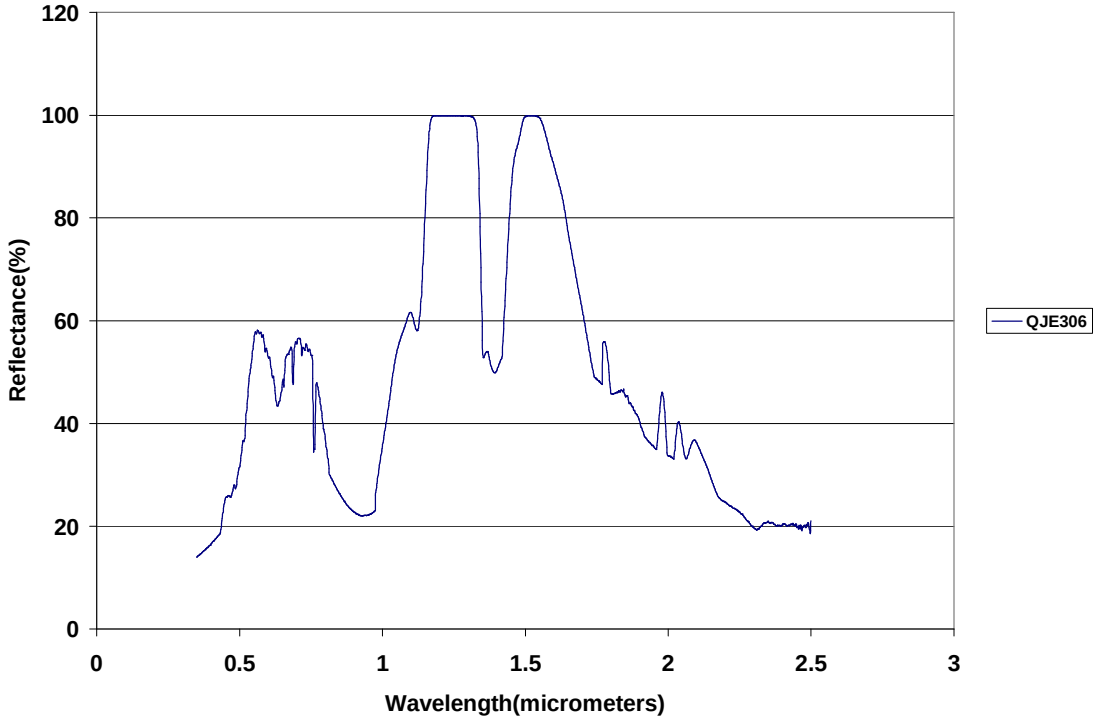

Figure 5.34. Spectral profile of Tremolite (QJE306) obtained from Kaapmniden, Mpumalanga.

Spectral Differentiation/ Separability of Asbestos Minerals

Figure 5.35 demonstrates the spectral separability of crocidolite, amosite and chrysotile at different wavelengths. Both minerals show a similar pattern of reflectance. However, they can be clearly separated because of the reflectance level within the region of 1.8 – 2.5 μm. Their mapping and identification may be effective in this wavelength region. Figure 5.36 shows the reflectance difference of amosite from crocidolite. These were the main minerals that were mined in Mafefe and Mathabatha area. Compared to crocidolite, amosite show low reflectance difference in most wavelengths which goes below 10 % in the region of 1.4 - 2.3 μm.

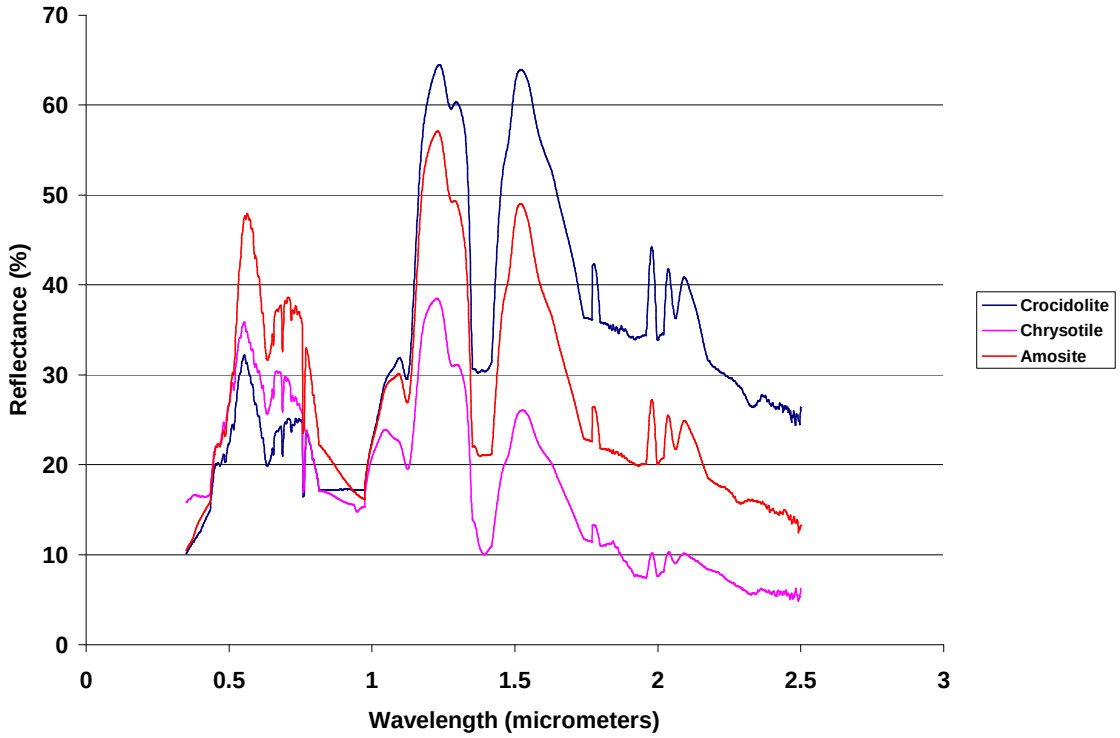

Figure 5.35. Spectral separability of crocidolite, amosite and chrysotile.

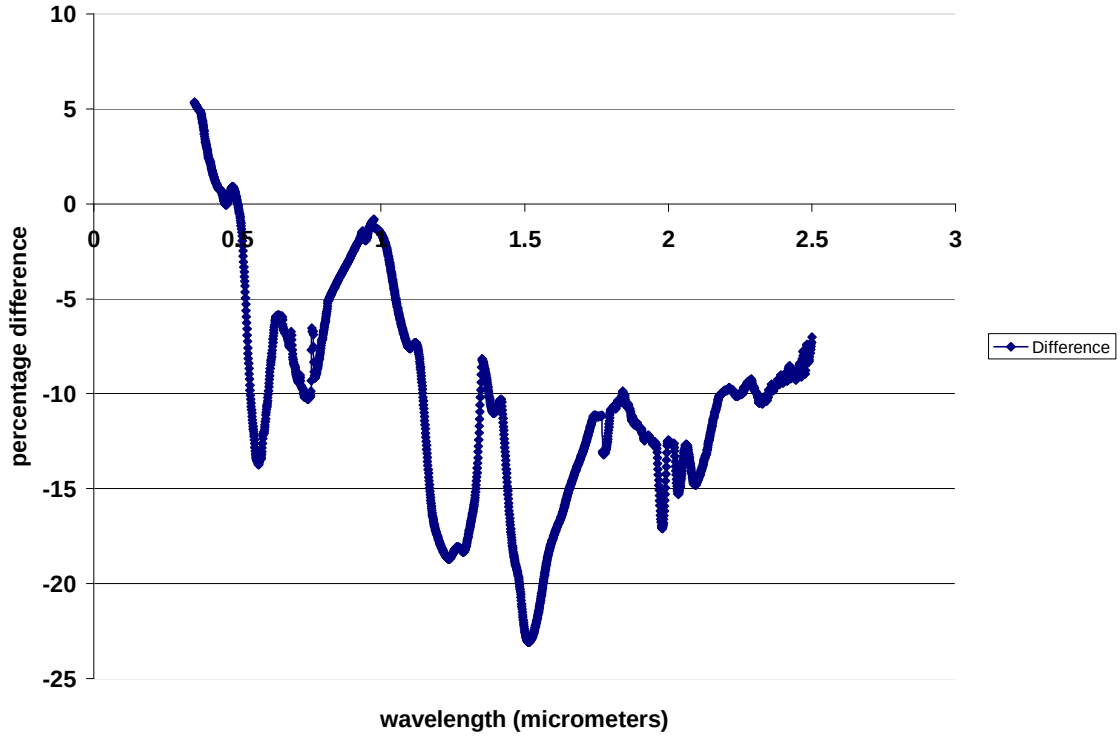

Figure 5.36. Spectral differencing of amosite from crocidolite.

5.5.3 Overview of Findings

Different asbestos minerals generally follow a similar pattern of reflectance and transmittance of electromagnetic radiation. Depending on the percentage or level of reflectance, different asbestos types can be distinguished. This can also be done effectively using the spectra differencing method as illustrated in Figure 5.36. On this basis, spectrally derived mineral mapping can be used as an important tool to map different minerals of the same genera with the aid of very high spectral resolution remote sensing images. Construction of this type of spectral libraries through time will contribute positively to the geo-information applications in the mining sector. Spectra differencing is presented here as the most appropriate method to conduct the spectral separability of different minerals. It helps in avoiding errors that may be encountered when undertaking visual interpretation. Through the use of reflectance spectroscopy, it is possible to use reflectance data to map the distribution of asbestos minerals in the former mining areas. Through continuous validation and calibration, this will contribute positively to monitoring asbestos pollution using space borne and airborne sensors.

5.5.4 Summary

This section demonstrated the feasibility of using remote sensing to distinguish different asbestos minerals through reflectance spectroscopy analyses. Determining separability of different types of asbestos is an important input for deriving spectrally based methods of detecting the spread of asbestos. However, this can clearly be expanded using high spectral resolution images. The information derived can be used as a valuable input to

carry out spectrally derived mapping of minerals. However, cost and accessibility of hyperspectral images may be a limiting factor.

5.6. Spectral Analysis of Soil and Water Samples

5.6.1 Introduction

This section investigates the potential use of reflectance spectroscopy in monitoring the distribution of asbestos minerals in soil and water. Spectral signatures of soil and water samples collected for laboratory analysis were recorded. The main purpose was to determine if traces of asbestos minerals can be detected from the collected samples based on the known spectral profiles of asbestos minerals.

5.6.2 Results and Discussion

Spectral Reflectance of the Collected Water Samples

Figure 5.37 shows the spectral profile of a normal drinking water to be used for comparison with the water samples collected from the rivers. The water running through the streams in Mafefe are used for drinking, irrigation and other domestic uses. Figure 5.38 and 5.39 shows the spectral reflectances of water collected from the flowing river at Cork. Compared to the control sample (Figure 5.37), a slight but insignificant pattern in reflectance is observed. However, figure 5.39 shows lower reflectance values. Figure 5.40 and 5.41 shows the spectral profiles of dirty water collected at Cork River. Compared to the spectral profile of the control water sample, both reflectances (Figure 5.40 and 5.41) show a significant deviation. This shows the presence of other substances which are reflecting radiation in other parts of the wavelength as compared to the control

sample profile. These elements are accounted for in the detailed laboratory analyses later in this chapter.

Figures 5.42 and 5.43 show the spectral reflectance of dirty water samples collected from Mohlapitse river. Compared to the control water sample, there is not much deviation except that the reflectance is much lower (below 18 and 12%, respectively). This shows the presence of materials that are absorbing electromagnetic radiation. Generally the spectral reflectance of drinking water did not exceed 25%. Figure 5.44 and 5.45 shows the spectral profiles of dirty water samples collected at Mohlapitse river. Despite the low reflectance values, a similar pattern of reflectance was observed compared to the control water sample. Compared to other substances, water absorbs a greater portion of radiation as expected (Qunshu *et al*., 1983).

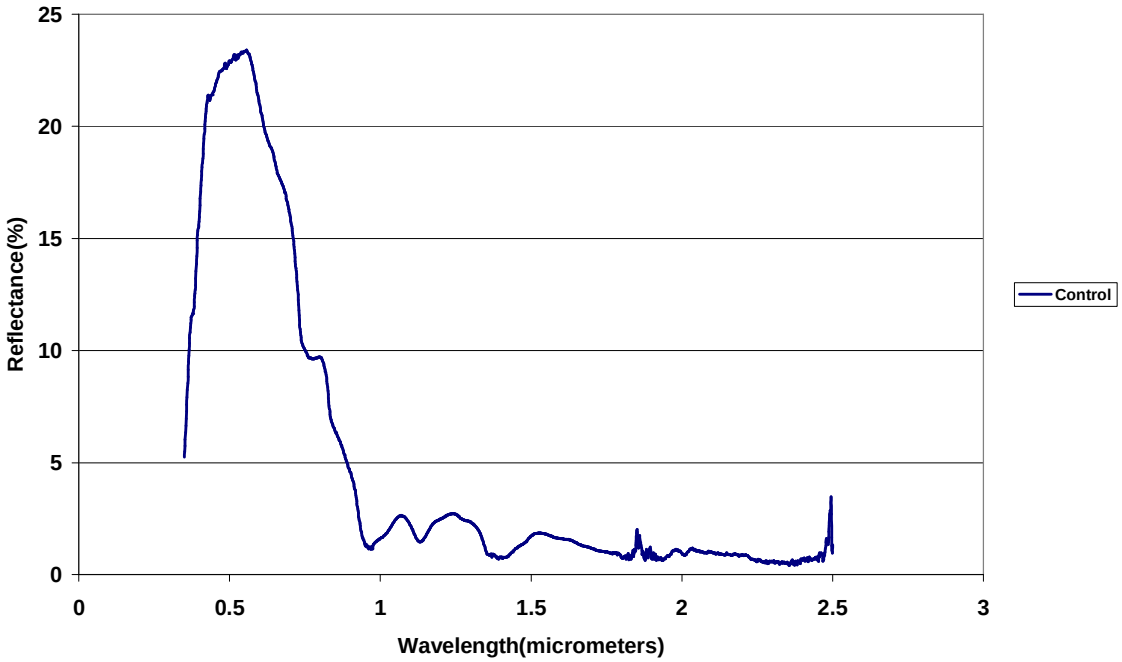

Figure 5.37. Spectral profile of clean potable water.

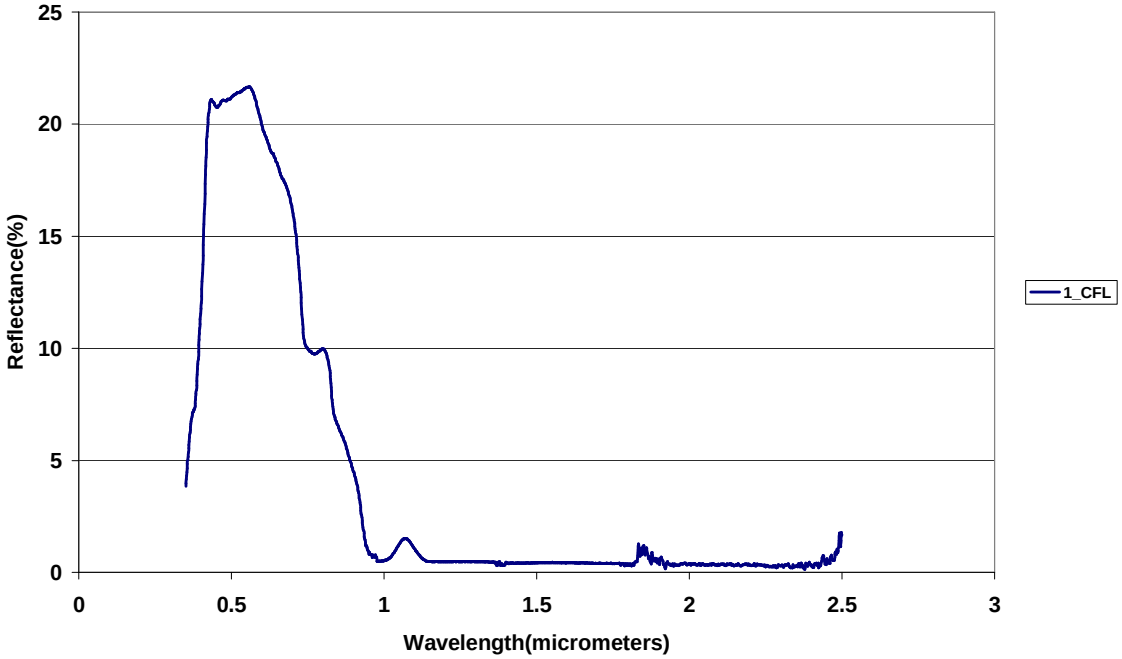

Figure 5.38. Spectral profile of sample 1 collected from flowing water at Cork River.

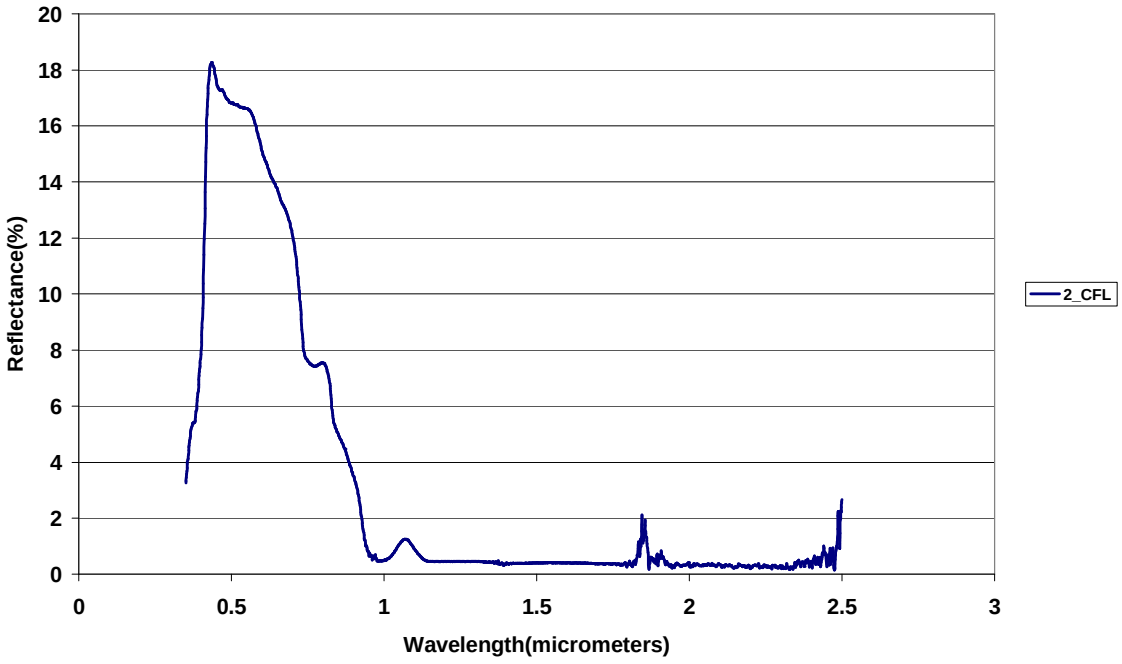

Figure 5.39. Spectral profile of sample 2 collected from flowing water at Cork River.

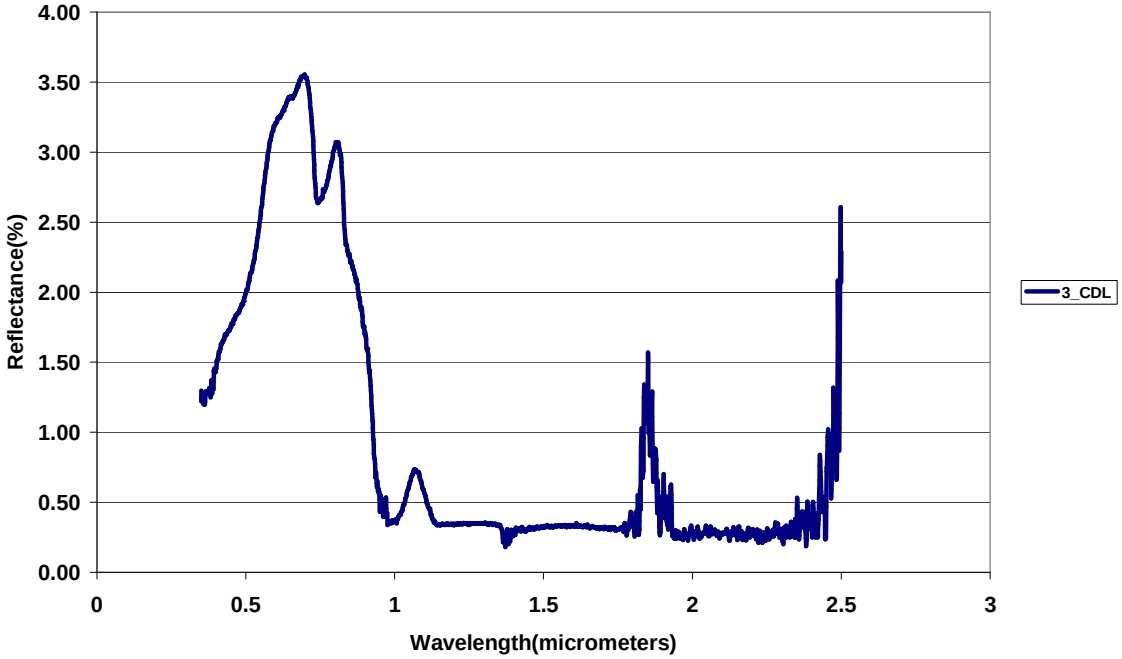

Figure 5.40. Spectral profile of sample 3 collected from dirty water at Cork River.

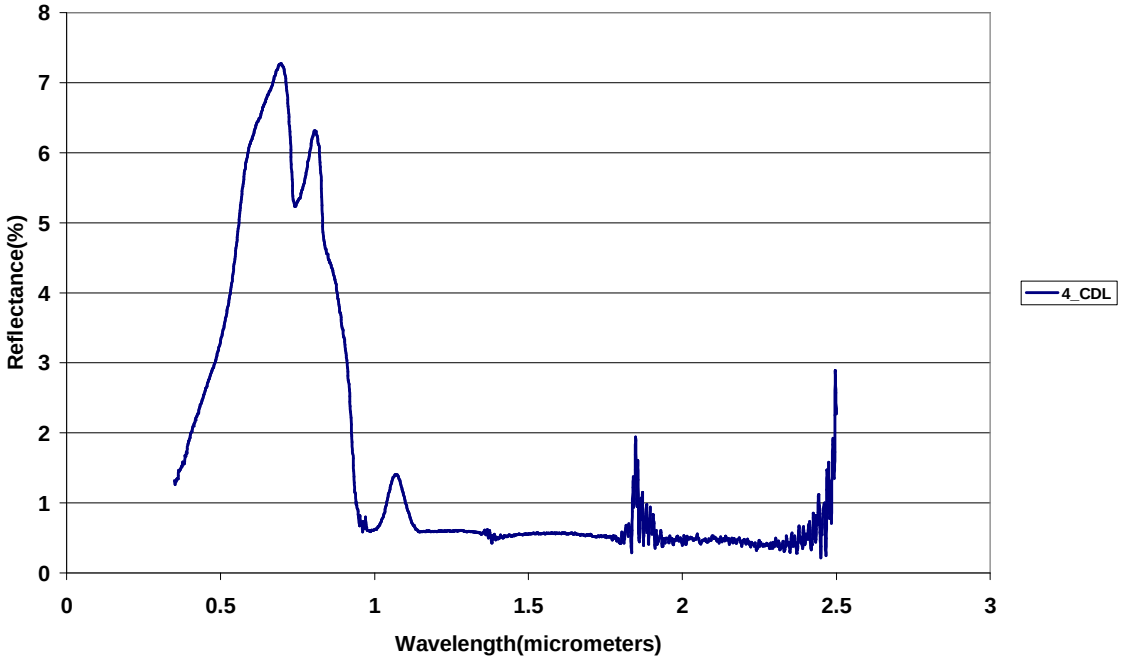

Figure 5.41. Spectral profile of sample 4 collected from dirty water at Cork River.

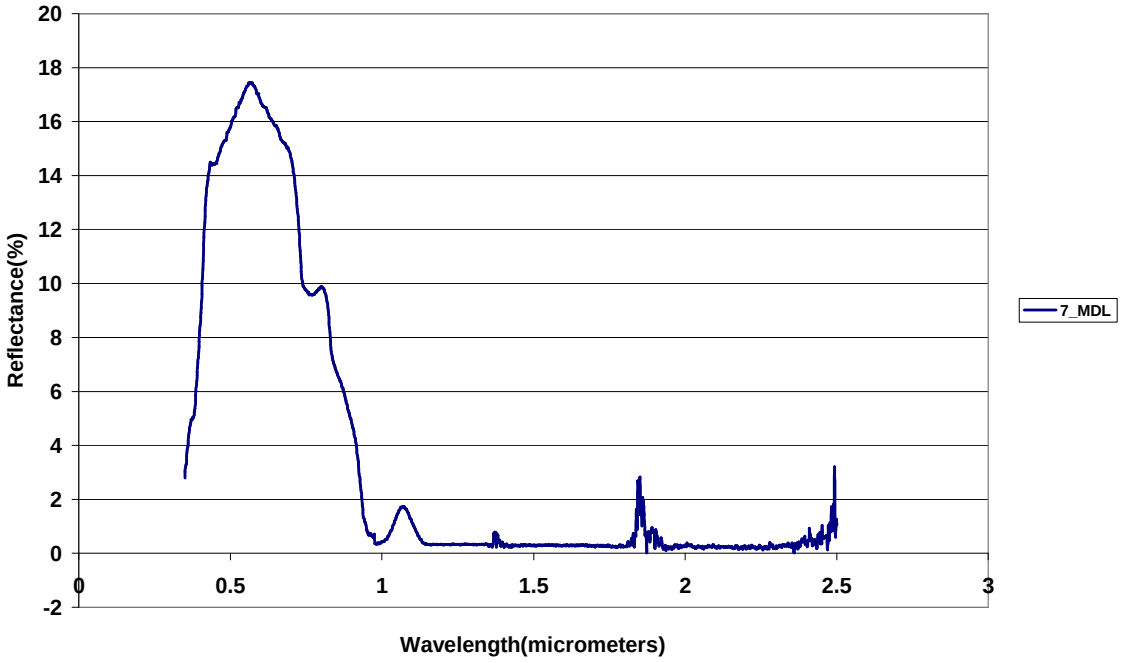

Figure 5.42. Spectral profile of sample 7 collected from dirty water at Mohlapitse (Mashilwane) River.

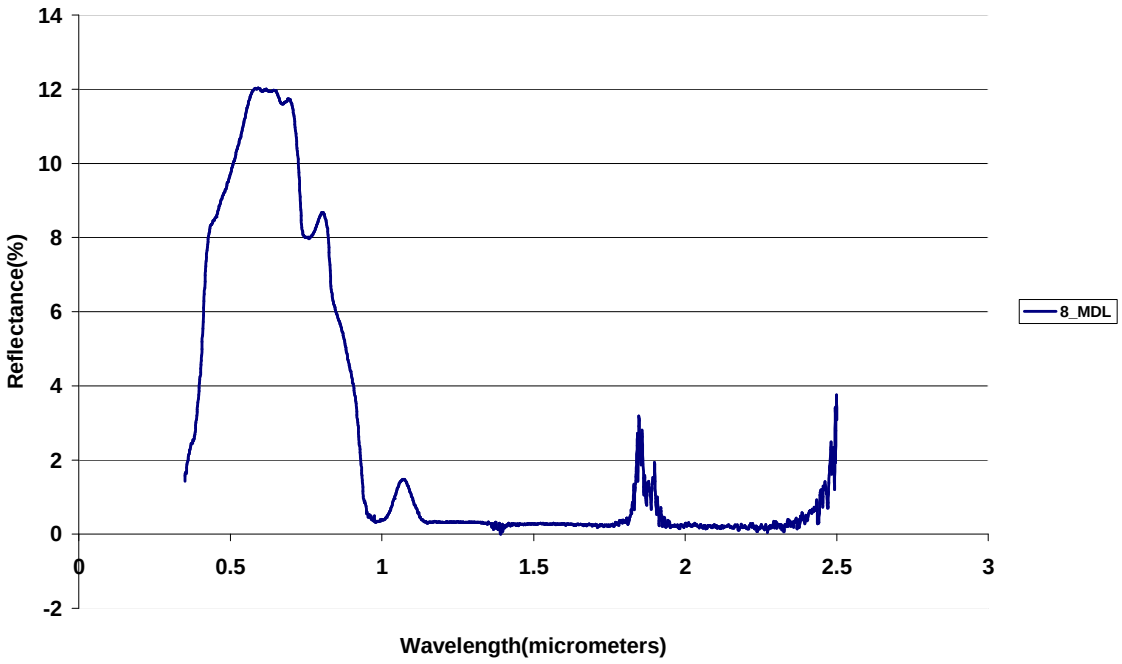

Figure 5.43. Spectral profile of sample 8 collected from dirty water at Mohlapitse (Mashilwane) River.

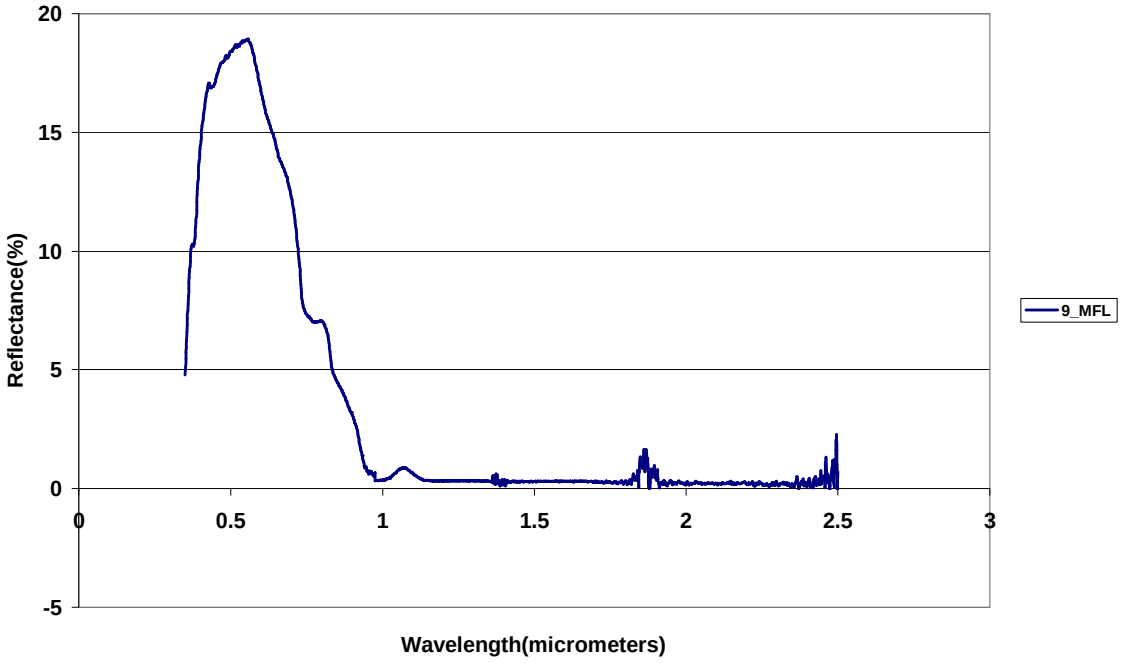

Figure 5.44. Spectral profile of sample 9 collected from flowing water at Mohlapitse (Mashilwane) River.

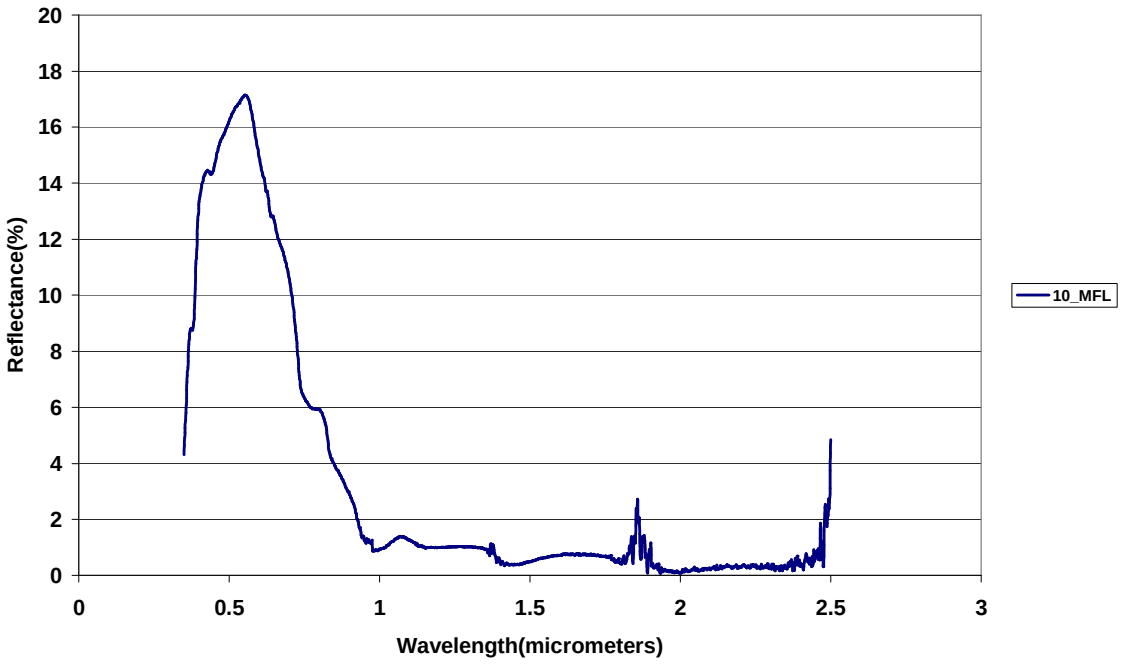

Figure 5.45. Spectral profile of sample 10 collected from flowing water at Mohlapitse (Mashilwane) River.

Spectral Reflectance of the Wet Soil Samples from the river

Figure 5.46 shows the spectral reflectance of the wet river bed soil collected from Mohlapitse river. A reflectance value above 8% was recorded between the wavelengths 0.8 – 1.4 μm with below 5% reflectance in the region 2.1 μm. A larger percentage of the radiation was absorbed. The reflectance pattern does not relate to that of a control water sample because of the presence of soil material. A relatively similar pattern is observed in Figures 5.47 and 5.48 with increased absorption in the region 1.4 – 2.4 μm in Figure 5.48. Figures 5.49 to 5.51 show the spectral profiles of the wet river bed soil samples collected at Cork river. Generally a similar pattern is observed compared to those at Mohlapitse despite the differences in reflectance values.

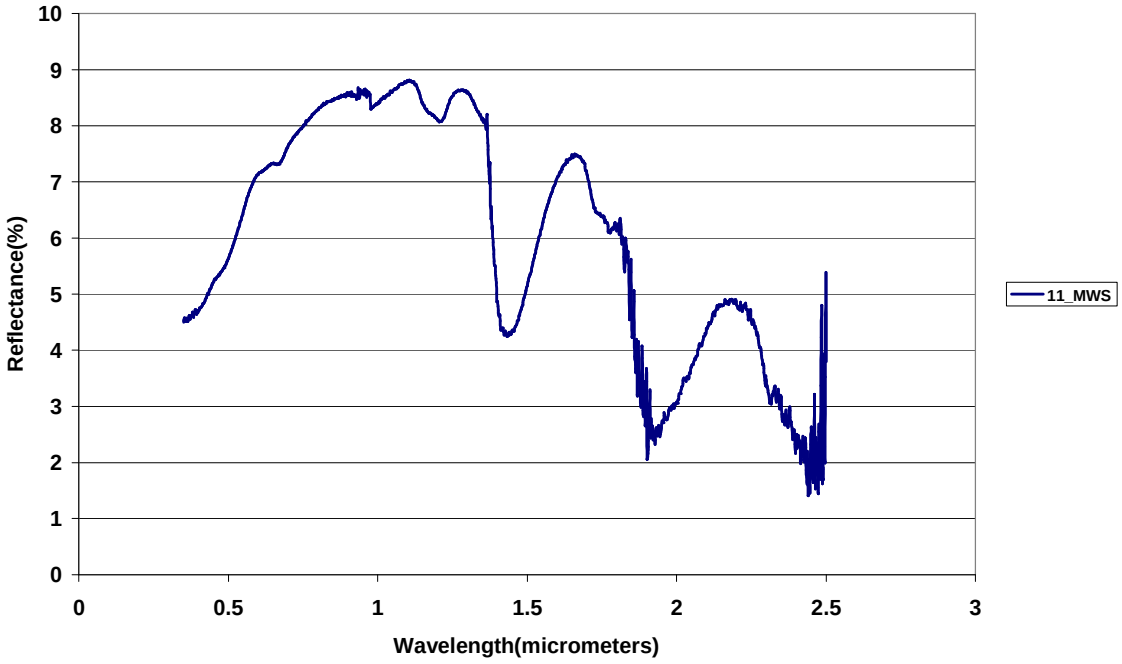

Figure 5.46. Spectral profile of sample 11 collected from river bed at Mohlapitse (Mashilwane) River.

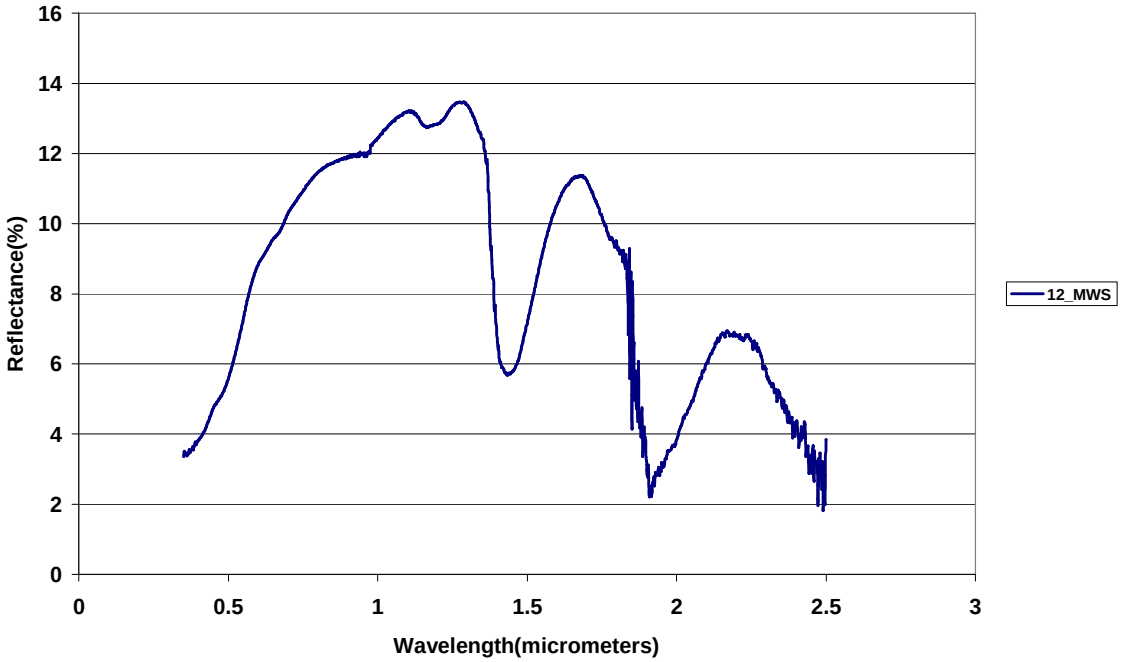

Figure 5.47. Spectral profile of sample 12 collected from river bed at Mohlapitse (Mashilwane) River.

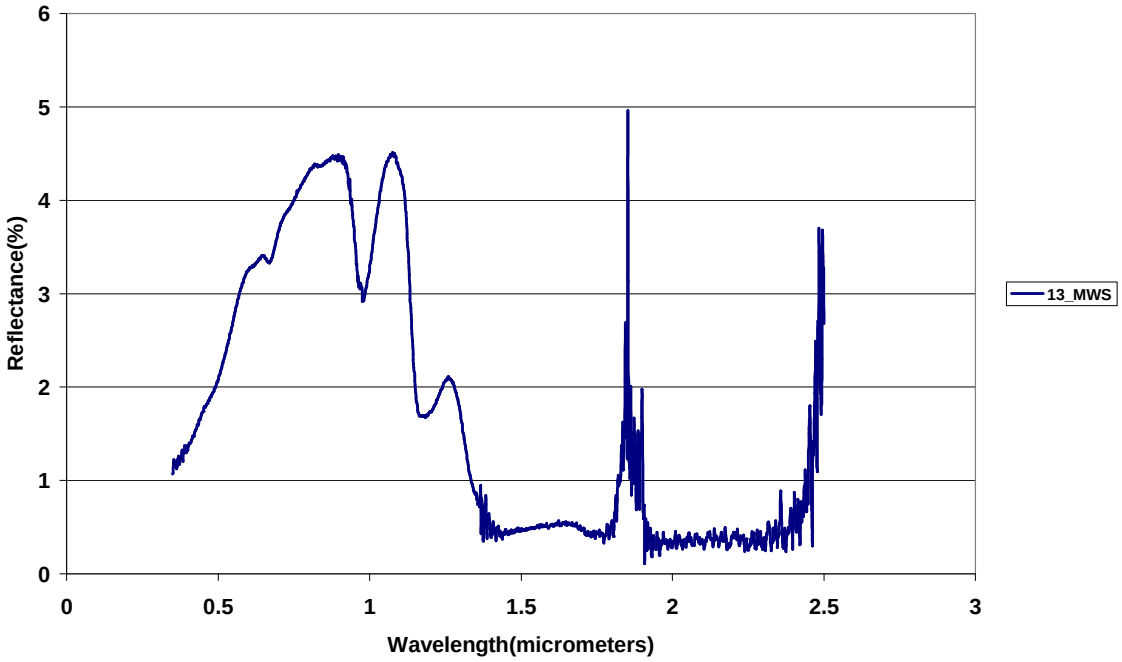

Figure 5.48. Spectral profile of sample 13 collected from river bed at Mohlapitse (Mashilwane) River.

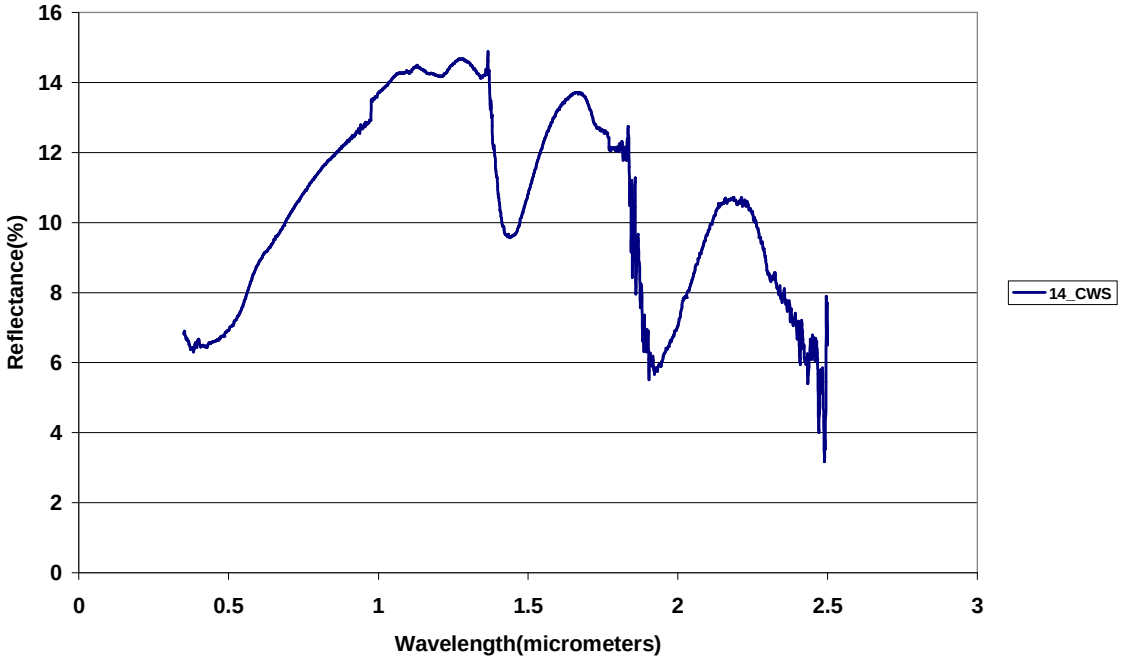

Figure 5.49. Spectral profile of sample 14 collected from river bed at Cork River.

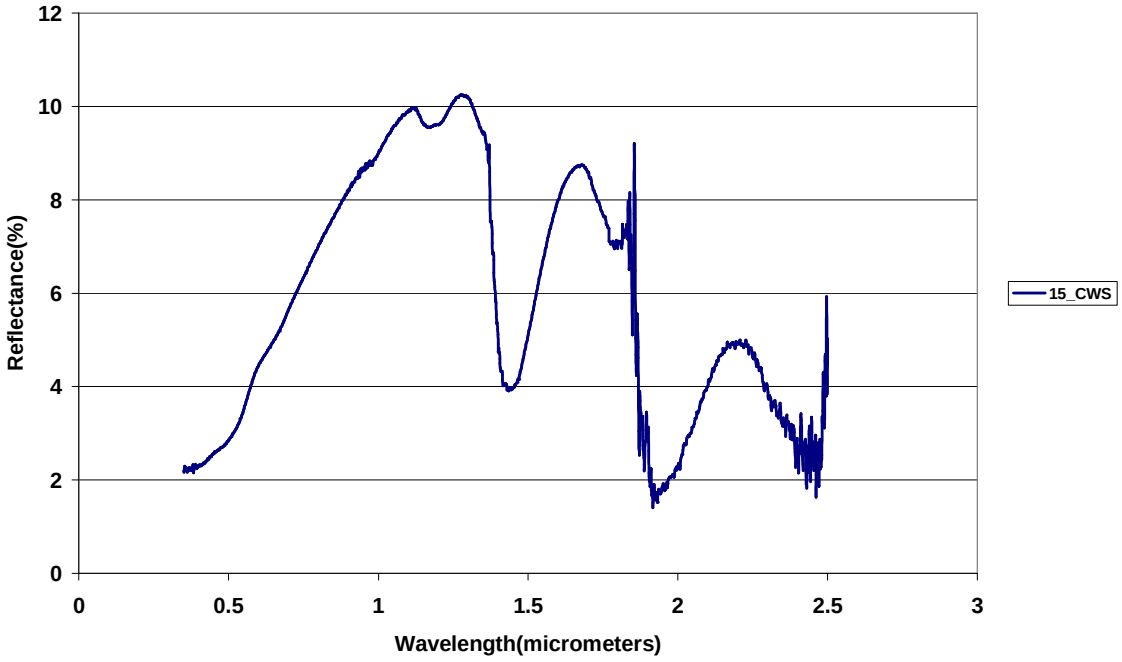

Figure 5.50. Spectral profile of sample 15 collected from river bed at Cork River.

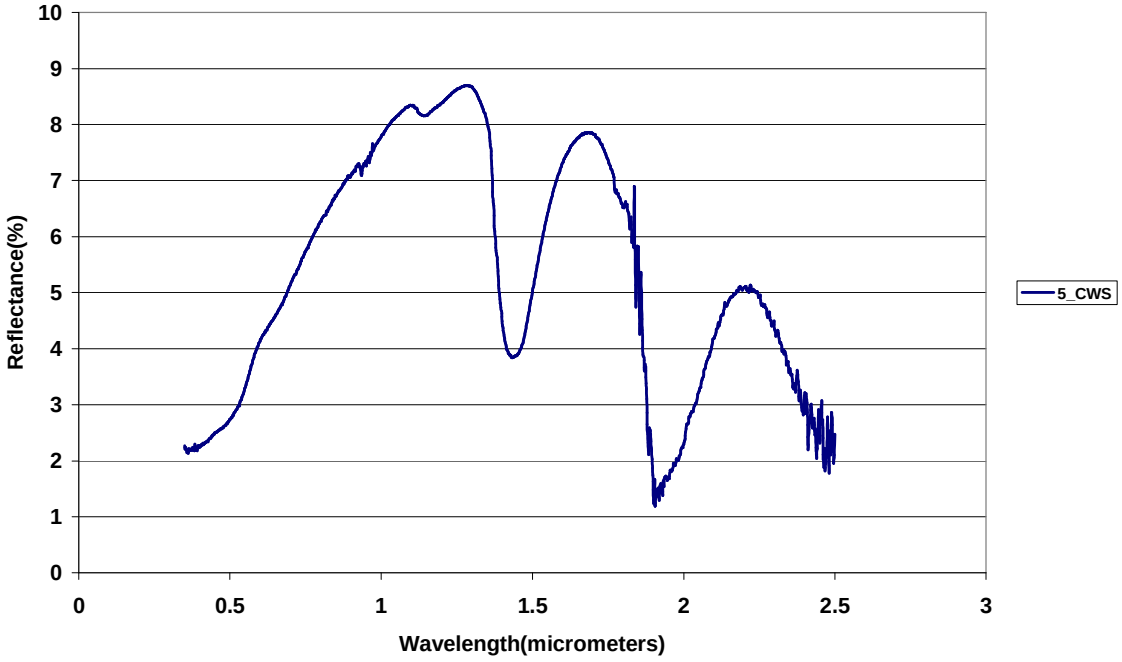

Figure 5.51. Spectral profile of sample 5 collected from river bed at Cork River.

5.6.3 Summary

From both the flowing and dirty water collected in the rivers, traces of asbestos minerals cannot be clearly detected. Wet soil samples collected from the river bed shows a slight reflectance of some materials although at a lower level. Because of the absorptive nature of water to electromagnetic radiation, it has been difficult to distinguish asbestos minerals in water. Further techniques (X-Ray Diffraction and Scanning Electron Microscopy) have been used to detect the presence of asbestos minerals in this case.

5.7. Laboratory based identification and characterization of asbestos minerals in soil and water samples from Mafefe and Mathabatha, Limpopo Province

5.7.1 Introduction

Sixteen soil and eight water samples were analyzed in the laboratory for identification and characterization of asbestos minerals. Asbestos is a geological term used for a group of naturally occurring silicate minerals with fibrous morphology. There are two classes of asbestos, based on the two mineral group to which they belong: serpentine asbestos and amphibole asbestos (Table 5.1). Chrysotile is the only asbestos mineral of the serpentine group, it is a sheet silicate and crystallizes in tubes and rods. All other asbestos, most common of which are actinolite, tremolite, grunerite, riebeckite and anthophyllite, belong to the amphibole family of minerals. Amphiboles are chain silicates most of which do not crystallize in asbestiform varieties. The term asbestiform is widely used in literature to describe appearance of minerals in the form of long, thin fibers or needle-like structures. It is also used to distinguish between fibrous and non fibrous varieties of the minerals from the serpentine and amphibole group. Those with fibrous morphology can separate easily along crystallographic planes to form extremely thin flat plates and fibrous or needle-like structures. All asbestos minerals have their non asbestiform analogues. The asbestos minerals are not classified on a mineralogical basis, but rather on a commercial basis because of their unique properties. Therefore, the asbestos variety commercially known as crocidolite is mineralogically identified as riebeckite and similarly amosite is a composite name for fibrous grunerite and cummingtonite. In this section all asbestos types are referred to by their proper mineral name.

Table 5.1. Common asbestos minerals

Commercial Name	Mineral Name	Mineral Group	Chemical Formula
Chrysotile	Chrysotile	Serpentine	(Mg, Fe)3Si2O5(OH)4
Crocidolite	Riebeckite	Amphibole	Na2(Mg,Fe2+)3Fe3+2Si8O22(OH)2
Anthophyllite	Anthophyllite	Amphibole	(Mg,Fe2+)7Si8O22(OH)2
Amosite	Grunerite-Cummingtonite	Amphibole	(Mg,Fe2+)7Si8O22(OH)2
Tremolite	Tremolite	Amphibole	Ca2(Mg,Fe)5Si8O22(OH)2
Actinolite	Actinolite	Amphibole	Ca2(Mg,Fe)5Si8O22(OH)2

5.7.2 Results and Discussion

X-ray Diffraction (XRD)

The XRD results of soil and water residue samples (Table 5.2) indicate a consistent soil mineral assemblage largely composed of quartz (between 29 and 97%); amphibole (trace-51%); mica (2-18%); calcite (1-33%) that is notably iron rich with hematite, goethite and magnetite present in varying proportions. Other phases identified in smaller amounts include smectite, Il/Sm Interstratifications (mixed clay), chlorite, serpentine, plagioclase and K-feldspar. Where Goethite/Hematite, Kaolinite/Chlorite and Kaolinite/Chlorite/Serpentine are reported and quantified together it should be considered as either one or the other or a bit of both to be present unless special sample preparation and instrumentation are used to confirm otherwise. This is due to peak interferences where closely spaced or overlapping XRD peaks and high background make trace mineral identification and quantification very difficult and have to be confirmed by Scanning Electron Microscopy (SEM) or other optical methods.

Small amounts (1-2%) of serpentine were identified in only three samples, namely C1 and C2, both wet soil and in dry soil sample Mt1. Determining the presence of chrysotile at very low

concentration levels is difficult due to the much higher amount of other crystalline substances contained in the sample and peak interferences with the rest of the serpentine minerals (lizardite and antigorite), kaolinite and chlorite having closely spaced reflection at 7.2 – 7.4 ´ region. This becomes even a bigger issue since the asbestiform and non asbestiform analogs of the serpentine and amphibole minerals are not distinguishable by XRD, so results may vary.

Amphibole was detected in all samples ranging from trace to ~51%. The highest concentrations were detected in samples WP 58 cork2 (51%), WP 58 cork1 (42%) and WP 66 (40%) all representing dry soil samples. The wet soil samples appear to contain noticeably less amphibole minerals (2-4%) and similarly this also applies to the water residue samples. Actinolite-tremolite, grunerite and riebeckite were positively identified in the samples where their concentrations exceed 10%.

Table 5.2. Bulk mineral compositions as determined by X-Ray Diffraction, expressed as semi quantitative estimates (wt%)

Sample	Description	Calcite	Goethite	Goethite/Hematite	Hematite	Magnetite	K-Feldspar	Plagioclase	Quartz	Kaolinite/Chlorite	Kaolinite/Chlorite/Serpentine	Serpentine	Amphibole	Mica	Smectite	II/Sm Interstratification
BW 1	dry soil	-	4	-	9	2	-	-	50	-	-	-	25	10	-	-
BW 2	dry soil	33	2	-	1	1	-	-	42	-	-	-	6	15	-	-
Mt 1	dry soil	-	-	-	-	-	-	2	42	9	-	1	29	17	-	-
Mt 2	dry soil	1	10	-	7	-	-	-	54	-	2	-	9	16	2	-
WP 58 cork1	dry soil	1	5	-	5	2	-	-	33	-	-	-	42	7	6	-
WP 58 cork2	dry soil	-	6	-	2	1	-	-	29	-	-	-	51	7	4	-
WP 66	dry soil	-	9	-	3	-	-	1	36	-	-	-	40	7	3	-
WP 71	dry soil	4	-	11	-	3	2	2	66	-	2	-	5	4	-	-
WP 72	dry soil	2	5	-	3	1	1	2	49	-	2	-	24	10	-	-
WP 74	dry soil	13	4	-	1	1	1	2	42	-	3	-	11	18	-	4
CS 1	wet soil	6	-	1	-	-	-	-	80	1	-	1	2	3	1	4
CS 2	wet soil	5	-	1	-	-	-	1	78	1	-	2	trace	4	2	6
MS 1	wet soil	-	-	trace	-	-	1	-	97	-	1	-	1	-	-	-
MS 2	wet soil	-	-	2	-	1	1	-	92	-	1	-	1	2	-	-
MS 3	wet soil	trace	-	2	-	trace	2	-	91	-	1	-	1	2	-	2
SS cork (streambed soil)	wet soil	5	-	2	-	-	-	2	81	-	3	-	3	4	-	-
W 1	water residue	No sufficient material for XRD														
W 2	water residue	No sufficient material for XRD														
W 3	water residue	3	3	-	1	-	-	2	75	-	3	-	2	3	-	9
W 4	water residue	13	3	-	1	-	-	1	61	-	3	-	2	4	4	8
W 7	water residue	5	-	3	-	-	2	2	65	-	3	-	3	6	3	10
W 8	water residue	4	-	1	-	-	1	2	70	-	3	-	2	4	3	10
W 9	water residue	No sufficient material for XRD														
W 10	water residue	No sufficient material for XRD														

Scanning Electron Microscopy (SEM) with Energy Dispersive Microanalysis System (EDS) analysis

Backscattered Electron (BSE) images of the identified asbestos minerals for each sample are presented in Figures 5.42 to 5.75 along with a short description of the morphology of the

fibres and their dimensions. The fibre size may not always correspond to actual size either because they are partially exposed or of submicron size. In case of fragment and bundle of fibres usually the dimensions of the longest and thinnest (smallest diameter) that might potentially be produced is given. The mineral chemistry of selected representative fibre identified for each sample is also supplied.

All minerals identified by XRD were also observed here as well as some trace minerals that were below the detection limits of the XRD. Those include ilmenite, Ti-oxide, REE –oxides, siliceous diatoms in the water residue samples.

The asbestos minerals were identified based on their fibrous or fibre-like morphology and their major element proportions. Some are observed as massive fragments with visible cleavage potentially separating into fibre and others as bundles of more defined fibrous morphology.

Serpentine (chrysotile) was positively detected in sample CS2 where it was also identified by XRD. In single occasions fibre of chrysotile composition was noted in the water residue samples W3 and possibly, but quite unclear W10.

Amphibole minerals, represented by actinolite, tremolite, grunerite, riebeckite and occasionally anthophyllite were detected in the soil as well as in the water residue samples (Figures 5.52 to 5.75 and Table 5.27)

Sample BW1

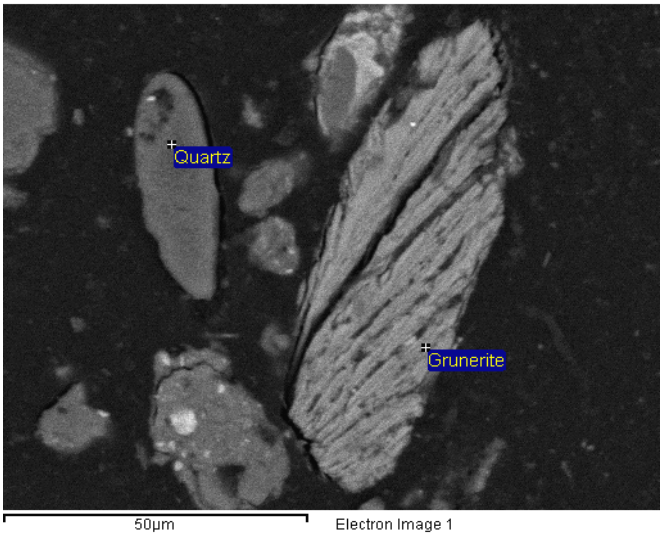

A bundle of straight to slightly curved fibers of grunerite
Fragment size: 83.51 x 25.25 µm
Fibre dimensions: 55.7 x 0.138 and smaller (the longest and the thinnest visible fiber)

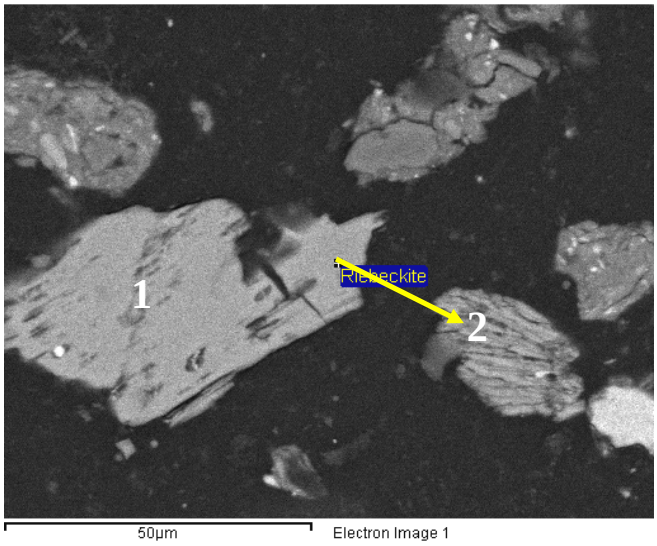

A fragment of massive riebeckite (1) with signs of cleavage that might become potential breakage planes and a bundle (2) of short curved fibers.

Massive fragment size: 54.43 x 34.65 µm
Fibre dimensions: 21.46 x 0.462 µm (visible)

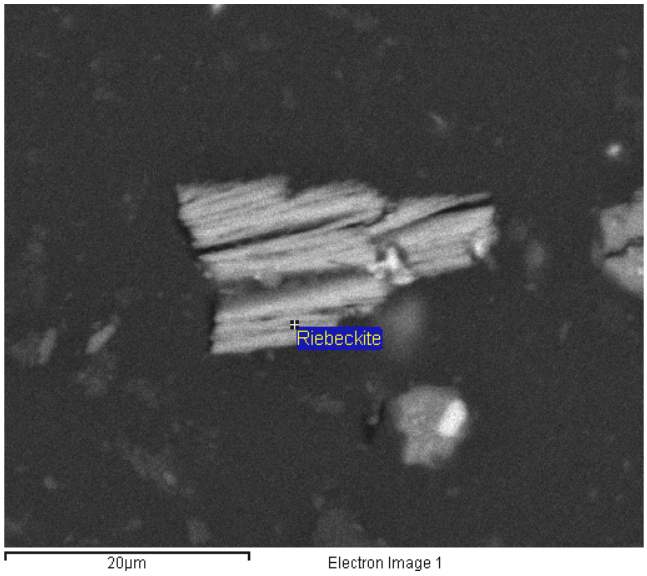

A bundle of fibrous riebeckite.
Fibre dimensions: 23.14 x 0.413 µm

Figure 5.52. BSE images of asbestos minerals identified in sample BW2

Table 5.3. EDS analyses of selected asbestos minerals from sample BW1

	Na2O	MgO	Al2O3	SiO2	K2O	CaO	FeO
Grunerite	0.51	8.3	0.28	55.06	0	1.33	35.37
Grunerite	0	7.71	0.17	55.62	0	0.35	36.4
Grunerite	0	7.87	0.11	55.99	0	0.3	35.83
Grunerite	0.13	7.96	0.19	54.89	0	0.66	36.53
Riebeckite massive	6.22	3.94	0	54.03	0.73	1.18	32.78
Riebeckite massive	5.58	4.04	0.01	55.02	0.93	1.64	33.25
Riebeckite massive	5.09	4.37	0	55.32	1.09	1.85	31.23
Riebeckite massive	5.63	4.12	0	54.79	0.92	1.56	32.42
Riebeckite fibre	6.29	5.04	0.22	57	0.85	1.35	30.1
Riebeckite fibre	6.03	5.2	0.26	57.3	1.11	1.67	29.39
Riebeckite fibre	5.44	4.22	0	54.39	1.24	1.45	29.34
Riebeckite fibre	5.84	4.23	0.08	54.86	0.91	1.38	31.32

Table 5.4. EDS analyses of selected asbestos minerals from sample BW2

	Na2O	MgO	Al2O3	SiO2	K2O	CaO	FeO
Grunerite	0.13	5.8	0.83	55.66	0.03	0.57	35.95
Grunerite	0.23	7.34	1.14	55.04	0.13	1.42	35.52
Grunerite	0	6.52	1.13	56.21	0	1.14	34.82
Grunerite	0.05	6.55	1.04	55.3	0.04	1.04	35.1
Tremolite	0.58	14.36	2.19	59.18	0.31	11.63	10.34
Tremolite	0.29	15.55	3.57	59.22	0	11.99	8.79
Actinolite	0.33	6.11	3.43	56.45	0.81	6.68	26.6
Actinolite	0.27	5.6	3.37	55.57	0.91	5.96	26.62
Actinolite	0	5.27	2.65	55.46	0.44	6.31	25.33

Sample BW2

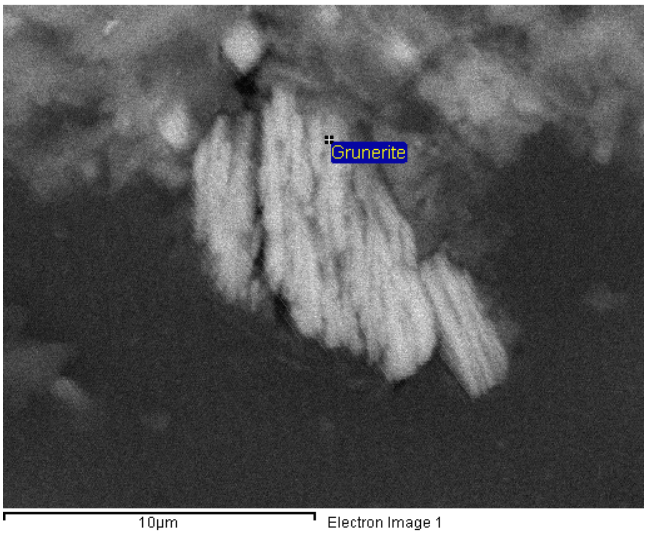

Grunerite bundle of straight rigid fibres
Individual fibre size: 7.68 x 0.200 µm

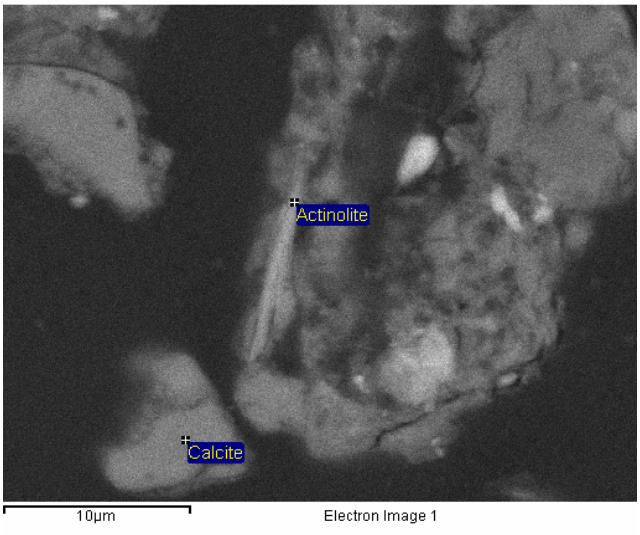

Single actinolite fibre in process of splitting further (bottom end)
Dimensions: 10.72 x 0.44 µm

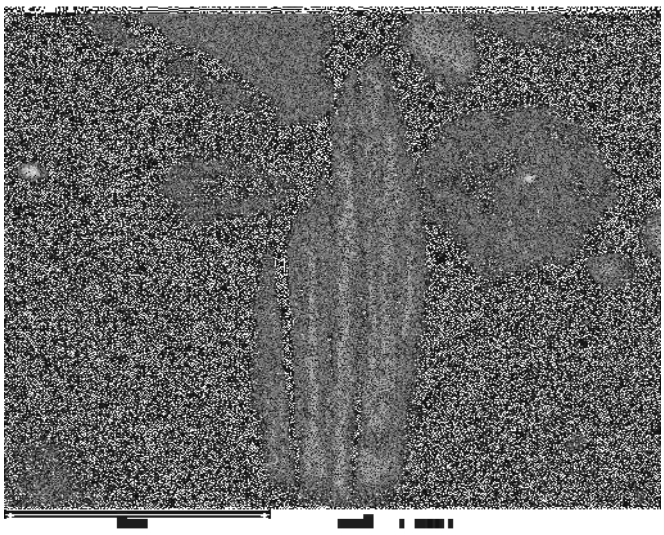

Tremolite bundle of straight composite fibres
Individual fibre size: 35.23 x <100nm

Figure 5.53. BSE images of asbestos minerals identified in sample BW2

Sample CS1

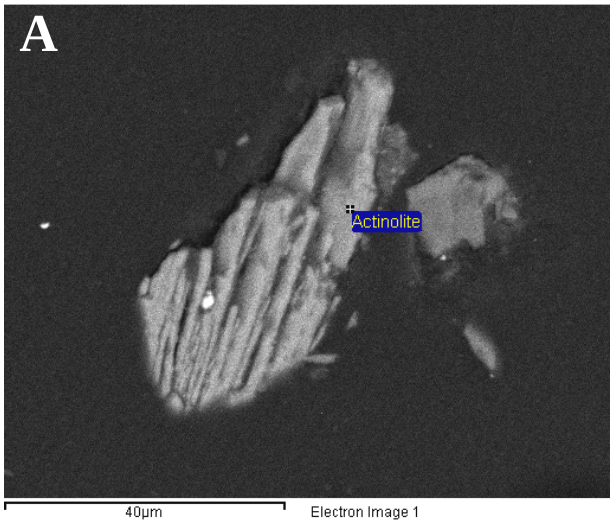

Actinolite bundle of straight rigid fibres
Individual fibre size: 53.72 µm x <0.165µm

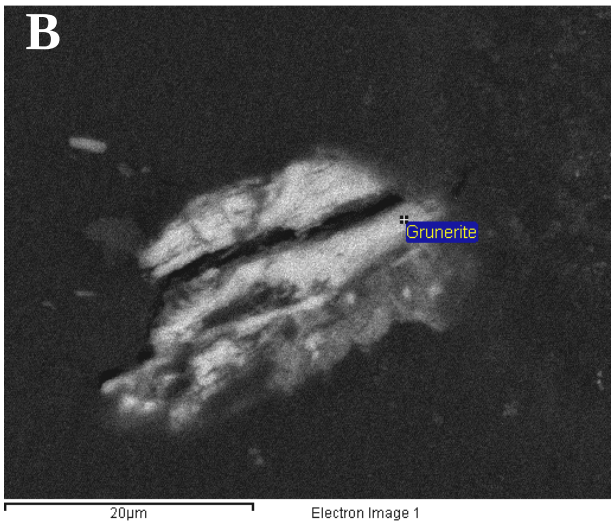

Grunerite (B)
Individual fibre size: 23.84 µm x 0.346µm

A composite fragment of massive and fibrous anthophyllite (C)
Individual fibre size: 41.06 µm x 26.46µm

Tremolite bundle of rigid fibre of various thickness (D)
Individual fibre size: 28.58 µm x 0.638 µm

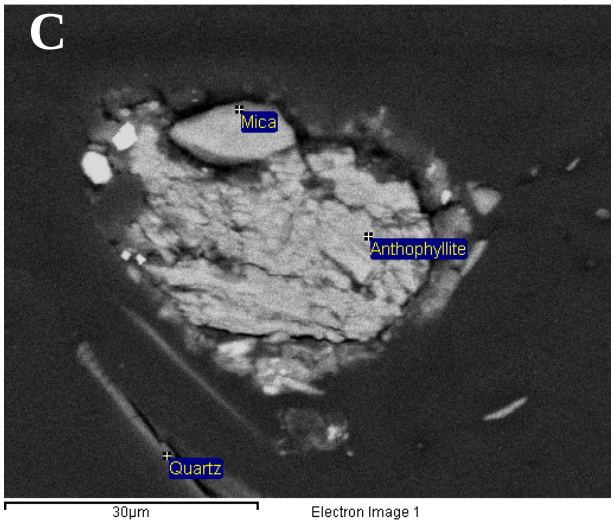

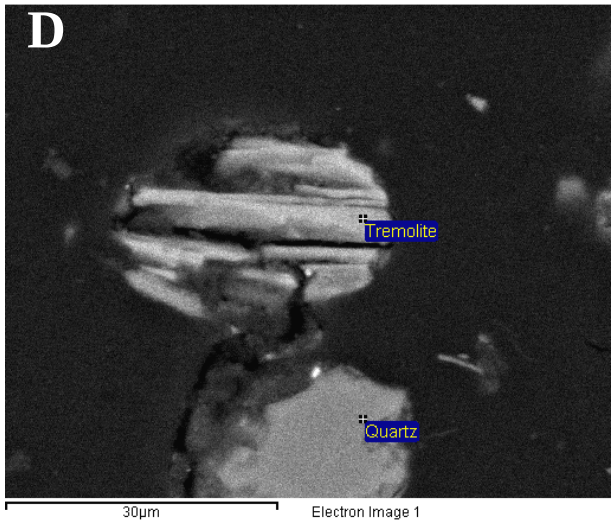

Figure 5.54. BSE images of asbestos minerals identified in sample CS1

Table 5.5. EDS analyses of selected asbestos minerals from sample CS1

	Na2O	MgO	Al2O3	SiO2	K2O	CaO	FeO
Grunerite	0.49	4.95	1.92	56.11	0.19	0.22	35.59
Grunerite	0	7.1	1.36	54.59	0.45	0.61	35.94
Grunerite	0	6.55	1.35	53.7	0.01	0.54	35.87
Grunerite	0	7.2	1.35	52.28	0	0.87	35.47
Anthophyllite	0.47	24.17	0	59.25	0.1	0.54	13.86
Anthophyllite	0.32	24.76	0.03	58.83	0	0.38	14.63
Anthophyllite	0.1	24.01	0.37	59.22	0	0.29	12.37
Anthophyllite	0.3	24.31	0.1	58.44	0	0.41	13.62
Tremolite	0.81	17.05	4.7	56.29	0.14	12.18	7.64
Tremolite	1.08	16.41	4.76	56.12	0.07	11.57	7.87
Tremolite	1.11	18.09	4.62	56.4	0.13	12.62	6.03
Tremolite	1	17.19	4.69	56.6	0.11	12.12	7.85
Ferro-actinolite	2.22	4.02	4.39	46.66	1.41	7.68	33.42
Ferro-actinolite	2.22	3.09	4.42	49.01	1.09	8	29.44
Ferro-actinolite	1.33	3.18	3.46	49.82	0.85	9.64	30.9
Ferro-actinolite	1.96	3.61	3.89	48.98	0.75	9.51	30.26
Ferro-actinolite	2.29	3.99	3.86	49.11	0.66	9.11	29.8

Table 5.6. EDS analyses of selected asbestos minerals from sample CS2

	Na2O	MgO	Al2O3	SiO2	K2O	CaO	FeO
Ferro-actinolite	1.29	13.51	4.14	52.58	0.3	8.12	18.16
Ferro-actinolite	1.36	14.57	4.13	50.96	0.22	8.88	18.25
Ferro-actinolite	1.52	12.08	4.74	52.9	0.52	7.74	19.02
Tremolite	0	20.87	0.72	60.4	0.15	12.13	4.38
Tremolite	0	20.4	0.43	58.75	0.22	13.24	4.11
Tremolite	0.23	22.6	0.55	58.42	0	13.15	3.57
Chrysotile	0	40.02	0.44	46.26	0	0.12	2.73
Chrysotile	0.14	37.31	1.07	43.48	0.11	0.15	2.67
Chrysotile	0.12	38.89	1.14	42.05	0.14	3.38	8.18
Chrysotile	0.07	39.41	1.58	42.46	0.07	3.5	7.24
Chrysotile	0	40	1.85	41.48	0	1.97	8.86
Chrysotile	0.25	35.09	4.88	39.92	0.13	0.5	7.97

Sample CS1

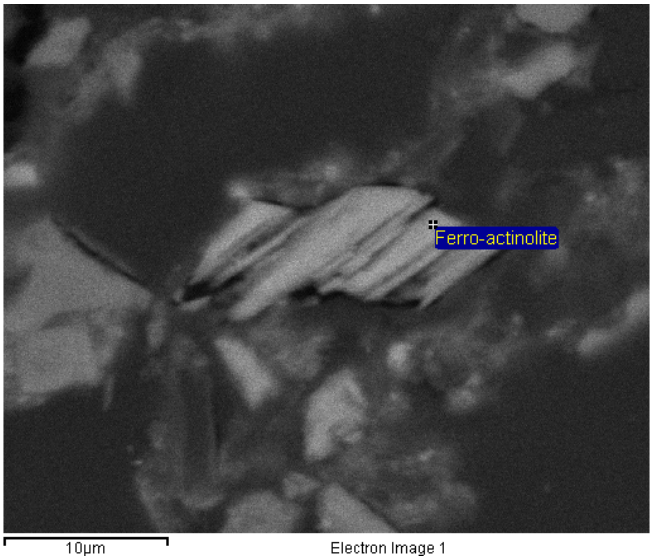

Fe-rich actinolite fibre
Individual fibre size: 13.58 x 0.570 µm

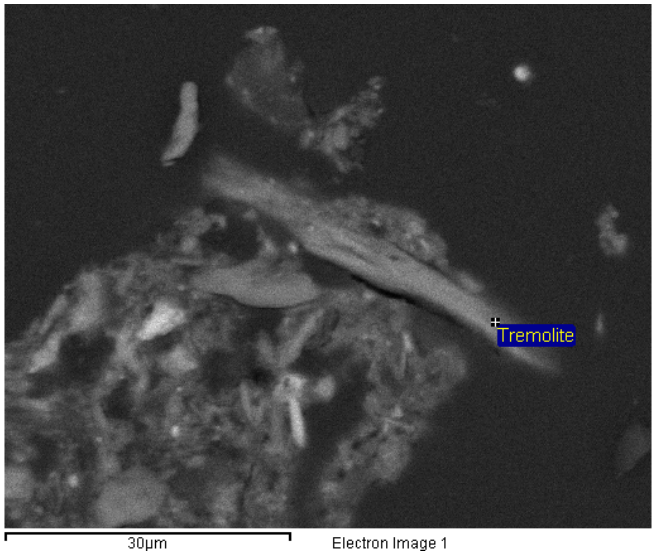

Thin elongated tremolite fibre with signs of further splitting
Individual fibre size: 40.53 x 2.880 µm

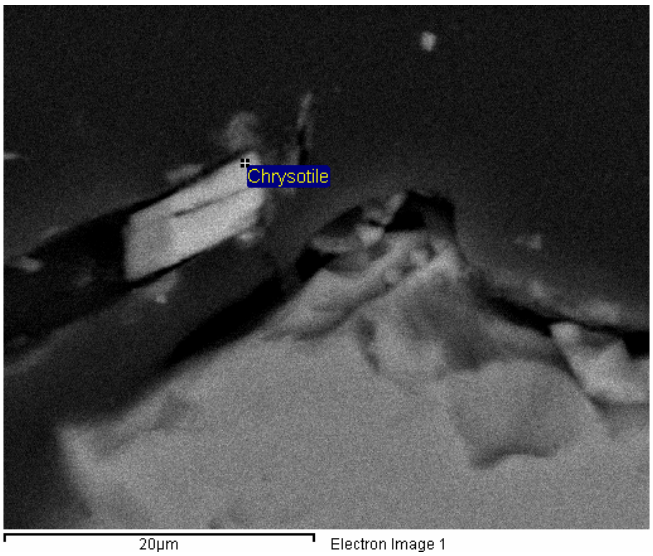

Chrysotile with individual fibre size of 7.73 x 2.15 µm

Figure 5.55. BSE images of asbestos minerals identified in sample CS2

Sample MS1

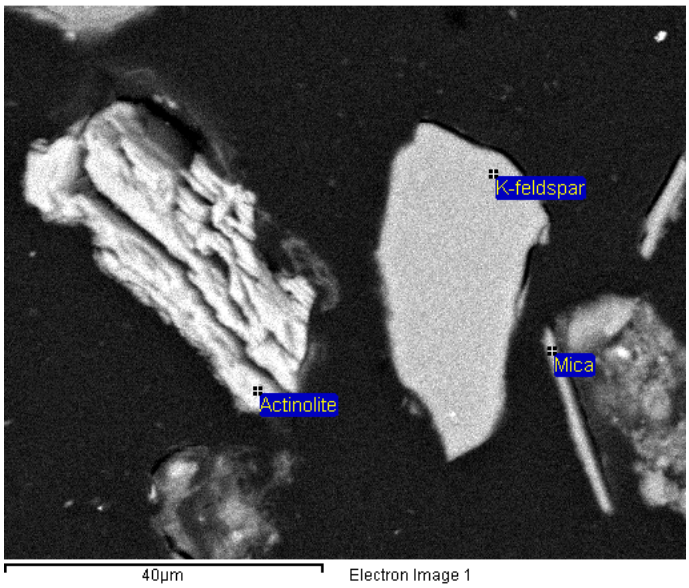

Actinolite bundle with straight to slightly curved fibers
Individual fibre size:
40.05 x 0.575 µm

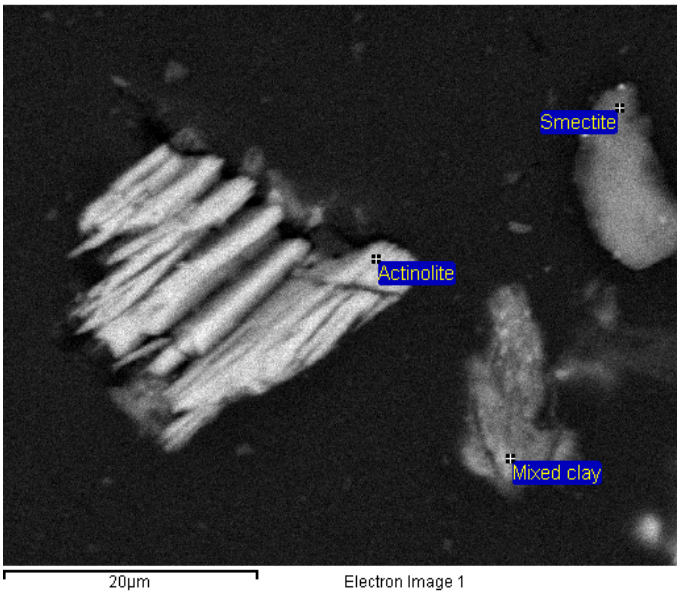

Well separated straight actinolite fibers
Individual fibre dimensions:
23.16 x 0.286 µm

Figure 5.56. BSE images of representative specimens of asbestos minerals from sample MS1.

Sample MS2

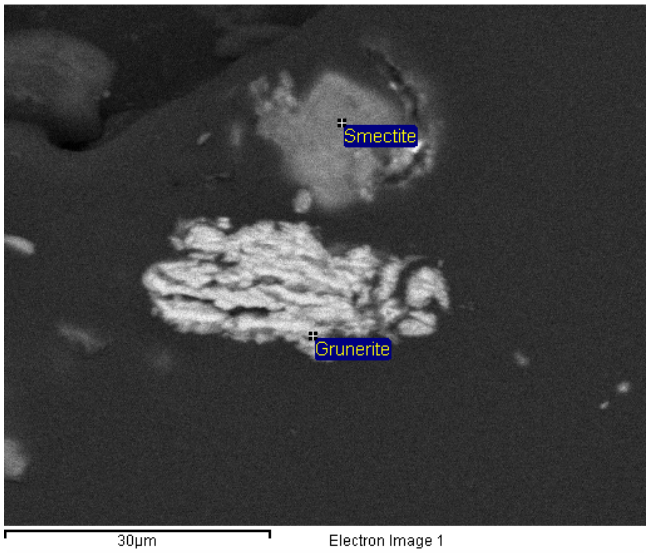

Grunerite bundle of curved fibers
Individual fibre dimensions:
23.13 x 0.416 µm

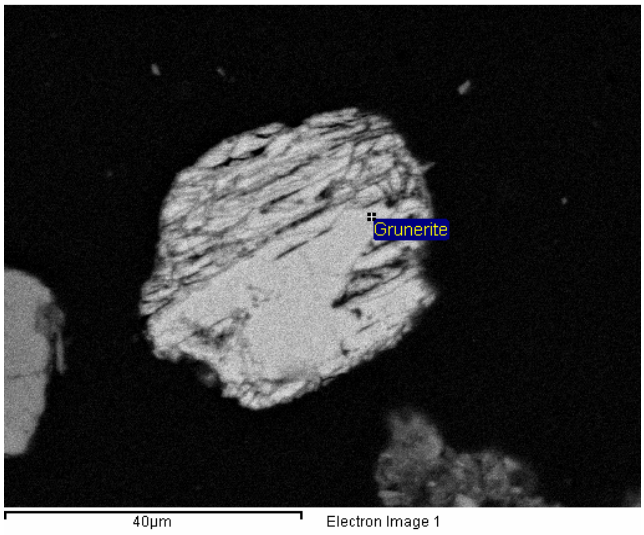

A composite fragment of fibrous and massive grunerite
Individual fibre dimensions:
41.37 x 0.235 µm

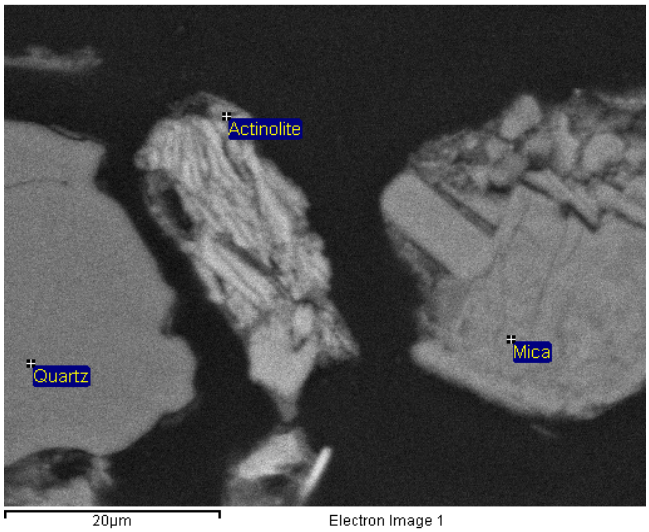

Actinolite bundle with straight to curved fibers
Individual fibre dimensions:
8.43 x 0.359 µm (the longest and thinnest)

Figure 5.57. BSE images of representative specimens of asbestos minerals from sample MS2.

Table 5.7. EDS analyses of selected asbestos minerals from sample MS1

	Na2O	MgO	Al2O3	SiO2	K2O	CaO	FeO
Actinolite	0	17.7	2.55	49.78	0.14	12.97	14.62
Actinolite	0	17.26	2.33	50.28	0.14	12.89	14.41
Actinolite	0.2	19.14	2.68	50.52	0	12.55	13.7
Actinolite	0	17.05	3.06	50.7	0	13.57	14.58
Actinolite	0.15	17.75	3.89	49.7	0	12.73	14.46

Table 5.8. EDS analyses of selected asbestos minerals from sample MS2

	Na2O	MgO	Al2O3	SiO2	K2O	CaO	FeO
Actinolite	0.31	14.14	1.18	55.59	0.24	11.86	15
Actinolite	0	14.26	1.64	55.71	0.26	12.38	14.81
Actinolite	0.22	13.01	2.24	55.03	0.21	11.94	15.83
Actinolite	0.17	13.8	1.69	54.44	0.24	12.06	15.21
Grunerite	0	4.9	0.13	51.01	0.36	0.11	41.77
Grunerite	0	4.51	0	52.07	0	0.2	41.87
Grunerite	0.19	4.85	0	50.21	0.02	0.14	41.64
Grunerite	0.37	6.37	0.1	55.05	0.21	0.32	36.11
Grunerite	0.35	6.89	0	54.54	0.01	0.04	36.42
Grunerite	0.63	6.55	0.11	54.3	0.04	0.33	36.86

Table 5.9. EDS analyses of selected asbestos minerals from sample MS3

	Na2O	MgO	Al2O3	SiO2	K2O	CaO	FeO
Actinolite	0.15	16	2.23	56.62	0.06	12.24	11.29
Actinolite	0.28	15.99	1.92	55.74	0.11	12.68	11.4
Actinolite	0.02	15.26	2.84	56.64	0.18	9.55	13.43
Actinolite	0.14	17.36	2.6	55.92	0.06	12.56	8.59
Actinolite	0	16.12	3.3	54.49	0	11.77	13.84
Tremolite	0	19.31	1.57	55.37	0	18.5	3.23
Tremolite	0.87	19.34	0.18	57.65	0.18	15.42	2.31
Tremolite	0.51	20.15	2.37	59.14	0	12.43	2.5
Riebeckite	6.5	3.44	0	57.72	0.17	0.32	33.31
Riebeckite	6.38	2.34	0.84	55.61	0.27	0	32.85
Riebeckite	5.33	3.03	0.03	54.79	0.07	0.08	35.45
Riebeckite	6.07	2.94	0.29	56.04	0.17	0.04	33.87

Sample MS3

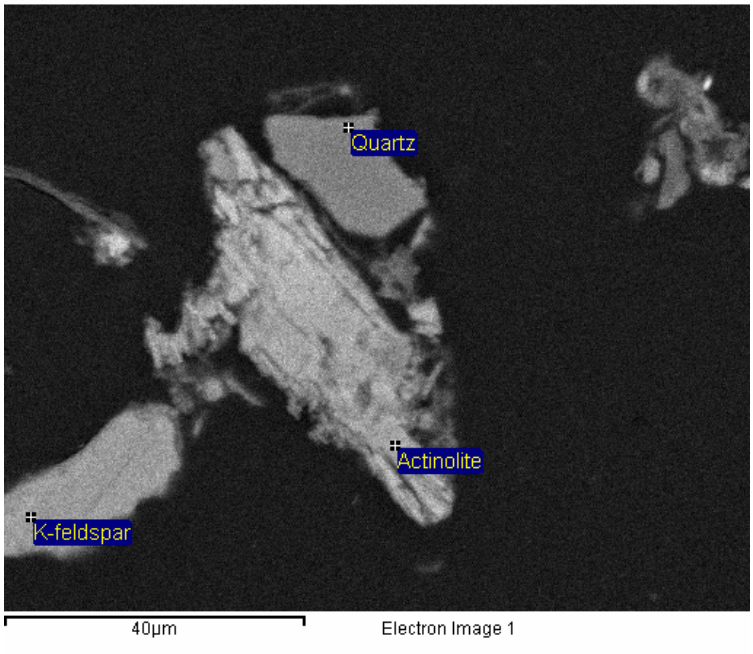

Actinolite fibre size:
47.82 x 0.280 µm

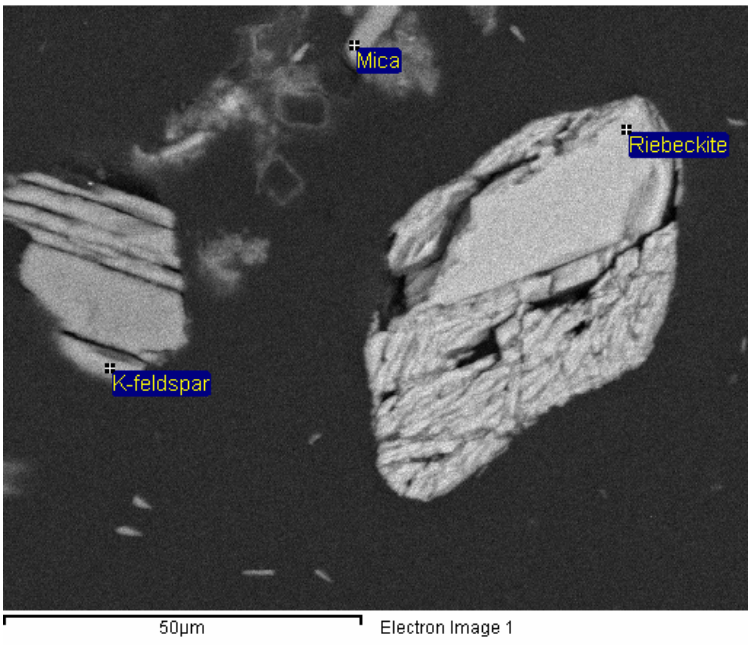

A composite fragment of massive and fibrous riebeckite. Individual fibre dimensions: the longest and the thinnest – 9.89 x 0.173 µm

Figure 5.58. BSE images of representative specimens of asbestos minerals from sample MS3.

Sample Mt1

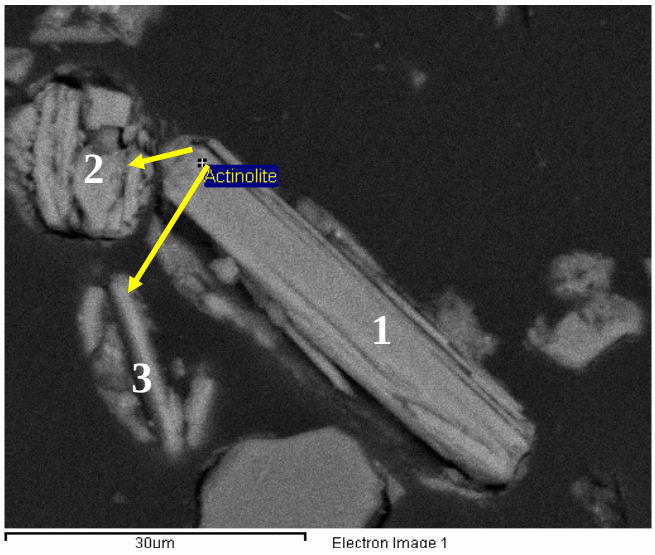

Elongate lath-like actinolite crystal (1), a bundle (2) and single actinolite fibre (3)
Dimensions: 1) 45.63 x 0.445 µm
2) 13.30 x 1.25 µm
3) 18.40 x 1.20 µm

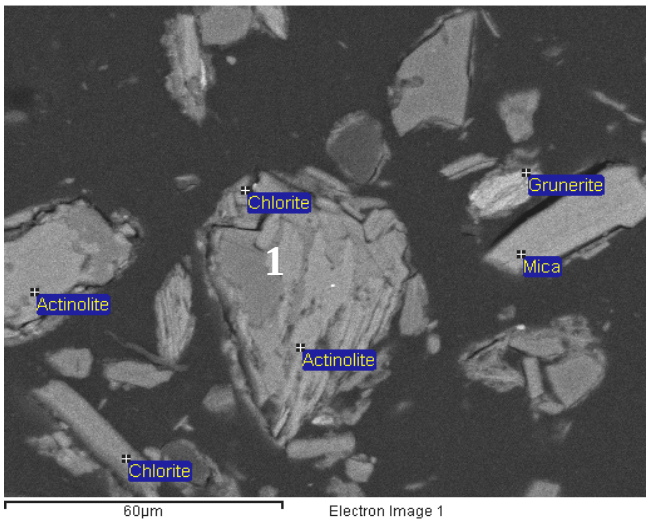

Aggregate of actinolite and chlorite (centre), massive actinolite (left) and grunerite (white, right). Note elongate prismatic "fibrous" chlorite in the bottom left corner.
Dimensions:
Actinolite: 17.82 x 1.645 µm
Grunerite: 13.56 x 0.456 µm

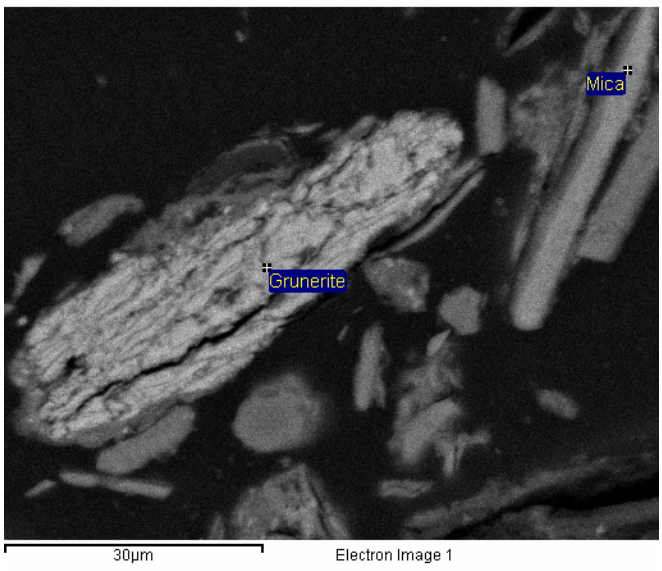

Grunerite bundle of curved fibre
Individual fibre size:
from 5.12 x 0.585 µm
to 13.50 x 1.23 µm

Note prismatic "fibrous" mica – top right corner

Figure 5.59. BSE images of representative specimens of asbestos minerals from sample Mt1

Table 5.10. EDS analyses of selected asbestos minerals from sample Mt1

	Na2O	MgO	Al2O3	SiO2	K2O	CaO	FeO
Actinolite	0.82	15.4	7.88	51.76	0.1	11.42	9.02
Actinolite	0.89	15.92	5.26	52.64	0.02	10.33	9.44
Actinolite	1.5	14.11	7.84	50.41	0	11.33	11.12
Actinolite	0.78	18.52	6.06	52.94	0.11	10.17	9.28
Actinolite	0.48	14.54	5.89	53.88	0.17	12.13	11.87
Actinolite	0.22	15.34	5.36	53.04	0.14	12.79	11.82
Actinolite	0.37	15.91	4.5	54.85	0	12.65	8.74
Grunerite	0	4.75	2.28	48.33	0.11	0.5	40.7
Grunerite	0	6.09	0.45	50.59	0.17	0.4	41.38
Grunerite	0.05	3.81	2.85	49.72	0.05	0.3	40.99
Grunerite	0.23	6.77	0.14	50.33	0.16	0.1	39.51
Grunerite	0.02	6.82	0.15	52.27	0	0.3	38.31
Grunerite	0	6.99	0.22	51.65	0.1	0.34	39.05

Table 5.11. EDS analyses of selected asbestos minerals from sample Mt2

	Na2O	MgO	Al2O3	SiO2	K2O	CaO	FeO
Grunerite	0.09	5.73	0.27	46.78	0	0.41	43.46
Grunerite	0	6.52	0	50.32	0.16	0.03	40.17
Grunerite	0.7	7.9	0.1	50.28	0.12	0.22	38.99
Grunerite	0.34	6.28	0.28	56.25	0.47	0.07	34.93
Grunerite	0	0.82	1.5	53.14	0.36	0.44	42.11
Grunerite	0.17	7.34	0	50.6	0	0.19	39.52
Grunerite	0.95	7.02	0.27	51.25	0	0.31	38.39
Tremolite-massive	0.05	19.82	2.27	55.45	0.12	13.19	6.68

Sample Mt2

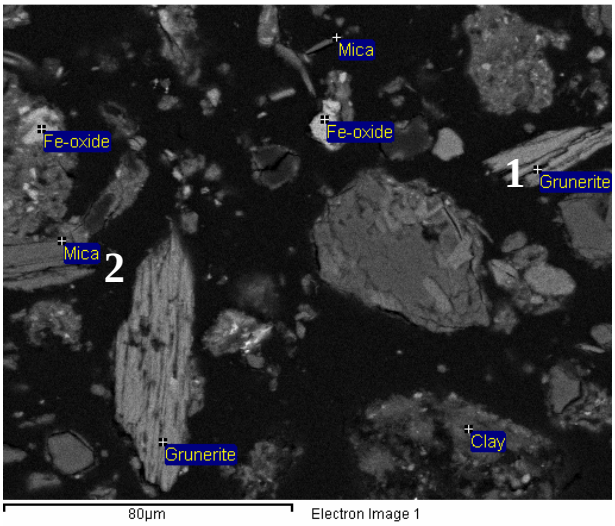

Grunerite bundles of straight to slightly curved fibre.
Dimensions:

1) 37.75 x 1.20 µm
2) 58.78 x 0.347 µm

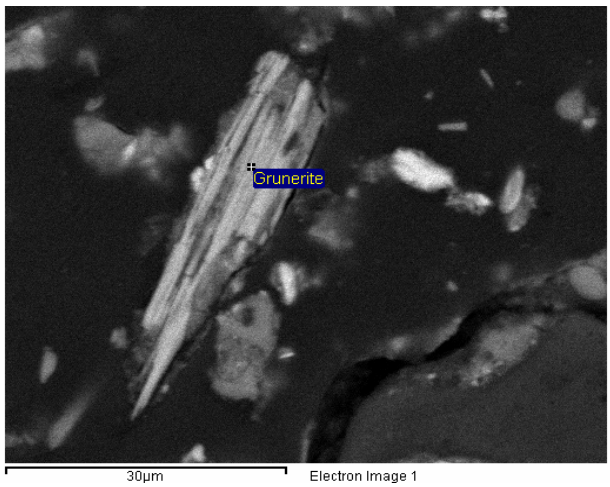

Grunerite bundle with straight rigid fibre
Individual fibre dimensions range from 4.00 x 0.531 µm to 42.48 x 1.037 µm

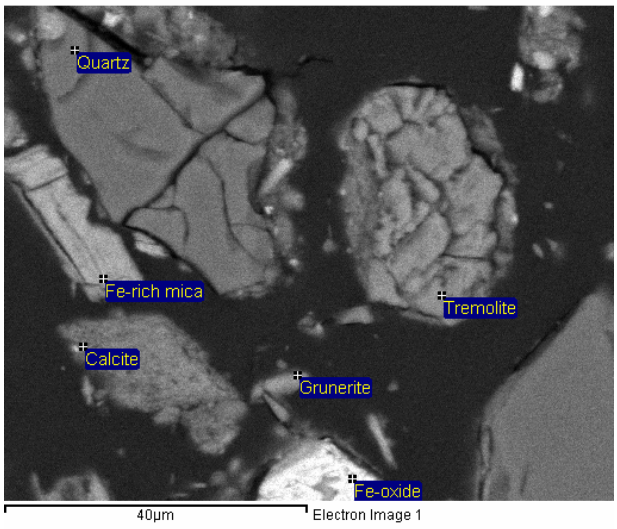

Single grunerite fibres (bottom) – 8.50 x 3.25 µm
and a fragment of massive tremolite.

Figure 5.60. BSE images of representative specimens of asbestos minerals from sample Mt2

Sample SS cork

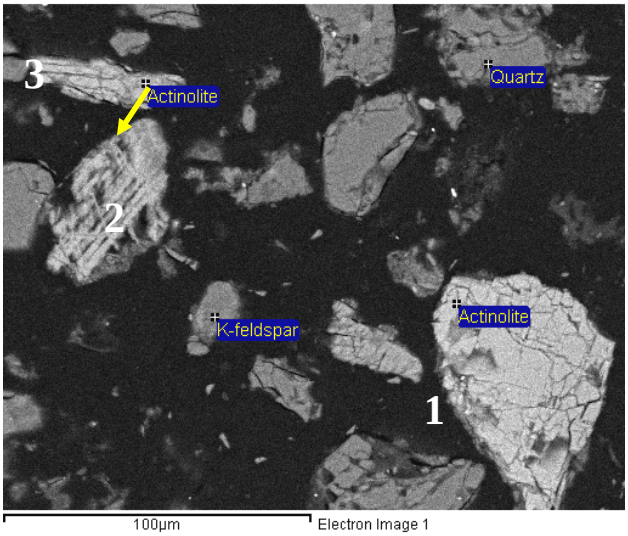

Actinolite – massive and blocky (1) and fibrous (2 and 3).
Visible fibre dimensions:
2) 52.15 x 1.012 µm
3) 46.70 x 2.84 µm

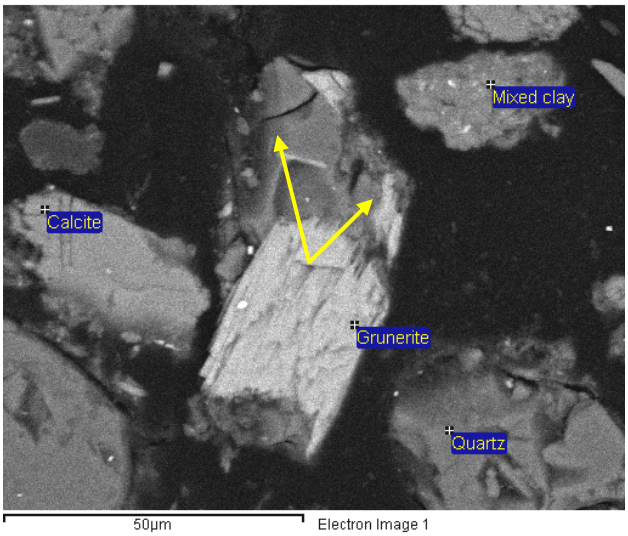

Grunerite columnar aggregate with liberated single needle-like fibre (yellow arrows) – 29.76 x 0.615 µm

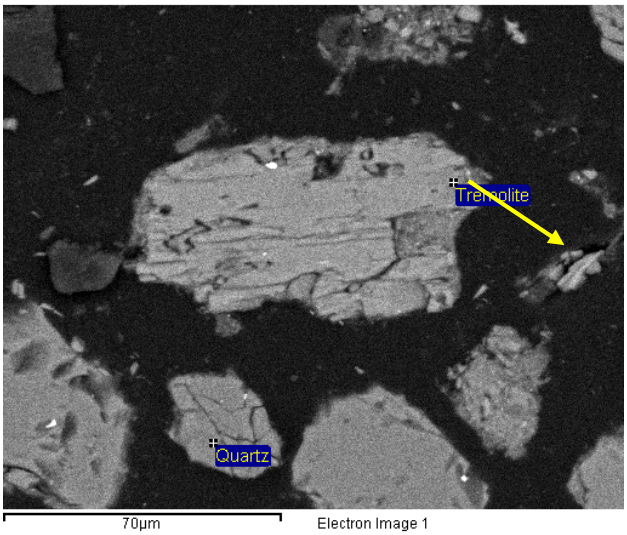

Fragment of tremolite with visible fibrolamellar structure and a single liberated fibre (arrow)
Visible fibre size: 84.43 x 1.233 µm

Figure 5.61. BSE images of representative asbestos minerals from sample SS cork

Sample WP 58 cork1

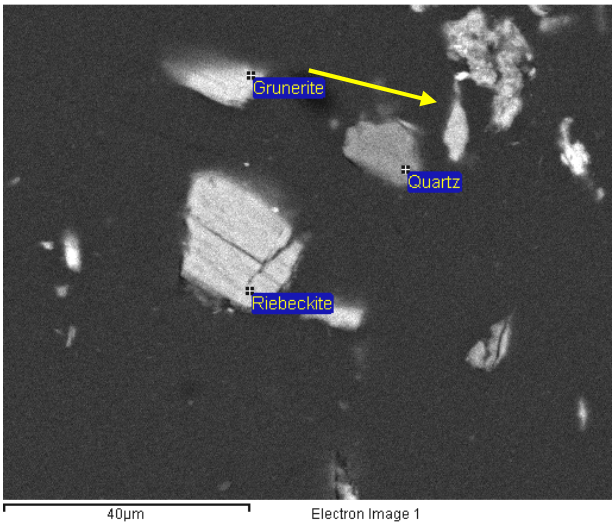

Fragment of stubby riebeckite (centre)with incipient fractionation along cleavage? planes and massive grunerite (top)
Riebeckite fragment size: 21.18 x 15.32 µm

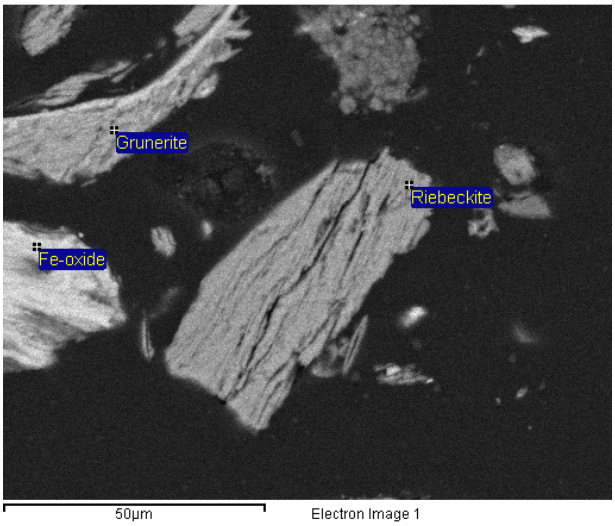

Straight to slightly curved riebeckite and curved fibrous grunerite (largely abundant)
Dimensions of individual fibre:
riebeckite – 56.77 x 0.572 µm and smaller diameter
grunerite -9.83 x 0.666 µm

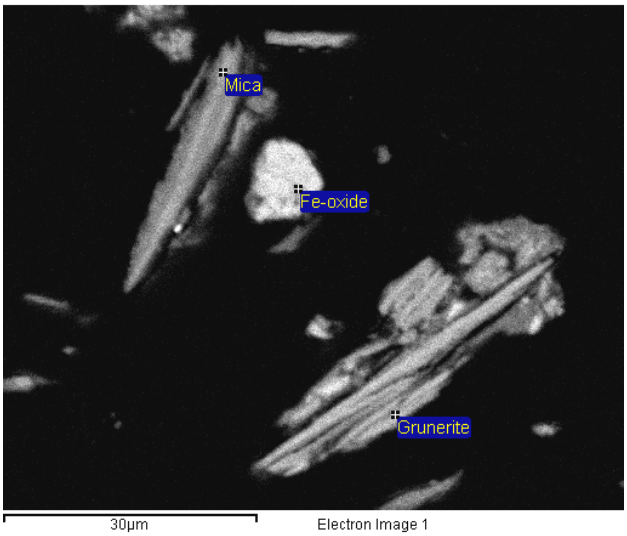

Straight and rigid grunerite fibre – 42.19 x 1.676 µm and smaller diameter visible
Note fibre-like mica with dimensions 30.71 x 5.036 and abundance of smaller crystals

Figure 5.62. BSE images of representative asbestos minerals from sample WP58 cork1

Table 5.12. EDS analyses of selected asbestos minerals from sample SS cork

	Na2O	MgO	Al2O3	SiO2	K2O	CaO	FeO
Grunerite	0.17	6.02	0	51.96	0.07	0.23	39.95
Grunerite	0.33	6.73	0	50.55	0	0.16	40.59
Grunerite	0.01	6.27	0	50.92	0.11	0.07	40.9
Grunerite	0.17	6.34	0	52.48	0	0.16	39.01
Actinolite	1.08	9.35	1.11	50.52	0	18.45	18.05
Actinolite	0	10.02	1.44	50.42	0	17.85	18.9
Actinolite	0.06	9.26	2.12	51.33	0.09	17.14	17.54
Actinolite	0.19	9.87	1.55	50.76	0	17.81	17.83
Tremolite	0.06	22.8	2.01	58.75	0	13.8	0.98
Tremolite	0	22.22	1.95	59.47	0	12.74	1.5
Tremolite	0.15	22.94	1.76	59.99	0	12.81	1.23
Tremolite	0.04	22.65	1.91	58.07	0	13.78	1.24

Table 5.13. EDS analyses of selected asbestos minerals from sample WP58 cork1

	Na2O	MgO	Al2O3	SiO2	K2O	CaO	FeO
Grunerite	0	6.61	0.1	49.26	0.77	0.87	40.87
Grunerite	0.07	6.88	0	53.02	0.21	0.85	37.59
Grunerite	0.24	6.56	0.34	53.68	0.07	0.18	37.48
Grunerite	0	6.68	0	52.99	0.35	0.63	38.31
Riebeckite	6.5	4.56	0.16	54.91	0.01	0.3	31.77
Riebeckite	6.73	4.28	0	53.54	0.55	0	32.35
Riebeckite	6.93	4.59	0.09	54.84	0.05	0.51	31.81

Table 5.14. EDS analyses of selected asbestos minerals from sampleWP58 cork2

	Na2O	MgO	Al2O3	SiO2	K2O	CaO	FeO
Grunerite	0.09	8.7	0	52.05	0.05	0.23	37.35
Grunerite	0.3	9.09	0	52.21	0.04	0	36.35
Grunerite	0	8.64	0.02	50.98	0	0.01	38.13
Grunerite	0.09	8.81	0	53.74	0.02	0.07	34.61
Riebeckite	5.71	3.63	0.25	54.56	0.15	0.26	33.59
Riebeckite	5.98	3.88	0.14	53.46	0	0.19	34.32
Riebeckite	6.15	3.73	0.42	52.64	0.05	0	34.06
Riebeckite	5.95	3.74	0.27	52.89	0.05	0.13	34.32

Sample WP58 cork2

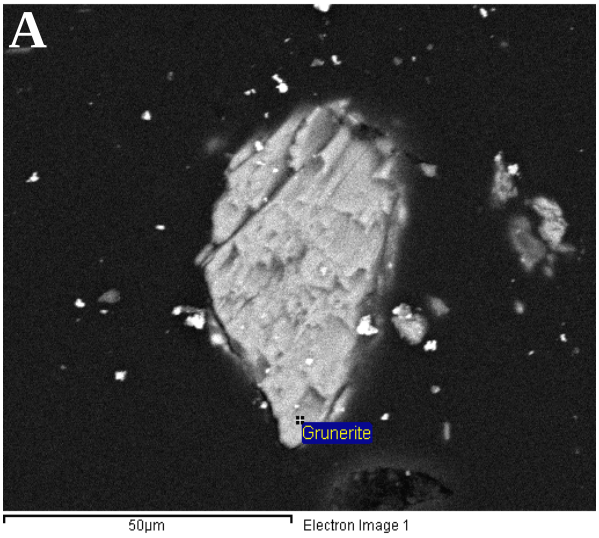

A - Grunerite fragment
Possible fibre dimensions of 43.29 x 0.509 µm measured

B – Straight rigid grunerite fibre (centre) – 13.74 x 0.475 µm

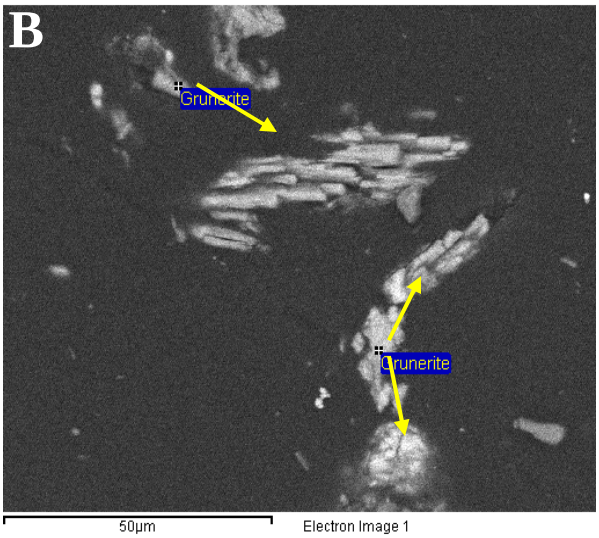

C – Grunerite in various morphologies:
curved fibre from bundle: 8.156 x 0.540 µm
elongate straight fibre: 40.99 x 0.350 µm

D - A bundle of thick rigid riebeckite fibre – 35.43 x 0.454 µm

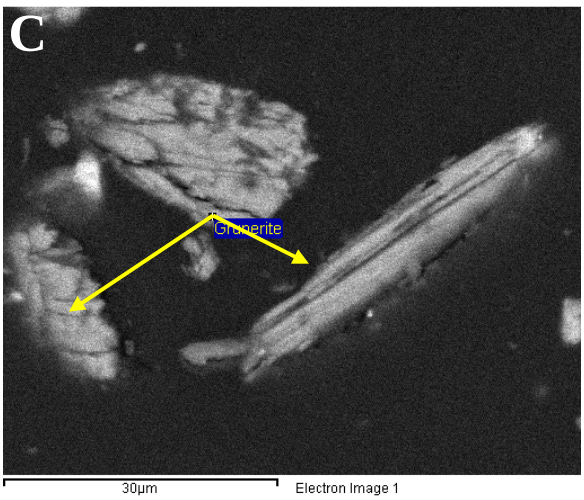

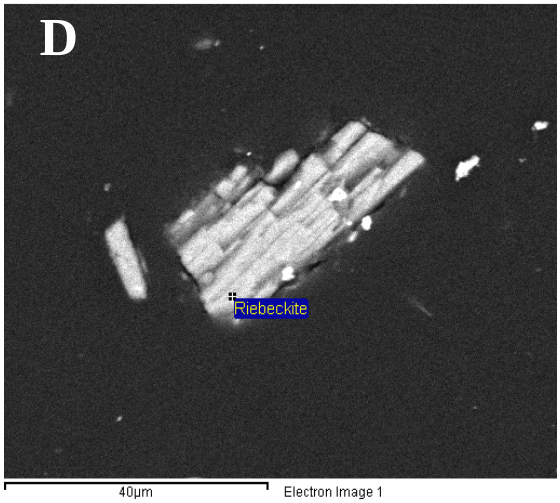

Figure 5.63. BSE images of representative asbestos minerals from sample WP58 cork2

Sample WP66

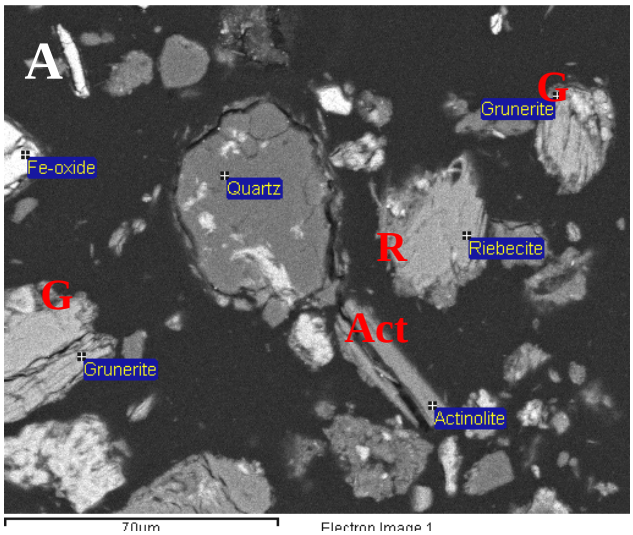

Grunerite bundles (G), actinolite (Act) elongate prismatic fibre aggregate and blocky riebeckite fragment (R).
Fibre dimensions:
G – from 23.54 x 0.502 µm
to 34.86 x 0.785 µm
Act – 38.60 x 1.105 µm
R – 35.83 x 1.056 µm

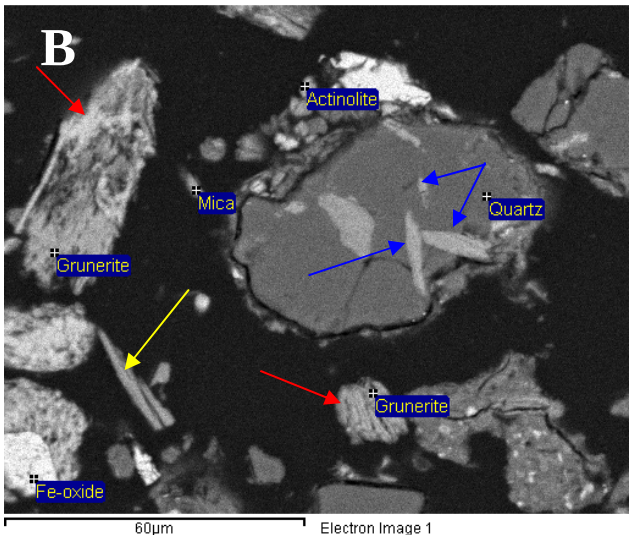

Grunerite in bundles (red arrows), enclosed within a quartz aggregate (blue arrows) and liberated single fibre embedded in epoxy (yellow).
Fibre in bundles: 46.90 x 1.02 µm
Fibre in quartz: 12.90 x 0.477 µm
Single fibre: 22.80 x 1.19 µm

Variation in grunerite forms of appearance: (D) - elongate aggregate with fibrolamellar structure and tightly spaced curved and short fibre in bundle (C)

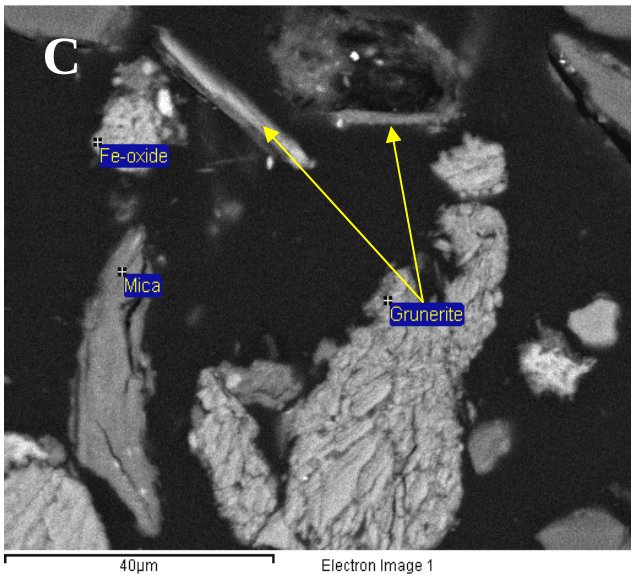

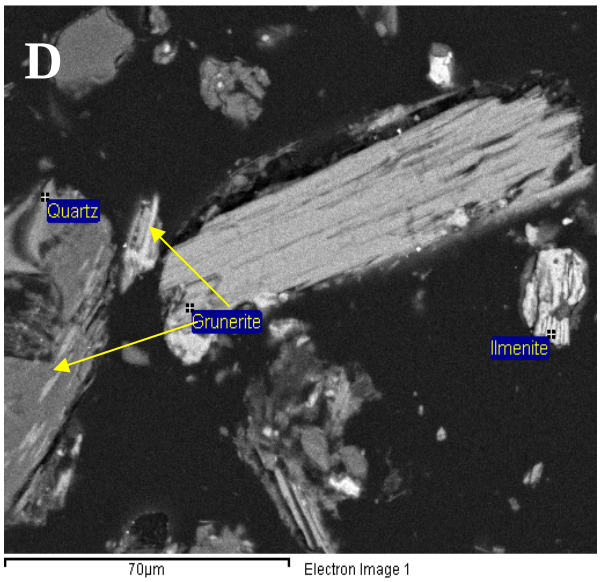

Figure 5.64. BSE images of representative asbestos minerals from sample WP66

Table 5.15. EDS analyses of selected asbestos minerals from sample WP66

	Na2O	MgO	Al2O3	SiO2	K2O	CaO	FeO
Grunerite	0	4.87	0	53.89	0.04	0.13	39.75
Grunerite	0	5.35	0	54.89	0	0.34	38.08
Grunerite	0	4.9	0.2	54.66	0	0.19	38.86
Grunerite	0	4.73	0	50.64	0	0.24	41.44
Grunerite	0.12	5.06	0	53.82	0	0.27	38.91
Riebeckite	5.88	4.69	0.76	54.68	0.59	0.87	30.94
Riebeckite	6.45	4.39	0.23	55.16	0.71	0.96	30.37
Riebeckite	6.08	4.6	0.38	54.49	0.68	0.75	31.37
Actinolite	0.37	15.61	4.8	52.87	0.1	10.65	12.6
Actinolite	0.64	17.2	2.34	54.04	0.03	11.31	12.82
Actinolite	0.42	15.61	3.52	54.52	0.22	10.55	12.99

Table 5.16. EDS analyses of selected asbestos minerals from sample WP71

	Na2O	MgO	Al2O3	SiO2	K2O	CaO	FeO
Grunerite	0.03	6.73	0.08	54.35	0.01	0.26	37.41
Grunerite	0	7.19	0.1	55.08	0.25	0.16	35.03
Grunerite	0	6.51	0.44	51.27	0.31	0.13	38.91
Grunerite	0	6.81	0.21	54.23	0.19	0.18	37.79
Riebeckite	5.97	3.21	0.39	54.43	0.22	0.35	33.27
Riebeckite	6.51	3.7	0	53.88	0.12	0.21	34.78
Riebeckite	6.62	3.87	0	54.17	0.1	0.4	33.37
Riebeckite	5.44	2.68	0	54.61	0.8	0.58	34.17
Tremolite	0.59	21.67	1.86	56.28	0.51	10.58	7.27
Tremolite	0.31	18.84	0.6	56.59	0.07	13.55	8.29
Tremolite	0	18.59	0.96	57.97	0	12.87	8.41
Tremolite	0.19	19.2	1.31	56.99	0.22	12.17	8.4

Sample WP71

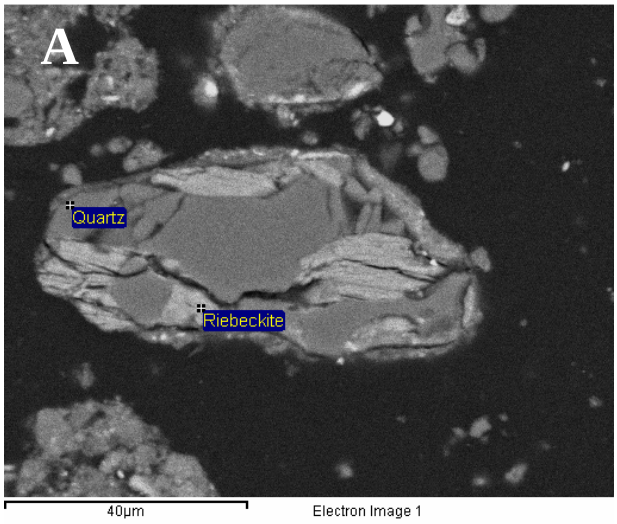

Straight to slightly curved riebeckite and quartz aggregate
Fibre size: 23.65 x 0.607 µm and smaller diameter

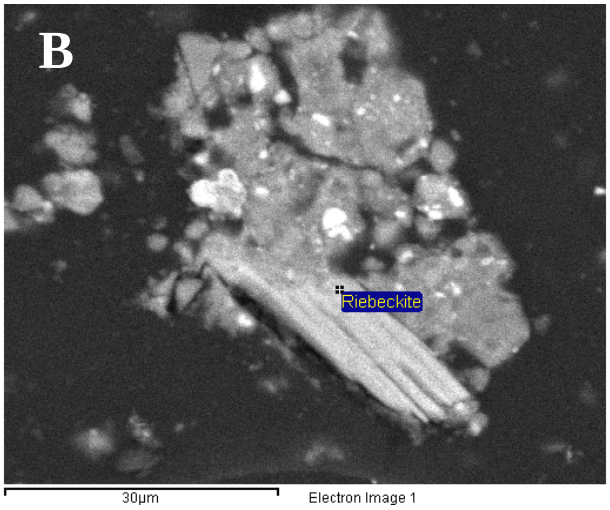

B - straight rigid riebeckite fibre – 28.19 x 0.369 µm

C – tremolite fibre: 15.01 x 0.596 µm

D – grunerite bundle – 3.80 x 0.396 µm

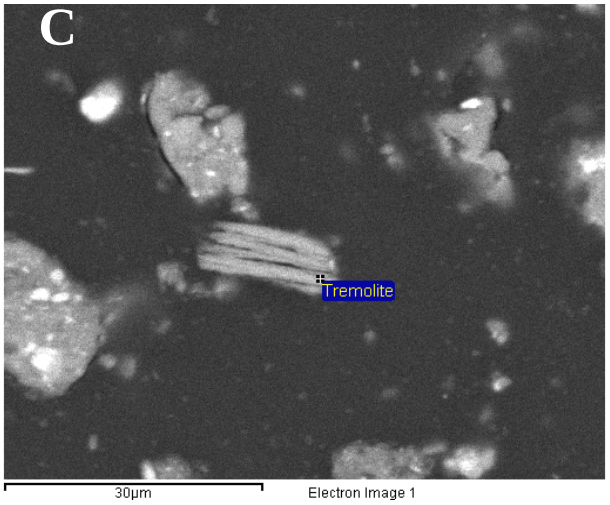

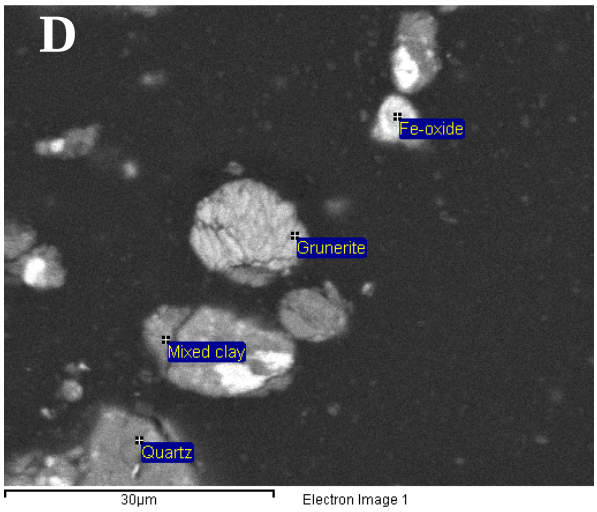

Figure 5.65. BSE images of representative asbestos minerals from sample WP71

Sample WP72

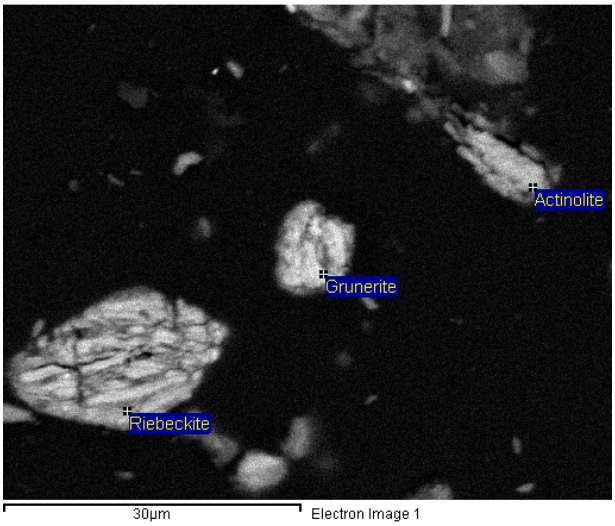

Actinolite fibre: 12.39 x 0.332 µm
Grunerite aggregate: 8.347 x 6.629 µm
Riebeckite fibre: 10.17 x 0.234 µm

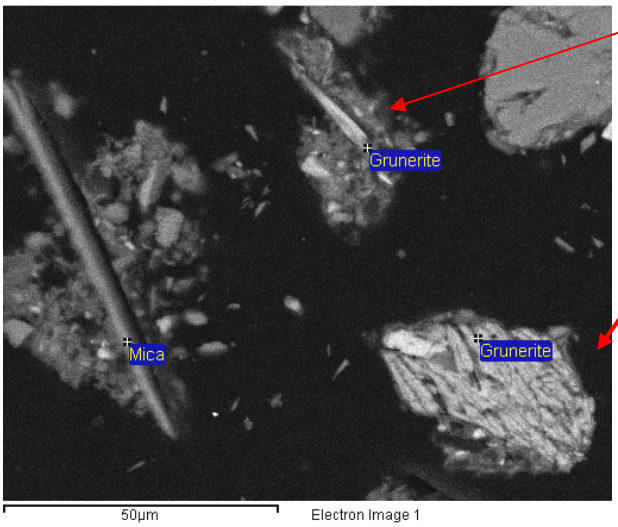

Grunerite single fibre - 19.50 x 1.814 µm

and

bundle: 20.07 x 0.507 µm

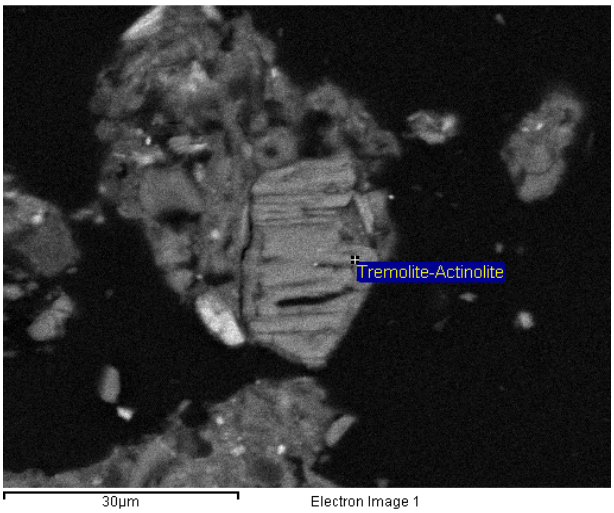

Fragment of tremolite-actinolite composition with visible cleavage-fracture planes.
Dimensions of possible fibre to be released: 12.66 x 0.444 µm

Figure 5.66. BSE images of representative asbestos minerals from sample WP72

Table 5.17. EDS analyses of selected asbestos minerals from sample WP72

	Na2O	MgO	Al2O3	SiO2	K2O	CaO	FeO
Grunerite	0.06	6.78	0	51.03	0.15	0.2	40.58
Grunerite	0.19	5.88	0.01	50.77	0.08	0.14	41.57
Grunerite	0	7.09	0.1	50.62	0	0	40.23
Grunerite	0	7.92	0	50.14	0	0.05	40.79
Riebeckite	6.51	4.5	0.3	56.23	0.34	0.58	29.84
Riebeckite	6.38	4.66	0	56.82	0.21	0.52	29.64
Riebeckite	6.56	4.71	0.04	56.92	0.22	0.46	29.75
Riebeckite	7.08	4.57	0.17	56.7	0.36	0.31	30.6
Actinolite	0.2	10.41	3.57	55.62	0.2	9.92	17.5
Actinolite	0.28	11.27	2.86	54.12	0.14	11.24	17.82
Actinolite	0.43	10.44	3.09	56.14	0.02	11.02	17.4
Tremolite-Actinolite	0.78	14.54	6.09	54.93	0.07	10.95	10.67
Tremolite-Actinolite	0.81	14.85	6.31	56.33	0.06	10.73	10.34
Tremolite-Actinolite	0.78	15.3	4.57	57.71	0.19	10	9.99
Tremolite-Actinolite	0.5	16.63	5.82	56.1	0.25	8.8	10.36

Table 5.18. EDS analyses of selected asbestos minerals from sample WP74

	Na2O	MgO	Al2O3	SiO2	K2O	CaO	FeO
Grunerite	0	9.94	0.42	54.96	0.04	0.08	32.13
Grunerite	0	10.89	0.33	54.07	0	0.59	33.83
Grunerite	0.18	10.48	0.36	53.93	0.16	0.45	33.78
Actinolite	0.3	19.52	4.93	53.75	0.12	10.12	10.03
Actinolite	0.02	20.84	3.07	52.3	0.28	4.53	15.76
Actinolite	0.42	19.84	5.24	51.53	0	12.27	8.96

Sample WP74

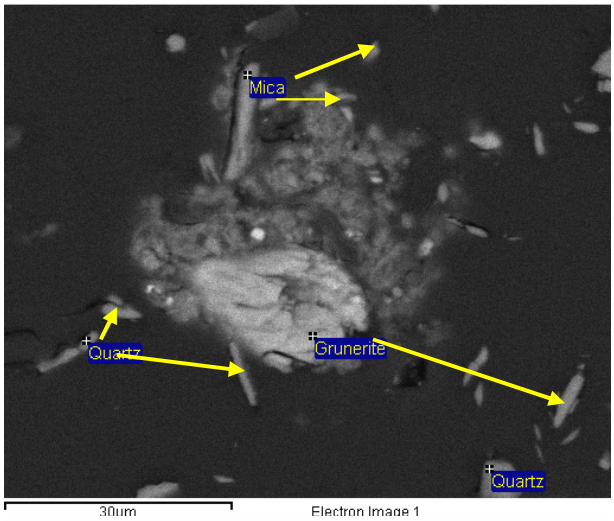

Bundle of grunerite: 8.9 x 0.779 µm on visible part of fibre
Note the majority of single needle-like "fibre" dispersed in the epoxy is quartz and mica and occasionally asbestos

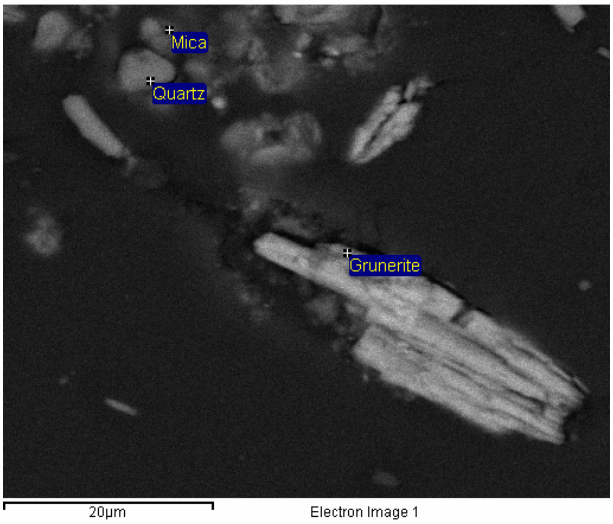

A bundle of straight, rigid fibre of grunerite
Individual fibre size: 33.86 x 0.661 µm

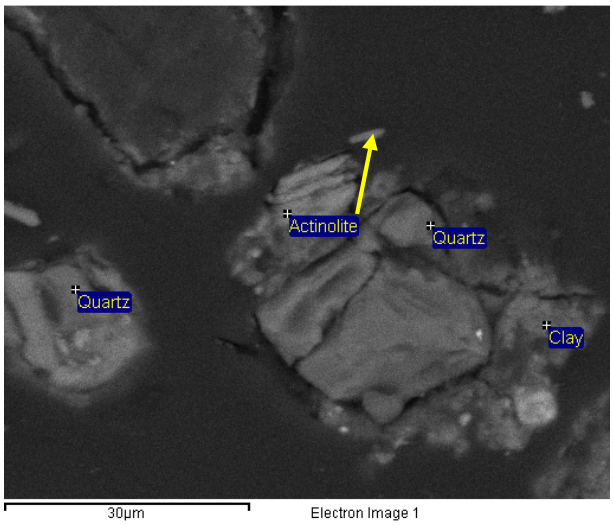

A group of short actinolite fibre – 9.18 x 0.806 µm and a single fibre in epoxy (arrow): 4.12 x 0.721 µm

Figure 5.67. BSE images of representative asbestos minerals from sample WP74

Water residue W1

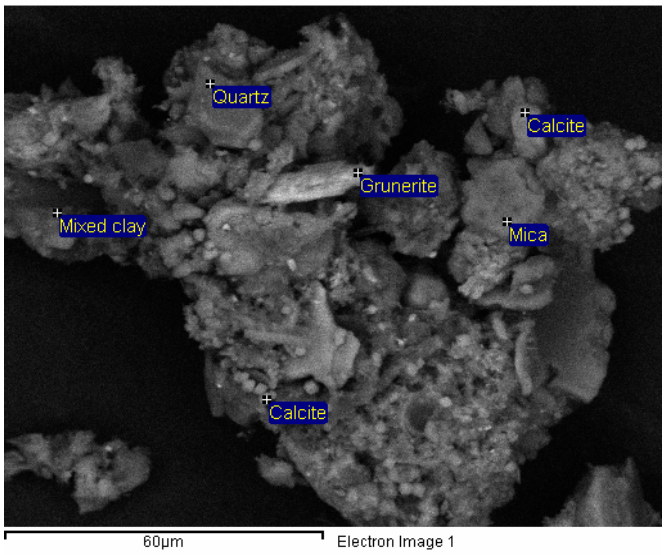

A bundle of grunerite with dimensions 21.40 x 6.5 µm

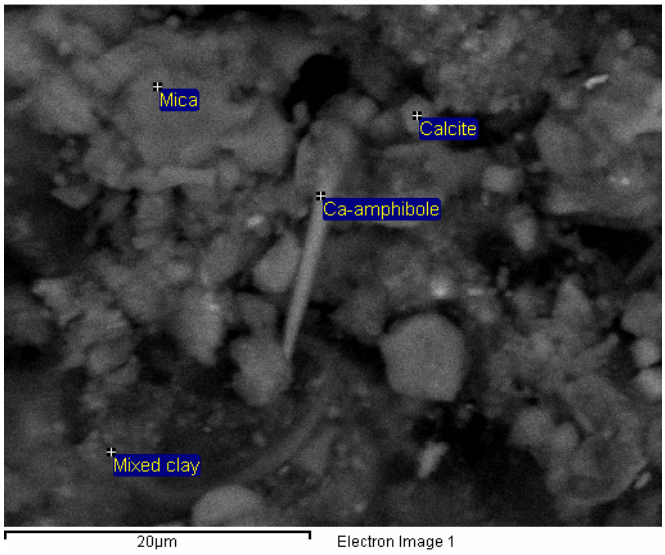

Single actinolite fibre measuring 12.62 x 1.00 µm

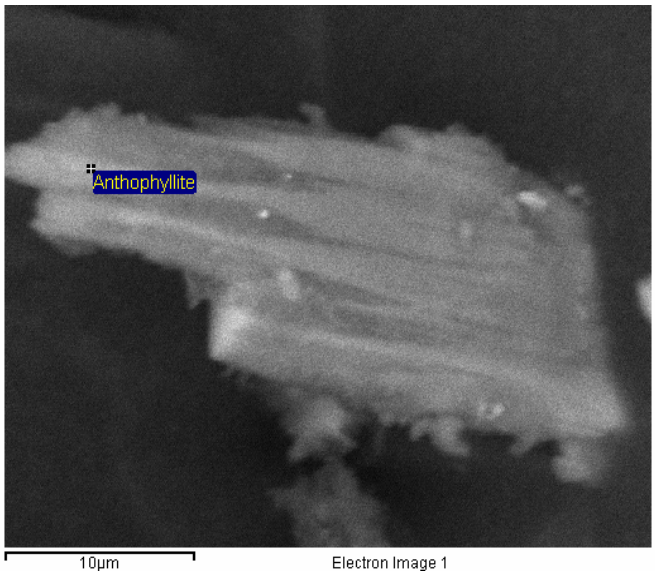

Anthophyllite thick cleavage fragmentation .
Possible fibre size: 32.20 x 1.80 µm

Figure 5.68. BSE images of representative asbestos minerals from water residue W1

Table 5.19. EDS analyses of selected asbestos minerals from water residue sample W1

	Na2O	MgO	Al2O3	SiO2	K2O	CaO	FeO
Grunerite	0.01	6.03	2.56	52.56	0.22	0.5	36.02
Grunerite	0.36	5.84	1.95	53.32	0.29	0.56	36.66
Grunerite	0.07	6.54	2.29	51.8	0.23	0.54	37.09
Grunerite	0.06	5.48	1.93	51.13	0.33	0.61	37.71
Anthophyllite	0	30.92	1.33	54.64	-0.01	1.64	9.03
Anthophyllite	0.11	30.13	1.33	55.58	0.07	0.64	9.51
Anthophyllite	0.3	31.94	2.02	54.15	0.14	0.96	8.26
Anthophyllite	0.05	29.69	2	56.2	0.16	3.67	6.97

Table 5.20. EDS analyses of selected asbestos minerals from water residue sample W2

	Na2O	MgO	Al2O3	SiO2	K2O	CaO	FeO
Grunerite	0.02	4.46	0.46	50.41	0.1	0.29	41.11
Grunerite	0.16	4.89	0.51	51.44	0.11	0.13	40.19
Grunerite	0.49	5.11	0.26	51.4	0	0.22	41.16
Grunerite	0	8.44	1.07	51.68	0.22	0.22	35.84
Grunerite	0.23	7.51	1.36	51.72	0.12	0.17	35.34
Grunerite	0.06	8.25	0.46	51.48	0.06	0.21	36.49
Grunerite	0.08	7.35	1.94	50.95	0	0.74	34.56

Table 5.21. EDS analyses of selected asbestos minerals from water residue sample W3

	Na2O	MgO	Al2O3	SiO2	K2O	CaO	FeO
Grunerite	0.04	7.81	0.48	54.84	0.2	0.1	33.5
Grunerite	0	6.66	0.94	55.82	0	0.36	30.79
Grunerite	0.11	6.98	0.85	52.62	0	0.37	37.2
Chrysotile	0	39.22	0.22	44.7	0	0.15	1.27
Chrysotile	0.21	40.47	1.15	42.68	0.06	0.21	1.1
Chrysotile	0.21	39.75	0.79	42.81	0.14	0.09	1.22
Chrysotile	0.11	41.19	0.54	42.2	0	0.14	1.38
Chrysotile	0.16	40.01	0.8	43.13	0.08	0.04	1.37
Chrysotile	0.15	42.3	1.12	43.89	0.07	0	1.24

Table 5.22. EDS analyses of selected asbestos minerals from water residue sample W4

	Na2O	MgO	Al2O3	SiO2	K2O	CaO	FeO
Grunerite	0	6.19	0.66	53.1	0	0.58	38.24
Grunerite	0.37	5.8	0.83	53.69	0	0.53	37.06
Grunerite	0.14	6.24	0.21	54.08	0	0.41	37.42
Grunerite	0.13	6.08	0.57	53.29	0	0.5	37.58
Actinolite massive	0.73	14.92	3.17	52.79	0	13.38	13.68
Actinolite massive	0.13	15.33	2.66	52.51	0	14.21	13.65
Actinolite massive	0.23	15	2.92	53.4	0	13.19	13.45
Actinolite fibre	0.49	12.52	2.71	51.33	0.13	5.62	23.45
Actinolite fibre	0	14.08	1.1	53.47	0.4	0.86	28.82
Actinolite fibre	0.22	12.64	3.2	52.71	0.12	5.33	22.62

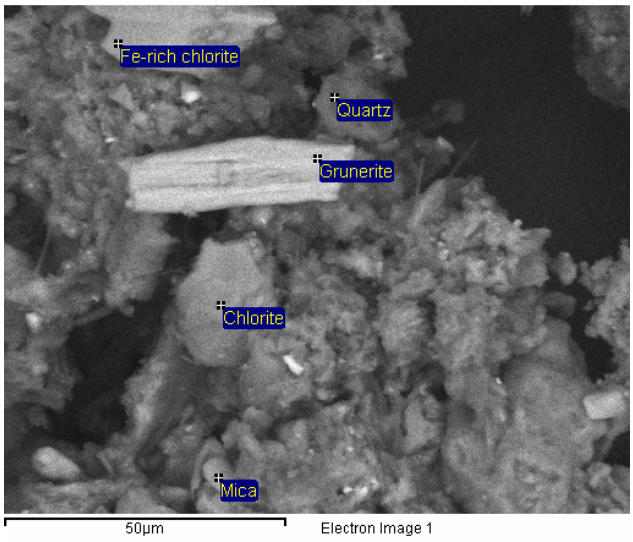

Grunerite fragment – 39.00 x 11.05 µm fibre

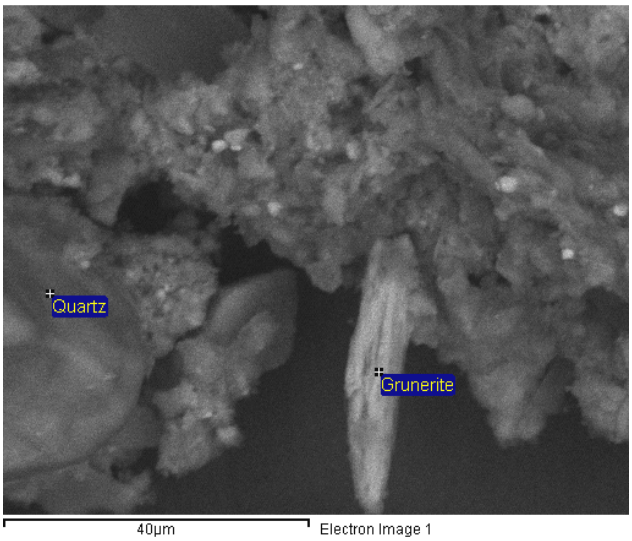

Grunerite – 36.1 x 7.15 µm

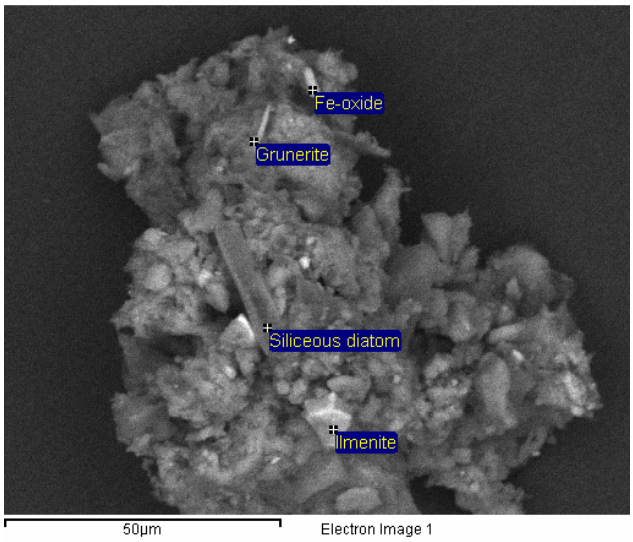

Single thin grunerite fibre – 9.75 x 0.655 µm

Figure 5.69. BSE images of representative asbestos minerals from water residue W2

Water residue W3

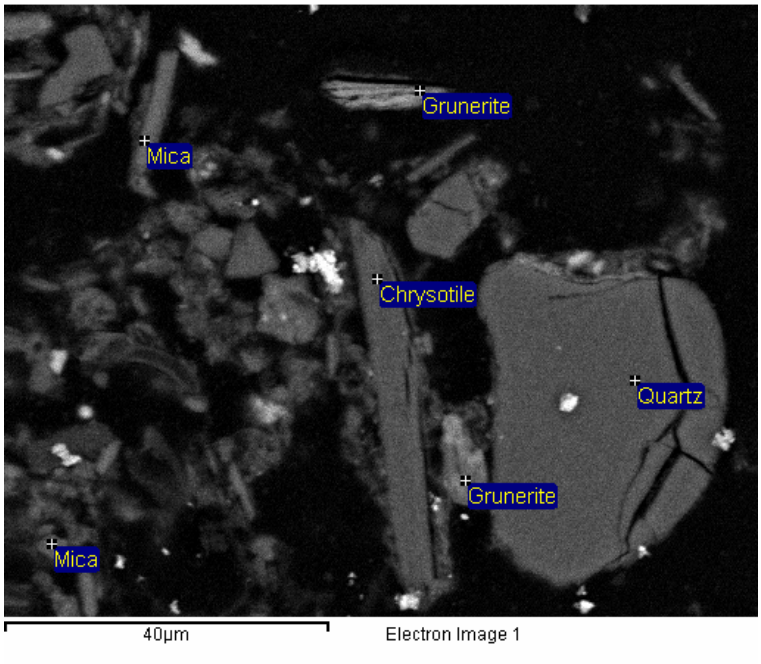

Grunerite – 15.41 x 0.353

Straight elongate chrysotile fibre – 45.47 x 5.00 µm

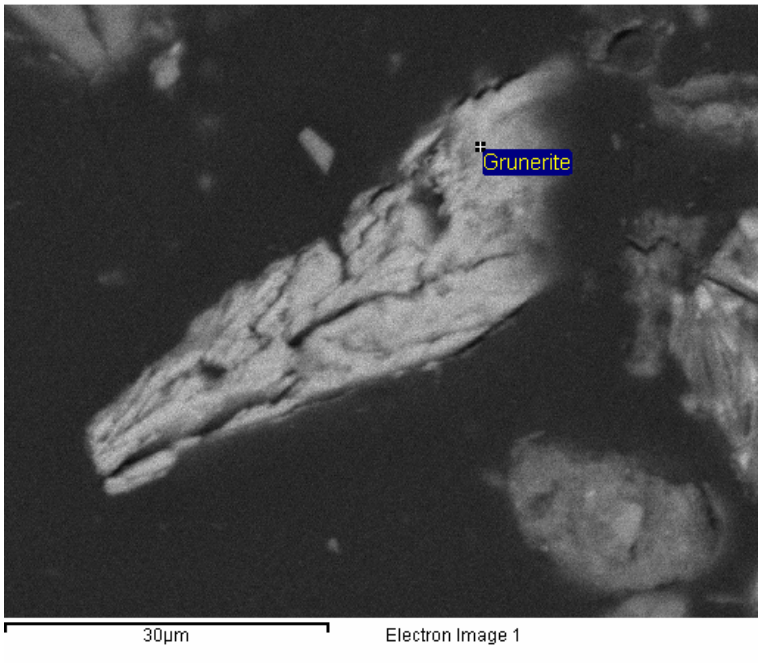

Grunerite bundle of slightly curved fibre –
50.02 x 1.195 µm

Figure 5.70. BSE images of representative asbestos minerals from water residue W3

Water residue W4

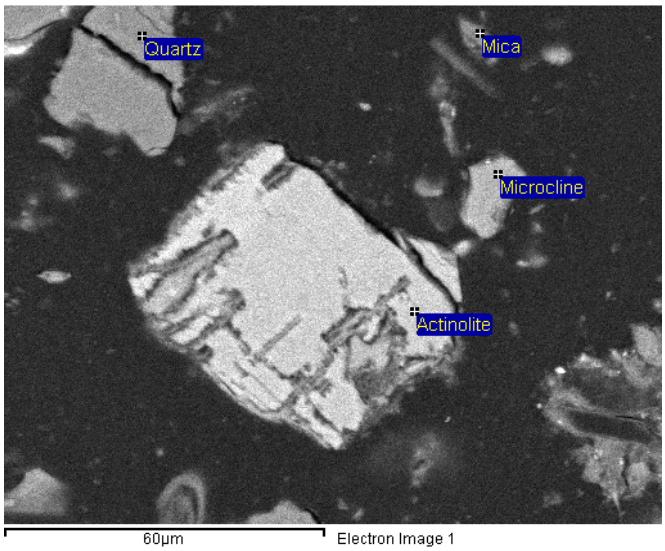

Massive actinolite

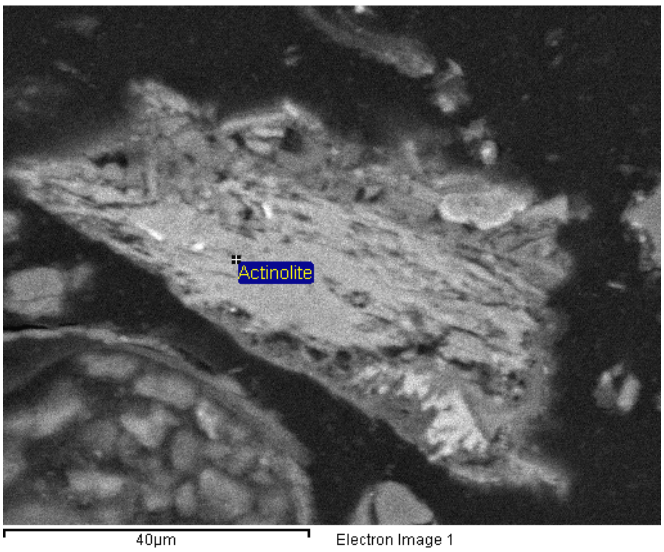

Actinolite fragment in the process of braking down into small thin fibre with visible thickness ~500 nm

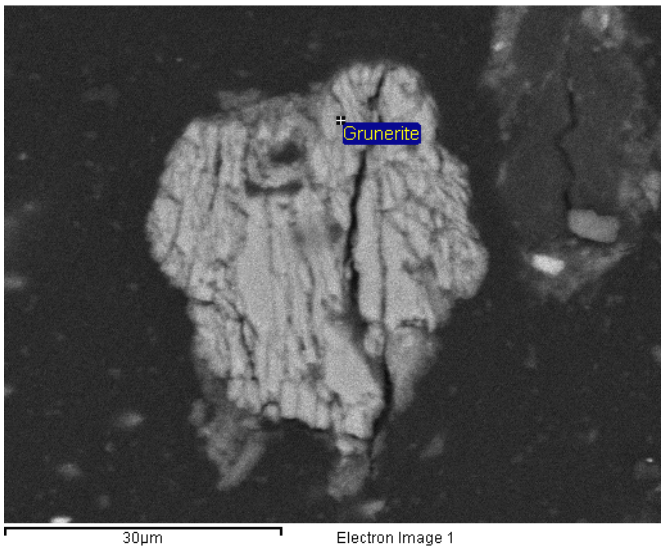

Bundle of grunerite.
Individual fibre dimensions:
15.45 x 0.307 µm

Figure 5.71. BSE images of representative asbestos minerals from water residue W4

Water residue W7

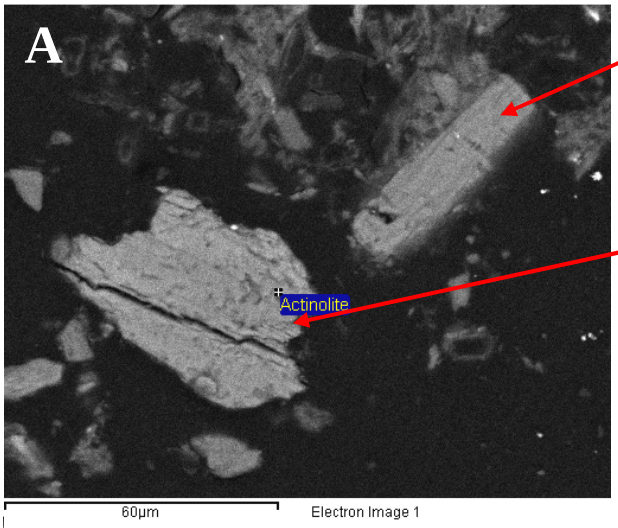

Elongate fragment of tremolite: fragment size 47.75 x 14.37 µm

Actinolite bundle:
fibre size 51.89 x 0.278 µm

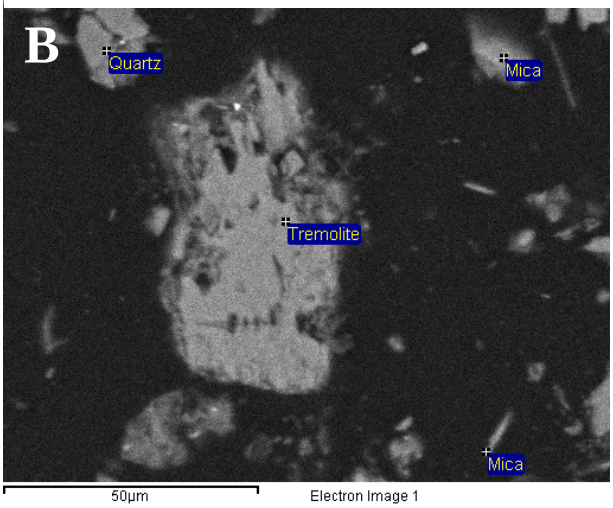

B - Fragment of massive tremolite in the process of braking down that might potentially produce fibre

C – Solid fragment of massive actinolite

D – Bundle of straight rigid fibre of riebeckite.
Dimensions of the longest and thinnest fibre - 30.98 x 0.503 µm

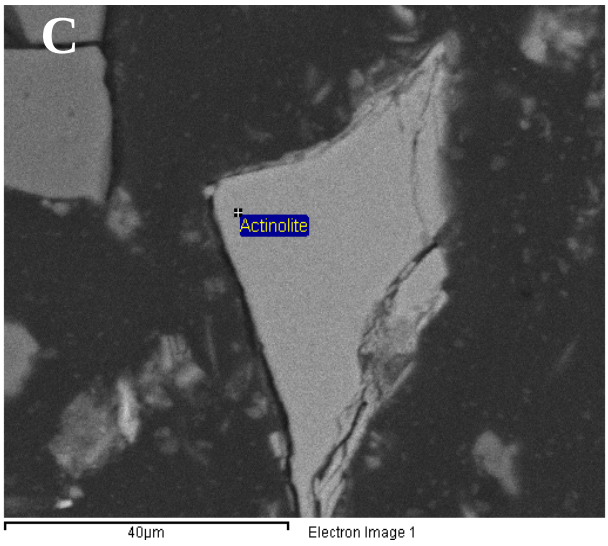

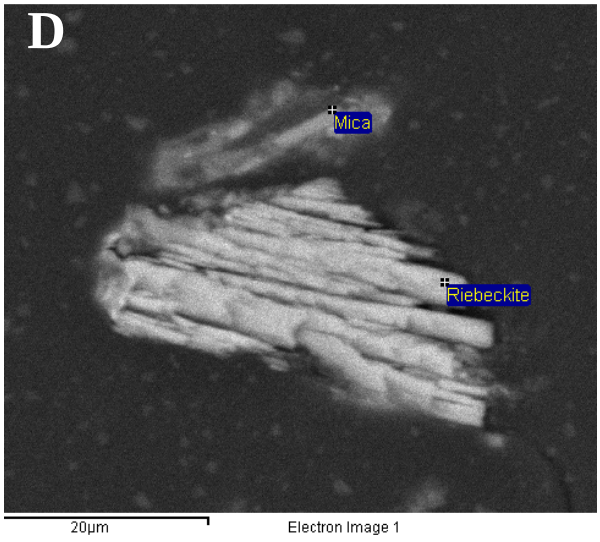

Figure 5.72. BSE images of representative asbestos minerals from water residue W7

Water residue W8

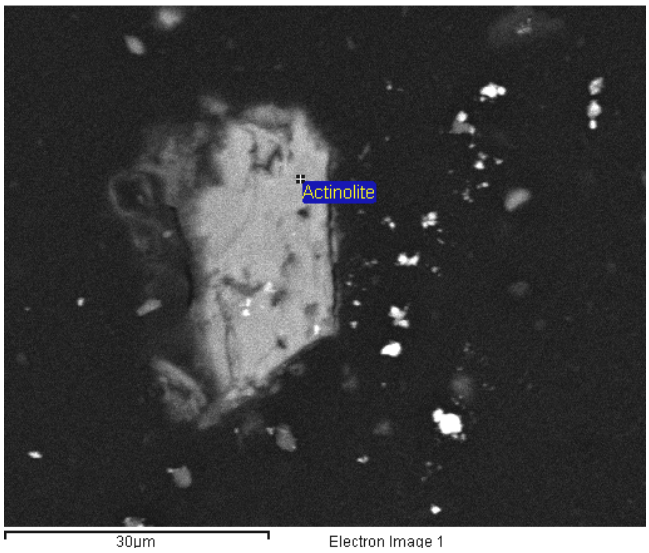

Massive blocky actinolite .
Fragment size – 30.15 x 14.22 µm

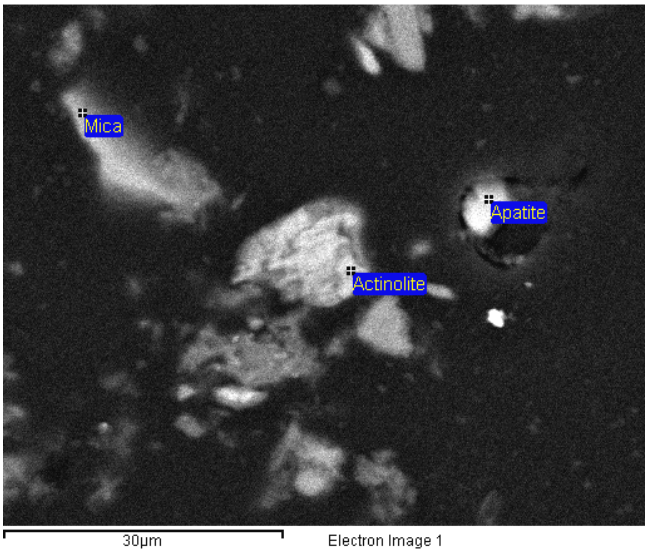

Fibrous actinolite bundle
Individual fibre size – 8.56 x 0.345 µm

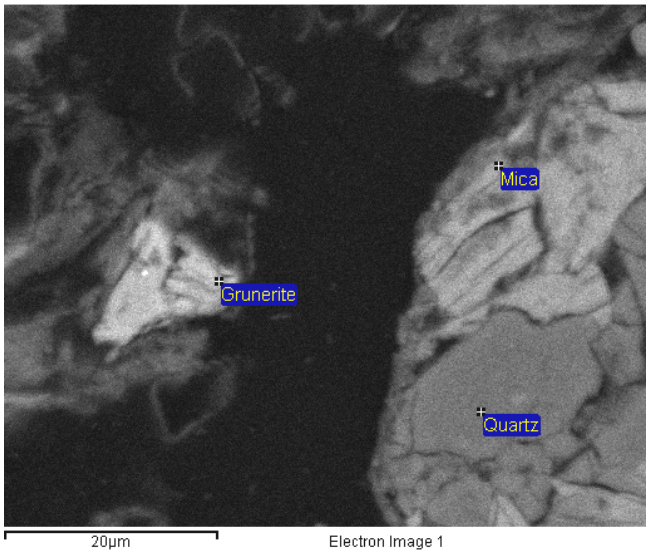

Grunerite fragment, partially fibrous
Fibre size – 5.75 x 0.235 µm

Figure 5.73. BSE images of representative asbestos minerals from water residue W8

Table 5.23. EDS analyses of selected asbestos minerals from water residue sample W7

	Na2O	MgO	Al2O3	SiO2	K2O	CaO	FeO
Tremolite massive	0	24.42	0.01	57.24	0.14	14.11	0.82
Tremolite massive	0.07	24.06	0.32	58.05	0.09	14.49	0.9
Tremolite massive	0.12	23.89	0	58.48	0.01	14.73	0.68
Tremolite massive	0.04	18.81	7.2	58.38	2.77	10.96	1.19
Actinolite massive	0.44	13.4	1.85	48.75	0.01	13.32	19.48
Actinolite massive	0.19	12.83	1.78	50.37	0	13.94	19.5
Actinolite massive	0.25	13.4	2.09	48.92	0.01	12.86	20.11
Actinolite massive	0.29	13.21	1.91	49.68	0	13.37	19.7
Actinolite aggregate	0	14.9	3.63	54.08	0.11	11.04	13.31
Actinolite aggregate	0.15	15.3	1.53	53.01	0.07	12.81	15.17
Actinolite aggregate	0.51	13.09	0.81	54.13	0	13.18	15.55
Actinolite aggregate	0	14.43	1.99	54.74	0.05	12.34	14.68

Table 5.24. EDS analyses of selected asbestos minerals from water residue sample W8

	Na2O	MgO	Al2O3	SiO2	K2O	CaO	FeO
Actinolite massive	0.85	7.91	2.69	48.78	0.17	9.41	26.38
Actinolite massive	0.25	9.63	2.32	51.87	0.24	3.22	30.97
Actinolite massive	0.75	7.53	3.16	49.87	0.11	9.22	27.17
Grunerite	0.62	7.49	0.87	53.07	0	0.03	35.61
Grunerite	0	9.08	0	53.4	0.24	0.47	35.55
Grunerite	0.78	8.03	0	50.52	0.37	0.04	37.55

Table 5.25. EDS analyses of selected asbestos minerals from water residue sample W9

	Na2O	MgO	Al2O3	SiO2	K2O	CaO	FeO
Grunerite	0	8.3	1.01	51.07	0.07	0.19	37.45
Grunerite	0.36	7.28	0.73	52.81	0.14	0.8	34.5
Grunerite	0	7.13	0.87	52.39	0	0.39	37.28
Grunerite	0.08	8.35	0.9	50.82	0.15	0.24	37.03
Grunerite	0.31	6.54	0.84	52.49	0.01	0.35	36.23

Table 5.26. EDS analyses of selected asbestos minerals from water residue sample W10

	Na2O	MgO	Al2O3	SiO2	K2O	CaO	FeO
Anthopyllite	0.06	27.27	0.45	57.24	0.02	0.72	13.92
Anthopyllite	0	26.67	0.54	55.95	0	0.59	14.58
Anthopyllite	0	25.84	0.71	57.1	0.16	0.79	14.17

Water residue W9

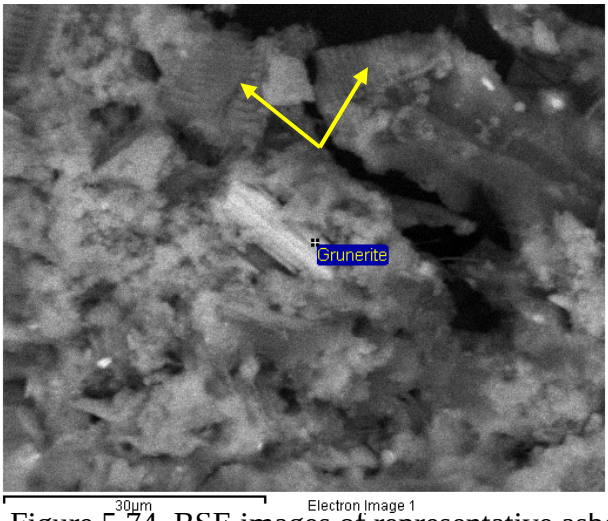

Grunerite bundle (15.58 x 5.00 µm) with visible fibre of ~ 400 nm diameter

Note cellular structure of siliceous diatoms (yellow arrows)

Figure 5.74. BSE images of representative asbestos minerals from water residue W9

Water residue W10

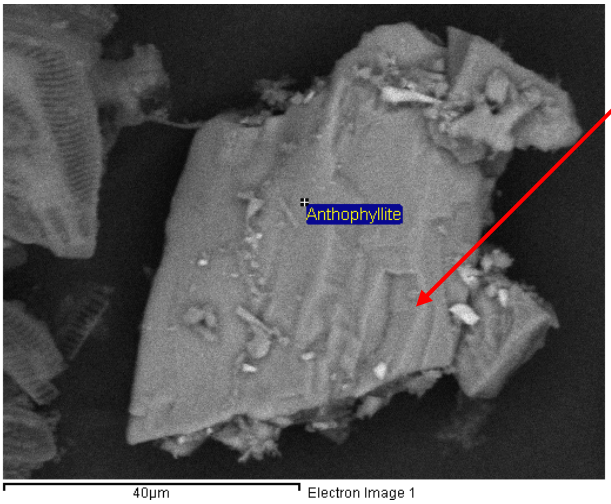

Massive anthophyllite – 65.1 x 44.6 µm with visible splitting plains

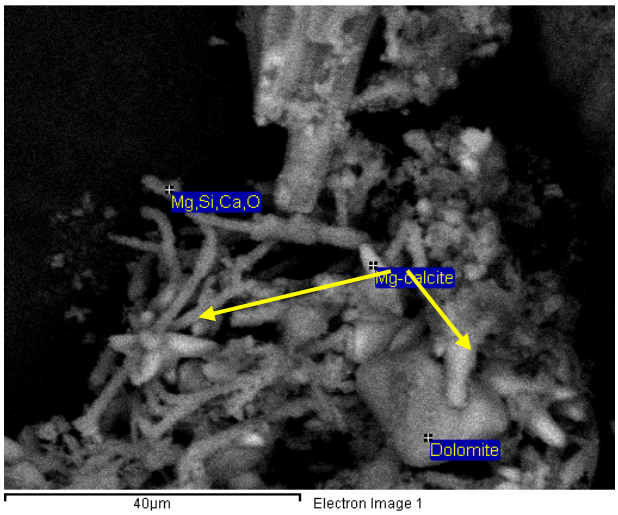

Fibres of Mg, Si, Ca, O composition, possibly chrysotile. Impossible to obtain accurate elemental compositions due to small size: diameter ~ 0.758 – 1.000 µm

Figure 5.75. BSE images of representative asbestos minerals from water residue W10

5.7.3 Summary

Table 5.27 presents the summarized results of this investigation. It shows that the most common asbestos mineral is grunerite (amosite), observed in the dry and wet soils as well as in the water residue samples, followed by actinolite and riebeckite (crocidolite), tremolite and occasionally anthophyllite. Serpentine asbestos (chrysotile) was identified only in one of the soil samples (wet soil CS2) and water residue samples W3 and W10.

In many instances it was very difficult to determine whether a specific amphibole grain is the result of fragmentation of precursor amphibole asbestos or of a common prismatic and more stubby amphibole. The morphological distinction between the asbestiform and non asbestiform varieties of amphibole and serpentine could not always be established beyond doubt. Commonly, due to their structure, natural amphiboles that are non-asbestiform will upon fracture of larger grains through cleavage produce fibre-like grains with aspect ratio (length to width ratio) of much greater than 3 (USEPA 2004a). Hence mean aspect ratio of chrysotile measured in soil samples here is 4:1 and in water residue 9:1. The amphibole asbestos minerals showed average aspect ratio as follows: grunerite – 193:1 (in soils) and 40:1(in water); riebeckite – 78:1 (in soils) and 62:1 (in water); actinolite – 30:1 (soils) and 18:1 (in water); tremolite – 38:1 (soils) and 25:1 (water); anthophyllite – 2:1 (in soils) and 18:1 (in water). According to Klein (1993) mean aspect ration of asbestiform amphiboles tend to be 20:1 or greater (>100:1) in fibres longer than 5 μm, whereas aspect ratios of non asbestiform varieties tend to be small, ranging from 2 to ~ 30.

The chemical composition of chrysotile is quite uniform in contrast to that of amphibole asbestos varieties. Considerable chemical substitution in the latter often occurs between the principal cations in the amphibole structure – magnesium, iron, calcium and sodium. The

elemental spectrum of each asbestos mineral combined with fibre morphology is in most instances characteristic enough for its identification (NIOSH - 77-169) (DHEW, 1976). Major and trace elements concentrations in the soil samples (XRF results) and ICP-MS analyses results for the water samples are provided in Appendix IV.

Table 5.27. Summary of results

Sample	Description	Serpentine		Amphibole					
		Total wt%	Chrysotile	Total wt%	Riebeckite (crocidolite)	Grunerite (amosite)	Anthophyllite	Tremolite	Actinolite
BW 1	dry soil	-		25	x	x			
BW 2	dry soil	-		6		x		x	x
Mt 1	dry soil	1		29		x			x
Mt 2	dry soil	-		9		x		x	x
WP 58 cork1	dry soil	-		42	x	x			
WP 58 cork2	dry soil	-		51	x	x			
WP 66	dry soil	-		40	x	x			x
WP 71	dry soil	-		5	x	x		x	
WP 72	dry soil	-		24	x	x		x	x
WP 74	dry soil	-		11		x			x
CS 1	wet soil	1		2		x	x	x	x
CS 2	wet soil	2	x	trace				x	x
MS 1	wet soil	-		1					x
MS 2	wet soil	-		1		x			x
MS 3	wet soil	-		1	x			x	x
SS cork (streambed soil)	wet soil	-		3		x		x	x
W 1	water residue					x	x		x
W 2	water residue					x			
W 3	water residue	-	x	2		x			
W 4	water residue	-		2		x			x
W 7	water residue	-		3	x			x	x
W 8	water residue	-		2		x			x
W 9	water residue					x			
W 10	water residue		x				x		

5.8. Synthesis of the Study and Overview of the Findings

5.8.1 The use of remote sensing to Monitor Environmental Change associated with mining

From a natural resource management perspective, satellite imagery plays a significant role in monitoring change in vegetation cover as a result of human activities. This applies to both changes made by environmental degradation and those made through environmental mitigation. Remote sensing provides a holistic view of change as a factor of spatial extent, temporal dynamics incorporating the influence of environmental factors. Mining environments are dynamic in nature and as such, traditional field based monitoring techniques normally do not account for changes that occur in between seasons. Remote sensing because of its repeat coverage is therefore ideal to monitor dynamic environments. As demonstrated in this study, the ecological setting of the area is a limiting factor in itself for conventional monitoring methods. The area is inaccessible and is characterized by steep slopes and rugged terrain. These among others demonstrate to some extent why the mine rehabilitation was not monitored to date by the government despite having invested a lot of money in this environmental mitigation programme.

The vegetation indices proved to be one of the most practicable remote sensing tools to monitor and detect change in a disturbed environment. Field validation of the vegetation indices using PAR/LAI Ceptometer helped to understand the positive growth of vegetation which resulted from the rehabilitation process. The results showed that the vegetation species used for the rehabilitation are efficient in capturing solar radiation for

the process of photosynthesis. This explained a relatively faster growth of vegetation on the rehabilitated sites when compared to the natural sites. Traditionally most remote sensing literature focused more on the relationship of *f*PAR/LAI with vegetation indices (NDVI) than to relate *f*PAR to LAI. However in this study the relationship between *f*PAR and LAI helped to explain the importance of the vegetation type, canopy structure and its receptive capability of radiation, which in turn has an impact on photosynthesis (vegetation growth). This study found an inverse linear relationship between *f*PAR and LAI.

Two methods of rehabilitation were used in the study area. These include revegetation and rehabilitation using gravel and soil to cover adits. Rehabilitation using soil and gravel to cover open cast mines is less effective compared to the one using vegetation. It takes a long time for adits covered with gravel to become suitable for vegetation growth. The process of ecological succession is slow at these sites. During the rainy season, water tend to erode some of the material from high lying slopes to the streams (see Figure 5.76). Unlike graveled sites, revegetated areas suppress the process of erosion. This helps to reduce the degradation and enhance ecosystem recovery.

Figure 5.76. Site rehabilitated using gravel and soil with loose asbestos fibres on a steep mountain slope (Site W58).

5.8.2 Spectral Separability of Vegetation using field spectrometry

Spectral profiling of different plant species in the study area showed that the indigenous species are spectrally separable from those used for rehabilitation. *Euphorbia terucalli* species have been used at most sites for mine rehabilitation. Other species occurring naturally in the study area grow gradually within rehabilitated sites through ecological succession. Both species were found to be spectrally separable from each other. Tswai (2003) used field spectrometry to specifically determine the wavelength at which varieties of one plant family can be differentiated. He computed the standard deviation of the spectra of those species for comparative analysis and concluded that the white and yellow maize cannot be differentiated in the red and green wavelengths but rather in the near infrared. Raychaundhuri and Bhattacharrya (2006) used a fuzzy rule base to

spectrally differentiate plants of the same species at different growing stages. The methodology was also based on reflectance averages. They experimented the model using the species of Cucurbitaceae family. They concluded that vegetation growth stages can be standardized on the basis of the overall reflectance percentage at certain visible wavelength of sunlight. They therefore defined a growth stage in terms of spectral reflectance.

5.8.3 Comparison of Reflectance Spectroscopy and Laboratory techniques in Monitoring Asbestos Pollution

The feasibility of using remote sensing to spectrally differentiate different types of asbestos minerals through reflectance spectroscopy was investigated in this study. The main objective was to experiment on spectral characteristics of minerals for potential use in asbestos pollution monitoring. These include investigating whether traces of asbestos minerals can be detected using spectral signature analysis from the soil and water samples of the rehabilitated environment. Laboratory investigations (X-Ray Diffraction and Scanning Electron Microscopy) were also conducted for identification and characterization of asbestos minerals which were found in the rehabilitated sites in the collected soil and water samples. This was done in order to validate and verify findings using reflectance spectroscopy.

X-ray Diffraction was able to detect amphibole asbestos in sample W58. The highest concentrations were detected in samples W58 cork2 (51%), W58 cork1 (42%) and W66 (40%) all representing dry soil samples. The wet soil samples contained notably less

amphibole minerals (2-4%) and similarly to the water residue samples. Actinolite-tremolite, grunerite and riebeckite were positively identified in the samples where their concentrations exceeds 10%.

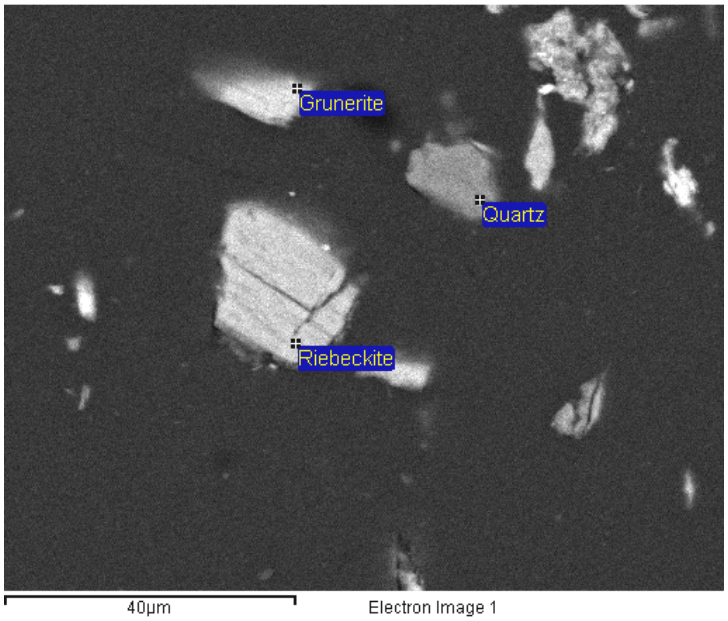

Figure 5.77. BSE image of sample W58 showing a fragment of stubby riebeckite with incipient fractionation along cleavage planes and massive grunerite (Riebeckite fragment size: 21.18 x 15.32 µm).

Figure 5.77 shows a Backscattered Electron (BSE) image of the identified asbestos minerals for sample W58 along with short description of the morphology of the fibres and their dimensions. This was detected using Scanning Electron Microscopy. All minerals identified by XRD were also observed here as well as some trace minerals that were below the detection limits of the XRD. Those include ilmenite, Ti-oxide, REE – oxides, siliceous diatoms in the water residue samples.

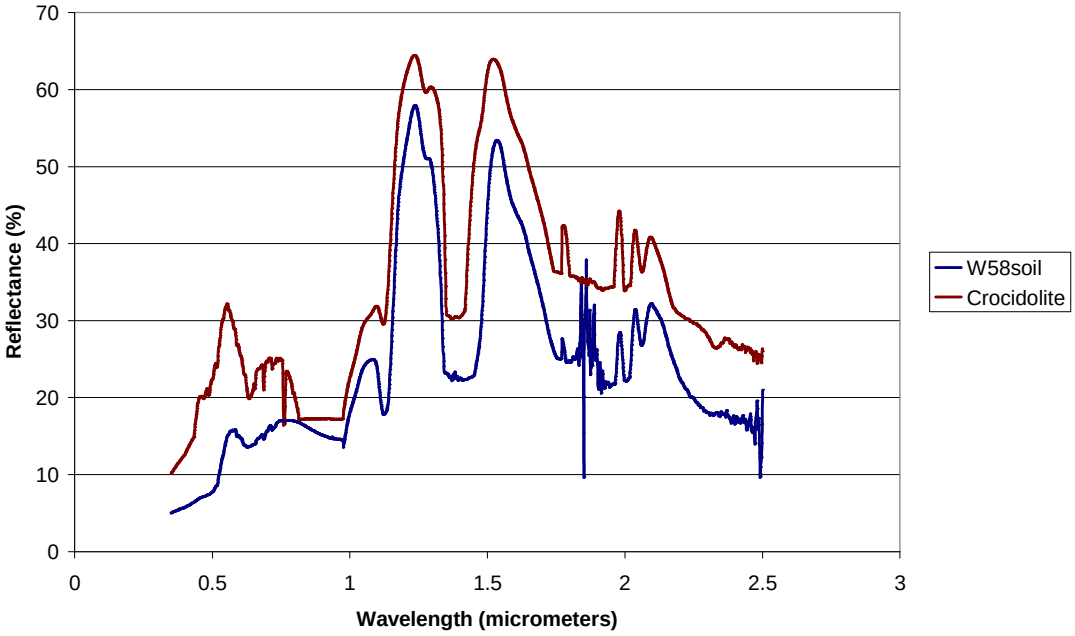

Figure 5.78. Spectral profiles of soil collected at Cork (W58) compared to the one of crocidolite.

Figure 5.78 shows the presence of crocidolite asbestos fibres in a soil sample collected at site W58. This confirms the laboratory results. The variation in reflectance may be attributed to other components such as the non asbestos top soil cover.

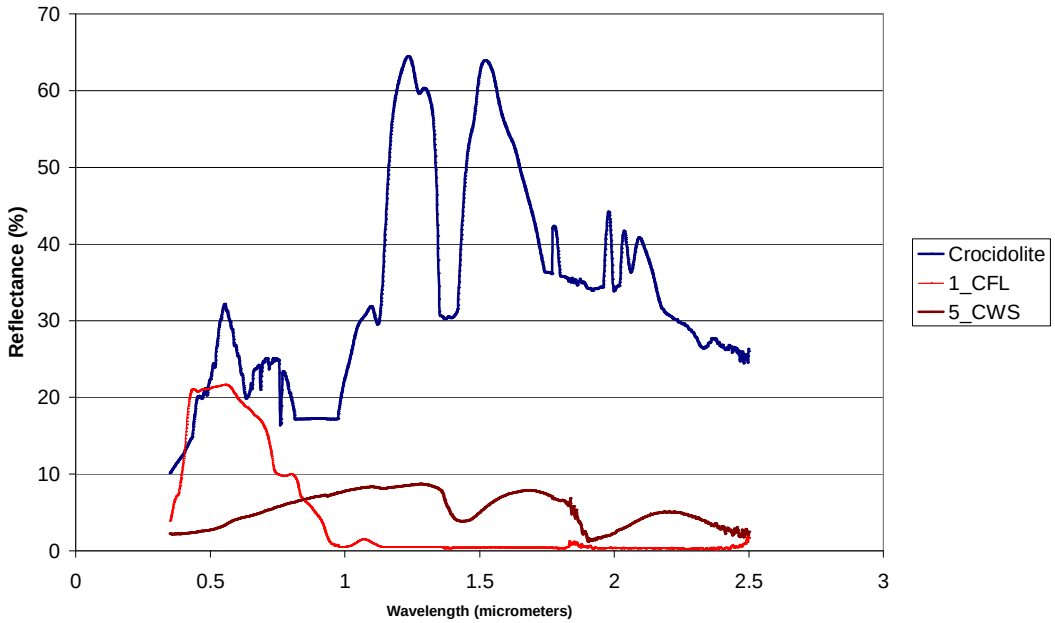

Figure 5.79. Spectral profiles of wet riverbed soil (CWS) and flowing water (CFL) collected at Cork (W58) compared to the one of crocidolite.

It has not been possible to associate the reflectance pattern with any of the asbestos minerals from the wet riverbed soil (Figure 5.79). However, the same samples showed the presence of asbestos minerals as indicated in the laboratory analysis which was recorded in lower quantities. Reflectance spectroscopy was unable to pick up asbestos minerals in water. This may be attributed to the fact that water naturally absorbs a large portion of the solar radiation.

Overall, laboratory techniques showed different capabilities and limitations in detecting the presence of asbestos minerals. Of all, the SEM produced the most detailed results, further validating the XRD results. Reflectance spectroscopy was able to detect traces of asbestos in dry soil samples. For wet soil samples together with flowing soil sample, this technique was unable to detect traces of asbestos. This therefore makes the reflectance

spectroscopy useful for mapping the distribution of asbestos over reasonably larger areas on the land surface. However, as this was experimented from the ground field campaign, it has positive implications for hyperspectral remote sensing images. This study revealed the presence of asbestos fibres on rehabilitated sites. Except for the water analysis, remote sensing techniques can be used to monitor asbestos pollution and its spatial distribution over the dry land surface. This will however be limited to hyperspectral imagery.

5.9 Overall Summary

This chapter provided the results and discussion of this research project. The results included findings of satellite derived monitoring of asbestos mine rehabilitation, the use of PAR/LAI ceptometer for measuring the fraction of photosynthetically active radiation and calculating leaf area index and its implications on the rehabilitated sites. It also covered ground based reflectance spectroscopy of vegetation, together with asbestos minerals, soil and water samples, and their significance in monitoring asbestos pollution. Detailed laboratory results for detecting and identifying asbestos minerals were also presented. An overview of the findings was also provided.

CHAPTER SIX

CONCLUSIONS AND RECOMMENDATIONS

6.1 Conclusions

This research used remote sensing techniques to study and monitor the process of asbestos mine rehabilitation and assessed its effectiveness in mitigating environmental degradation. Field surveys and laboratory analysis were conducted to validate and confirm data obtained using remote sensing techniques. The main thrust was to assess the progress of asbestos rehabilitation against objectives of environmental mitigation and to determine whether there is any significant improvement in the rehabilitated environment. The overall objective was to use remote sensing for the monitoring of mine rehabilitation for the purpose of improving sustainable mining and general environmental management in South Africa. It has not been possible for the government to deploy mine environmental inspectors throughout the country to physically audit the rehabilitated mines. This was largely due to limited capacity and poor access to rehabilitated mines. Therefore, satellite remote sensing played an important role in observing mine rehabilitation for the purpose of monitoring progress achieved. This study was conducted in a typical rural setting of South Africa which has been severely affected by the negative impacts of asbestos mining.

The study demonstrated that satellite imagery are important tools to monitor the extent to which mine rehabilitation mitigate environmental degradation. It was able to demonstrate both positive and negative change on the environment. It would have been more costly and time consuming to rely on the traditional field based methods of

natural resource monitoring. The physiography of the study area makes it impossible for frequent field based surveys.

The vegetation indices showed the rate of vegetation growth /change as a result of mine rehabilitation and that revegetation is suppressing degradation in most sites. Rehabilitation using soil and gravel to cover open cast mines has been ineffective when compared to revegetation. Such sites pose a danger of resurfacing asbestos due to soil erosion, especially because of the steepy nature of the slopes. The increasing species density and diversity is suppressing erosion of asbestos fibres to the streams in most sites except for the partially rehabilitated sites.

Field based assessment of photosynthetic capability of the vegetation species used for rehabilitation made a significant contribution to this study. This has explained to a larger extent why a positive vegetation growth was experienced in the rehabilitated sites. It also makes an important contribution to literature on the relationship of leaf area index and fraction of absorbed photosynthetically active radiation. Landsat TM satellite images used in this research were obtained from the Council for Scientific and Industrial Research (South Africa) free of charge. The vegetation indices results for change monitoring were presented in temporal and quantifiable dimensions. The NDVI values of the rehabilitated sites were compared to those of the natural sites and results/findings confirms the hypotheses that satellite imagery provides cost effective monitoring of open cast mining and dump rehabilitation, and that they provide a quantifiable timeous monitoring of vegetation establishment on the rehabilitated sites. Landsat TM imagery has a spatial resolution of 30 m. A sub-pixel based approach was used to extract NDVI values that were used for change detection. This was to ensure that an average NDVI value for investigated sites were captured for analysis with the

aim of making maximum information extraction out of medium resolution imagery. This sub-pixel modeling was integrated with the use of Global Positioning System (GPS) in order to produce site specific results. This confirms the hypothesis that modeling of medium spatial resolution imagery assist in maximizing the use of such images in monitoring the progress of rehabilitation on rehabilitated sites.

Reflectance spectroscopy/field spectrometry also played a significant role in this study. Based on the reflectance and emittance characteristics of the targets, this study was able to spectrally differentiate various plant species, asbestos minerals and to detect the presence of asbestos minerals over the land surface. Reflectance spectroscopy is a useful remote sensing technique in monitoring asbestos pollution over land surfaces. This was confirmed through the use of laboratory based methods (X-Ray Diffraction and Scanning Electron Microscopy). Because of the lower quantities of asbestos in water and the absorptive nature of water to radiation, it proved to be difficult to detect asbestos particles in water bodies using reflectance spectroscopy. For detecting the presence of asbestos minerals in water, laboratory analysis remains a priority. This study revealed that there is a considerable presence of asbestos fibres on rehabilitated sites. Except for the water analysis, remote sensing techniques can be used to monitor asbestos pollution and its spatial distribution over the land surface. The derived information can be used as a valuable input to carry out spectrally derived mapping of minerals and pollution in the mining environment. Therefore, the findings of this study make positive contributions to imaging spectroscopy.

The use of satellite imagery proved to be cost effective in many ways. First they were donated, therefore acquired without cost. Secondly, the image processing and value

adding tasks for about twenty six images required only a single individual to complete in a period of less than a month. This resulted in an output that would inform the decision maker of the progress of mine rehabilitation. The initial results were obtained and published within the first six months of the study. Using field based surveys, it would have taken more than two years to come up with preliminary results to advice the government. This therefore confirms the hypothesis that satellite derived assessment of asbestos rehabilitation can be more cost effective when compared to intensive field based surveys. Because of extensive spatial coverage, regular temporal coverage and reasonable cost, satellite imagery provides an opportunity to undertake routine natural resource monitoring in developing countries. This contributes to efficient decision making in natural resource management. In conclusion, this study was able to use remote sensing data to monitor asbestos rehabilitation process and assess its effectiveness as a strategy of environmental management.

6.2 Recommendations

6.2.1 Recommendation for Land Use Audit and Integrated Land Use Policy

A comprehensive land use audit is recommended for Mafefe and Mathabatha areas. This will help to identify sustainable development alternatives (agriculture, conservation and other uses of societal benefit) which will be suitable for the post mining environment. The communities are now subjected to abject poverty as they now have no meaningful and sustainable livelihood, they who previously depended on mining for employment and as a source of income. The people are now turning to agriculture as an alternative source of food and income. The area has not been adequately surveyed for alternative land uses and most of the subsistence agricultural activities are currently undertaken on the wetlands and previous mine dumping sites.

The situation calls for the need to undertake an agricultural development audit. The agricultural development and land use audit will help to identify the risks associated with practicing agriculture in the post asbestos mining environment and to identify development opportunities. It will also help to identify possible conventional and biological controls for minerals such as asbestos. In addition, the audit will help to identify and prioritize areas suitable for agricultural development. It will also help to identify capacity building requirements to promote sustainable land management practices which will ensure minimal or no adverse impact on both riparian zones and wetlands. This will contribute positively to sustainable land use management that promotes sustainable agricultural development.

A land use audit will normally give rise to the implementation of an integrated land management policy. This will help to effectively manage development in these areas, reduce hazards and minimize potential disaster. Rehabilitated sites should be declared areas of conservation to ensure full ecosystem recovery. No other land uses should be conducted in such areas. A land use policy should demarcate areas suitable for production and also the ones which cannot be used. This will help in avoiding the risk of resurfacing asbestos. GIS and Remote Sensing will contribute positively in this regard.

6.2.2 Recommendation for Further Research

It is recommended that a detailed air quality assessment be conducted in Mafefe and Mathabatha. This will help to determine the presence of asbestos fibres in the air and evaluate them against the national air quality standards. It will also help to determine

the risk of further contamination of respiratory diseases by the community that may be contracted through environmental exposure to asbestos fibres.

This research has laid a foundation for permanent monitoring of ecosystem recovery using remote sensing. It is therefore recommended that the distribution of asbestos over the land surface be regularly monitored using imaging spectroscopy. This will require support from government in terms of finance.

6.2.3 Community Participation in Planning and Policy

Government and/or stakeholders should involve the community in any decision making. Projects should not be dictated to the communities in a top – down approach, especially those that affect the various communities directly and indirectly. They should be involved in the planning and policy stages before the actual implementation. This will ensure the sustainability of the projects by getting enough support from the community. Without community participation, any decision-making will either fail or will not achieve its intended objectives.

6.2.4 Periodic Assessment and Monitoring

It is recommended that regular monitoring and assessment of progress in the rehabilitated areas be conducted. This evaluation system should be implemented by the regulatory authority (Department of Minerals and Energy). Relevent officials should be tasked to observe and monitor the mining environment situation using user friendly tools such as satellite imagery and geospatial information analysis. This review should be continuous, especially during the post closure period of the mines.

References

Alexander, S.S., Dein J. and Gold D.P. (1973). The use of ERTS-1 MSS data for mapping strip mines and acid mine drainage in Pennsylvania. *Proceedings of the Symposium on Significant Results obtained from Earth Resources Technology Satellite-1, Maryland, USA, 5-9 March 1973*. (Washington D.C.: NASA), 1, 569-575.

Alforque, M. (1996). Trace Metals Analysis By ICP-MS. US Environmental Protection Agency website: http://yosemite.epa.gov/R10/LAB.NSF/b8b7c39a103a235088256c3e007a4dd9/9f18a1f3cf600033882565e2006d287d!OpenDocument. Date accessed: December 2006.

Almeida-Filho, R. and Shimabukuro, Y.E. (2002). Digital processing of a Landsat TM time series for mapping and monitoring degraded areas caused by independent gold miners, Roraima State, Brazilian Amazon. *Remote Sensing of the Environment*, 79, 42-50.

Analytical Spectral Devices Inc, (2002). *FieldSpec ® Pro: User Guide*, Boulder, USA.

Anderson, A.T. and Shubert, J. (1976). ERTS-1 data applied to strip mining. *Photogrammetric Engineering and Remote Sensing*, 42, 211-219.

Anderson, A.T., Schultz, D., Buchman, N. and Nock, H.M. (1977). Landsat imagery for surface mine inventory. *Photogrammetric Engineering and Remote Sensing*, 43, 1027-1036.

Anuta, M.A. and Bahethi, O.P. (1982). *Mine waste location by satellite imagery*. United States Department of the Interior, Bureau of Mines, Washington D.C., Mining Research Contract Report, Number J0208030.

Apan, A.A. (1997). Landcover mapping for tropical forest rehabilitation using remotely sensed data. *International Journal of Remote Sensing*. 18(5), 1029-1049.

Asner, G.P., Braswell, B.H., Schimel, D.S. and Wessman, C.A. (1998). Ecological research needs from multiangle remote sensing data. *Remote Sensing of Environment*. 63, 155-165.

Boyd, D.S. and Petitcolin, F. (2004). Remote sensing of the terrestrial environment using middle infrared radiation (3.0 – 5.0). *International Journal of Remote Sensing*, 25 (17), 3343-3368.

Biot, Y., Blaikie, M.P., Jackson, C. and Palmer-Jones, R. (1995). *Rethinking Research on Land Degradation in Developing Countries: World Bank Discussion Paper no 289*. The World Bank, Washington DC.

Blaikie, P. and Brookfield, H. (1987a). Defining and Debating the Problem. In Blaikie, P. and Brookfield, H. (eds) *Land Degradation and Society*. Methuen, London.,1-26.

Blaikie, P. and Brookfield , H. (1987b). Colonialism, Development and Degradation. In Blaikie P and Brookfield H (eds) *Land Degradation and Society*. Methuen, London, 100-121.

Brime, C. (1985). The accuracy of X-ray diffraction method for determining mineral mixtures*, Mineralogical Magazine*. 49, 531-538

British Asbestos Newsletter (1999). Issue 33 : Winter 98/99 website on internet at http://www.lkaz.demon.co.uk/ban33.htm

Chase, P.E. and Pettyjohn, W. (1973). ERTS-1 investigation of ecological effects of strip mining in eastern Ohio. *Proceedings of the Symposium on Significant Results obtained from Earth Resources Technology Satellite-1, Maryland, USA, 5-9 March 1973*. (Washington D.C.: NASA), 1, 561-568.

Chen, J.M. (1996). Canopy Architecture and Remote Sensing of the Fraction of Photosynthetically Active Radiation Absorbed by Boreal Conifer Forests. *IEEE Transactions on Geoscience and Remote Sensing*, 34,6, 1353-1368.

Clark, R. N. (1999). Chapter 1: Spectroscopy of Rocks and Minerals, and Principles of Spectroscopy. In Rencz, A.N. (ed), *Manual of Remote Sensing, Volume 3, Remote Sensing for the Earth Sciences*, John Wiley and Sons, New York, 3- 58.

Clark, R.N., Hoefen, T.M., Swayze, G.A., Livo E.K, Meeker, G.P., Sutley, S.J., Wilson, S., Brownfield, I.K. and Vance, S.J. (2003). Reflectance Spectroscopy as a Rapid Assessment Tool for the Detection of Amphiboles from the Libby, Montana Region. *U.S. Geological Survey Open-File Report 03-128*.

Coops, N.C., Goodwin, N. and Stone, C. (2006). Predicting *Sphaeropis sapinea* Damage in *Pinus radiata* canopies using spectral indices and spectral unmixture analysis. In *Photogrammetric Engineering and Remote Sensing*, 72(4), 495-416.

Coetzee, C.B., Brabers, A.J., Malherbe, S.J., and van Biljon, W.J. (1992). Asbestos, In Coetzee, C.B.(ed) *Mineral resources of South Africa.* 5th edition. Geological Survey, Pretoria.

Crankshaw, P. (1999). Revealing Africa's mineral wealth. *African mining.* Business Print Centre, Pretoria.

Deacagon Devices Inc. (2004). AccuPar PAR/LAI Ceptometer Model *LP-80*: Operator's Manual Version 1.2. Deacagon Devices Inc. Pullman, Washington.

Deacagon Devices Inc. (2005). *How the LP80 Measures Leaf Area Index: Application Note*. Website: http://www.decagon.com/appnotes/MeasureLAI.pdf. Date accessed: May 2006.

Deer, W.A., Howie, R.A. and Zussman, J. (1992). *An introduction to the Rock Forming Minerals*, 2nd edition John Wiley and Sons, New York, 691p.

DHEW (1976) NIOSH. *Publication No. 77-169, Revised Recommended Asbestos Standard.* Department of Health, Education and Welfare, USA.

ERDAS. (1997). *ERDAS Field Guide, Fourth Edition.* ERDS Inc, Atlanta, GA.

Foody, G.M., Palubinskas, G., Lucas, R.M., Curran, P.J. and Honzak, M. (1996). Identifying terrestrial carbon sinks: classification of successional stages in regenerating tropical forest from Landsat TM data. *Remote Sensing of Environment*, 55, 205-216.

Geerken, R. and Ilaiwi, M. (2004). Assessment of rangeland degradation and development of a strategy for rehabilitation. *Remote Sensing of Environment*, 90, 490-504.

Ghitter, G.S., Hall, R.J. and Franklin, S.E. (1995). Variability of Landsat Thematic Mapper data in boreal deciduous and mixed-wood stands with conifer understory. *International Journal of Remote Sensing*. 16(16), 2989-3002.

Håme, T., Heiler, I. and Miguel-Ayanz, J.S. (1998). An unsupervised change detection and recognition system for forestry. *International Journal of Remote Sensing*. 19(6), 1079-1099.

Harms, B., Knaapen, J.P. and Rademakers, J.G. (1993). Landscape planning for nature restoration : comparing regional scenarios. In Vos,C.C. and Opdam, P. (eds) *Landscape ecology of a stressed environment.* Chapman and Hall, London.

Haralick, R.N. and Fu, K.S. (1983).Pattern recognition and classification. In Colwell R.N.(ed) *Manual of Remote Sensing*. American Society for Photgrammetry and Remote Sensing: Falls Church, 793-804.

Henebry, G.M. (1993). Detecting change in grasslands using measures of spatial dependence with Landsat TM data. *Remote Sensing of Environment*, 46, 223-234.

Herman, P. and Baud-Mony, A. Th. (2000). The asbestos conspiracy, *Le Monde diplomatique*, July 2000.

Huemmrich, K. F. and Goward, S.N. (1992). Spectral vegetation indexes and the remote sensing of biophysical parameters. Proceedings of the International Geoscience and Remote Sensing Symposium (IGARSS), Houston, Texas. Institute of Electrical and Electronics Engineers, 1017-1019.

Institute for Ecological Rehabilitation. (1999). Report for the working group meeting, Bewaarkloof. Potchefstroom University for CHE, Noordbrug.

Institute for Ecological Rehabilitation. (2000). Report for the working group meeting, Island Blue. Potchefstroom University for CHE, Noordburg.

IOM Consulting. (2003). Sampling and Analysis of Crude vermiculite samples for possible asbestiform fibre and quartz content based on vermiculite from Palabora, South Africa (DECEMBER 2003) website: http://www.schundler.com/06-04palabora.htm, Date accessed 04 October 2006.

Irons, J.R. and Kenhard, R.L. (1986). The utility of Thematic Mapper sensor characteristics for surface mine minitoring. *Photogrammetric Engineering and Remote Sensing*, 52, 389-396.

Jakubaskas, M.E. (1996). Thematic Mapper characterization of lodgepole pine seral stages in Yellowstone National Park, USA. *Remote Sensing of Environment*. 56, 118-132.

Justice, C.O., Townshend, J.R.G., Holben, B.N. and Tucker, C.J. (1985). Analysis of the phenology of global vegetation using meteorological satellite data. *International Journal of Remote Sensing*, 6(8),1271-1318.

Karnieli, A., Gabai, A., Ichouku, C., Zaddy, E. and Shachak, M. (2002). Temporal dynamics of soil and vegetation responses in a semi-arid environment. *International Journal of Remote Sensing*. 23(193), 4073-4087.

Klein, C. (1993). Review in Mineralogy, Vol 28

Lawrence, R.L. and Ripple, W.J. (1999). Calculating change curves for multitemporal satellite imagery: Mount St Helens 1980 – 1985. *Remote Sensing of Environment*. 67, 309-319.

Legg, C.A. (1986). Monitoring of open cast coal mining and reclamation works in the United Kingdom using MSS and TM imagery. *Proceedings of the 20th International Symposium on Remote Sensing of Environment,* Ann Arbor: Environmental Research Institute of Michigan, 2, 931-941.

Legg, C.A. (1990). Applications of remote sensing to environmental aspects of surface mining operations in the United Kingdom. *Proceedings of Conference on Remote Sensing: An Operational Technology for Mining & Petroleum Industries held at London, 29-31 October 1990* (London: Institution of Mining and Metallurgy), 159-164.

Liu, H. and Zhou, Q. (2004). Accuracy analysis of remote sensing change detection by rule based rationality evaluation with post classification comparison" *International Journal of Remote Sensing*, 25(5), 1037-1050.

Lu, L., Li, X., Huang, C.L., Ma, M.G., Che, T., Bogaert, J., Veroustraete, F., Dong, Q.H. and Ceulemans, (2005). Investigating the relationship between ground – meaured LAI and vegetation indices in the alpine meadow, North-west China. In *International Journal of Remote Sensing*, 26(20), 4471-4484.

Lucas, R., Rowlands, A., Niemann, O., Merton, R. N. (2004). Chapter 1: Advanced Image Processing Techniques for Remotely Sensed Hyperspectral Data. In Varshney, P. K. and Arora, M. J.(eds) *Hyperspectral Sensors and Applications*. Springer-Verlag, 11 - 49.

Luque, S.S. (2000). Evaluating temporal changes using Multi-Spetral Scanner and Thematic Mapper data on the landscape of the natural reserve: the New Jersey Pine B arrens, a case study. *International Journal of Remote Sensing*. 21(13&14), 2589-2611.

MacDonald, D. and Archer, M. (1993). *Rural Land Degradation*. Hodder and Stoughton, London.

Malila, W.A. (1980). Change vector analysis: An approach for detecting forest changes with Landsat. *Proceedings of machine processing of remotely sensed data symposim*. Purdue University, West Lafayette, Indiana, Ann Arbor: ERIM, 326-335

Mattikalli, N.M. (1995). Integration of remotely sensed raster data with a vector based geographical information system for land use change detection. *International Journal of Remote Sensing*. 16(15), 2813-2828.

Mikkola, K. (1996). A remote sensing analysis of vegetation damage around metal smelters in the Kola Peninsula, Russia. *International Journal of Remote Sensing*. 17(18), 3675-3690.

Ministry of Northern Development Mines, Ontario (2000). Website on internet at webmaster@ndm.gov.on.ca.

Monteith, J.L. (1973). *Principles of Environmental Physics*, Edward Arnold.

Mroczynski, R.P. and Westmiller, R.A. (1982). Aerial photography: a tool for strip mine reclamation. In Johannsen, C.J. and Sanders, J.L. (eds) *Remote Sensing of Resource Management,* Ankeny: Soil Conservation Society of America, 331-337.

Munyati, C. (2000). Wetland change detection on Kafue flats, Zambia, by classification of a multitemporal remote sensing image dataset. *International Journal of Remote Sensing*. 21(9), 1787-1806.

Mutanga, O., Skidmore, A.K. and Prins, H.H.T. (2004). Discriminating Sodium Concentration in a mixed grass species environment of the Kruger National Park using field spectrometry. *International Journal of Remote Sensing*, 25(20), 4191-4201.

Mnyneni, R.B., Maggion, S., Iaquinta, J., Privette, J.L., Gobron, N., Pinty, B., Verstraete, M.M., Kimes, D.S. and Williams, D.L. (1995a). Optical Remote Sensing of Vegetation: Modeling, Caveats and Algorithms, *Remote Sensing of Environment*, 51, 169-188.

Myneni, R.B., Hall, F.G., Sellers, P.J. and Marshak, A.L. (1995b). The Interpretation of Spectral Vegetation Indices, IEEE Transactions on Geoscience and Remote Sensing, 33, 481-486.

Myneni, R.B., Nemani, R.R. and Running, S.W. (1997). Estimation of Global Leaf Area Index and Absorbed PAR using Radiative Transfer Models, In IEEE Transactions on Geoscience and Remote Sensing, 35(6), 1381-1393.

Myneni, R., Running, W., Glassy, J. and Votava, P. (1999). FPAR, LAI (ESDT: MOD15A2) 8-day Composite NASA MODIS Land Algorithm User's Guide

http://modland.nascom.nasa.gov

Nel, M.E., Wessman, C.A. and Veblen, T.T. (1993). Digital and visual analysis of thematic mapper imagery for differentiating old growth from younger spruce fir stands. *Remote Sensing of Environment*, 48, 291-301.

Peplies, R.W., Fishman, N.S. and Tanner, C.E. (1982). Detection of abandoned mined lands: a case study of the Tug Fork Basin. Johannsen, C.J. and Sanders, J.L.(eds) *Remote Sensing of Resource Management*, Ankeny: Soil Conservation Society of America, 362-376.

Petja, B.M. (2001). *An evaluation of the rehabiltation process in the post asbetos mining environment of Mafefe and Mathabatha, Northern Province*. Unpublished Honours Dissertation, Department of Ecology and Resource Management, University of Venda, Thohoyandou.

Petja, BM., Malherbe, J. and Mudau, H.A. (2003). *Evaluation of new satellite systems for use in natural agricultural resource management*. Report No. GW/A/2003/18. ARC – Institute for Soil, Climate and Water, Pretoria.

Prakesh, A. and Gupta, R.P. (1998). Land-use mapping and change detection in a coal mining area – a case study of Jharia Coalfield, India. *International Journal of Remote Sensing*. 19(3), 391-410.

Qunzhu Z., Meisheng, C., Xuezhi, F., Fengxian, L., Xianzhang, C. and Wenkun, S. (1983) A study of spectral reflection characteristics for snow, ice and water in the north of China. *Hydrological Applications of Remote Sensing and Remote Data Transmission* (Proceedings of the Hamburg Symposium, August 1983). IAHS Publ. no. 145., 451 – 462.

Rathore, C.S. and Wright, R. (1993). Monitoring environmental impacts of surface coal mining. *International Journal of Remote Sensing*. 14(6), 1021-1042.

Rashed, T., Week, J.R., Stow, D. and Fugate, D. (2005). Measuring temporal compositions of urban morphology through spectral mixture analysis: towards a soft approach to change analysis in crowded cities. *International Journal of Remote Sensing*, 26(4), 699-718.

Raychaudhuri, B. and Bhattacharyya, S. (2006). Fuzzy Analysis of Laboratory Spectroscopy of Vegetation for Remote Sensing Applications. In *International Journal of Remote Sensing*, 27(1-2), 191-201.

Sader, S. A., Hayes, D. J., Hepinstall, J. A., Coan, M. and Soza, C. (1991). Forest change monitoring of a remote biosphere reserve. *International Journal of Remote Sensing*, 22(10), 1937–1950.

SAEP. (2000). Asbestos. Website on internet at http: // www.saep.org/n subject/ law_policy/ ASBESTOS.html.

Saidi, T.A. (2000). *Research Methodology Module*. Department of Ecology and Resource Management, University of Venda, Thohoyandou.

Saldanha, D.L., Lima E Cunha, M.C. and Haertel, V. (2004). Spectral analysis of soils from mafic/ ultramafic rocks of Cerro Mantiqueira, south-west of Rio Grande do Sul, Brazil. *International Journal of Remote Sensing*. 25(20), 4381-4393.

Serra, P., Pons, X. and Sauri, D. (2003). Post classification change detection with data from different sensors: some accuracy considerations, *International Journal of Remote Sensing*, 24(16), 3311-3340.

Schmidt, H. and Glaesser, C.(1998). Multitemporal analysis of satellite data and their use in monitoring of the environmental impacts of open cast lignite mining areas in Eastern Germany. *International Journal of Remote Sensing*. 19(12), 2245-2260.

Sellers, P.J. (1989). Theory and Applications of Optical Remote Sensing. In Asrar G. (ed) *Vegetation – Canopy Spectral Reflectance and Biophysical Processes*. John Wiley and Sons, New York, 297-333.

Sengupta, M.(1993). *Environmental Impacts of Mining: Monitoring, Restoration and Control*. Lewis Publishers, Boca Raton.

Simonett, S.D. (1976). Remote sensing applications: analysis, interpretation and resource management. In Lintz Jr, J. and Simonett, S.D. (eds) *Remote sensing of environment*. Addison – Wesley Publishing, Reading.

Sohl, T.L., Gallant, A.L. and Loveland, T.R. (2004). The characteristics and interpretability of land surface change and implications for project design. *Photogrammetric Engineering and Remote Sensing*, 70(4),439-448

Stats SA. (2006). Population data obtained from Statistics South Africa via e-mail (Edroy Christians, edroyc@statssa.gov.za).

Steininger, M. K. (1996). Tropical secondary forest regrowth in the Amazon: age, area and change estimation with Thematic Mapper data. *International Journal of Remote Sensing.* 17 (1), 9-27.

Steininger, M.K. (2000). Satellite estimation of tropical secondary forest above-ground data from Brazil and Bolivia. *International Journal of Remote Sensing.* 21(6&7), 1139-1157.

Sunar, F. (1998). An analysis of changes in a multidate data set: a case study in the Ikitelli area, Instanbul, Turkey. *International Journal of Remote Sensing*. 19(2), 225-235.

Torres – Vera, M.A. and Prol – Ledesma, R.M. (2003). Spectral enhancement of selected pixels in Thematic Mapper images of Guanajuato district (Mexico) to identify hydrothermally altered rocks. In *International Journal of Remote Sensing*, 24(24), 4357-4373.

Tswai, D.R. (2003). *Spectral Differentiation of Summer Crops in South Africa.* CETEL/DESS Masters Report, University of Paris 6, Paris.

Turkington, T. (2000). The town that battles blue death : where breathing can kill you in *True Love Magazine* August 2000. Naspers, Sandton, Vol 258 .

Twumasi, Y.A. (2005). Park Management in Ghana using Geographic Information System (GIS) and Remote Sensing Technology. Edwin Mellen Press, Lewiston.

UNEP WCMC. (2007). Potlake Nature Reserve Website: http://www.unep-wcmc.org/sites/pa/0622p.htm, Date Accessed, March 2007.

University of Virgnia. (2006). X-Ray Diffraction, website: http://galileo.phys.virginia.edu/classes/317.gbh.fall05/xray/xray.html Date accessed, December 2006.

Upper Midwest Aerospace Consortium. (2002). *Weekly vegetation maps*, website http://www.umac.org/farming/2c.html.

USEPA. (2004a). What is asbestos? *U.S. Environmental Protection Agency website: www.epa.gov*.

Vermaak, C.F. (1979). *The global status of the South African Minerals economy and Data summaries of its key commodities : Review paper no 1*, Geological Society of South Africa, Johannesburg.

Wier, C.W., Wobber, F.J., Orville, R.R. and Amato, R.V. (1973). Fracture mapping and strip mine inventory in the Midwest by using ERTS-1 imagery. *Proceedings of the Symposium on Significant Results obtained from Earth Resources Technology Satellite-1, Maryland, USA, 5-9 March 1973*. (Washington D.C.: NASA), 1, 553-560.

Xavier, A.C. and Vettorazzi, C.A. (2004). Mapping Leaf area index through spectral vegetation indices in a subtropical watershed. In *International Journal of Remote Sensing*, 25(9),1661-1672.

Zhou, X., Zhu, Q., Tang, S., Chen, X. and Wu, M. (2002). Interception of PAR and relationship between FPAR and LAI in summer maize canopy. In Proceedings of IEEE International Geoscience and Remote Sensing Symposium, 6(2002),3252 – 3254.

Cited South African Legislation (Published by Government Printer)

Atmospheric Pollution Prevention Act, Act 45 of 1965.

Compensation for Occupational Injuries and Diseases Act, Act 130 of 1993.

Constitution of Republic of South Africa, Act 200 of 1993.

Constitution of Republic of South Africa, Act 108 of 1996.

Minerals Act 1991, Act 50 of 1991.

Mining Rights Act, Act 20 of 1967.

National Environmental Management Act, Act 107 of 1998.

APPENDIX I: Minimum and Maximum Temperatures of the Study Area

Lekgalametse Maximum Temperatures

maxT/month	1996	1997	1998	1999	2000	2001	2002	2003	2004
Jan		28.7	28.5	28.6	26.3		29.8	30.9	30.2
Feb				27.6			28.0	31.1	
Mar			30.9		27.1	25.7		29.8	
Apr	23.9	24.8			24.2	26.4		27.8	
May	22.9							24.6	
Jun	22.1	23.6	24.3	23.1			21.1	21.2	
Jul	20.2	20.7					23.5		
Aug	22.3	23.7	24.6	24.2	23.5	24.1			
Sep	27.3	24.4	26.5	24.9	26.0	26.6	26.0	27.0	
Oct		25.2	26.2	26.1	27.6	25.2	27.9	27.5	
Nov		28.1	27.0				28.2	-999	
Dec	28.1	28.5	26.8				27.5	29.9	

Lekgalametse Minimum Temperatures

minT/mont	1996	1997	1998	1999	2000	2001	2002	2003	2004
Jan		19.1	19.4	18.4	17.7		17.8	18.4	19.5
Feb		17.9		18.0			17.9	19.0	
Mar	16.4		18.1		18.3	17.6		17.4	
Apr	14.0	13.4				16.1		15.6	
May	12.6							13.2	
Jun	9.6	10.3	9.7	9.1			9.5	9.9	
Jul	8.3	8.1		9.1			9.6		
Aug	10.3	10.2	10.3	12.2	9.2	10.8			
Sep	12.7	13.4	12.4	11.5	13.2	13.0	12.1	11.0	
Oct		13.9	14.4	13.3	15.7	15.4	14.6	15.1	
Nov		15.8	16.7				14.9		
Dec	18.2	17.4	17.7				18.1	18.1	

APPENDIX II: Population

Populations Size weighted by income

	No income	R 1 - R 400	R 401 - R 800	R 801 - R 1600	R 1601 - R 3200
Mafefe	9044	669	1329	84	66
Mafefe SP	363	4	36	-	-
Dublin	121	5	24	3	3
Fertilis	1314	89	112	6	8
Ga Mafefe	2834	268	572	33	31
Ga-Mokgotho	351	77	47	11	-
Gemini	852	34	119	7	8
Geneva	229	16	32	5	-
Mahlatjane	1320	62	165	5	3
Masusele	143	3	30	-	-
Mataung	518	60	85	8	3
Mobosobohlogo	279	22	32	3	3
Osterd	259	21	21	-	3
Setaseng	460	9	54	3	-
Mathabatha	376	14	38	9	3
Madikeleng Kuduskop	376	14	38	9	3

Source: Stats SA (2006).

	R 3201 - R 6400	R 6401 - R 12800	R 12801 - R 25600	R 25601 - R 51200	R 51201 - R 102400
Mafefe	72	34	3	-	-
Mafefe SP	3	-	-	-	-
Dublin	-	-	-	-	-
Fertilis	11	-	-	-	-
Ga Mafefe	42	26	-	-	-
Ga-Mokgotho	-	-	-	-	-
Gemini	-	-	-	-	-
Geneva	-	-	-	-	-
Mahlatjane	9	3	-	-	-
Masusele	-	-	-	-	-
Mataung	5	3	-	-	-
Mobosobohlogo	3	-	-	-	-
Osterd	-	-	-	-	-
Setaseng	-	-	-	-	-
Mathabatha	3	3	-	-	-
Madikeleng Kuduskop	3	-	-	-	-

	R 102401 – R 204800	R 204801 or more
Mafefe	8	-
Mafefe SP	-	-
Dublin	-	-
Fertilis	-	-
Ga Mafefe	-	-
Ga-Mokgotho	-	-
Gemini	-	-
Geneva	-	-
Mahlatjane	-	-
Masusele	-	-
Mataung	8	-
Mobosobohlogo	-	-
Osterd	-	-
Setaseng	-	-
Mathabatha	-	-
Madikeleng Kuduskop	-	-

APPENDIX III: Acquired Landsat TM images and Field Survey Sites

Imagery Acquisition Dates

Landsat TM	169/077
19890512	19890816
19900616	19910705
19920621	19920808
19930608	19930811
19940627	19940814
19950614	19950801
19970502	19960819
19980606	19970822
19990508	19980910
20000510	19990828
20020508	20000830
20030409	20010910
20040606	20020727

WAYPOINT	58	-24.18950099	30.14268335	Mafefe
WAYPOINT	59	-24.19043818	30.14335432	Mafefe
WAYPOINT	60	-24.19043742	30.14335658	Mafefe
WAYPOINT	62	-24.19045863	30.14331442	Mafefe
WAYPOINT	63	-24.27829687	30.22155697	Mafefe
WAYPOINT	64	-24.26902455	30.21297223	Mafefe
WAYPOINT	65	-24.27911108	30.22217187	Mafefe
WAYPOINT	66	-24.22836495	30.18432825	Mafefe
WAYPOINT	67	-24.22895243	30.18299628	Mafefe
WAYPOINT	68	-24.23270308	30.17858271	Mafefe
WAYPOINT	69	-24.23259697	30.17857541	Mafefe
WAYPOINT	70	-24.17033133	30.09830779	Bewaarkloof
WAYPOINT	71	-24.16925484	29.7819979	Bewaarkloof
WAYPOINT	72	-24.17324882	29.77888905	Bewaarkloof
WAYPOINT	73	-24.17410813	29.77883784	Bewaarkloof
WAYPOINT	74	-24.18526202	29.78884005	Bewaarkloof
WAYPOINT	75	-24.18524802	29.78887383	Bewaarkloof
WAYPOINT	76	-24.26415425	29.9261948	Potlake
WAYPOINT	77	-24.26029882	29.92814108	Potlake
WAYPOINT	78	-24.26001971	29.92173504	Potlake
WAYPOINT	79	-24.25619689	29.91351642	Potlake
WAYPOINT	80	-24.25626503	29.91348892	Potlake
WAYPOINT	81	-24.25250541	29.91061494	Potlake
WAYPOINT	82	-24.25850065	29.92987898	Potlake
WAYPOINT	83	-24.26043821	29.93626541	Potlake
WAYPOINT	84	-24.26222582	29.94325507	Potlake
WAYPOINT	85	-24.26231476	29.92874458	Potlake
WAYPOINT	86	-24.26267166	29.93098179	Potlake
WAYPOINT	87	-24.26614579	29.92721178	Potlake
WAYPOINT	88	-24.26641585	29.92959324	Potlake
WAYPOINT	89	-24.26872456	29.92641642	Potlake
WAYPOINT	90	-24.27073773	29.92991846	Potlake
WAYPOINT	91	-24.27230649	29.93288297	Potlake
WAYPOINT	92	-24.27199124	29.91907354	Potlake
WAYPOINT	93	-24.18730913	29.79496764	Bewaarkloof
WAYPOINT	94	-24.18750677	29.79612837	Bewaarkloof

APPENDIX IV: XRF AND ICP-MS Analyses

XRF Analyses

Results of major (wt%) and trace (ppm) elements analysed by X-ray fluorescence spectrometry

Sample	BW-1	BW-2	CS-1	CS-2	MS-1	MS-2	MS-3	MT-1
SiO_2	45.29	42.09	64.57	56.49	91.21	87.20	87.28	55.92
TiO_2	0.28	0.26	0.51	0.58	0.14	0.14	0.15	0.96
Al_2O_3	3.34	4.13	5.19	6.46	2.96	2.82	2.83	13.89
Fe_2O_3(t)	44.20	15.59	7.14	8.14	2.31	6.02	6.82	14.79
MnO	0.213	0.402	0.588	0.728	0.089	0.100	0.100	0.218
MgO	0.72	1.83	1.20	1.38	0.50	0.46	0.47	4.12
CaO	0.25	16.64	3.92	3.70	0.69	0.74	0.53	2.64
Na_2O	0.28	0.15	0.21	0.21	0.10	0.17	0.11	0.57
K_2O	0.95	1.56	0.67	0.78	1.03	1.09	1.02	1.90
P_2O_5	0.10	0.18	0.11	0.14	0.02	0.02	0.02	0.06
Cr_2O_3	0.015	0.022	0.012	0.015	0.010	0.009	0.010	0.040
L.O.I.	3.19	16.60	15.61	21.14	1.28	1.42	0.92	4.30
TOTAL	98.82	99.45	99.73	99.76	100.35	100.19	100.26	99.40
H_2O^-	1.46	1.91	2.53	4.24	0.22	0.27	0.23	1.24
As	<4	10	<4	7.1	4.1	<4	<4	12
Ba	301	230	154	188	155	161	179	534
Bi	5.3	3.3	<3	<3	<3	<3	<3	<3
Br	<2	6.7	17	22	<2	<2	<2	2.8
Ce	54	40	39	46	15	<10	21	59
Co	12	18	19	22	4.5	4.8	4.9	35
Cr	102	224	86	102	40	40	41	379
Cs	<5	<5	<5	<5	<5	<5	<5	<5
Cu	28	32	48	59	5.7	6.3	7.0	52
Ga	6.8	7.0	6.8	8.4	3.3	3.3	3.4	19
Ge	3.5	3.2	<1	1.1	<1	<1	<1	1.5
Hf	4.7	3.0	<3	3.9	<3	<3	<3	3.9
La	17	22	14	21	<10	<10	<10	37
Mo	<2	<2	<2	<2	<2	<2	<2	<2
Nb	3.4	3.7	4.6	5.1	1.5	1.7	1.8	13

Nd	14	12	14	20	<10	<10	<10	25
Ni	42	83	55	65	15	15	16	129
Pb	11	14	12	13	7.4	7.3	6.8	28
Rb	157	113	36	42	24	25	25	103
Sc	8.5	<3	10	12	<3	<3	3.5	20
Se	1.5	<1	<1	<1	<1	<1	<1	<1
Sm	<10	<10	<10	<10	<10	<10	<10	<10
Sr	14	45	18	20	12	13	13	58
Ta	<2	<2	2.2	<2	<2	<2	<2	2.7
Th	4.3	<3	3.6	4.3	<3	<3	<3	14
Tl	<3	<3	<3	<3	<3	<3	<3	<3
U	<2	2.0	<2	<2	<2	<2	2.0	4.1
V	40	57	65	74	13	13	15	145
W	<3	<3	<3	<3	<3	<3	<3	7.0
Y	6.9	8.8	14	18	4.8	6.4	4.6	21
Yb	<2	<2	<2	<2	<2	<2	<2	2.3
Zn	25	51	37	45	8.1	8.0	8.0	97
Zr	67	48	82	96	55	51	56	145

Sample	MT-2	STREAM	WP-58-1	WP-58-2	WP-66	WP-71	WP-72	WP-74
SiO_2	45.78	58.23	42.29	40.50	45.76	54.50	48.56	45.85
TiO_2	0.22	0.58	0.06	0.06	0.29	0.23	0.25	0.41
Al_2O_3	2.49	6.26	0.72	0.90	4.47	3.00	3.94	6.20
Fe_2O_3(t)	43.54	9.14	48.43	50.11	34.42	36.05	35.90	17.79
MnO	0.229	0.710	0.285	0.270	0.537	0.275	0.359	0.445
MgO	1.00	1.33	2.17	2.54	1.76	0.58	1.57	2.70
CaO	0.83	3.55	1.68	1.22	0.93	1.21	1.99	8.36
Na_2O	0.19	0.24	0.23	0.28	0.31	0.12	0.41	0.23
K_2O	1.13	0.78	0.59	0.75	1.00	0.54	1.23	1.91
P_2O_5	0.09	0.13	0.13	0.20	0.22	0.06	0.13	0.23
Cr_2O_3	0.014	0.014	0.007	0.008	0.019	0.013	0.020	0.033
L.O.I.	3.90	18.79	2.75	2.54	9.70	2.89	4.81	15.32
TOTAL	99.42	99.76	99.34	99.39	99.42	99.48	99.17	99.47
H_2O^-	1.49	2.48	1.50	1.11	3.33	1.50	1.84	3.06
As	7.7	11	<4	<4	13	<4	<4	16
Ba	224	189	46	52	138	227	263	232

Bi	4.3	<3	6.7	7.7	5.4	3.5	3.4	3.3
Br	4.8	20	<2	<2	6.3	<2	7.4	6.6
Ce	38	40	10	23	17	39	35	51
Co	8.2	20	6.9	3.2	14	7.3	12	20
Cr	107	105	12	15	153	96	175	316
Cs	<5	<5	<5	<5	<5	<5	<5	<5
Cu	24	58	11	12	31	26	32	40
Ga	5.2	8.7	<1	1.7	6.8	5.3	7.1	8.5
Ge	4.6	<1	3.4	3.8	4.9	3.7	4.7	3.7
Hf	5.3	<3	<3	<3	3.9	<3	<3	<3
La	12	26	<10	<10	<10	24	<10	20
Mo	<2	<2	<2	<2	<2	<2	<2	<2
Nb	2.1	5.6	<1	<1	2.6	2.8	3.0	5.3
Nd	12	17	<10	<10	<10	14	12	17
Ni	43	65	10	13	66	41	63	103
Pb	14	14	8.7	6.5	12	10	13	17
Rb	139	42	92	114	79	89	114	138
Sc	8.6	11	<3	<3	9.6	6.9	6.3	7.8
Se	1.3	<1	2.4	2.1	1.6	<1	1.2	<1
Sm	<10	<10	<10	<10	<10	<10	<10	<10
Sr	23	20	20	24	25	22	46	45
Ta	<2	<2	<2	<2	<2	<2	<2	<2
Th	<3	<3	<3	<3	<3	<3	<3	4.8
Tl	<3	<3	<3	<3	<3	<3	<3	<3
U	3.2	<2	2.3	<2	<2	<2	<2	<2
V	40	73	<3	<3	49	40	48	74
W	<3	<3	<3	<3	<3	<3	<3	<3
Y	7.6	18	6.9	11	13	13	7.4	13
Yb	<2	<2	<2	2.2	<2	<2	<2	<2
Zn	43	44	20	21	73	23	40	74
Zr	43	96	8.8	11	51	56	59	77

ICP-MS Analyses

Note: all ICP-MS values in ppb

Samples	Li (7)	Be (9)	B (10)	Na (23)	Mg (24)	Al (27)	K (39)	Ca (43)
SAMPLE 1	3	8	136	2 561	18 942	120	654	31 404
SAMPLE 2	4	< 1	98	2 767	19 606	< 100	763	31 854
SAMPLE 3	1	< 1	93	2 985	19 440	< 100	1 374	33 353
SAMPLE 4	2	< 1	79	2 911	19 693	< 100	1 145	33 852
SAMPLE 7	2	< 1	65	3 009	15 498	< 100	837	30 128
SAMPLE 8	2	< 1	63	2 358	15 813	< 100	799	28 977
SAMPLE 9	1	< 1	60	2 380	15 670	< 100	824	25 288
SAMPLE 10	< 1	< 1	53	2 432	15 780	< 100	806	24 586

Samples	V (51)	Cr (52)	Fe (54)	Mn (55)	Co (59)	Ni (60)	Cu (63)	Zn (66)
SAMPLE 1	6	174	749	15	< 5	72	16	279
SAMPLE 2	4	180	798	23	< 5	85	21	464
SAMPLE 3	3	180	659	19	< 5	75	17	574
SAMPLE 4	2	176	661	19	< 5	72	14	287
SAMPLE 7	< 2	169	468	12	< 5	72	17	314
SAMPLE 8	< 2	175	659	22	< 5	70	9	219
SAMPLE 9	< 2	170	739	20	< 5	74	17	475
SAMPLE 10	< 2	161	743	19	< 5	75	18	490

Samples	Ga (69)	As (75)	Se (82)	Rb (85)	Sr (88)	Mo (95)	Ag (107)	Cd (111)
SAMPLE 1	< 5	< 1	12	2	14	< 5	2	< 2

SAMPLE 2	< 5	< 1	< 5	2	14	< 5	< 1	< 2
SAMPLE 3	< 5	< 1	< 5	2	14	< 5	< 1	< 2
SAMPLE 4	< 5	< 1	< 5	3	15	< 5	< 1	< 2
SAMPLE 7	< 5	< 1	< 5	2	17	< 5	< 1	< 2
SAMPLE 8	< 5	< 1	< 5	1	17	< 5	< 1	< 2
SAMPLE 9	< 5	< 1	< 5	1	16	< 5	< 1	< 2
SAMPLE 10	< 5	< 1	< 5	1	17	< 5	< 1	< 2

Samples	Te (128)	Ba (137)	Tl (205)	Pb (208)	Bi (209)	U (238)
SAMPLE 1	< 1	17	< 1	22	1	1
SAMPLE 2	< 1	19	< 1	23	< 1	< 1
SAMPLE 3	< 1	23	< 1	22	< 1	< 1
SAMPLE 4	< 1	20	< 1	20	< 1	< 1
SAMPLE 7	< 1	19	< 1	14	< 1	< 1
SAMPLE 8	< 1	22	< 1	11	< 1	< 1
SAMPLE 9	< 1	22	< 1	27	< 1	< 1
SAMPLE 10	< 1	24	< 1	26	< 1	< 1

Note: all IC values in ppm

Samples	F	Cl	NO_2	Br	NO_3	PO_4	SO_4
1	0	5	0	0	0	0	1
2	0	5	0	0	0	0	1
3	0	6	0	0	1	0	1
4	0	6	0	0	1	0	1
7	0	5	0	0	1	0	2
8	0	5	0	0	1	0	2
9	0	5	0	0	0	0	2
10	0	5	0	0	0	0	2

APPENDIX V: PAR/LAI Values and Parameters

07-Jun-06

Time	Above	Below	Tau (τ)	Chi (X)	Fb	Zenith Angle	Cosθ	2Cosθ
762	1641.59	16.2	0.009868	1.00,	0.9	49	0.656059	1.312118
774	1789.4	36	0.020118	1.00,	0.9	49	0.656059	1.312118
834	1452.59	148.39	0.102155	1.00,	0.9	55	0.573576	1.147153
846	1614.69	58.09	0.035976	1.00,	0.9	56	0.559193	1.118386
852	1678.09	205.5	0.122461	1.00,	0.9	57	0.544639	1.089278

Time	K	1/2K	a	A	lnτ	L
762	0.762127	0.656059	0.9	0.86071	-4.61841	2.137694
774	0.762127	0.656059	0.9	0.86071	-3.90612	1.808
834	0.871723	0.573576	0.9	0.86071	-2.28126	0.942385
846	0.894146	0.559193	0.9	0.86071	-3.3249	1.34466
852	0.918039	0.544639	0.9	0.86071	-2.09997	0.83083

08-Jun-06

Time	Above	Below	Tau (τ)	Chi (X)	Fb	Zenith Angle	Cosθ	2Cosθ
624	1819.69	33.9	0.01863	1	0.9	54	0.587785	1.175571
630	1784	83.3	0.046693	1	0.9	54	0.587785	1.175571
642	1452.4	766.4	0.527678	1	0.9	52	0.615661	1.231323
684	1451.4	240.1	0.165426	1	0.9	49	0.656059	1.312118
702	1685.09	137.19	0.081414	1	0.9	49	0.656059	1.312118
768	1504.3	38.29	0.025454	1	0.9	49	0.656059	1.312118
774	1556	347.29	0.223194	1	0.9	50	0.642788	1.285575
780	1316.4	400.1	0.303935	1	0.89	50	0.642788	1.285575

Time	K	1/2K	a	A	lnτ	L
624	0.850651	0.587785	0.9	0.86071	-3.98301	1.67952
630	0.850651	0.587785	0.9	0.86071	-3.06416	1.292071
642	0.812135	0.615661	0.9	0.86071	-0.63927	0.280313
684	0.762127	0.656059	0.9	0.86071	-1.79923	0.832798
702	0.762127	0.656059	0.9	0.86071	-2.50821	1.160958
768	0.762127	0.656059	0.9	0.86071	-3.67089	1.699124
774	0.777862	0.642788	0.9	0.86071	-1.49971	0.682155
780	0.777862	0.642788	0.9	0.86071	-1.19094	0.548995

09-Jun-06

Time	Above	Below	Tau (τ)	Chi (X)	Fb	Zenith Angle	Cosθ	2Cosθ
654	1687.5	261.79	0.155135	1.00,	0.9	51	0.62932	1.258641
660	1236.19	839.79	0.679337	1.00,	0.87	51	0.62932	1.258641
672	1452.59	80.19	0.055205	1.00,	0.9	50	0.642788	1.285575
684	1157.3	539.79	0.466422	1.00,	0.81	49	0.656059	1.312118
738	1391.5	247.5	0.177866	1.00,	0.9	48	0.669131	1.338261
744	1340.4	864.7	0.645106	1.00,	0.88	49	0.656059	1.312118
804	928	1023.5	1.102909	1.00,	0.68	52	0.615661	1.231323
822	1579.3	130.5	0.082632	1.00,	0.9	53	0.601815	1.20363

Time	K	1/2K	a	A	lnτ	L
654	0.794508	0.62932	0.9	0.86071	-1.86346	0.832466
660	0.794508	0.62932	0.9	0.86071	-0.38664	0.179897
672	0.777862	0.642788	0.9	0.86071	-2.8967	1.317585
684	0.762127	0.656059	0.9	0.86071	-0.76266	0.395876
738	0.747238	0.669131	0.9	0.86071	-1.72673	0.812857
744	0.762127	0.656059	0.9	0.86071	-0.43834	0.208252
804	0.812135	0.615661	0.9	0.86071	0.097952	-0.05719
822	0.83082	0.601815	0.9	0.86071	-2.49336	1.072486

14-Jun-06

Time	Above	Below	Tau (τ)	Chi (X)	Fb	Zenith Angle	Cosθ	2Cosθ
590	1579.3	130.5	0.082632	1.00,	0.9	53	0.601815	1.20363

Time	K	1/2K	a	A	lnτ	L
590	0.83082	0.601815	0.9	0.86071	-2.49336	1.072486